Dynamic ubiquitin modification regulated and interpreted by endosomal sorting complexes.

Francesca Frigenti

Thesis submitted in accordance with the requirements of the University of Liverpool for the degree of doctor in philosophy.

August 2023

Abstract

Ubiquitin is a fundamental signalling protein that can be appended onto substrate proteins to affect their function. E3 ligases and DUBs (deubiquitylases) are the enzymes that attach and cleave the isopeptide bond formed by ubiquitin, respectively. Lys63-linked poly-ubiquitin (K63-ubiquitin) on cargo receptors is a signal recognised by the ESCRT complexes to induce the translocation of cargo receptors to intra-luminal vesicles of the late-endosome or multi-vesicular body (MVB). The DUB AMSH/STAMBP localises to endosomes and has been proposed to affect the trafficking of endocytosed receptors like EGFR and CXCR4 by virtue of its ability to cleave their K63-ubiquitin chains, but whether it targets other proteins in this pathway is not known.

Here, I describe the generation of HeLa AMSH knockout cells to investigate the effect upon the ubiquitin landscape. I found that there was a global increase of K63-linked polyubiquitin associated with intracellular membranes in AMSH knockout cells compared to parentals.

I asked which specific proteins are differentially modified with K63-ubiquitin in AMSH KO cells compared to parentals. To this end, I carried out an unbiased approach to analyse the proteome enriched for K63-linked poly-ubiquitin using a specific ubiquitin binding domain called K63-Superbinder. The data indicate that AMSH may be regulating exosome biogenesis and/or exosome protein composition by exerting its K63-ubiquitin specific DUB activity. Exosomes are relevant for cell-to-cell communication because of their carrier activity for proteins and RNA molecules modulating the immune response.

In addition, I generated Flag-APEX2-AMSH cells that can be used in conjunction with proteomics to perform proximity labelling experiments in order to search for novel co-regulators of AMSH function.

In conclusion, I suggest a novel physiological role for AMSH as a DUB as a regulator of the maturation process that generates exosomes from MVBs.

Table of contents

List of figures

List of tables

Abbreviations

ABIN	A20 Binding and Inhibitor of NFkB
ACN	Acetonitrile
ADP	Adenosine-
AIM2	absent in melanoma 2
ALG-2	Apoptosis-linked gene 2
ALIX	ALG-2-interacting protein X
AMBIC	Amonium bicarbonate
AMP	Adenosine monophosphate
AMSH	Associated molecule with the SH3 domain of STAM
APC	anaphase promoting complex
APEX2	Apurinic/Apyrimidinic Endodeoxyribonuclease 2
AQUA	absolute quantification
ATP	adenosine triphosphate
BDNF	Brain-derived neurotrophic factor (
BIRC7	Baculoviral IAP repeat-containing protein 7
BRCA1	Breast cancer type 1 susceptibility protein
BRCC36	BRCA1/BRCA2-containing complex subunit
BSA	bovine serum albumine
CCV	clathrin coated vesicle
CHC	clathrin heavy chain
CHMP	charged multivesicular body proteins
CME	clathrin mediated endocytosis
CPY	Carboxypeptidase Y
CRISPR	Clustered Regularly Interspaced Short Palindromic Repeats
CRL	cullin ring ligase
CSF	Macrophage colony-stimulating factor 1
CSN5	COP9 signalosome complex subunit 5
CTCF	corrected total cell fluorescence
CUE	Coupling of Ubiquitin conjugation to Endoplasmic reticulum
CXCR4	C-X-C motif chemokine receptor 4
DAB	Diaminobenzidine
DAMP	Damage-associated molecular patterns
DAPI	4′,6-diamidino-2-phenylindole
DMEM	Dulbecco’s Modified Eagle’s Medium
DMSO	Dimethylsulfoxide
DNA	Deoxyribonucleic acid
dNTP	Deoxynucleotide triphosphates
DUIM	double-sided ubiquitin-interacting motif
ESCRT	endosomal sorting complex required for transport

EDTA	Ethylenediaminetetraacetic acid
EEA1	Early endosome antigen 1
EGF	epithelial growth factor
EGFR	epithelial growth factor receptor
EGTA	ethylene glycol-bis (β-aminoethyl ether)-N,N,N′,N′-tetraacetic acid
EM	electron microscopy
EV	extracellular vesicle
FAM21	family with sequence similarity 21
FBXL2	F-Box and Leucine Rich Repeat Protein 2
FC	fold change
FDR	false discovery rate
FRT	flippase recombinase recognition target sequences
FYVE	(Fab1/ YOTB/Vac1/EEA1) domain
GEF	guanine nucleotide-exchange factor
GFP	green fluorescent protein
GLUE	gramlike ubiquitin-binding in Eap45
GST	Glutathione S-transferase
GTP	Guanosine-5'-triphosphate
H_2O_2	hydrogen peroxyde
HANL	HA-NanoLuciferase tag
HCD	higher-collisional dissociation
HDL	High-density lipoprotein
HDPTP	His domain–containing tyrosine phosphatase
HECT	homologous to the E6AP carboxyl terminus
HEK293	Human embryonic kidney 293 cells
HEPES	hydroxyethylpiperazine ethane sulfonic acid
HERC	HECT and RLD domain containing E3 ubiquitin protein ligase
HGS	Hepatocyte growth factor-regulated tyrosine kinase substrate
HIV	human immunodeficiency virus
HOIL	heme-oxidized IRP2 ubiquitin ligase 1
HOIP	HOIL-1-interacting protein
HOPS	homotypic fusion and protein sorting
HPLC	High Performance Liquid Chromatography
HRS	Hepatocyte growth factor-regulated substrate
IBR	In Between Ring fingers
ICAM	Intercellular adhesion molecule-1
IFNAR1	Interferon alpha and beta receptor subunit 1
IFNAR1	type-1 interferon (IFN) receptor chain 1
ILV	intraluminal vesicle
IPTG	Isopropyl β-D-1-thiogalactopyranoside
ISG15	Interferon-stimulated gene 15

IST1	IST1 factor associated with ESCRT-III
ITAM	immune-receptor tyrosine-based activation motif
JAB1	c-Jun activation domain-binding protein-1
JAMM	JAB1/MPN/MOV34
LAMP1	Lysosomal Associated Membrane Protein 1
LBPA	lysobisphosphatidic acid
LC3	Microtubule-associated proteins 1A/1B light chain 3B
LDL	Low-density lipoprotein
LFQ	label free quantification
MDM2	Mouse double minute 2 homolog
MHC	major histocompatibility complex
MIC-CAP	microcephaly capillary syndrome
MIM	MIT-interacting motif
MIT	microtubule-interacting domain
MJD	Machado–Joseph disease
MMP2	Metalloprotease-2
MOPS	3-(N-morpholino)propanesulfonic acid
MPI	mammalian protease inhibitors
MS	mass spectrometry
MVB	multivesicular body
MW	molecular weight
MYSM1	Myb Like, SWIRM And MPN Domains 1
NEAA	Non-Essential Amino Acids
NEB	New England Biolabs
NEDD4L	neural precursor cell expressed developmentally down-regulated 4-like
NEDD8	Neural precursor cell expressed developmentally down-regulated protein 8
NEM	N-Ethylmaleimide
NEMO	NF-kappa-B essential modulator
NES	nuclear export signal
NGF	neuronal growth factor
NHEJ	non homologous end joining
NLR	NOD-like receptors
NLRP3	LR family pyrin domain containing 3
NLS	nuclear localisation signal
NMDA	N-methyl-D-aspartate
NMR	nuclear magnetic resonance
NPC	Niemann Pick C2 protein
NPC1	Niemann Pick C2 protein complex1
NSCLC	non-small cell lung cancer cells
NT1	non targeting 1
NUFIP1	Nuclear FMR1 Interacting Protein 1

NZF	zinc finger
OD	optical density
ORF	open reading frame
OTU	ovarian tumour proteases
OTUD	OTU Deubiquitinase
PAGE	Polyacrylamide gel electrophoresis
PAMP	Pathogen-associated molecular patterns
PAR	Protease-activated receptors
PBL	peripheral-blood leucocytes
PBS	phosphate buffer saline
PCR	polymerase chain reaction
PCSK9	Proprotein Convertase Subtilisin/Kexin Type 9
PDCD6IP	Programmed cell death 6-interacting protein
PDGF	platelet-derived growth factor
PDZ	Post-synaptic density protein 95 domain
PFA	Paraformaldehyde
PFU	PLAA family ubiquitinbinding domain
PHD	Pleckstrin-homology domain
PI	Phosphatidylinositol
PI3K	Phosphoinositide 3-kinases
PI3P	phosphatidylinositol 3-phosphate
PIP2	Phosphatidylinositol 4,5-bisphosphate
PLAA	Phospholipase A2 Activating Protein
PM	plasma membrane
PNS	post-nuclear supernatant
POI	protein of interest
PRD	protein region disordered
PSD95	Postsynaptic density 95
PSMD14	26S proteasome non-ATPase regulatory subunit 14
PTPN23	Protein Tyrosine Phosphatase Non-Receptor Type 23
RAF	Rapidly Accelerated Fibrosarcoma
RAP80	receptor-associated protein 80
RAS	Rat sarcoma virus
RBR	RING-between-RING
RIG	retinoic acid-inducible gene I
RING	Really Interesting New Gene
RIPA	Radioimmunoprecipitation assay buffer
RLD	RCC1 (MIM 179710)-like domain
RNA	Ribonucleic acid
SAMD1	Sterile alpha motif domain-containing protein 1
SAPP	soluble amyloid precursor protein
SBM	STAM-binding motif

SDCBP	syndecan binding protein
SDS	sodium dodecyl sulphate
SH3	Src homology 3 domain
SHMT	serine hydroxymethyltransferase
SILAC	Stable isotope labeling by amino acids in cell culture
SLUG	Zinc finger protein SNAI2
SNAI1	Zinc finger protein SNAI1
SNAP	Synaptosomal-Associated Protein
SNARE	Soluble N-ethylmaleimide-sensitive factor activating protein receptor
SNX	sorting nexin
SOUBA	solenoid of overlapping UBAs
STAM	Signal Transducing Adaptor Molecule
STAMBP	STAM binding protein
STAMBPL	STAM binding protein-like 1
SUMO	small ubiquitin-like modifier
SWIP	strumpellin and WASH interacting protein
TBS	Tris-buffered saline
TBST	Tris-buffered saline with 0.1% Tween® 20 detergent
TDP	thymidine diphosphate
TERM	tetraspanin-enriched microdomains
TGF	Transforming growth factor
TGN	trans-Golgi network
THP	Tohoku Hospital Pediatrics-1
TREX	Transcription Factor Regulatory Element X
TSC2	Tuberous Sclerosis Complex 2
TSG101	Tumor susceptibility protein 101
TUBES	tandem-repeated ubiquitin-binding entities
UBA	ubiquitin-associated proteins
UBAN	ubiquitin binding in ABIN and NEMO
UBAP1	ubiquitin associated protein 1
UBB	ubiquitin B
UBC	ubiquitin C
UBD	ubiquitin C
UBICREST	Ubiquitin Chain Restriction
UBM	ubiquitin-binding motif
UBP	ubiquitin-binding protein
UBPY	ubiquitin isopeptidase
UBZ	ubiquitin-binding zinc finger
UCH	Ubiquitin carboxyl-terminal hydrolase
UEV	ubiquitin E2 variant
UIM	ubiquitin interacting motif
ULM	ubiquitin-like modifiers

USP	ubiquitin-specific proteases
VAMP	Vesicle-associated membrane protein
VATP	vacuolar ATP-ase
VEGF	vascular endothelial growth factor
VEGFR	vascular endothelial growth factor receptor
VHS	Vps27/Hrs/STAM
VPS	Vacuolar protein sorting-associated protein
WASH	Wiskott–Aldrich syndrome protein and SCAR homolog complex
WB	western blot
WT	wild type
WWP1	WW domain containing E3 ubiquitin protein ligase 1
ZUP1	Zinc Finger Containing Ubiquitin Peptidase 1

Aknowledgements

I would like to express my profound gratitude to my supervisors Professors Sylvie Urbé and Michael Clague for giving me the opportunity to carry out my PhD in their lab. Thank you for all the support, the precious teachings, and the good times together as a team!
I would like to thank Dr. Alfred Vertegaal, Dr. Fredrick Trullsson, Dr. Gunnar Dittmar and Dr. Marta Mendes for the important collaboration.

The completion of this thesis work would have not been possible without the endless support from my family. I would like to thank my parents, Anna and Franco, my sisters Floriana and Antonella, and my brother-in-law Sam.
Thanks to all the people from MCSU lab and 5th floor who contributed to make the time in the lab enjoyable. In no particular order I would like to thank Emma Rusilovicz-Jones, Katy McCarron, Francesca Querques, Joana Gomes-Neto, Anne Clancy, Andreas Kallinos, Jane Jardine, Hannah Elcocks, Hannah Glover, Francesco Barone, Hannah Warren, Pei Yee Tey, Ioanna Georgiou, Liam Pollock, Georgia Guilbert, Svetlana Telnova, Fiona Hood, Ailbhe Brazel, Horacio Maldonado Lorca, Valeria Marotta, Martina Tripari, Sonia Fanelli, Jan Schulze, Eritelgi Bertsoulaki, Elena Marcassa. Thanks for the support, the collaborative environment, the exchange of ideas and the nights out!
A big thank you to my friends who were always there to cheer me up: Marica, Lella, Maky, Tina, Alfonso, Luca, Marghe, Cristiano, Laura.

Chapter 1: Introduction

1.1 Ubiquitin

The discovery of the “ubiquitously expressed” 76-amino-acid polypeptide ubiquitin in the 1970’s changed the history of molecular and cellular biology.

This protein is historically linked to protein degradation of a mutant haemoglobin in cell-free reticulocyte extracts (Etlinger & Goldberg, 1977). Etlinger and colleagues found that degradation of haemoglobin was ATP dependent, and they promptly isolated an ATP-dependent proteolysis factor 1 (APF-1) in one of the fractions of the cell-free extract. This factor was required to activate the ATP-dependent proteolysis in the remaining fractions of the lysate (Hershko et al., 1979; Etlinger & Goldberg, 1977).

In 1980, Wilkinson, Urban and Haas pointed out that APF-1 was identical in sequence to a protein discovered in the 1975 by Schlesinger et al. (Keith D. Wilkinson, 1980; Schlesinger & Goldstein, 1975). This protein was ubiquitin, and it had first been identified to play a role in lymphocyte differentiation and was later also found in the nucleus conjugated to the histone H2A through an iso-peptide bond (Goldstein et al., 1975) (Goldknopf & Busch, 1977).

1.2 Ubiquitylation

Ubiquitin is a reversible post-translational modification (Hershko & Ciechanover, 1998) (**Figure 1.1**).

It is through an isopeptide bond that ubiquitin is mostly conjugated onto substrate proteins. This process termed “ubiquitylation” or “ubiquitination”, occurs between the C-terminal carboxyl group of a ubiquitin moiety and most commonly the ε-amino group of a Lys (K) in the substrate. Ubiquitylation or ubiquitination results from a cascade of reactions mediated by the sequential action of E1 ubiquitin-activating, E2-conjugating and E3 ubiquitin-ligase enzymes (Pickart et al., 2001).

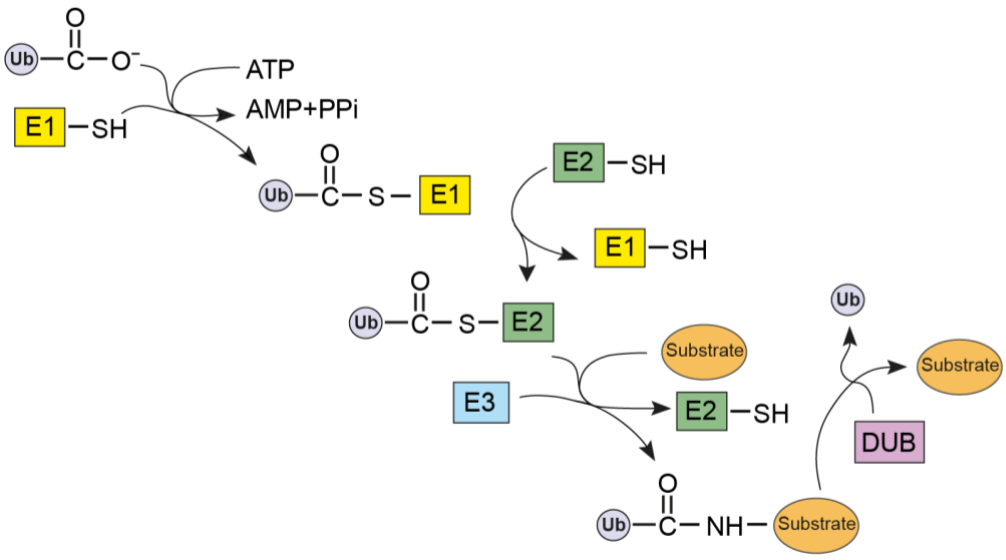

Figure 1.1 Ubiquitylation is a reversible modification.
Schematic of the ubiquitylation cascade of a substrate. E1, E2 and E3s carry out ubiquitylation, while deubiquitylases (DUBs) are the enzymes that remove ubiquitin (Heride et al., 2014). The C-terminus of ubiquitin is conjugated to the E1 enzyme via a thioester bond in an ATP-dependent manner. The ubiquitin is transferred to the E2 enzyme via a trans-thioesterification reaction. The ubiquitin-charged E2 is then able to transfer the ubiquitin to a lysine residue of a substrate protein with the help of an E3 ligase protein. The substrate is conjugated with ubiquitin via an isopeptide bond formed between the ubiquitin C-terminal Glycine of ubiquitin and the epsilon amino group of a Lysine side chain of the substrate. Deubiquitylases (DUBs) remove ubiquitin from substrates by hydrolysing the isopeptide bond.

There are two E1 enzymes in vertebrates, UBA1 and UBA6 with the former enzyme being the most abundant in HeLa cells, about 10x more abundant than UBA6 (Kulak et al., 2014). The E1 enzyme needs to firstly activate free ubiquitin in an activation step in which ATP is used to form an adenosine monophosphate-ubiquitin (Ub-AMP) intermediate with the E1 enzyme alongside the release of pyrophosphate (PPi). Then this Ub-AMP species is charged on the E1 via a thioester bond (Haas et al., 1982).

From the E1, the activated ubiquitin is transferred to an E2 enzyme which undertakes a nucleophilic attack with its active site Cys on the C-terminal carboxyl group of ubiquitin thereby forming a thioester bond. The final step of isopeptide bond formation is then performed by the E3s that recognise the ubiquitin-loaded E2 and the substrate in a specific manner (N. Zheng et al., 2017).

1.2.1 E2 enzymes

E2 enzymes can associate with many different E3 enzymes to transfer the activated ubiquitin and by doing this they determine ubiquitin chain topology and length which carry biological information (Clague et al., 2015; Komander and Rape, 2012).

There are approximately 40 E2s that operate the transfer of both ubiquitin and ubiquitin-like proteins (Ubl) and can be divided in three groups. E2s that transfer ubiquitin onto a target protein residue (monoubiquitylating or priming E2s); E2s that transfer ubiquitin onto another ubiquitin (chain-building E2s); and promiscuous E2s that can do either (Stewart et al., 2016). E2s are important to define specific chain linkage types when ubiquitin chains become extended by the action of E2s and E3s together (Pruneda et al., 2012; Dou et al., 2012; Plechanovov et al., 2012). UBE2N (Ubc13), for example, helps elongate K63-ubiquitin chains via its E2-like subunit which directs the correct positioning of the Lys63 of the acceptor ubiquitin towards the active site of the donor ubiquitin (Eddins et al., 2006). The mammalian Ubc13 specifically mediates the assembly of K63-ubiquitin chains, and its activity depends on the association with a Ubc variant (Uev) (R. M. Hofmann & Pickart, 1999; McKenna et al., 2001). Ubc13 can pair with either of two variants of the cofactor Ubc (Uev), Uev1A or Mms2 to coordinate K63-ubiquitin ubiquitylation in vitro. The Ubc13-Mms2 pairing plays a role in the DNA damage response, whereas Ubc13-Uev1A works in the activation of NF-kB pathway (Andersen et al., 2005).

1.2.2 E3 enzymes

E3 ligases are a vast family of ligases which can mediate the formation of a thioester bond between ubiquitin and a target substrate (Komander & Rape, 2012b; Scheffner et al., 1995). The activity of E2s and E3s together translates into different physiological outcomes, as E3 enzymes transfer ubiquitin onto regulated substrates and generate a diverse range

of ubiquitin topologies (Clague & Urbé, 2010; Dikic & Schulman, 2022; Scheffner et al., 1995).

The most abundant class of E3 ligases in humans are the RINGs (really interesting new gene) which are encoded by 200-300 genes (Freemont, 2000; Metzger et al., 2014; N. Zheng & Shabek, 2017). RINGs can be composed either of a single protein like c-Cbl (Casitas B-lineage lymphoma) or be divided in multipartite subunits like the BRCA1 (breast cancer 1) BRCA1-BARD1 (BRCA1-associated RING domain 1) heterodimer, cullin–RING ligases (CRLs), and the anaphase-promoting complex (APC) (Baer & Ludwig, 2002; Chang & Barford, 2014; Deshaies, 1999; N. Zheng & Shabek, 2017; Zimmerman et al., 2010).

RINGs are considered to be actual ligase enzymes connecting the E2 and the substrate. In fact, RINGs mediate transfer of ubiquitin from the E2-conjugating enzyme to the substrate via their RING/U-box catalytic site which involves binding to the E2-ubiquitin thioester to discharge ubiquitin from the E2 (N. Zheng & Shabek, 2017). An example of this mechanism was provided by the crystal structure of RNF4 and BIRC7 complex with the ubiquitin-E2 (UbchH5) where the C-terminal tail of the donor ubiquitin folds in a cleft in the E2 close to the E2's active site. The hydrophobic Ile44 patch of the donor ubiquitin contacts the E2 internal alpha helix (closed conformation of E2-Ub), and this interaction is stabilised by the RING binding to the donor ubiquitin (Buetow & Huang, 2016) . Another non-covalent interaction important for RING-mediated ubiquitylation is formed by the Arg residue in the RING domain that bridges ubiquitin and E2 (N. Zheng & Shabek, 2017). These interactions confer processivity to RING ligases when they extend a single-linkage ubiquitin chain (Pruneda et al., 2012; Dou et al., 2012; Plechanovov et al., 2012).

The family of HECT (homologous to the E6AP carboxyl terminus) E3 ligases were first identified in a study by the group of Jon Huibregtse where they showed that E6-AP can form a thioester bond with ubiquitin by its C-terminal region and ubiquitylate p53 as a substrate. This C-

terminal region was named HECT domain (Scheffner et al., 1995). The HECT family includes ~30 members in humans and is subdivided in 3 main groups, based on structural divergencies of the N-terminal domain: Nedd4, HERC and the other HECTs (Rotin & Kumar, 2009).

HECT E3s possess a C-terminal bilobate catalytic domain composed of a C-lobe that forms a thiol-ester intermediate with the ubiquitin C-terminus, and an N-lobe that contacts the E2 (Rotin & Kumar, 2009). The two lobes become juxtaposed thanks to the flexibility of the hinge and this conformational change is required to transfer ubiquitin onto substrates by trans-thiolation (L. Huang et al., 1999; Ogunjimi et al., 2005; Pickart, 2001; Verdecia et al., 2003). Nedd4 members of the HECT E3 ligase family are characterised by a common C2 domain at the N-terminus, followed by 2-4 WW domains. The C2 region can bind lipids at the plasma membrane, endosomes, multi-vesicular bodies (MVBs), annexin A13b, Grb (Grb7-Grb10-Grb14 family) adaptor proteins, while the WW domains recognise phosphorylated Tyr (Dunn et al., 2004; Plant et al., 2000; Kanelis et al., 2001; Staub et al., 1996). Finally, HERCs are a sub-family of HECT enzymes that are characterised by a HECT catalytic domain which relies on a conserved catalytic Cys, and also contain regulator of chromosome condensation 1 (RCC1)-like domains (RLDs) at their N-terminus (Garcia-Gonzalo et al., 2005). HERCs are further subdivided into large HERCs (>500kDa) with multiple RLDs, and small HERCs (>100kDa) with single RLDs. The RLDs are thought to bind chromatin and are known to have a guanine nucleotide-exchange factor (GEF) property towards Ran GTPase (Renault et al., 2001; Rotin & Kumar, 2009).

More recently, a third family of ubiquitin ligases, the RING-between-RING (RBR) has been described as a new class of RING-HECT hybrid enzymes. RBRs were discovered by investigating the RING-binding capability of UBCH7, an E2 previously shown to activate HECT E3 ligase activity (Brzovic et al., 2003; A. Huang et al., 2009). Ubch7 was demonstrated to have a Cys-dependent activity towards RBR E3 ligases.

These enzymes are named after the central in-between-RING (IBR) zinc-binding domain that separates the two ring finger domains RING1 and RING2 (Wenzel et al., 2011). The RBR family includes 14 members including parkin, HOIP (HOIL-1-interacting protein) and HOIL-1 (heme-oxidized IRP2 ubiquitin ligase 1). RBRs use the Cys in the c-terminal catalytic site to directly ubiquitylate substrates and have unique structures like the C-terminal Rcat (required-for- catalysis) domain and the non-catalytic central BRcat (benign-catalytic) domain lacking a Cys residue (Spratt et al., 2014).

1.3 Ubiquitin chain structure

Ubiquitin is a 76 amino acid long polypeptide that is encoded by UBB, UBC, UBA52 and RPS27A genes in the human genome. UBA52 provides a single copy fused to the N-terminus of the ribosomal protein subunit L40, while RPS27A encodes a ubiquitin fused to the S27a subunit (Baker & Board, 1991). The UBB and UBC genes, encode linear polyubiquitin stretches of 3 and 9 units, respectively. To produce active ubiquitin molecules, these fusion proteins are cleaved by the enzymes that remove ubiquitin, Deubiquitylases (DUBs) (Özkaynak et al., 1984; Wiborg et al., 1985).

With the exception of 3 conservative changes, ubiquitin has a highly conserved sequence from yeast to human. The structure of ubiquitin itself can be described as a β-grasp fold with a flexible six-residue C-terminal tail (Komander and Rape, 2012). Additionally, the sequence contains distinct hydrophobic patches important for ubiquitin-recognition purposes: I44, I36 and F4 surfaces can be recognised by E3 ligases, Deubiquitylases enzymes (DUBs) and ubiquitin-binding proteins (UBP)/ubiquitin-binding domains (UBDs) (Dikic et al., 2009).

Ubiquitin can also form chains; this is because one ubiquitin can be covalently linked via its carboxy-terminal (C-terminal) Gly to the epsilon amino group of either of 7 internal Lys or to the N-terminal Met of another ubiquitin moiety (Ciechanover & Ben-Saadon, 2004). In fact, eight types of different linkages exist that are named after the Lys (K) or Met (M) to

which ubiquitin is conjugated onto the substrate: M1, K6, K11, K27, K29, K33, K48, K63 (Heride et al., 2014). The rotational immobility of the iso-peptide linked ubiquitin moieties generates distinct topologies that can be bound by ubiquitin binding proteins (UBPs) (Komander & Rape, 2012a).

Different types of ubiquitylated products can be found. Mono- or multi-mono- ubiquitylation of a substrate is the attachment of a single ubiquitin to one or multiple sites (Heride et al., 2014). A homotypic chain is a ubiquitin polymer wherein the C-terminus of the distal ubiquitin is linked to the proximal ubiquitin by the same Lys along the chain. Conversely, when the distal ubiquitin in a chain is attached to the proximal one by a different Lys, this generates a mixed ubiquitin chain; lastly, a ubiquitin polymer can include different Lys linkages thereby generating branched chains (Komander & Rape, 2012a) (Figure 1.2).

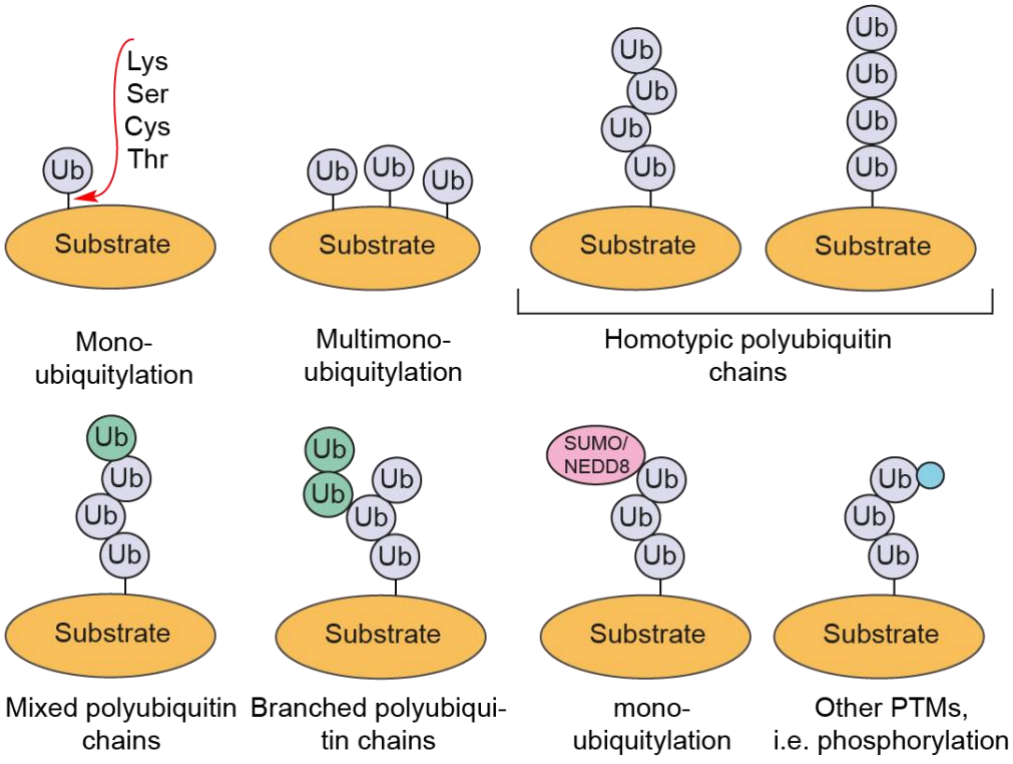

Figure 1.2 Schematic of ubiquitin chain structure.

The diagram shows that Lys, Ser, Cys and Thr are all the different amino acid residues within a substrate that can be used to attach ubiquitin. A substrate can be modified with mono-ubiquitin, multimono-ubiquitin or with ubiquitin polymers (chains) subdivided in homotypic, mixed, branched. Lastly, different PTMs such as SUMO, NEDD8 or phosphates

can be conjugated to ubiquitin chains. Adapted from (Dikic & Schulman, 2022).

The Lys linkages in a ubiquitin chain can generate different topologies or structures that are dictated by different levels of “conformational freedom” around the isopeptide bond. For example, in K48-linked ubiquitin chains, ubiquitin moieties show a more compact structure and interact with each other through Ile44/Ile36 patches. This earns K48-linked ubiquitin chains the denomination of “closed conformation” that is also assumed by K6 and K11 chains (Cook et al., 1992; Eddins et al., 2007; Tenno et al., 2004; Varadan et al., 2002). On the other hand, the K63-linked and the so called “linear” M1-linked ubiquitin chains adopt an “open conformation”. This is because here the ubiquitin moieties are arranged like beads on a string and have more freedom to be contacted by ubiquitin binding proteins proteins (Tenno et al., 2004, Varadan et al., 2004; Datta et al., 2009; Komander, Reyes-Turcu, et al., 2009; Weeks et al., 2009) (**Figure 1.3**). Lastly, unanchored ubiquitin chains come from: a) the synthesis of ubiquitin from UBB and UBC genes, b) internal or en-bloc removal of ubiquitin chains from substrates, c) synthesis by ubiquitin ligases of free chains used in signal transduction which play active roles in immunity (Clague et al., 2019; Pickart, 2001; Xia et al., 2009; Zeng et al., 2010).

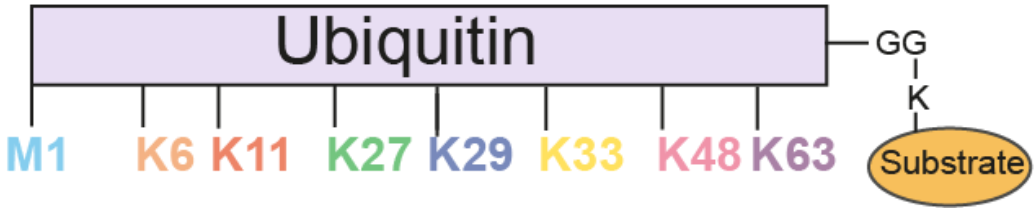

Figure 1.3 Ubiquitin linkages generate different polyubiquitin chains. The diagram depicts the eight amino acids that can be used to form an iso-peptide linkage to attach a proximal ubiquitin onto a distal ubiquitin in a poly-ubiquitin chain. Adapted from (Heride et al., 2014).

Ubiquitin itself can also be modified by other post-translational modifications such as acetylation (on Lys residues) (Ohtake et al., 2015) or phosphorylation (on its Tyr, Ser and Thr residues)(Hornbeck et al., 2015a; Swaney et al., 2013). In addition, ubiquitin can be found in mixed polymers or

heterotypic chains, which consist of ubiquitin conjugated with other ubiquitin-like (UbLs) molecules like SUMO, NEDD8 or ISG15. Lastly, unconventional modifications of ubiquitylation can be found, in bacteria wherein Ser ADP-ribosylation of ubiquitin of host proteins during pneumophila infection (Clague et al., 2019; Bhogaraju et al., 2016).

1.3.1 Ubiquitin chain functions

The ability of the ubiquitin chains to create different topologies is exploited by a plethora of ubiquitin binding domains (UBDs) that recognise them (reviewed hereafter in section 1.4). Binding of ubiquitin binding proteins (UBPs) like for example on endosomes translates into degradation of ubiquitylated cargo receptors. ESCRT-0 proteins HRS and STAM, for example, both bear multiple ubiquitin binding domains by which they recruit and concentrate ubiquitylated EGFR molecules to the endosomal membrane prior to endolysosomal degradation (Mizuno et al., 2003; Ren & Hurley, 2010). The physiological outcome of such interactions also depends on the sub-cellular localisation and timing of enzymes' activities (Husnjak & Dikic, 2012). Extensive research in the field of ubiquitin was conducted to associate specific functions to recognition of the different ubiquitin chain topologies (Akutsu et al., 2016).

1.4 Ubiquitin binding domains

The different ubiquitin chain topologies, that make up the ubiquitin code, can be recognised (or "read") by proteins that bear ubiquitin binding domains (UBDs) and can change the fate of a ubiquitylated substrate (Komander & Rape, 2012a).

A plethora of approximately 20 families of UBDs that are all structurally different can bind to ubiquitin topologies in a non-covalent fashion (Dikic et al., 2009). The main sub-families of UBDs can be grouped based on some common structural features. Single or multiple α-helices containing domains include ubiquitin associated (UBA) domain, ubiquitin interacting motif (UIM), double sided ubiquitin interacting motif (DUIM), motif

interacting with ubiquitin (MIU), coupling of ubiquitin conjugation to endoplasmic reticulum degradation (CUE), GGA and Tom1 (GAT), Vps27/Hrs/STAM (VHS), ubiquitin binding in ABIN and NEMO (UBAN) protein (Husnjak & Dikic, 2012). In addition, there are zinc finger containing UBDs which are quite variable and are suggested to bind long ubiquitin chains. The Znf-containing UBDs include the nuclear protein localization 4 zinc finger (NZF), zinc-finger ubiquitin-binding protein (ZnF UBP), zinc finger in A20 protein (ZnF A20) and ubiquitin-binding zinc finger (UBZ) (Husnjak & Dikic, 2012). Pleckstrin-homology domain (PHD) containing UBDs were found to be involved in the binding of ubiquitin by the N-terminus of the proteasomal ubiquitin receptor Rpn13 (Schreiner et al., 2008). PHDs include gram like ubiquitin-binding in Eap45 (GLUE) and pleckstrin-like receptor for ubiquitin (PRU) (Husnjak & Dikic, 2012). Another sub-group of UBDs is distinguished as ubiquitin-conjugating-like ubiquitin E2 variant (UEV) and UBC, while other unrelated structures exist such as Src homology 3 domain, ubiquitin-binding motif (UBM), PLAA family ubiquitin binding domain (PFU), Jab1/MPN (Husnjak & Dikic, 2012).

The binding affinity of a single UBD to ubiquitin is very modest (K_d = 10^{-5} to 10^{-3}M), whilst that of tandem repeat UBDs can reach affinities in the order of nM (Choi et al., 2019). UBPs that hold multiple or multipartite UBDs are efficient modulators of downstream signals (Dikic et al., 2009).

Specificity of different UBDs towards ubiquitin chains, can be exemplified by the K63-specific binding of the tandem UIMs of RAP80. RAP80 recognises K63-linked polyubiquitin on the histones H2A and H2AX to recruit the Abraxas-BRCC36 (BRCA1/BRCA2-containing complex subunit 36) to BRCA1-associated RING domain protein 1 (BARD1) and to damaged DNA (J. Yan & Jetten, 2008).

Importantly, the structural information about the UBA domains, led to the development of tandem-repeated ubiquitin-binding entities (TUBEs). TUBES are used as a gold standard tool to enrich ubiquitylated proteins in cell extracts. TUBES that either bind both the total of ubiquitylated proteins or specific Lys-linked ubiquitin polypeptides are available and can be used for biased and unbiased approaches like ubiquitin-specific

proteomics or “ubiquitylome studies” (Hjerpe et al., 2009). In addition to TUBEs, ubiquitin sensors based on the structure of different types of ubiquitin linkage specific UBDs have been independently generated and produced. An example of a ubiquitin sensor is the tandem repeated 3x (UIM) of the RAP80 which can be employed to enrich protein lysates for K63-linked poly-ubiquitin (Thorslund et al., 2015).

1.5 DUBs (Deubiquitylases)

1.5.1 Overview of DUB families

Compared to E3s, the inventory of DUBs is much smaller, comprising around 100 DUBs in humans. These enzymes cleave the isopeptide bond linking one ubiquitin moiety to another or to a substrate.

The main outcomes of deubiquitylation are changing protein turnover and regulating protein-protein interaction and activity (Clague et al., 2019).

Seven families of DUBs have been identified in humans and can be classified based on their catalytic site. Six DUB families are Cys proteases: USP/ ubiquitin-specific proteases family (56 members in humans and 2 pseudo-DUBs), OTUs/ovarian tumour proteases (17 members and 2 pseudo-DUBs), UCHs/ubiquitin C-terminal hydrolases (4 members), MJDs/ Josephins (4 members) MINDYs/motif interacting with ubiquitin (MIU)- containing novel DUB family (4 members), and the last discovered ZUP1 family (Clague et al., 2019). In distinction to all other DUBs, the family of JAMM/MPN^{+} (JAB1/MPN/MOV34) enzymes are Zn+ metalloproteases. The JAMM family is composed of 16 DUBs, five of which are pseudo-DUBs (Walden et al., 2018). DUB families are collected in **Table 1.**

Table 1 Deubiquitylases families.
DUBs can be subdivided into seven families, six of which are characterised by cysteine catalytic site (Cys proteases), while JAMMs are metalloproteases that are characterised by a catalytic site which requires a metal ion for their activity. Different cell colours highlight cysteine proteases (light blue) and metalloproteases (light pink). Shown is the total number of family members including the inactive ones that are indicated in brackets. Adapted from Clague and Urbé, 2019.

DUB family	Name abbreviation	Key property	Number	Example

			(inact.)	
Ubiquitin specific proteases	USPs	Cysteine proteases	69 (5)	USP1
Ovarian tumour proteases	OTUs	Cysteine proteases	17 (2)	A20
Josephins	MJD	Cysteine proteases	4	ATXN3
Ubiquitin C-terminal hydrolases	UCHs	Cysteine proteases	4	BAP1
Motif Interacting with Ubiquitin (MIU)- containing novel DUB family	MINDYs	Cysteine proteases	5 (1)	MINDY1
Zinc Finger Containing Ubiquitin Peptidase 1	ZUP1s	Cysteine proteases	1	ZUP1
JAB1/MPN/MOV34	JAMMs	Metalloproteases	13 (5)	AMSH

Cys proteases like the USPs, use a Cys residue in the catalytic site to cleave the scissile bond. They contain a catalytic triad that is analogous to the enzyme papain (Cstorer & Ménard, 1994): an adjacent His lowers the pKa of the catalytic Cys, in this way this Cys is more likely to undergo a nucleophilic attack, while a third residue, an Asp or Asn polarises and aligns the His (Clague et al., 2013).

JAMM metalloproteases distinguish themselves by an active site composed of two His, an Asp and a Ser. A Zinc atom is coordinated by the conserved His, Asp and a water molecule. Also, a Glu is needed to de-protonate water so that the resulting hydroxyl anion can perform a nucleophilic attack onto the carbonyl group of the substrate (C=O of Gly). This reaction produces a transient tetrahedral structure which is destroyed by hydrolysis of water (Clague et al., 2013).

Most of the DUBs are ubiquitin-specific, meaning they exclusively cleave the ubiquitin-chain linkage rather than other types of ubiquitin-like modifiers (i.e. NEDD8). This specificity exists because they bind to the C-terminus of ubiquitin and specifically interact with the Ile 36 and Ile 44

patches, differently from the requirements to recognise ubiquitin-like modifiers (ULMs) (Abdul Rehman et al., 2016; Komander, Clague, et al., 2009; Komander & Rape, 2012a). Exceptions include the JAMM protein CSN5, which can cleave Nedd8 from CRLs (cullin-RING E3 ligases) and USP18 which specifically acts on the ISG15 ubiquitin-like modifier (Cope et al., 2002; Basters et al., 2017; Malakhov et al., 2002). Another example of a Cys protease active on ubiquitin-like modifiers is USPL1 which specifically removes SUMO from substrates, but not ubiquitin (Schulz et al., 2012).

Having taken these features into account, it is not surprising that some DUBs can also specifically cleave certain ubiquitin-ubiquitin linkages. Examples for such specificity can be found in the JAMMs, OTUs, Josephins and MINDY families. On the other hand, DUBs like UCHs and most USPs are not linkage-specific, but rather substrate-specific DUBs. In fact, the latter can cleave several different iso-peptide bonds in the ubiquitin-ubiquitin conjugate as well as the proximal ubiquitin that is the ubiquitin directly attached to the substrate (Clague et al., 2019; Mevissen & Komander, 2017).

Notably, in contrast to the broad selectivity seen for the majority of the USPs, many members of the JAMM family enzymes show a very high degree of specificity towards K63-ubiquitin chains, for example AMSH (McCullough et al., 2004, 2006), AMSH- LP (Sato et al., 2008) and BRCC36 (Cooper et al., 2009). Linkage-specific DUBs are collated in **Table 2**.

Table 2 Linkage specific DUBs.
The table shows the DUBs that cleave linkage-specific ubiquitin chains across different families. Adapted from (Clague et al., 2019).

DUB	Linkage specificity	Reference
AMSH, AMSH-LP, BRCC36, OTUD1, ZUP1, CYLD, phospho-OTUD4	Lys63	(Cooper et al., 2010; Haahr et al., 2018; Hermanns et al., 2018; Hewings et al., 2018; Komander, Reyes-Turcu, et al., 2009; Kwasna et al., 2018; McCullough et al., 2006; Mevissen et al., 2013; Sato et al., 2015; Zhao et al., 2018).
OTUB1, OTUD4, A20, MINDY	Lys48	(Abdul Rehman et al., 2016; Mevissen et al., 2013).
TRABID	Lys29 and Lys33	(Virdee et al., 2010).
Cezanne	Lys11	(Bremm et al., 2010; Mevissen et al., 2016).

OTULIN and CYLD	Linear	(Keusekotten et al., 2013; Komander, Reyes-Turcu, et al., 2009; Rivkin et al., 2013; Sato et al., 2015).
PSMD14 and USP14	En bloc	(Yao & Cohen, 2002)
USP30	Lys6	(Cunningham et al., 2015; Gersch et al., 2017; Sato et al., 2017).

An important approach for the study of ubiquitylation makes use of DUBs and is referred to as Ubiquitin Chain Restriction (UbiCRest). This allows one to determine the ubiquitin chain architecture of a specific substrate. This approach consists of incubating a purified substrate with a panel of linkage-specific DUBs and analysing the result of the ubiquitin chain digestion by western blot (Hospenthal et al., 2015).

1.5.2 Focus on JAMM metalloproteases.

The JAMM/MPN+ family is an interesting one. Firstly, because the JAMM domain is found in all three domains of life (Maytal-Kivity et al., 2002). JAMMs took their name from the larger MPN (Mpr1-Pad1-N-terminal) family, as they are distinguishable by the 'H-x-H-P-x[6]-S-x[2]-D' amino acidic sequence within the catalytic domain that supports the zinc-atom needed for catalysis (Maytal-Kivity et al., 2002).

Several JAMMs show selectivity for specific ubiquitin chains or ubiquitin-like proteins. AMSH, AMSH-LP and BRCC36 are highly linkage-specific DUBs and preferentially cleave the non-canonical K63-linked ubiquitin polymers (Sato et al., 2008). MYSM1 and PSMD14 can instead cleave ubiquitin chains en bloc whereas CSN5 cleaves Nedd8 from the Cullin component of the Cullin RING ligases (Cope et al., 2002; Yao & Cohen, 2002; Zhu et al., 2007). Another feature many JAMMs have in common is that they form part of macromolecular assemblies that play essential roles such as the proteasome components PSMD14/PSMD7 and the CSN5/CSN6 components of the COP9 signalosome (discussed in **section 1.5.3) (**Maytal-Kivity et al., 2002; Cope et al., 2002; Cope & Deshaies, 2003). BRCC36 is involved in DNA repair either together with BRISC or BRCA1-RAP80 (Cooper et al., 2009; Shao et al., 2009). MYSM1 is a histone H2A associated DUB that functions in complex with the p/CAF acetyltransferase (Zhu et al., 2007).

1.5.3 AMSH and AMSH-LP are K63-specific JAMMs.

AMSH was the first JAMM-containing protein to be linked with isopeptidase activity (Mevissen & Komander, 2017; McCullough et al., 2004). Importantly, it was demonstrated to preferentially cleave K63-linked ubiquitin chains but is incapable of removing the proximal ubiquitin from substrates (en bloc) (McCullough et al., 2006; McCullough et al., 2004; Bremm et al., 2010; Komander, Reyes-Turcu, et al., 2009).

AMSH-LP (AMSH-like protein) was identified by Kikuchi and colleagues as a protein very similar in sequence and structure to AMSH (Kikuchi et al., 2003). Like AMSH, AMSH-LP is also specific for K63-ubiquitin and the structure of the human in complex with K63-linked di-ubiquitin has been resolved by crystallography (Sato et al., 2008).

The S1 site of a DUB is the main site of ubiquitin recognition and dictates the formation of enzyme-substrate complex. In members of the USP family, this site does not determine substrate specificity. USPs rely on accessory motifs for substrate specificity and use at least one S1 site (ubiquitin-binding site) to guide the catalytic site to the ubiquitin c-terminus and the scissile bond. When cleaving di-ubiquitin, the S1 is occupied by the distal ubiquitin, whereas the S1' is contacted by the proximal ubiquitin (Mevissen & Komander, 2017).

The mode of K63-ubiquitin recognition by a JAMM protein can be exemplified by AMSH-LP. This isopeptidase contains a canonical JAMM domain with 2 His and one Glu and one Asp. The distal ubiquitin binds to the Ins-1 part, a conserved insertion in AMSH made of a pair of anti-parallel β-sheets and the JAMM core of AMSH-LP, while the proximal ubiquitin binds to the Ins-2 and JAMM. What confers the K63-specificity is a surface created by the Zn^{+}- coordinating loop of Ins-2 region and a loop in the JAMM core. The JAMM core and the proximal ubiquitin establish hydrogen bonds which are required for efficient cleavage. Moreover, the Ins1 region and the JAMM core of AMSH-LP establish two important hydrophobic interactions with the distal ubiquitin that are fundamental for

the binding affinity of the enzyme to K63-linked di-ubiquitin (Clague et al., 2013; Davies et al., 2013; Sato et al., 2008; Shrestha et al., 2014) (**Figure 1.4**).

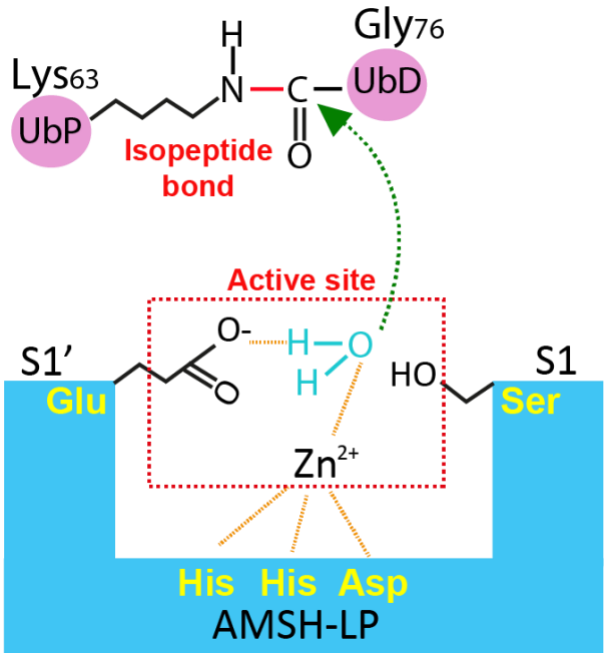

Figure 1.4 Catalytic mechanism of AMSH-LP.
The diagram shows the catalytic site of AMSH-LP, which is the best example of JAMM catalytic mechanism and was characterised by crystallography (Sato et al., 2008). S1 and S1' sites coordinate binding to the Distal (UbD) and Proximal ubiquitin (UbP). The Zinc atom in the active site is coordinated by a water molecule, the conserved catalytic triad (His, His, Asp) and the S1' Glu residue of AMSH-LP. The water molecule becomes activated by the Glu residue and performs a nucleophilic attack onto the carbon atom in the isopeptide bond. Adapted by Clague et al., 2013.

1.5.4 JAMMs in macro-molecular complexes

The proteasome is a barrel-shaped multi-protein machinery for the destruction of un-needed or aberrant proteins (Beck et al., 2012). The JAMM isopeptidase POH1/Rpn11/PSMD14 is part of the lid of the proteasome. This structure is associated with Adrm1/Rpn13 and is localised on top of the AAA-ATPase N-ring. The metalloprotease POH1/PSMD14 plays a fundamental role in the 19S regulating particle of the 26S proteasome: by removing ubiquitin chains from the substrates en

bloc from the proximal to the last ubiquitin, this DUB allows unfolding of the proteasomal substrate by the AAA-ATPase (Verma et al., 2002; Yao & Cohen, 2002) . It has also been shown that POH1 (Rpn11) tightly binds an inactive JAMM protein, PSMD7 (Rpn8) that facilitates its positioning at the top of the 20S core of the proteasome to allow recycling of ubiquitin from polypeptides as they enter the 20S barrel for degradation (Worden et al., 2014).

BRCC36 is another JAMM deubiquitylase that takes part in a multi-protein complex. It works as a component of the BRCA1-A machinery in the nucleus that is involved in genome maintenance. The complex is composed of BRCA1, MERIT40, BRCC45, BRCC36, RAP80 and ABRAXAS1 (an inactive JAMM-like protein). RAP80 recruits the complex to K63-polyubiquitin chains created by RNF8 at the histone H2AX and on the L3MBTL2 protein (Cooper et al., 2009; Feng et al., 2010; Shao et al., 2009). The role of BRCC36 is to remove these ubiquitin chains and in doing so initiates the NHEJ (non-homologous end-joining) pathway of the DNA damage response (DDR) at double-strand brakes. Interestingly, BRCC36 can also form another complex, the cytosolic BRISC complex together with BRCC45, MERIT40, ABRAXAS2 and SHMT2 adaptor protein that limits interferon 1 receptor-chain 1 (IFNAR1) lysosomal-mediated degradation (Rabl et al., 2019; H. Zheng et al., 2013a).

Among the JAMM enzymes, another pairing of an active with an inactive member of the family, are the COPS5 and COPS6 subunits of the COP9 signalosomes, that remove Nedd8 from the Cullin subunit of the CRLs thereby inactivating the ligase (Cavadini et al., 2016).

1.6 Endocytic trafficking

The plasma membrane operates the ingress (endocytosis) or egress (recycling and secretion) of macromolecules to and from of the cell and enables quick responses to changes in the extracellular environment (Norris & Grant, 2020). Endocytosis is the process by which extracellular material is taken up by the external leaflet of the plasma membrane to generate intra-cellular membranes filled with cargo molecules (Doherty &

McMahon, 2009; Huotari & Helenius, 2011) Macro-pinocytosis and phagocytosis are classified as macro-endocytic mechanisms, as they are required to ingest large material like pathogens (Kumari et al., 2010).

On the other hand, micro-endocytic sorting involves the ingestion of particles which are smaller than 200nm and can be distinguished as clathrin coated vesicles (CCVs) (El-Sayed & Harashima, 2013). Clathrin mediated endocytosis (CME) is distinguished from clathrin independent endocytosis (CIE) by the presence of Clathrin, a peculiar protein having typical triskelial structure that coats CCVs (Kanaseki & Kadota, 1969; Pearse, 1975). Upon bending of the membrane to endocytose cargo receptors, Clathrin forms basket-like structures around CCVs and recruits a large variety of adaptors and accessory proteins that are proposed to be cargo-specific (E. M. Schmid & McMahon, 2007).

Once endocytosed and sorted into endosomes, cargo material can be either recycled to the plasma membrane or degraded in lysosomes (Cullen & Steinberg, 2018).

1.6.1 Early and late endosomes

Early endosomes are dynamic tubulovesicular compartments and the main sorting station in cells that are generated from the fusion of endocytic vesicles derived from the plasma membrane and receive cargo from the Golgi apparatus. The early endosome is a sorting station for many endocytosed cell surface receptors. From here they can be either recycled to the plasma membrane or be sent for degradation in the lysosome (Gruenberg & Maxfield, 1995). Endosomes base their identity on protein-lipid composition, and as a consequence, proteins that modify these lipids change the characteristics and function of an endosome (Huotari & Helenius, 2011). The advent of immune-labelling coupled to electron microscopy allowed to finely measure the size of endosomal sub-domains and to visualise them at high resolution: endosomes are made of a central vacuole (100-500 nm in diameter), tubular membrane extensions (20-50nm in diameter) and intraluminal vesicles (ILVs) (40-60 nm in diameter) (Klumperman & Raposo, 2014).

Intralumenal vesicles are formed by inward budding of the early endosome limiting membrane. It is the presence of multiple ILVs (>3) in an endosome that structurally discriminates a late endosome from an early endosome (Dupré et al., 2001; Hicke, 2001). Consequent to accumulation of ILVs into the late endosome lumen and progressive acidification from pH = 5.5 to pH = 4, late endosomes fuse with lysosomes to deliver proteins which need to be degraded (Futter et al., 1996). An overview diagram of the endo-lysosomal network is displayed in **Figure 1.5**.

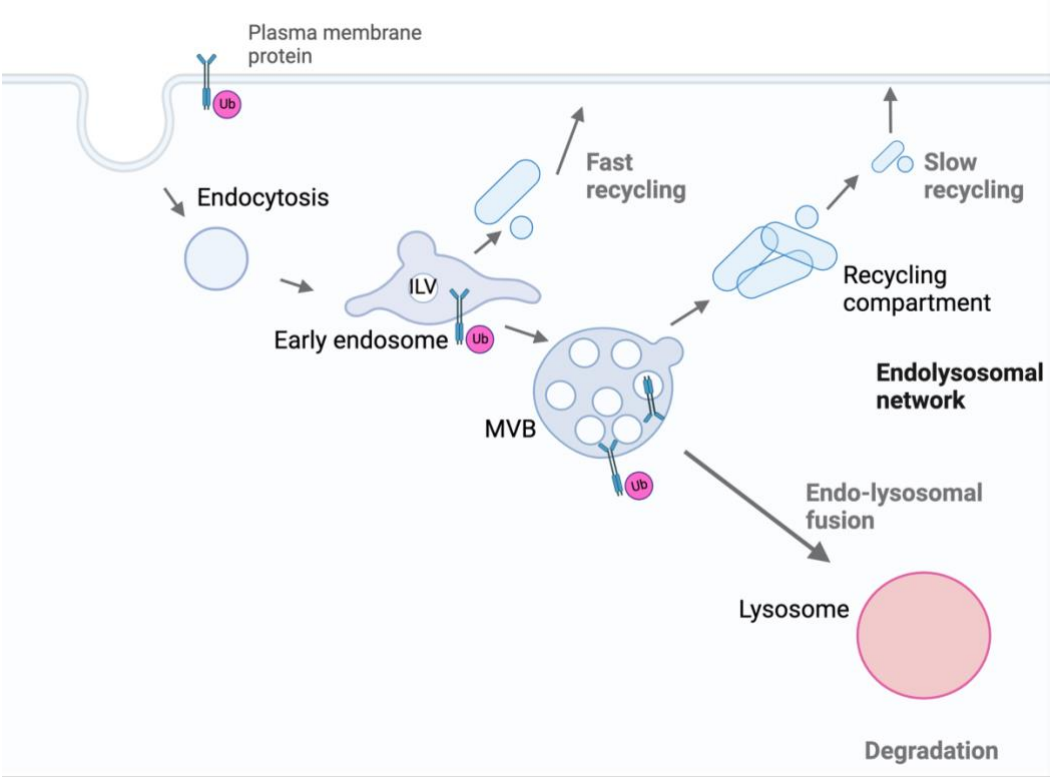

Figure 1.5 Overview of endocytosis.
The diagram shows the secretory pathway and the endolysosomal network. Endocytosis of plasma membrane proteins involves their sorting into early endosomes which mature to late endosomes as they accumulate intraluminal vesicles (ILVs). Late endosomes fuse with the lysosome to degrade the endocytosed cargos. Adapted from Cullen and Steinberg, 2018.

Intralumenal organellar acidity plays an important role in determining dissociation of ligand from carrier receptors that need to be recycled to the plasma membrane prior to ligand degradation in lysosomes. Indeed, the affinity of ligands for their receptors decreases at pH <5.5 pH and this

switch in acidity allows fine tuning of metabolism. Examples of this pH-guided dissociation process were shown for the cholesterol bound low-density lipoprotein receptor (LDL) and iron loaded transferrin receptor (TfR) (Antonescu et al., 2014; Dautry Varsat et al., 1983; Seidah et al., 2012).

1.6.2 Markers of endosomal maturation

Early endosomes can undergo maturation into a late endosome or multivesicular body (MVB). An early endosome can be distinguished mostly by the presence of the small GTPase Rab5, while a key step for endosome maturation is the replacement of this GTPase with Rab7 (Poteryaev et al., 2010; Sönnichsen et al., 2000). Rab GTPases can arrange in endosomal microdomains and by doing so, they assign different functions to the micro-domain they localise to. Rink and colleagues uncovered the very dynamic association of Rab5 on endosomal membranes (Rink et al., 2005). Rab5 also mediates upon homotypic fusion (endosomes of the same type), then Rab5 is rapidly replaced with Rab7 (late endosome Rab GTP-ase). While new Rab5-positive endosomes are continuously generated at the periphery of the cell, those that fuse together move towards the cell centre where they finally undergo Rab conversion. Rab5 is recycled and forms new early endosomes with material coming from the plasma membrane. Homotypic fusion thus generates late endosomes that contain degradative material. Also, they are bigger and less abundant than early endosomes. The transition from Rab5 to Rab7 was found to be regulated by the VPS/HOPS complex that has GEF activating activity towards Rab5 (Rink et al., 2005).

While the endosome maturation process occurs, endosomes are loaded with cargo. Cargoes can still be recycled back to the plasma membrane or brought to the Golgi from the sorting endosome. Alternatively, cargo can be sorted to the late endosome for final degradation in the lysosome (Norris & Grant, 2020).

1.6.3 Recycling pathways

The alternative fate that endosomal cargo can follow is to be either recycled to the plasma membrane, or to be transported back to the Golgi apparatus (Cullen & Steinberg, 2018). Recycling occurs by enriching cargo at the cytosol-facing tubular structures of endosomes to prevent cargo from entering the internal vesicles (Klumperman & Raposo, 2014; Maxfield & McGraw, 2004).

There are specialised endosomal microdomains which are typically decorated with distinct members of the Rab family of small GTP-ase proteins which allow fast and slow recycling mechanisms regulated by the GTP-ase Rab4 and Rab 11 positive microdomains, respectively (S. L. Schmid et al., 1988; Van Der Sluijs et al., 1991).

Retromer is an endosomal coating complex for recycling of cargo through the formation of tubules and vesicles to recycle endosomal material either to the Golgi or to the plasma membrane. These complexes form solenoids and help build tubular structures by forming oligomers around the endosomal membrane (Kovtun et al., 2018; Leneva et al., 2021).

Studies in yeast showed that retromer is made up of SNX-BAR (sorting nexins) complexes with a core cargo-recognition heterotrimer composed of Vps35, Vps29, and Vps26 (Seaman et al., 1998). The second retromer sub-complex is made of a dimer of the SNX family members Vps5p and Vps17p that are the cargo-selective components of retromer (Horazdovsky et al., 1997; Nothwehr & Hindes, 1997).

In mammals, the heterotrimer consists of VPS35, VPS29 and one of two paralogues of VPS26, A or B. Snx1 and Snx2 can both associate with either of Snx5 and Snx6 containing BAR domains that can apply curvature to large membrane portions to bud tubules. In addition, it is thought that SNX polymers confer the ability to bud tubules.

Differently from yeast, the mammalian retromer can interact with the WASH (Wiskott-Aldrich syndrome protein and scar homologue) complex, an actin nucleation complex important for Retromer-dependent recycling that nucleates the assembly of F-actin (filamentous actin). The WASH complex is made of FAM21 A/B/C (WASHC2A/B/C), CCDC53

(WASHC3), SWIP (strumpellin and WASH interacting protein; WASHC4) and strumpellin (WASHC5) (Harbour et al., 2012).

Ultimately, actin is polymerised at tubules which are positive for Actin-related protein 2/3 (Arp2/3) and Vps35 and act as a docking point for downstream sorting complexes (McNally & Cullen, 2018).

1.6.4 Lysosomes

Late endosomes are vacuolar compartments of 250-1000 nm in diameter which ultimately fuse with lysosomes to degrade cargo (Cullen & Steinberg, 2018).

The lysosome is a tightly regulated degradative compartment that was discovered by De Duve and colleagues in the 60's (de Duve & Wattiaux, 1966). It is characterised by a single membrane and preserves high acidity in its lumen (pH<4) thanks to the vacuolar ATP-ase proton pump (VATP-ase) which is essential for the activation of the lysosomal hydrolases. The acidic hydrolases in the lysosomal lumen dispose of proteins, nucleic acids, carbohydrates, and lipids. Lysosomes can undergo fusion with a number of other membrane enclosed organelles such as phagophores as a way of digesting un-necessary or non-functional material. The importance of lysosomes for health, is highlighted by the fact that lysosome malfunctioning is associated with very severe genetic and life impairing neuronal disorders (Ballabio & Bonifacino, 2019).

The degradative fate of cargo is determined by binding of the endosome phospholipid phosphatidylinositol 3-monophosphate (PtdIns (3)P), by the ESCRT-0 component HRS via its FYVE domain. Both the ubiquitin and PI(3)P binding properties of HRS determine its endosomal localisation. HRS determines the recruitment of the downstream (endosomal sorting complexes required for transport) ESCRT complex ESCRT-I component TSG-101 via its Pro-rich tetrapeptide region (PSAP, Bache et al., 2003) . ESCRTs are a series of complexes for ILV sorting of cargo receptors (discussed in more details in following sub-sections) (Raiborg et al., 2006, 2002, 2001; Sachse et al., 2002).

1.6.5 Major discoveries in yeast

The yeast vacuole is functionally equivalent to the lysosome in animal cells, thus yeast have played an important role as model organism in the uncovering the very first insights into the molecular mechanisms involved in endocytosis. The genes involved in vacuolar protein sorting in yeast were uncovered by Scott Emr and colleagues (Bankaitis et al., 1986). Emr and colleagues used a mutational screen to identify the vacuolar protein targeting (vpt) genes able to complement for vacuolar localisation of the yeast invertase CPY (Bankaitis et al., 1986).

Later on, Raymond et al. assigned 41 genes into vacuolar protein sorting (vps) mutant groups as they accumulate cargos into aberrantly enlarged prevacuolar (endosome-like) compartments, as shown by fluorescence microscopy (Raymond et al., 1992). Importantly, 13 vps genes of the class E variety encode proteins required for pre-vacuolar maturation. A pre-vacuolar compartment is strongly immunostained for the V-ATPase, CPY proteinase and the vacuolar proteases A and B which could not progress to the vacuole (Raymond et al., 1992)

Stevens' group studied temperature sensitive Vps27 (orthologue of mammalian HRS) mutants and showed that Vps27 positive compartments are intermediates between Golgi and vacuoles, as shown by electron microscopy (Piper et al., 1995). Later on, a major breakthrough into the mechanistic function of the class E vps genes in pre-vacuolar (early endosomal) physiology derived from studies developed by Scott Emr's lab. Emr and colleagues firstly described the role of the AAA ATPase Vps4 in preserving normal pre-vacuolar morphology (Babst et al., 1997, 1998).

Importantly, Emr and collaborators showed that Vps27 and all other 13 class E encoded proteins assemble into ESCRT complexes (described in more detail in **section 1.7**). In particular, the authors described the zinc-finger Vps27 as a ubiquitin binding protein fundamental to maintain a normal pre-vacuolar morphology and ensure degradation of the endocytosed material in the vacuole (Babst, Katzmann, Estepa-Sabal, et al., 2002; Babst, Katzmann, Snyder, et al., 2002; Bilodeau et al., 2002; Bowers et al., 2004; Katzmann et al., 2001, 2003).

1.5 Ubiquitin and lysosomal sorting

Early studies in yeast reported on the role of ubiquitin in the endo-lysosomal pathway. Hicke and Riezmann first discovered that the G-protein coupled plasma membrane receptor Ste2 becomes ubiquitylated upon activation of its cognate receptor (Hicke & Riezman, 1996).

The role of ubiquitylation had been historically linked to that of targeting proteins for proteasomal degradation, as K48-linked ubiquitin chains were first found to induce this process (Finley, 2009).

A breakthrough in our understanding of endocytosis regulation, was the discovery that ubiquitin is a sorting signal for endocytosis and importantly lysosomal degradation of many plasma membrane transporters and growth factor receptors (Haguenauer-Tsapis & André, 2004). Whilst mono-ubiquitylation, is sufficient for internalisation. it is currently accepted that, from yeast to plants and mammals, K63-linked ubiquitin chains is the primary sorting signal that directs cargo receptors for lysosomal degradation. For example, studies on *S. cerevisiae* ubiquitin mutants showed that the appendage of K63-ubiquitin on the yeast Gap1 permease and the carboxypeptidase S. is required for sorting in the MVB (Haguenauer-Tsapis & André, 2004; Lauwers et al., 2009).

The ubiquitin on the cargo receptor or transporter is recognised by a series of multimeric complexes called ESCRTs (endosomal sorting complexes required for transport), reviewed in more detail in the following section. ESCRTs are essential in many multicellular organisms, for example, severe developmental phenotypes result from defective ESCRTs components. It is now appreciated that ESCRTs carry out a vast number of cellular processes that include nuclear envelope repair, HIV-1 release from host cells, cytokinesis, exosomes and small vesicle biogenesis, plasma membrane wound repair, micro- and macro-autophagy (Hurley, 2015).

1.7.1 ESCRT-0: HRS-STAM

Hepatocyte growth factor-regulated substrate (HRS) is the mammalian counterpart of the Yeast Vps27 protein of the class E vacuolar protein sorting protein that, if mutated, causes mis-sorting of proteins through endosomes (Raymond et al., 1992; Piper et al., 1995).

The structure of HRS contains several domains: a VHS domain, a FYVE domain, a double-sided UIM (DUIM), a coiled coil region through which HRS binds the signal transducing adaptor molecules STAM1 and 2 (Endo et al., 2000; Takata et al., 2000; Asao et al., 1997, Raiborg et al., 2001). In addition, HRS has also been shown to bind clathrin via a clathrin binding motif (CBM). Diagram of protein domains for HRS, STAM1/2 and AMSH are displayed in **Figure 1.6**. As already mentioned earlier (**section 1.6**), clathrin is a coating molecule involved in the formation of CCVs at the plasma membrane upon endocytosis of cargo receptors. Clathrin is made of 3 heavy and 3 light chains which together form peculiar structures named “triskelia”. Clathrin usually functions as a coat for endocytic vesicles or for the tubular recycling endosomes. However, HRS creates endosomal microdomains in association with clathrin. HRS binds the β-propeller domain of clathrin heavy chain by its C-terminus thereby recruiting it to the early endosome (Raiborg et al., 2001). This flat clathrin coat is a means of concentrating cargo receptors before they are sent to lysosomes and HRS is proposed to act as an adaptor between receptors and the clathrin coat (Sachse et al., 2002; Clague, 2002).

Human HRS includes 30 Tyr residues, nevertheless Urbé et al. showed that HRS is phosphorylated at Y334 or alternatively at Y329 upon EGF-stimulation. Both modifications are ablated when the UIM is deleted from the protein. A ΔUIM HRS mutant fails to create peri-nuclear clusters of enlarged endosomes. Also, HRS is itself mono- and poly-ubiquitylated and this occurs independently from phosphorylation. The expression of phosphorylation-defective HRS creates severely abnormal endosomes where the M6PR is blocked (not able to be recycled), whereas the same is not seen upon ΔUIM HRS mutant expression. On the other hand, the

UIM domain of HRS is necessary to retain EGFR at the membrane of early endosomes, as the ΔUIM HRS mutant fails to suppress the inclusion of the EGFR in the ILVs (Urbé et al., 2003). HRS is phosphorylated upon growth-factor stimulation i.e the epidermal growth factor (EGF) stimulation, platelet-derived growth factor (PDGF), IL-2 and granulocyte-macrophage factor (Asao et al., 1997; Komada & Kitamura, 1995; Omerovic et al., 2012).

HRS localises at the endosome via its FYVE (Fab1/ YOTB/Vac1/EEA1) domain that recognises PI3P (phosphatidylinositol 3-phosphate) at the endosomal membrane. EGF-induced phosphorylayion of HRS on (Y334) was shown to be inhibited by treatment with Wortmannin, an inhibitor of phosphatidylinositol 3-kinase (PI3K) (Komada et al., 1997;Patki et al., 1997) Since, the activity of PI3K is required for localisation of HRS to the endosome via FYVE domain, HRS phosphorylation is believed to occur at the early endosomes. Moreover, EGF-dependent HRS phosphorylation depends on concomitant localisation of activated EGFR at the endosome (Urbé et al., 2000).

Over-expression of HRS severely alters endosomal morphology by creating enlarged endosomes and blocks the lysosomal route of endocytosed receptors whilst also hindering TfR recycling (Urbé et al., 2000). HRS is required for ventral folding morphogenesis of mouse embryos, and deletion of HRS in mice causes accumulation of enlarged endosomes and death at the 11-day stage (Komada & Soriano, 1999).

1.7.2 ESCRT-0: STAM

STAM1 and 2 are two paralogues that share 55% sequence identity. STAM 1 is a 70 kDa protein discovered in 1996 by Takeshita et al. that is phosphorylated in response to stimulation with IL-2 and a number of other cytokines (IL-3, IL-4, IL-7, GM-CSF, EFG, PDGF) (Takeshita et al., 1996). STAM comprises of an Src-homology 3 (SH3) domain and immunoreceptor Tyr-based activation motif (ITAM) (Takeshita et al., 1996).

SH3 domains are conserved protein-protein interaction motifs widely found in membrane-associated proteins, cytoplasmic proteins and adaptor proteins. An SH3 domain assumes the common topology of a compact β-barrel composed of 5 anti-parallel β-strands where a typical hydrophobic patch binds to a Pro-rich regions of partner proteins (Morton & Campbell, 1994; H. Yu et al., 1994). The ITAM is a conserved motif very often found in T-cell receptors, B-cell receptors, and other receptors on cells of the immune system. Upon phosphorylation of two Tyr in the ITAM, this domain becomes a signalling platform to recruit downstream signalling molecules and activates several SRC family members including Lyn and Syk (Johnson et al., 1995).

Soon after STAM1 was discovered, STAM2 was identified by Mass Spectrometry as a protein sharing 55% of its identity with STAM1 that is Tyr-phosphorylated after stimulation by growth factors and cytokines (i.e IL-3)(Pandey et al., 2000). In fact, STAM2 is phosphorylated on Tyr after EGF, and this depends on activation of Jak1 pathway. Furthermore, STAM2 can increase IL-2 dependent c-Myc promoter activation and needs an SH3 domain to carry out this function (Takeshita et al., 1997).

With 525 amino acids, the primary sequence of STAM2 is just a bit shorter than STAM1 (540 amino acids) and has an expected molecular weight of 59 kDa. STAM2 has an expected molecular weight of 57kDa. Like STAM1, STAM2 possesses an SH3 domain and an ITAM motif. Their ITAMs are 72% identical, and 12 of the 16 Tyr of STAM2 are conserved between the two proteins (Pandey et al., 2000).

Shortly after STAMs were discovered, they were found to tightly bind to the early endosome protein HRS by their coiled-coil regions (Asao et al., 1997;Takata et al., 2000). Like HRS, STAM1 and 2 contain a UIM which can bind two ubiquitin molecules (K. Hofmann & Falquet, 2001).

The yeast orthologue of STAM, Hse1 was shown to be involved in UIM-dependent sorting of ubiquitylated proteins through the endo-lysosomal pathway strongly (Bilodeau et al., 2002). Like HRS, STAM proteins

contain a second ubiquitin-binding domain at their N-terminus, the VHS (Vps27/Hrs/STAM) present in 8 mammalian proteins including Hrs, Tom1 and GGA proteins (Lohi & Lehto, 2001; Lohi et al., 2002).

The VHS domain of STAM1 and 2 can bind ubiquitin alone but needs the UIM to strengthen this binding. When low levels of STAM1 and 2 are expressed, they localise at the endosomal membrane and partially co-localise with HRS on punctate structures in the cytoplasm. STAM1 and 2 over-expression causes an endosomal enlargement similar to when HRS is over-expressed (Komada et al., 1997; Mizuno et al., 2003). When STAM are over-expressed, these enlarged early endosomes accumulate ubiquitinated proteins (Mizuno et al., 2003).

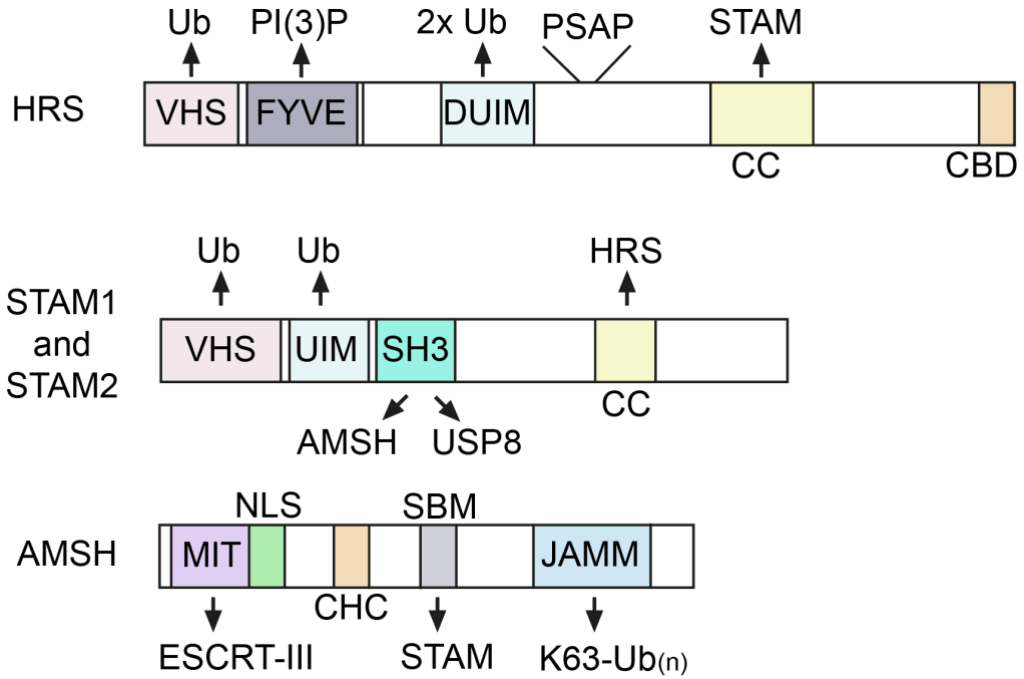

Figure 1.6 Protein domains of ESCRT-0 (HRS and STAM1/2) and AMSH.
The diagram depicts the protein domains of HRS, STAM1/2 and AMSH. Abbreviations: VHS, Vps27/Hrs/STAM; FYVE, Fab1/ YOTB/Vac1/EEA1; DUIM, double-sided ubiquitin binding motif; PSAP Pro-rich tetrapeptide region; CC, coiled coil motif; CBD, clathrin minding domain; SH3, Src-homology 3 (SH3) domain; MIT, microtubule-interacting domain CHC, clathrin heavy chain region; SBM, STAM binding motif; JAMM, JAB1/MPN/MOV34. Adapted from Clague and Urbé, 2006; Raiborg et al., 2001; Bache et al., 2003).

1.7.3 ESCRT complex and MVB biogenesis

In the last decade there has been an increasing amount of data that provided insight into the mechanism of ESCRT assembly and disassembly at intra-cellular membranes.

Among the different pathways that the ESCRT multi-protein complexes can carry out, they can orchestrate the so-called “canonical” pathway for MVB biogenesis. ESCRT-0 is the first ESCRT to recruit ubiquitylated receptors on endosomes and serves to sequester them in clathrin-coated microdomains. The ESCRT-0 complex component HRS recruits the ESCRT-I component Tsg101 via the PSAP region (Bache et al., 2003). ESCRT-I and ESCRT-II are upstream of the ESCRT-III protein charged MVB protein 6 (CHMP6) that recruits CHMP4, CHMP2 and CHMP3 (in mammals). CHMP2 and CHMP3 recruit the vacuolar protein sorting-associated 4 (VPS4), an ATPase of the AAA type that is required for disassembly of the ESCRT-III filament from the endosomal membrane (Schöneberg et al., 2016).

VPS4 consists of a hexamer where each monomer contains an N-terminal MIT (microtubule-interacting domain) and a catalytic AAA+ ATPase domain. Each sub-unit of VPS4 can bind ATP with equal affinity, whereas 4 subunits bind ADP with a different affinity compared to the remaining 2. This ATPase has been shown to play an important role in recycling the ESCRT-III and there are speculations that ESCRT-III subunits might cross the central pore for their recycling, though its functions are not entirely understood (Schöneberg et al., 2016). VPS4 uses its MIT domain to interact with the MIMs (MIT-interacting motif) of ESCRT-III proteins, in particular with the MIM1 domain in CHMP2b, CHMP1a and IST1. While the MIM2 (MIT-interacting motif 2) of CHMP4-5 is bound by the MIT of VSP4 with much lower affinity than CHMP6. CHMP3 does not interact with VSP4 by such motif. Nevertheless, CHMP3 can bind to other MIT domains such as the deubiquitylases AMSH/STAMBP (McCullough et al., 2006; Row et al., 2007).

.

1.7.4 ESCRT-I /II/ III complexes

ESCRTs were first discovered by Katzmann and colleagues in 2001, when they identified ESCRT-I consisting of a hetero-tetramer of TSG101 (Vps23 in yeast), VPS28, VPS37A and MVB12A or MVB12B/UBAP1 having ubiquitin-binding capacity through the UBC-like domain of TSG101. Importantly, they show that ubiquitin binding is required for sorting of receptors into MVB (multivesicular bodies) thus linking ubiquitin to cargo downregulation by the lysosome (Katzmann et al., 2001).

ESCRTs carry out both budding and vesicle-neck severing. Internal vesicles (ILVs), that characterise MVBs, derive from the inward budding of the limiting endosomal membrane that takes material away from the cytosol. This process is named “reverse-topology scission”, as opposed to the “normal-topology membrane scission” (budding towards the cytosol, Schöneberg et al., 2016). A crucial difference between the two types of scissions lies in the fact that the scission complex can only access the vesicle neck from the cytosolic side (Schöneberg et al., 2016).

ESCRT-II is a hetero-trimeric complex made up of EAP45 (Vps36), EAP30 (Vps22) and EAP20 (Vps25), this latter present in two copies. The ESCRT-I subunit VPS28 contacts the VPS36 subunit of ESCRT-II to form a saddle-shaped ESCRTI-II supercomplex that derives its name from the fact that it contains both a negative curvature (concave) and positive curvature (convex, Boura et al., 2012; Mercker & Marciniak-Czochra, 2015).

The structure of ESCRTs is described as either rod shaped (ESCRT-I), Y-shaped (ESCRT-II) or filamentous (ESCRT-III) after its beads-on-a-string conformation. The filament can form a spiral-like or circular arrangement in the 3D space, so that, upon constriction or expansion of the filament, the neck of the budding vesicle is severed (Hurley, 2015). ESCRT-I is recruited to the endosomal membrane via the binding of the UEV domain of its TSG101 component to ubiquitin and to the PSAP domain in HRS (Katzmann et al., 2001). The ESCRT-I component VPS28 interacts with

the ESCRT-II component EAP45 (VPS36), while ESCRT-II recruits the ESCRT-III component CHMP6 (VPS20) via EAP20 (Saksena et al., 2009; Teis et al., 2008).

Unlike the other ESCRT complexes, ESCRT-III are the outsiders of all the ESCRT multimers. Firstly, they can't bind ubiquitin, and second, they are monomeric until ESCRT-II or ALIX binds to them thereby inducing ESCRT-III monomers polymerisation. Humans have 12 different ESCRT-III proteins which include IST1 and the CHMPs (charged multivesicular body proteins). Rather than acting in MVB biogenesis, IST1 plays a central role in nuclear envelope fusion, forming a tubular structure together with CHMP1B (Schöneberg et al., 2016).

CHMP1-7 are all composed of a core structure of α1-α6 helices. While the α6 is involved in interactions, the α5 has an autoinhibitory function. By deleting the last 40 amino acids at C-terminus of these proteins induces their polymerisation and binding to membranes. The so-called "closed conformation" is adopted when the α5 helix folds back onto the conserved α1-α4 stretch, involving major protein reorganisation (Shim et al., 2007; Zamborlini et al., 2006). At the C-terminus they bear microtubule interaction and transport (MIT) domain-interacting motifs (MIM1 or MIM2). In CHMP4 and IST1 both MIM1 and MIM2 are present, while the others have only either one or the other. The ESCRT-III proteins are found as inert monomers in the cytosol. Once they are recruited, they polymerise in a large variety of structures that have been defined through electron microscopy (EM). CHMP4 and CHMP2A can form spirals, while CHMP2A-CHMP3 tubes or CHMP1B "bells" have been observed. IST1-CHMP1B also can form tubular structures (Shim et al., 2007; Zamborlini et al., 2006). A diagram depicting ESCRTs assembly and concerted binding to the ubiquitylated cargo receptor is shown in **Figure 1.7**.

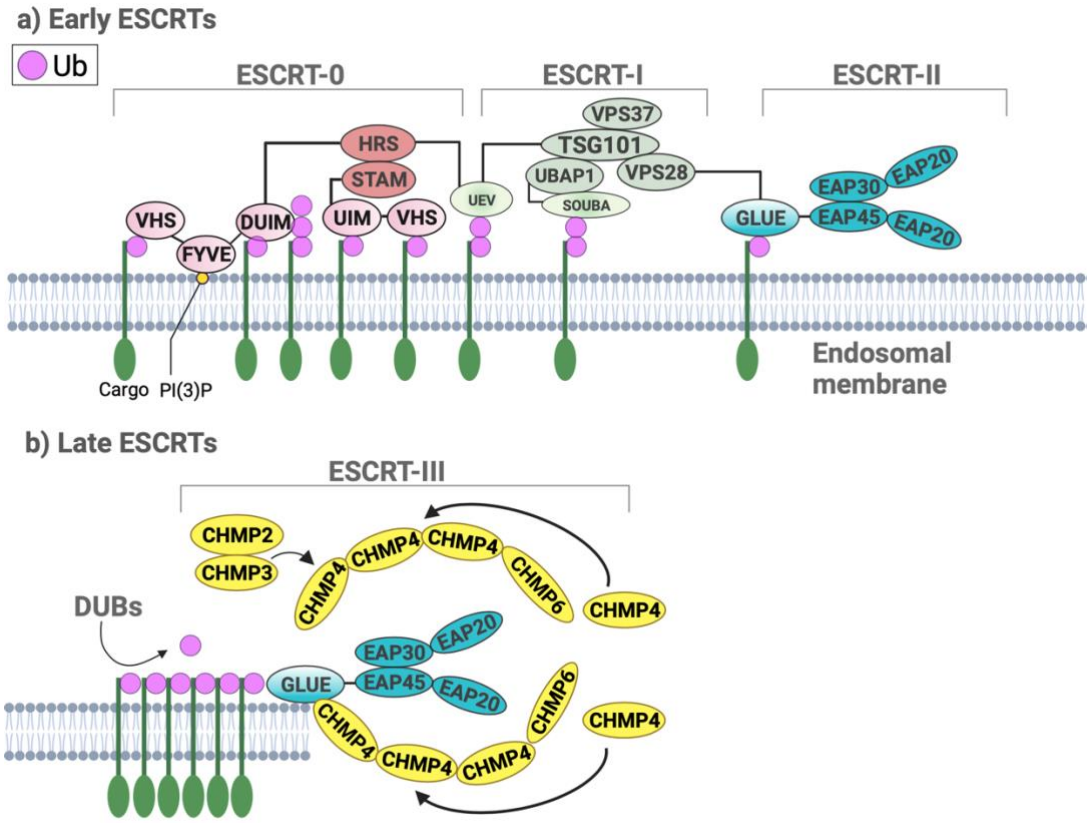

Figure 1.7 ESCRTs degrade ubiquitylated cargo receptors.
a) The diagram depicts binding of ubiquitylated cargo at the PI (3)P positive endosomal membrane of the early complexes ESCRT-0/I//II by a set of ubiquitin binding domains. In the ESCRT-0 complex HRS binds ubiquitin via VHS and DUIM domains, while STAM uses VHS and UIM ubiquitin binding domains. TSG101 and UBAP1 of the ESCRT-I complex use UEV and SOUBA domains to bind ubiquitylated cargo, respectively. The ESCRT-II component VPS36 bears a GLUE ubiquitin binding domain.
b) The late ESCRT-III filaments cannot bind ubiquitin but bind ESCRT-I via the GLUE domain of VPS36 thereby growing into a spiral structure around the clustered cargos that displaces early ESCRTs and deforms the endosomal membrane to form ILVs. The two endosomal DUBs USP8 and AMSH deubiquitylate cargo receptors prior to their sorting to ILVs. Adapted from Cullen and Steinberg, 2018.

1.7.5 Alternative ESCRTs

ALIX (Bro1 in yeast) is an accessory ESCRT protein that, together with ESCRT-0, ESCRT-I and ESCRT-II can recruit proteins through ubiquitin signals (in yeast) (Shields & Piper, 2011). ALIX is composed of a BRO1 domain, a V domain and a Pro-rich domain. The BRO1 domain is a domain also shared with HD-PTP phosphatase (an ESCRT component with similar domain structure to ALIX, discussed below) (Ali et al., 2013a).

The BRO1 domain in ALIX binds to the C-terminal helix of CHMP4 (Snf7 in yeast) on a concave surface(McCullough et al., 2008). The V domain in Bro1 can bind ubiquitin through its N-terminal tri-helical arms made of a shorter and a longer arm. Moreover, the V domain is required for cargo sorting in MVBs, likely in a cargo-specific way, when ESCRT-0 function is compromised. ALIX is thought to have an overlapping function with ESCRT-0 (Pashkova et al., 2013). ALIX can homodimerise via its V domain to adopt a conformation that resembles the ESCRT-II component that recruits the ESCRT-III. This conformation is hindered by the C-terminal PRD domain that autoinhibits the V domain; the PRD also binds to other proteins and other ESCRTs (Pires et al., 2009; Zhai et al., 2011).
The role of ALIX as an alternative means in recruiting ESCRT-III via CHMP4 interactions, is shown in HIV release and cytokinesis. In these processes, CHMP4 can be directly recruited by ALIX instead of the ESCRT-I-II-CHMP6 cascade used in MVB biogenesis (Schöneberg et al., 2016). ALIX is not the only alternative to ESCRT-I/II super-complex. The His domain phospho-Tyr phosphatase (HD-PTP) works as Tyr phosphatase and can replace ALIX in recruiting CHMP4 in a non-canonical ESCRT pathway (Parkinson et al., 2015). HD-PTP contains a V-domain that shares ~15% of identity with the V-domain of ALIX. HD-PTP can bind ubiquitin, ESCRT-I and ESCRT-III and localise to endosomes. Interestingly, HDPTP depletion by siRNA changes endosomal morphology and accumulates ubiquitylated proteins (Doyotte et al., 2008; Pashkova et al., 2013). Interestingly, the yeast orthologue Bro1 has been shown to recruit the DUB Doa4 (UBPY/USP8 in humans) that recycles ubiquitin from the sorted cargo (Amerik et al., 2006; Richter et al., 2007). HD-PTP recruits USP8 to endosomes. In fact, deleting HD-PTP recapitulates the USP8 depletion phenotype (Ali et al., 2013b).

1.7.6 ESCRTs in sorting ubiquitylated cargo proteins

Extensive research is being conducted to understand the mechanisms by which these complexes form intralumenal vesicles in the multivesicular bodies. This process is of particular importance for the downregulation of

RTKs (receptor-Tyr kinases), cytokine receptors and transporters and ion channels (Vietri et al., 2020).

HRS and STAM1/2 constitute the heterodimeric ESCRT-0 complex. This is the first point of contact of ubiquitylated receptors that are endocytosed. HRS and STAM concentrate these ubiquitylated cargoes in clathrin coated microdomains of the endosomal membrane (Clague, 2002; Sachse et al., 2002). As mentioned above, HRS localises at the endosome via its FYVE domain that recognises PI3P (phosphatidylinositol 3-phosphate) at the endosomal membrane. Instead, STAM localises to the membrane through association with HRS, with which it forms a tight heterodimeric complex (Mayers et al., 2011). As mentioned above, both HRS and STAM encode multiple UBDs (VHS and DUIM or UIM respectively). Importantly, reconstituted ESCRT-0 is able to bind to K63-linked polyubiquitin 50 times stronger than K48-linked polyubiquitin by virtue of their multiple ubiquitin binding motifs (Ren & Hurley, 2010).

Similar to other adaptor proteins working in endocytosis such as TSG101 and ALIX, HRS can be mono-ubiquitylated. This modification results in intramolecular interactions between ubiquitin and the UBD (DUIM) that prevents HRS from binding in trans to ubiquitylated substrates (Hoeller et al., 2006).

1.8 DUBs and lysosomal sorting

Ubiquitylation plays an important regulatory role when appended onto the C-terminus of endocytosed cargo receptors like the EGFR to direct down regulation by lysosomal degradation. Interestingly, much of the ubiquitin appended to activated EGFR is monoubiquitin, but the ubiquitin chains attached to EGFR are mainly linked through K63- polyubiquitin (F. Huang et al., 2013).

Endosomal DUBs include (multifunctional enzyme of the OTUD family) and AMSH (STAMBP) acting on K63-ubiquitin chains, and USP8 (UBPY), which, like most USPs, is a promiscuous enzyme (Faesen et al., 2011; Komander, Reyes-Turcu, et al., 2009; McCullough et al., 2006; Pareja et al., 2012) . USP8 and AMSH DUBs both have multivalent interactions and

compete for binding to the Src homology 3 (SH3) domain of STAM (ESCRT-0). In addition, they both bind to a distinct set of CHMP proteins (ESCRTIII) via their MIT domain (Clague & Urbé, 2006; McCullough et al., 2006; Row et al., 2006; Weissenhorn et al., 2011; Naviglio et al 1998). In addition, USP8 has been shown to stabilise the STAM component of ESCRT-0 via K48-linked ubiquitin cleavage (Row et al., 2006). USP8 also has been implicated in the trafficking of the cation-independent mannose 6-phosphate receptor (ci-M6PR). Indeed, depletion of USP8 leads to redistribution of the ci-M6PR from the Trans-Golgi network (TGN) to endosomes concomitant to the accumulation of ubiquitin in endosomes (Mcdonald et al., 2014). In contrast to USP8, AMSH depletion has been shown to induce a faster degradation of ligand-activated EGFR, suggesting a role in preventing cargo receptor degradation via a chain editing function (Bowers et al., 2006a; McCullough et al., 2004; Row et al., 2006, 2007) (**Figure 1.8**).

Whilst control of ESCRT stability explains many of the functions of USP8, physiological functions of AMSH remain to be fully explored. I will review AMSH related studies and its proposed role in cellular biology in the following section.

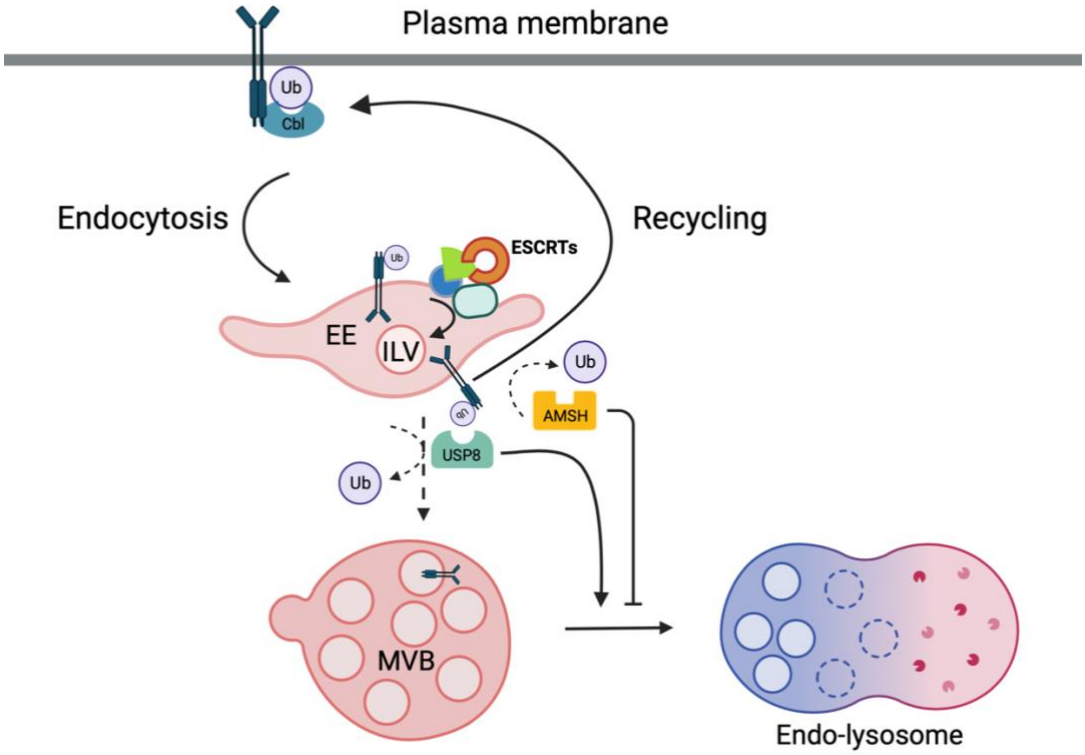

Figure 1.8 Endosomal DUBs that regulate the trafficking of plasma membrane proteins.
The diagram shows the two major endosomal DUBs. AMSH is proposed to oppose lysosomal degradation of MVB cargos, while USP8 was shown to induce degradation. Adapted from (Clague and Urbé, 2017, FEBS; Clague and Urbé, 2006, Trends in cell biology).

1.8.1 AMSH/STAMBP Discovery

AMSH (associated protein to the SH3 domain of STAM), also called STAMBP (STAM binding protein) was identified in a far Western screen for interactors of the STAM component of ESCRT-0. The authors first expressed a human leucocyte derived phage display cDNA library in E. coli. The transduced bacteria were plated until plaques were visible. At this point the plates were incubated for 4h with an IPTG soaked nitrocellulose membrane to induce protein expression. The nitrocellulose was then incubated with the GST-tagged SH3 domain of STAM. After western blotting, STAM interactors were identified by sequencing of the cDNA extracted from the GST-STAM-SH3 domain reactive plaques

(Tanaka et al., 1999). A cDNA clone was isolated that coded for a 48kDa, 424 amino acids long protein. This protein was predicted to have a JAB-1 subdomain homologous (JSH) module almost identical to the c-Jun activation-binding protein 1 (JAB1) and a bi-partite nuclear-localisation signal (NLS) homologous to that of p53 (**Figure 1.6**).

AMSH was found to interact with STAM in human T-cells (MOLTβ) irrespective of IL-2 stimulation and specifically interacts with the SH3 domain of STAM via a PXXP motif, referred to as the STAM binding motif (SBM) in the C-terminal region of AMSH spanning Arg^{234}-Arg^{424} (**Figure 1.6**). The authors hypothesised that AMSH is involved in the IL-2 and GM-CSF mediated signalling along with STAM (Tanaka et al., 1999).

1.8.2 Structure and function of AMSH

AMSH is a metalloprotease of the JAMM family of deubiquitylases. The domain structure of AMSH comprises an N-terminal MIT domain, a partially overlapping NLS, a poorly characterised clathrin heavy chain binding region (CHC), followed by the STAM-binding motif, (SBM), as mentioned above. The C-terminal half of the protein bears the JAMM catalytic domain (Dupré et al., 2001; McCullough et al., 2004, 2006; Nakamura et al., 2006; Clague & Urbé, 2006a) (**Figure 1.6)**. In addition, AMSH is able to bind ESCRT-III proteins via its functional MIT domain contrary to the MIT of AMSH-LP. Lastly, AMSH can bind the STAM component of the ESCRT-0 complex via its STAM-binding motif (addressed in detail in **subsection 1.7.1**). AMSH protein sequence is very conserved among different species (**Figure 1.9**).

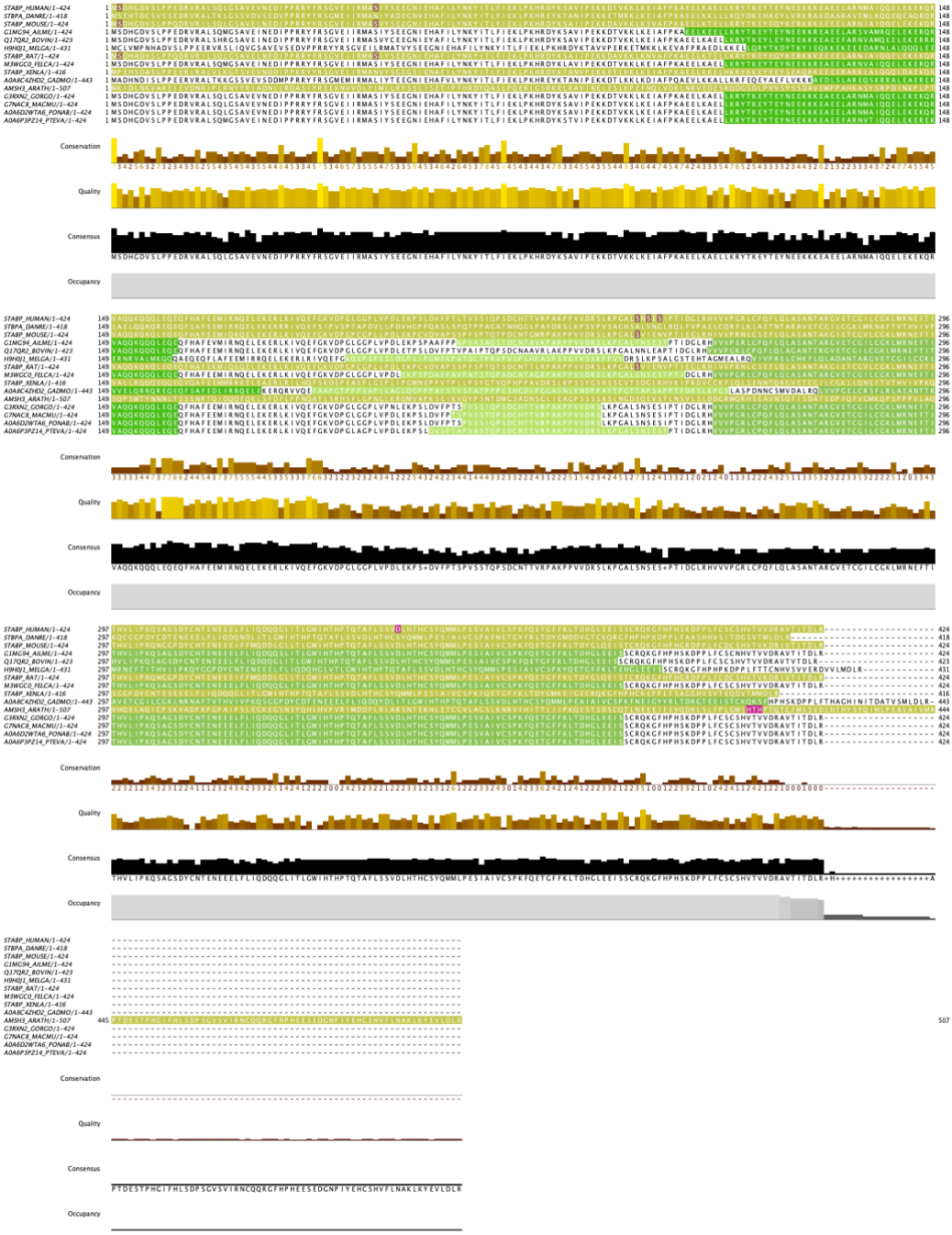

Figure 1.9 Protein Sequence alignment of AMSH across different species.

The protein sequences of AMSH from Human and a few species were sourced from Uniprot and aligned in Jalview. DANRE = Danio rerio; MOUSE = Mus musculus; Ailuropoda melanoleuca (Giant panda); BOVIN = Bos taurus (Bovine); MELGA = Meleagris gallopavo (Wild turkey); RAT = Rattus norvegicus (Rat); FELCA = Felis catus (Cat) (Felis silvestris catus); XENLA = Xenopus laevis (African clawed frog); GADMO = Gadus morhua (Atlantic cod); ARATH = Arabidopsis thaliana (Mouse-ear cress); GORGO = Gorilla gorilla gorilla (Western lowland gorilla); MACMU = Macaca mulatta (Rhesus macaque); PONAB = Pongo abelii

(Sumatran orangutan); PTEVA= Pteropus vampyrus (Large flying fox). Shown in green are the conserved portions.

Interestingly, the paralogue of AMSH, called AMSH-LP (STAMBPL) shares its K63-ubiquitin chain specificity, and like AMSH is localised to the endosomal membrane by its association with clathrin (Nakamura et al., 2006). In humans, AMSH-LP lacks the SBM motif, but shares the clathrin binding motif of AMSH (Agromayor & Martin-Serrano, 2006; Kyuuma et al., 2006; McCullough et al., 2004; Sierra et al., 2010a; Weissenhorn et al., 2011). AMSH-LP was shown to oppose the E3 ligase RNF167 and deubiquitylate Sestrin2, thereby disrupting its interaction with Gator2. This was shown to induce mTOR1 activation in cancer cells (Wang et al., 2022).

McCullough and colleagues produced the first report on AMSH specificity of cleavage towards K63-linked ubiquitin chains in an in vitro assay using purified chains (McCullough et al., 2004, 2006). They found that AMSH depletion caused a faster degradation of EGFR upon EGF stimulation. When overexpressed, GFP-tagged AMSH is primarily distributed between cytoplasm and nucleus with only a small fraction residing on endosomes. Over-expressed catalytically inactive GFP-AMSH (D348A), localised more strongly at early endosomes concomitant to an accumulation of conjugated ubiquitin and elevated recruitment of HRS. McCullough et al. speculate on a role for AMSH in promoting recycling of receptors by removing ubiquitin from them before they are committed to lysosomal degradation. In addition, overexpression of AMSH (D348A), led to both an enhanced interaction with STAM and accumulation of a ubiquitylated form of STAM that is dependent on the UIM domain of STAM (McCullough et al., 2004).

In a second study, McCullough and colleagues report on the wider network of AMSH interactors. Clathrin binds to STAM, HRS and AMSH, and in this way it may promote recruitment of the latter to endosomes. Binding of AMSH to STAM but not a UIM or SH3 deleted mutant of STAM, increases its catalytic activity towards K63-linked ubiquitin.

Moreover, AMSH binds simultaneously to STAM and the ESCRT-III subunit CHMP3 protein (McCullough et al., 2006). In addition, AMSH has been shown to interact with other ESCRTIII subunits including CHMP1A/B, CHMP2A/B, CHMP4A/B/C, CHMP5 and CHMP6 (Row et al., 2007; Agromayor et al., 2006; Babst, Katzmann, Estepa-Sabal, et al., 2002).

A strong interaction is established between AMSH and ESCRT-III protein CHMP3 both in open and closed conformation. The C-terminal region of AMSH is required for such interaction that is thought to relieve CHMP3 auto-inhibitory status (Lata et al., 2008). An overview of AMSH protein-protein interactions with the ESCRT complexes is shown in **Figure 1.10**.

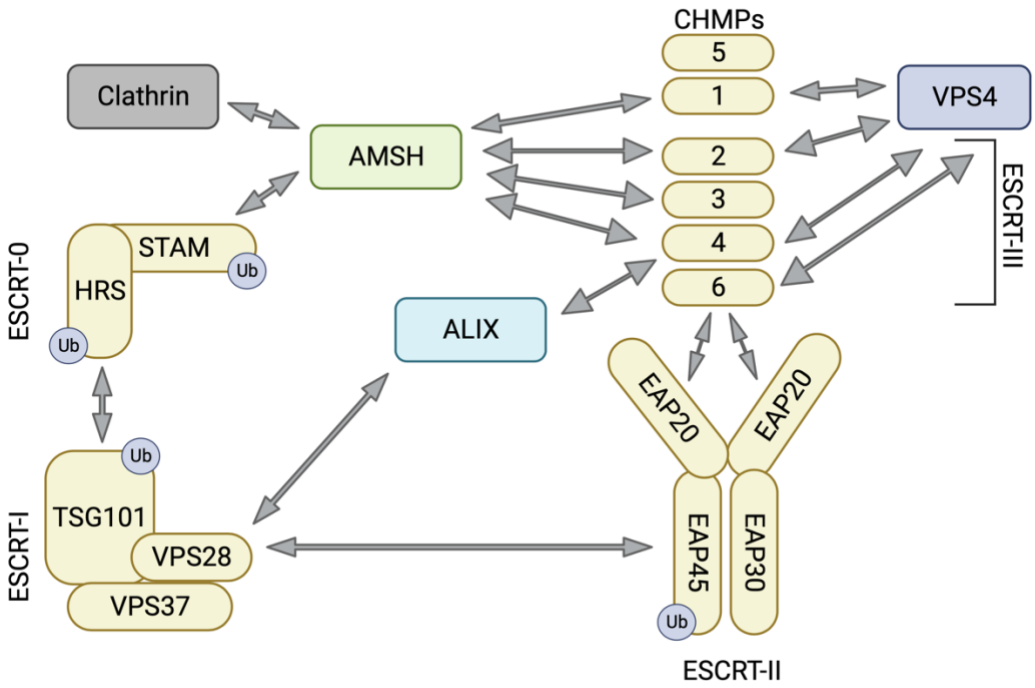

Figure 1.10 Overview of interactions between AMSH and the ESCRT machinery in mammals.
AMSH establishes a series of interactions with both ESCRT-0 (via STAM) and ESCRT-III components (CHMP1/2/3/4). The alternative ESCRT protein ALIX binds both to the ESCRT-III (CHMP4) and to ESCRT-I (VPS28). Adapted from Clague and Urbé, 2006.

1.8.3 AMSH involvement in developmental disease (MIC-CAP syndrome)

AMSH mutations are causative of a severe developmental disease, the MIC-CAP syndrome. The condition is characterised by severe microcephaly with progressive cortical atrophy, intractable epilepsy, profound developmental retardation, and multiple capillary malformations of the skin. McDonnell et al. found that different AMSH mutations can cause this autosomal recessive condition. The authors studied the capillary malformation (CM) phenotype which is a characteristic of dysfunctional RAS-MAPK (RAS-mitogen activated protein kinase) pathways. All 10 patients under study had visible CMs at birth, whereas one patient had also a cerebellar angioma and a second one had vascular liver malformations (McDonell et al., 2013).

Five out of six missense mutations map to the MIT domain of AMSH that is used to recruit the ESCRT-III subunit CHMP-III, the sixth missense mutation is in the JAMM domain at Thr^{313} which likely disturbs ubiquitin binding. Finally, they found Arg^{424*} and $Arg^{38}Cys$ as additional mutational hotspots. Interestingly, the authors found the accumulation of ubiquitylated protein aggregates both in a medulloblastoma cell line (Thr98Gly) and in LCLs (lymphoblastoid cell line) derived from AMSH-lacking patients. This phenotype was accompanied by apoptosis induction (caspase 3 and annexin V levels) after 24h starvation. Strikingly, the authors observed activation of autophagy in these cells pointing to a role of AMSH in regulating autophagy (McDonell et al., 2013).

AMSH patients derived LCLs displayed elevated levels of GTP-bound RAS, pERK1/2 and pRAF as well as high levels of pPI3K, pS6 and pTSC2 in starved and non-starved cells (McDonell et al., 2013).

AMSH importance in development has also been highlighted in animal models. AMSH is fundamental for post-natal development, as AMSH knockout mice die at P19 (post-natal day 19) and P23. Ishii et al report that the knockout mice have a significantly low body weight in comparison to the WT (wild type) (Ishii et al., 2001). Similar to MIC-CAP patients,

AMSH knockout mice showed severe neuronal loss, in particular at the hippocampal level. In fact, the mice experienced apoptosis within the CA1 (cornu-ammonis) sub-region of the hippocampus and the cerebral cortex was damaged. Therefore, the authors hypothesise a specific role of AMSH in promoting survival of hippocampal cells. AMSH interacts with the adaptor protein Grb2 that is known to induce survival and neuronal differentiation through Ras/MAPK pathway activated by NGF and BDNF (Ishii et al., 2001).

In more recent work, Suzuki and colleagues produced AMSH knockout mice to investigate the role of AMSH in the clearance of ubiquitylated protein aggregates (Suzuki et al., 2011). Interestingly, by developmental stage P8, ubiquitylated protein levels had increased significantly in insoluble fractions (membrane fractions) in AMSH KO mice neurons. Immuno-histochemistry showed that hippocampal and cortex neurons are the main areas that accumulate these ubiquitinated aggregates. These defects are reminiscent of the aggregates found in MIC-CAP patients' cells that lack AMSH protein (Suzuki et al., 2011).

The authors checked whether these accumulations were due to an inefficient removal of ubiquitylated proteins by autophagy. At P20 no LC3-positive puncta were detected. On the other hand, p62 aggregates were found in pyramidal cells of CA1 region, cortex and caudate putamen, where they colocalised with ubiquitin. Moreover, accumulation of TDP-43 positive and ubiquitin negative structures (a cytoplasmic protein) was shown to occur in the same regions of AMSH knockout mice brain in glial cells (astrocytes are suggested). Lastly, the CA1 region showed increased staining of ubiquitin positive Glu receptor aggregates that were also positive for PSD95 (DLG4). The latter is ubiquitylated by the E3 ubiquitin ligase MDM2 upon NMDA (Glu) receptor activation and is thought to be degraded by the proteasome (Suzuki et al., 2011).

1.8.4 AMSH and cancer

AMSH depletion in two melanoma cell lines (UACC257 and SK-MEL-28) attenuates migrative properties and invasiveness in these cells, whereas it had no effect on cell survival (Iwakami et al., 2018). The authors tested

effects on deubiquitylation, and they reported that, unexpectedly, AMSH depletion upon proteasomal inhibition (MG132 treatment) cause an increase in K48-ubiquitin chains. This points to a possible role of AMSH in directing, at least a sub-group of substrates, towards proteasomal degradation. In addition, they report the reduction of SLUG (SNAI), a transcription factor regulating melanocyte migration during development. While the protein expression decreases consequent to AMSH depletion, the transcript did not. Moreover, AMSH depletion strongly attenuates UACC257 melanoma derived-lung metastasis in mice (Iwakami et al., 2018).

More recently miR-378a-5p was shown to correlate with invasiveness in melanoma. miR-378a-5p targets the gene expression of AMSH to decrease both its transcript and protein in a cohort of melanoma patients' cells. miR-378a-5p promotes the migration of melanoma cell lines and acquisition of invasive features associated with cancer progression. In fact, this miRNA induces the expression of Metalloprotease-2 (MMP2) and urokinase receptor (uPAR) required to digest the extracellular-matrix. This points to a tumour-suppressor function of AMSH (Tupone et al., 2020).

This evidence strengthens the hypothesis that AMSH could be involved in regulating a subset of genes/proteins ultimately leading to cancer cell morphological changes in vivo (Tupone et al., 2020).

1.8.5 AMSH implication in Ubiquitin-dependent immune responses: inflammasomes

Inflammation is a defensive process built by host organisms against damage or infections with acute inflammation as a first line of defence. The process involves secretion of cytokines/chemokines by cells of the innate immune response, increase of blood pressure, vasodilation, extravasation of cells to the point of damage. Pattern recognition receptors (PRRs) on resident immune cells of the host detects pathogen associated molecular patterns (PAMPs) and damage-associated molecular patterns (DAMPs). PAMPs are conserved pathogen

determinants, while DAMPs include components released upon cell-damage or death (Bednash & Mallampalli, 2016).

Inflammasomes are self-oligomerising macromolecular assemblies that are initiated when PAMPs or DAMPs activate nucleotide-binding oligomerisation domain receptors (NOD-like receptors or NLRs) or AIM2-like receptors (ALRs)(Schroder & Tschopp, 2010). Different inflammasome complexes are activated depending on the upstream receptor.

Ubiquitylation can regulate inflammasomes, as K48-linked, K63-linked, linear and unanchored ubiquitin chains are conjugated to NLRP3 upon microphage stimulation with bacterial endotoxin. Moreover, inhibition of DUBs using non-selective inhibitors decreases IL-1β secretion and caspase-1 activation. NLRP3 is both K48- and K63 ubiquitylated (Bednash & Mallampalli, 2016). It is constitutively ubiquitylated by the SCF subunit FBXL2 for proteasomal degradation, while it has also been shown to be ubiquitylated by MARCH7 for degradation by autophagosome (Han et al., 2015),(Y. Yan et al., 2015). Another DUB BRCC3 is required for activity of the NLRP3 complex, thus further delineating a dynamic picture of its working mechanism (Py et al., 2013).

AMSH has been shown to participate in the modulation of the NACHT, LRR and PYD domains-containing protein 7 (NALP7) inflammasome component (Bednash et al., 2017a). Bednash et al. reported that AMSH can deubiquitylate NALP7 and thereby inhibit its lysosomal degradation. NALP7 can be induced to form an inflammasome with the adaptor protein ASC, as shown in THP-1 cells stimulated with LPS or Pam3CSK4 (a synthetic acylated peptide). The authors demonstrate that NALP7 stability is dependent on K63-ubiquitin chains appended onto K288. STAM knock down showed that the substrate is likely brought along to AMSH by STAM. AMSH depletion severely decreased IL-1β secretion in human-derived macrophages stimulated with LPS or an acylated peptide (acLP) thereby affecting inflammasome activity. Lastly, they confirmed that AMSH depletion increases NALP7 co-localisation with M6PR (mannose 6-phosphate receptor) upon leupeptin inhibition of lysosomal enzymes (Bednash et al., 2017b).

1.9 Exosome biogenesis

Extracellular vesicles (EVs) were first described by Peter Wolf who found that a phospholipid-rich minute particulate material (platelet-dust) was separated from platelets by ultracentrifugation (Wolf, 1967). EVs can be subdivided into three categories: apoptotic bodies, cellular macrovesicles and exosomes (Gould & Raposo, 2013).

Exosomes are non-degradative cell compartments with a diameter of 30-150 nm and are formed through invagination of the limiting membrane of the MVBs to form internal vesicles. They are called exosomes when they are released upon fusion of the limiting membrane of the MVBs with the plasma membrane (Yáñez-Mó et al., 2015) (**Figure 1.11**).

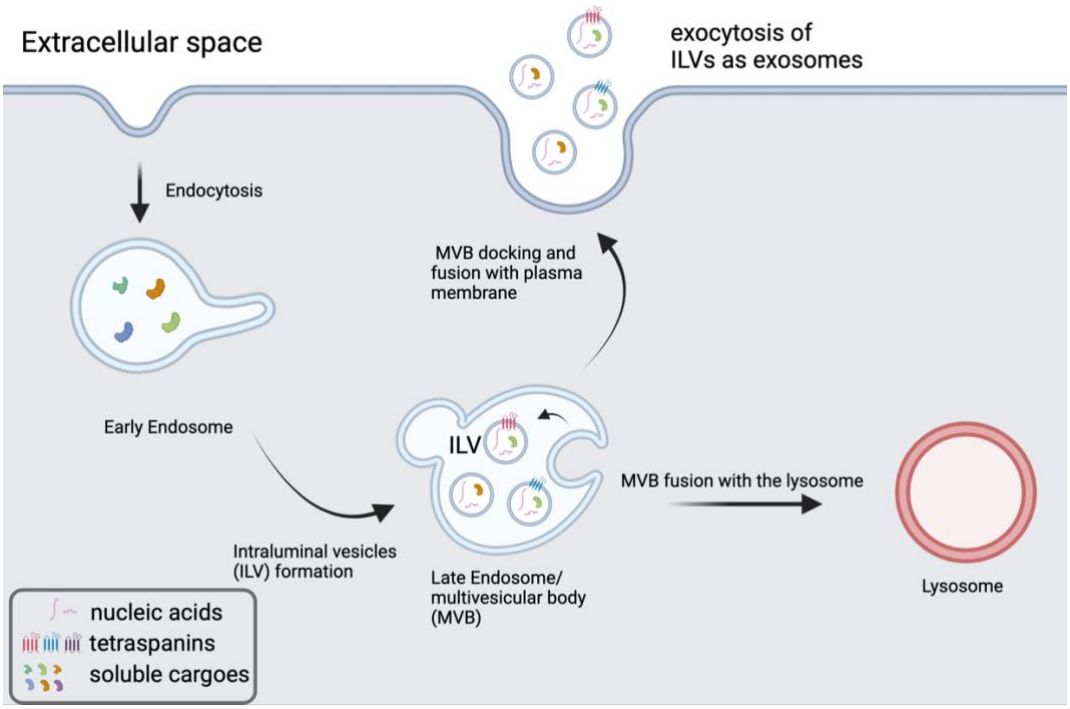

Figure 1.11 Exosome biogenesis.
The diagram shows the biogenesis of exosomes via the fusion of multi-vesicular bodies with the plasma membrane to release ILVs in the extracellular environment. Adapted from (Gurung et al., 2021).

Both exosomes and microvesicles contain endosomal proteins and are enriched in tetraspanins CD63, CD9 and CD81. Microvesicles have a similar size to exosomes (100-150nm diameter), making it difficult to separate them from exosomes. For this reason, they are grouped under

the name of small extracellular vesicles (sEVs) (Booth et al., 2006; Mastoridis et al., 2018).

The pathways and triggers that induce exocytosis have as yet not been fully elucidated. Nevertheless, it has become clear that a cytosolic increase in Ca^{2+} is a trigger for exosome secretion in response to plasma membrane repair. This process is mediated by Annexin A6 which acts as a calcium sensitive tether between CD63-positive MVBs and the plasma membrane (J. K. Williams et al., 2023)**.** Exosomes play an important role in inter-cellular communication, as they can be secreted by tumour cells and have important impacts on the tumour microenvironment. For example, the entry of pro-tumorigenic exosomes into endothelial cells can induce angiogenesis via the expression of VEGF, VEGFR and ICAM-1 proteins (Conigliaro et al., 2015). Exosome secretion is achieved thanks to the polymerisation and dynamic remodelling of subcortical actin (Li et al., 2018). In the final step of secretion of MVBs, the fusion of MVBs with the plasma membrane is mediated by the VAMP2, VAMP3, VAMP7 and VAMP8 in different cell types (Fader et al., 2009; Kumar et al., 2020; Z. Yu et al., 2020).

In recent years, there has been increasing interest in studying the relationship between exosome secretion and cell protrusions. Invadopodia are specialised actin-rich structures and form cellular protrusions which confer invasive properties to cancer cells (Murphy & Courtneidge, 2011). Invadopodia were found to be active secretion sites for CD63- and Rab27A-positive exosomes. MVBs are recruited at invadopodia and can induce both invadopodia formation and maturation (Hoshino et al., 2013). Filopodia and lamellipodia are thin, actin-rich plasma membrane protrusions specialised in probing the extracellular environment and cell adhesion, respectively (Mattila & Lappalainen, 2008; Murphy & Courtneidge, 2011). Interestingly, filopodia have been found to be sites where exosomes are recruited and that these are sites where the exosome docks to recipient cells. This process requires subcortical actin polymerisation (Heusermann et al., 2016).

An RNAi screen monitoring exosome secretion by trapping them using an anti-CD63 antibody, identified multiple ESCRT proteins as regulators. This study demonstrated that depletion of either HRS, STAM1 or TSG101 reduced exosome secretion. Depletion of VPS4B, VTA1 and ALIX increased it. ALIX depletion alters the composition of exosomes, as HSC70 and CD63 were decreased in exosomes from ALIX depleted cells (Colombo et al., 2013).

Syndecans are heparan-sulphate proteoglycan membrane proteins that work as co-receptors to modulate the intracellular response to extracellular stimuli (Couchman, 2003). Syntenin is a plasma membrane and cytosolic protein which plays a role in sorting syndecans to exosomes via ALIX interaction (M. F. et al. Baietti, 2012). Binding of Syntenin to Syndecans and ALIX has been proposed to facilitate the formation of ILVs. In addition, the tetraspanin CD63 is proposed to be sorted by Syntenin binding (Roucourt et al., 2015). Syntenin bears PDZ motifs which are protein-protein interacting motifs and can bind ubiquitin in an unconventional manner. In fact, Syntenin strongly binds ubiquitin C-terminal Arg^{72}, Leu^{73}, and Arg^{74} residues. Together with CD63, Syntenin can bind equally well to both K48 and K63 linked poly-ubiquitin through one of its 3 LYPXL motifs ($L^{4}YPSL^{8}$). Importantly, Syntenin1 recruitment to CD63-positive late endosomes relies on an intact $L^{4}YPSL^{8}$ motif thereby suggesting that Syntenin1 has a central role of as an adaptor to sort ubiquitylated proteins to CD63 positive Evs (Rajesh et al., 2011).

Interestingly, exosomes contain poly-ubiquitylated proteins, and a proteomics study conducted on specific ubiquitin chain linkages determined that K63-linked ubiquitin is the main chain type contained in exosomes (Buschow et al., 2005; Huebner A.R. et al., 2016). The mechanism of action by which ubiquitylated proteins are sorted to exosomes has not been elucidated.

1.10 Aims of the thesis.

This project began from the important findings from Dr. John McCullough. He showed that AMSH is specific for K63-linked ubiquitin chains and that

AMSH depletion affects the turn-over of stimulated EGFR (McCullough et al., 2004). One of the two ubiquitin binding ESCRT-0 components, STAM, can interact with AMSH and promote its catalytic activity at the endosomal membrane (McCullough et al., 2006). Therefore, the authors implicated AMSH in the downregulation of plasma membrane proteins through the endolysosomal pathway. In addition, the observation that depletion or deletion of AMSH causes accumulation of ubiquitin in mice and MIC-CAP patients' cells led us to speculate that its specificity towards K63-ubiquitin chains is key to its function.

As AMSH function is still not well understood, I generated tools to obtain a complete picture as to how AMSH regulates the endocytic pathway.

1. I used CRISPR-Cas9 to generate AMSH KO cells which will help me to assess whether there is a perturbation in the endosomal morphology and ubiquitin homeostasis.
2. I used an unbiased approach by analysing the K63-ubiquitin associated proteome in AMSH KO cells to identify new regulators of AMSH.
3. I generated and characterised a new tool: HeLa Flag-APEX2-AMSH Flp-In cells that can be used to discover novel interactors of AMSH.

Chapter 2: Materials and methods

2.1 Mammalian cell culture

2.1.1 Cell culture reagents

Dulbecco's Modified Eagle's Medium (DMEM) + GlutaMAX-I and pyruvate supplement (#31966-021), Fetal bovine serum (FBS) (#10270) and Minimum Essential Medium/Non-Essential Amino Acids (MEM/NEAA) (#11140-035) were purchased from Thermo-fisher Scientific. Trypsin-EDTA (#15400) and Opti-MEM (#409864), and Hygromycin B (#10687010) were purchased from Invitrogen (UK). GeneJuice Transfection reagent (#70967-3) was purchased from Sigma. Flp-In kit (#K6035-01) and Zeocin (#R25005) were purchased from Thermo-Fisher scientific. Plastic materials for cell culture were all purchased from Corning Inc. (NY, USA). Primers for PCR and cell line generation were purchased by Dharmacon.

2.1.2 Cell lines

HeLa S3 Flp-In Parental and HEK 293 T-REX were purchased from Invitrogen. HeLa S3 GFP-HRS Flp-In cells were generated by Dr. Han Liu (University of Liverpool) and are described in (MacDonald et al., 2018).

2.1.3 Cell line maintenance and seeding

Cells were cultured in in DMEM + GlutaMAX^{TM} medium supplemented with 10% Fetal bovine serum (FBS) and 0.1mM MEM/Non-essential amino acids (MEM/NEAA). All cells were kept at 37°C and in a 5% CO_2 humidity condition. Cells were maintained in 10cm^2 dishes. Freezing of cell batches was achieved from a confluent T75 flask from which 3 vials were cryo-stored at -80°C in 1 ml of freezing medium.

2.1.4 Generation of AMSH knock out HeLa cells by CRISPR Cas9

HeLa S3 GFP-HRS AMSH knockout (AMSH KO) cells were generated by CRISPR-Cas9 strategy. Three different single-guide RNAs (sgRNA1, sgRNA3 and sgRNA4), were generated by annealing two complementary primers that targeted the N-terminus (exon 1) or C-terminus of the protein (exon 7 and 8). At 24h post-transfection with the annealed sgRNAs, the cells were checked under a Nikon-Ti epifluorescent microscope for positivity in both the GFP and Tx-Red channel and then were sorted by fluorescence activated cell sorting (FACS) selecting double GFP and mCherry positive singlets in 96-well plates. The clones transfected with each sgRNA were cultured and then screened by western blotting and PCR on genomic DNA (**Table 3**).

Table 3 Sequence of primers annealed as sgRNAs for subcloning into the pU6-(BbsI)-CBh-Cas9-T2A-mCherry plasmid. The table shows the sequence of the sgRNA targeting different exons of AMSH.

Primer names	Annealed sgRNA name	Target	sgRNA sequence
FF-AMSH MIT-sgRNA1-Fw	sgRNA1	Exon 2	CACCGCTCTACCGCACTACCCAGCT
FF-AMSH MIT - sgRNA1-Rv	sgRNA1	Exon 2	AAACCAGCTGGGTAGTGCGGTAGAG
FF-AMSH JAMM-gRNA3-Fw	sgRNA3	Exon 7	CACCGTTCCTCATACAGGATCAGCA

FF-AMSH JAMM - sgRNA3-Rv	sgRNA3	Exon 7	AAACCTGCTGATCCTGTATGAGGAA
FF-AMSH JAMM - sgRNA4-Fw	sgRNA4	Exon 8	CACCGGTCGACACTGGAGAGAAACG
FF-AMSH JAMM - sgRNA4-Rv	sgRNA4	Exon 8	AAACCCGTTTCTCTCCAGTGTCGAC

After sgRNA production by complementary primer annealing, the pU6-(BbsI)-CBh-Cas9-T2A-mCherry plasmid (Addgene, #64324) was digested with the BbsI restriction enzyme to generate sticky ends. The BbsI site served to subclone the sgRNAs in the vector. The final plasmid product of this ligation, pU6-(sgRNAn)-CBh-Cas9-T2A-mCherry was transfected into 250,000 of HeLa GFP-HRS Flp-IN cells.

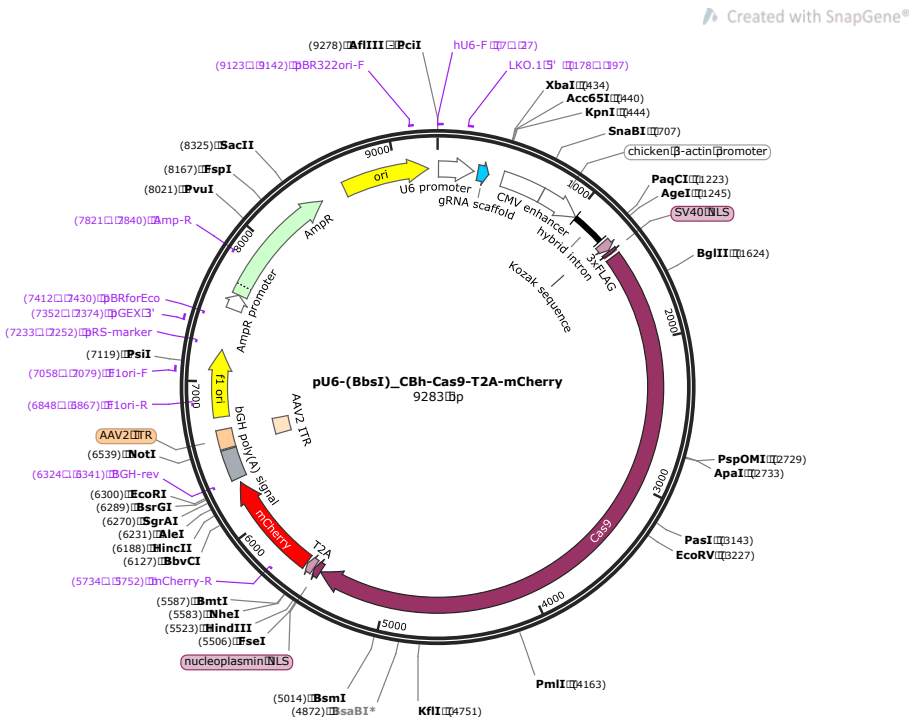

Figure 2. 1 Plasmid map of pU6-(sgRNAn)-CBh-Cas9-T2A-mCherry used to transfect HeLa GFP-HRS Flp-In.

Unique restriction sites in the pU6-(sgRNAn)-CBh-Cas9-T2A-mCherry plasmid are indicated.

At 24h post-transfection the media was changed, and the cells were observed in brightfield with a Nikon epi-fluorescent microscope at 40X magnification. The transfection efficiency was checked by imaging the cells in the Tx-Red channel. Around 30% of the transfected cells were mCherry-positive for either of sgRNA1, sgRNA3 or sgRNA4. Single cells were sorted by FACS (fluorescence-activated cell sorting) through an ARIA-III machine using double mCherry and GFP lasers to sort single cells in each well of 96 well plates. Single cell-derived clones were left to grow for 3 weeks and then were cultured in 6 well plates for Western blotting- based screening to assess AMSH protein deletion. After this stage, the genomic DNA (gDNA) was extracted from the cell clones to check for the genomic modification leading to AMSH protein deletion. The genomic regions of AMSH corresponding to exons 1, 7 or 8 were amplified by PCR using different sets of primers. Between 0.5-4 µl of the amplicon was ligated into the PCR4-Topo vector by blunt-end reaction at room temperature for 5min. The PCR4-TOPO-AMSH genomic reaction was transformed into TOP10 bacteria that were plated onto solid agar plates o/n at 37°C.

2.1.5 Flp-In cell system

The pEF5/FRT/V5 Directional TOPO® Expression Kit for Flp-In cells generation was purchased as a kit from Thermo-fisher Scientific (Catalog no. K6035-01). The kit was used to generate stable cells which express a gene of interest in a host cell line under a constitutive promoter. The system makes use of the pEF5/FRT/V5-D-TOPO® expression construct carrying a gene of interest that can be integrated at a unique FRT location in the host cell line genome. The FRT site contains a specific sequence that is required for Flp recombinase binding, strand cleavage and recombination after which the hygromycin resistance gene in the pEF5/FRT/V5-D-TOPO® is in a correct frame with both the ATG initiation codon and the gene of interest. The Flippase enzyme is provided by the pOG44 plasmid such that co-transfection of the two constructs is necessary for the

integration to occur. The FRT site in the parental cell line had been previously introduced for the expression construct to be inserted into.

2.1.6 Sub-cloning APEX2 at the N-terminus to AMSH

Cloning of the APEX2 sequence at the N-terminus of AMSH ORF was achieved through an LR reaction (gateway cloning) involving homologous recombination between a donor plasmid (PBR-AMSH) containing flanking attR sites and an entry vector (pENTR-Flag-APEX2-NES) containing the attL sites flanking the APEX2 and a nuclear export signal (NES).

The resulting plasmid obtained from the LR reaction was called pENTR-Flag-APEX2-NES-AMSH and was subcloned into a pEF5-FRT expression vector through restriction digestion and ligation reaction. The resulting pEF5-Flag-APEX2-AMSH plasmid can be integrated at a single specific FRT site in the genome of Flp-In cells by co-transfecting it with the pOG44 recombinase-encoding plasmid.

2.1.7 Generation of HeLa S3 Flag-APEX2-AMSH Flp-In

HeLa S3 Flp-In host cells carry a single integrated FRT site in their genome which is expressed along with a zeocin resistance gene. Prior to co-transfection, HeLa S3 Flp-In were cultured in DMEM supplemented with 1:400 dilution of Zeocin (Invitrogen). The cells were seeded (~0.5 $x10^6$ cells) onto 10cm dishes at day 1. At day 2, HeLa S3 Flp-In reached a 60-70% confluency and were co-transfected with 100ng pEF5-Flag-APEX2-AMSH Flp-In and 900 ng of the pOG44. The next day they were seeded onto two 10cm dishes at 1:6 and 1:4 dilution in the presence of 150µg/ml Hygromicin B for selection of positive clones.

After 3-4 weeks of selection, most of the cells had died and only small colonies were visible. The colonies were observed under a 40X objective in bright field and small single cell derived colonies were trypsinised in 10µl and picked with a p10 pipette. Each colony was grown in one well of a 96 well plate in Hygromycin B to select for clones that integrated Flag-APEX2-AMSH into their genome.

Surviving clones were assayed for Flag-Apex2-AMSH protein expression by Western Blot analysis and immunofluorescence.

2.2 Cell biology

2.2.1 Cell biology reagents

Lipofectamine RNAiMAX (#13778075), Opti-MEM™ Reduced Serum Medium and GlutaMAX™ Supplement (#51985034) were all purchased from Invitrogen (UK). GeneJuice Transfection Reagent (#70967) was purchased from Merck Millipore (Dorset, UK). siRNA oligonucleotides were purchased from Dharmacon (Cambridge, UK). IBIDI products purchased from Thistle Scientific (Glasgow, UK). Hoechst 33342 (#62249) was purchased from Thermo-fisher Scientific. Bafilomycin A1 from Streptomyces griseus (#B1793) was purchased Sigma.

2.2.2 siRNA-mediated knock-down

At day 1, HeLa cells were seeded into 6 well plates at a density of 1.5 $x10^5$ per well. At day 2 cells, were transfected with siRNA (40 nM) with Lipofectamine RNAiMAX in Opti-MEM medium at a 1:1 ratio following the manufacturer's instructions. The reaction was added to the cells for 6 hours, after which the media was exchanged with normal media. Reactions were left for 72 hours. Cells were lysed at day 5. The siRNA sequences used are indicated in **Table 4.**

Table 4 siRNA oligonucleotide sequences
The table shows the sequence of the siRNA oligonucleotides used for siRNA experiments.

Target	Cat. No.	Species	Sequence
NT1	single D-001810-01-50	control	TGGTTTACATGTCGACTAA

Syntenin1	Pool of 4 SDCBP (Human)-ON-TARGETplus Human PDCD6IP siRNA. Catalog ID:L-008270-00-0005	human	GGAGAGAAGAUUACCAUGA; GACCAAGUACUUCAGAUCA; GGAUGGUCUUAGAAUAUUU; GCAUUUGACUCUUAAGAUU
ALIX	Pool of 4, PDCD6IP (Human-ON-TARGETplus Human PDCD6IP siRNA. Catalog ID:L-004233-00-0005	human	CAGAUCUGCUUGACAUUUA; UCGAGACGCUCCUGAGAUA; GCGUAUGGCCAGUAUAAUA; GUACCUCAGUCUAUAUUGA
VPS26	Pool of 4, L-013195-00-0005	human	CCGUAUGGCUCAACUUCGA, AGGCAGGCGUCGAAGAGUA, GCUCUACGAAGAUCUGGAA, GGAGCGCAUUGCACAUCAA
HRS (HRS-1 oligo)	Custom single oligo, Catalog ID: Hum HRS-155, #URBSA 000003	human	GUCAACGACAAGAACCCAC
HRS (HRS-2 oligo)	Custom single oligo, Catalog ID: Hum HGS, #J016835-07	human	AAAGAACUGUGGCCAGACA
STAM1	Custom single oligo, Catalog ID: URBSA-000005	human	NNCCAAAGAUCCUCACGUU

STAM2	Custom single oligo, Catalog ID: URBSA-000007	human	NNUCAUAAGGUUCCACAUGUU

2.2.3 Transfections

For DNA transfection, cells were seeded at day 1 to be at 60-70% of confluency at day 2. The transfection reaction was obtained by diluting Genejuice reagent in OptiMEM serum free medium incubated for 5 minutes at room temperature. The oligos/DNA were added to the mixture and incubated for 15 minutes at room temperature. Prior to dropwise addition of the reaction onto cells, the media was exchanged with fresh media. Typically, the cells were imaged or collected at 24 hours post-transfection.

2.2.4 Drug treatments

HeLa GFP-HRS Flp-In parental and AMSH KO cells were treated with Bafilomycin A (100 µM) for 18 hours to inhibit the V-ATPase. The expression of HANL, HANL-CD63 and HANL-Syntenin1 in HEK 293 TREX cells was induced with both 0.1 µg/ml and 1 µg/ml doxycycline as indicated in figure legends. The cells were treated in normal media and duration of treatments is indicated in the appropriate figures.

2.2.5 NanoLuciferase assay

A protein of interest can be fused with NanoLuciferase which photoactivates a provided substrate by oxidation in presence of ATP and oxygen. The NanoLuciferase reacts with the provided substrate and realeases luminescence from the protein of interest. In this thesis, I have employed plasmids constitutively expressing the HA tag in frame with the NanoLuciferase (HANL) fused to either CD63 or Syntenin1. I then measured the luminescence emitted by HANL-tagged CD63 or Syntenin1 constructs from transiently transfected HeLa Parental and AMSH KO cells to determine their level of extracellular secretion.

For the Nano Luciferase assay, 3 x 10^4 cells were seeded into a well of a 24 well plate. At day 1, cells were transfected with 200µg of either of the constitutively expressing HANL (HA-NanoLuciferase tagged) plasmids: pEF5-HANL-CD63 or pEF5-HANL-Syntenin1. After 24 hours, they were either left untreated or treated with 100 nM of Bafilomycin A for 5h. To assay exosome secretion within this time window, the “media + EV fraction” (release) was collected from each well of the 24-well plate, spun down at 16,000g for 5 minutes in the cold. The supernatant (release) was transferred into fresh tubes. The cells remaining on the plate were permeabilized with 0.2% TritonX for 2 minutes. The released content was collected, named “total cell” (TC) fraction and spun at max speed for 5 minutes in the cold. 5 µl from the TC fraction and 50 µl from the release fraction were transferred to a 96-well plate in triplicate. The substrate and the buffer from the NanoGlo luciferase assay kit were mixed in a 1:50 ratio to reconstitute the active reagent. For the NanoGlo assay, 25µl of reconstituted reagent was added to each well and the luminescence from each condition measured using the standardized program of the NanoGlo plate reader (Promega). Fractional release from each condition was calculated as the ratio of luminescence in the release fraction /luminescence in the total cell fraction.

2.3 Molecular biology

2.3.1 Reagents

The QIAprep MiniPrep Kit (#27106), PCR clean up kit (#28104) and HiSpeed Maxiprep kit (#12633) were purchased from Qiagen. All restriction enzymes, T4 DNA ligase reagents, 1 kb DNA ladder (#N3232) and 100bp DNA ladder (#N3231) were purchased from New England Biolabs. BL21 biotinylation competent cells (#27462) were from TebuBio.

TAE buffer was purchased from National Diagnostics. S.O.C. medium (#1554-034), DH5α subcloning efficiency cells (#18265-017), electrophoresis grade agarose was obtained from Invitrogen. PCR nucleotide mix (#C1441) and PCR reagents were purchased from

Promega. pEF5/FRT/V5 Directional TOPO® Expression Kit (#K6035-01) was purchased from Thermo-fisher.

2.3.2 DNA PCR for cloning

As stated in the previous sections, HeLa S3 Flag-APEX2-AMSH Flp-In were generated by integrating the Flag-APEX2-AMSH at their single FRT site in their genome. The pEF5-Flag-APEX2-NES-AMSH constitutive expression plasmid was generated by amplification of the Flag-APEX2-NES-AMSH ORF in the pENTR-Flag-APEX2-NES-AMSH vector as a template. The forward primer carries the 5'-CACC stretch recognised by the recombinase enzyme. The resulting pEF5-Flag-APEX2-AMSH was co-transfected with pOG44 plasmid to generate Flag-APEX2-NES-AMSH HeLa S3 Flp-In cells (**Tables 5-6**). The PCR reaction mix was set up as described in Tables 5 and 6. The template (100 ng) was then added to the reaction mix **(Table 7)** and a control reaction without template was set up in parallel. After PCR, the amplicon was run on a 1% agarose gel in TAE buffer, the band at 2 kb was excised from the gel and the DNA was extracted and eluted from the gel piece using a Qiagen QIAquick Gel Extraction Kit. The concentration of the PCR product was determined, then was diluted to 20 ng/µl and was used in the TOPO® reaction at both a 0.5:1 and 1:1 ratio with the host pEF5-FRT-V5 vector DNA (**Table 7**).

Table 5 PCR primers used for cloning.

ORF	Sequence
Forward primer -Flag-Apex2-AMSH	caccATGGACTACAAGGATG
Reverse primer -Flag-Apex2-AMSH	GTGtcatcgaaggtctgtga

Table 6 PCR mix for DNA amplification.

component	Volume (µl)
H_2O	-

10x Pfu-buffer	10
dNTPs (25mM)	1.25
Forward primer (10µM)	3
Reverse primer (10µM)	3
DNA template (100ng)	-
Pfu Ultra-II fusion	2.5
total	100µl

Table 7 TOPO recombination reaction.

component	Volume (µl)	
H_2O	-	-
Fresh PCR product	1.5 µl	3 µl
Salt Solution	1 µl	1 µl
TOPO® vector	2.5 µl	1 µl
total	6µl	6µl

2.3.3 Bacterial transformation

TOP10 and BL21 Escherichia coli cells were employed in plasmid DNA preparation and protein preparation, respectively. The competent cells (50 µl) were thawed on ice for 5 minutes before adding 100 ng of plasmid DNA. Following a 20-minutes incubation on ice, the cells were heat shocked for 60 seconds in a 42°C water bath. Cells were then placed on ice for 2 minutes. SOC media (350 µl) was added to cells followed by shaking at 245 rpm for 1 hour at 37°C. Reactions were plated on LB agar plates with an antibiotic selection marker and incubated at 37°C overnight.

For a typical colony screening, 12-24 clones were picked and each inoculated into 5 ml of LB broth + antibiotic and grown shaking at 245 rpm at 37°C overnight. Plasmid DNA was isolated using a Qiagen MiniPrep kit. After a first test based on double restriction digest, positive colonies were sent for sequencing to a DNA sequencing facility (MRC-PPU, Dundee).

For glycerol stocks, the original cultures from colonies containing positively evaluated plasmids were inoculated in 5 ml antibiotic supplemented LB broth for overnight culture. After 16-18 hours, the cultures were pelleted at 4400 rpm and the pellet resuspended in 40% glycerol/LB broth and stored at -80°C.

2.3.4 Restriction digest

Typically, restriction digests were used to screen plasmids for the insert of interest or as a reaction to produce sticky ends to subclone DNA into the desired vector. For digests, 1 µg DNA was incubated with the selected restriction enzymes in NEB CutSmart buffer for at least 90 minutes at 37 °C. An undigested plasmid was run alongside restriction digests on a gel to serve as a negative control.

2.3.5 agarose gel electrophoresis

Agarose gel electrophoresis was always carried out in 1% agarose gels in TAE buffer. Agarose was dissolved by heating the solution in a microwave, the gel was left to cool before addition of SYBR Safe DNA gel stain (1x). The gels were poured in a sealed cassette and left to set. DNA samples were diluted in 6X loading buffer prior to loading in horizontal midi electrophoresis tank (Fisher Scientific) in TAE buffer at 120V for 45 minutes.

2.4 Biochemistry

2.4.1 Reagents

2-mercaptoethanol (#M6250), Bovine IgG (immunoglobulin G), Ponceau S stain (#P7170), Goat Serum Donor Herd (#G6767),

mammalian protease inhibitor (#P8340), (±)-6-Hydroxy-2,5,7,8-tetramethylchromane-2-carboxylic acid (Trolox) (#238813), biotin-phenol (#SML2135), Sodium L-ascorbate (#A-7631) and biotin (#B4501) were obtained from Sigma-Aldrich (Poole, UK). Marvel skimmed milk powder was ordered from Premier Brands, UK. BCA protein assay kit (#23225) was ordered from Pierce Biotechnology (Rockford, IL, USA). Nu-PAGE Bis-Tris 4-12% gels (#NP0321BOX) as well as NuPAGE MOPS and MES running buffers, SimplyBlue SafeStain (#LC6060), DAPI (4'6-Diamidino-2-Phenylindole Dihydrochloride) (#D1306) were purchased from Invitrogen (Paisley, UK). Amersham Protran 0.45 µm nitrocellulose membrane (#10600002). PD-10 Columns (GE17-0851-01), IPTG (#I6758), Lysozyme (#1052810001), DNase (#DN25), Protease inhibitor cocktail powder (#P8465), and Mowiol (#475904) were purchased from Merck Millipore (Darmstadt, Germany). Pre-stained broad range molecular weight marker (#P7708S) as well as unstained broad range marker (#P7704) were ordered from New England Biolabs (NEB) (Hitchin,UK). Bovine serum albumin (BSA, #40-00-410) was purchased from First Link (UK). BL21 BirA-transformed E. coli cells BL21(DE3) cells (tebu-bio #27462). Streptavidin agarose beads (cat. #S1638, Sigma) and 2-chloroacetamide (CAA) were purchased from Sigma. Nano-Glo® Luciferase Assay System catalogue (#N1110) was purchased from Promega. Ni NTA agarose (#30210) beads were purchased from Qiagen. Sodium Azide (#AA14314-22) was bought from VWR (Leicestershire, UK).

2.4.2 Cell lysis

For cell lysis, cells were seeded in 6-well plates for lysis unless used for proteomics, whereby 15cm^2 dishes were used. Cells were washed three times with ice-cold PBS. Cells were lysed with of either NP-40 (0.5% NP-40, 25mM Tris pH 7.5, 100mM NaCl, 50mM NaF), high-stringency RIPA (500mM NaCl, 50mM Tris-HCl pH 7.5, 0.1% sodium deoxycholate, 1mM EDTA, 1% NP-40) or TUBES buffer (20mN sodium phosphate pH 7.4, 1% NP-40) supplemented with phosphatase inhibitors and mammalian protein inhibitors (1:250). HS-

RIPA lysis buffer was always supplemented with 50mM 2-chloroacetamide (CAA) directly added to the buffer as a powder to inhibit ubiquitylation and de-ubiquitylation while NP-40 was supplemented with 20mM NEM (N-ethyl maleimide) prepared in DMSO where indicated (**Figure 5.3**). The plates were rocked for 10 minutes, lysates were collected in conical tubes and centrifuged at 14,000 rpm for 15 minutes to remove debris and transferred to a fresh tube.

2.4.3 Protein lysates sample preparation

Protein concentration of cell lysates was typically determined by BCA protein assay kit. A standard curve was generated using a bovine IgG standard in duplicate. Reagent A and B from the BCA kit were mixed in a 50:1 ratio in 96-well plates and incubated a 37°C for 30 minutes prior to absorbance detection at OD_{562} using a Thermo Labsystems Multiskan Spectrum plate reader samples were assayed in triplicate. After determining the protein concentrations. Samples were diluted to the same protein concentrations in lysis buffer and in 5x sample buffer (312.5mM Tris-HCl, pH6.8, 15% w/v SDS, 50% w/v glycerol, 16% w/w 2-Mercaptoethanol, 0.05% w/v Bromophenol Blue) to 1x final concentration before heating them at 95°C for 5 minutes.

2.4.4 Sodium Dodecyl Sulphate Polyacrylamide gel electrophoresis (SDS-PAGE) and Western Blotting

Protein lysates were loaded onto a 4-12% Bis-Tris precast NuPAGE gel run in 1x MES or MOPS buffer. Gels were run at 150V for 90 minutes. For western blotting, proteins were transferred onto a nitrocellulose membrane in transfer buffer (3.03g Tris, 14.4g Gly, 200ml methanol, topped up to 1L with distilled H20) at a constant current 1A, 25V for 2 hours on ice or 1 hour at room temperature. Membranes were incubated in blocking buffer for 1h at RT either in 5% Marvel milk powder/ TBS-T (0.1% w/v Tween20) or in 5% bovine serum albumin (BSA)/ TBS-T. The conditions for primary antibody use are reported in **Table 8**. Membranes were washed three times for 5 minutes in TBS-T and then incubated with secondary antibodies. After a further three washes in TBS-T for 5 minutes, the membranes

were imaged by an Odyssey (LI-COR) scanner. Molecular weight marker position shown on all western blots in this thesis are in kDa. Conditions used for secondary antibodies are in **Table 9**.

Table 8 Primary Antibodies used for western blot.

Primary antibody	Species	Catalogue No.	Conditions
ATP6-V0D	Mouse	Abcam, ab56441	1:2000, o/n, 4°C
AMSH	Rabbit	Home-made, 850-3	1:1000, 1h, RT
GFP	Sheep	Home-made, SK3493	1:1000, 1h, RT
USP8	Sheep	R&D systems, AF7735	1:500, 2h, RT
AMSH-LP	Rabbit	Home-made, U10	1:400, 2h, RT
ALIX	Mouse	Santa Cruz, sc-53540	1:500, 1h, RT
Syntenin1	Mouse	Abnova-Biotechne, H00006386-B01P	1:1000, 1h, RT
EGFR	Rabbit	Cell Signalling Technolog 4267	1:1000, o/n, 4°C
K63-ubiquitin	Rabbit	Millipore (Sigma), #05-1308	1:1000, 1h, RT
VU1(ubiqu n)	Mouse	Life sensors, VU101	1:2000, o/n, 4°C
CD63	Mouse	Novus Biologicals, NBP 42225SS	1:500, o/n, 4°C
HRS	Rabbit	Abcam, ab 155539	1:1000, o/n, 4°C
STAM1	Rabbit	Abcam, ab 155527	1:1000, o/n, 4°C
STAM2	Rabbit	Abcam, ab151545	1:1000, o/n, 4°C
Actin	Mouse	Proteintech, 66009-1-Ig	1:10000, 1 hr, RT
Actin	Rabbit	Proteintech, 20536-1-AP	1:10000, 1 hr, RT
VPS26	Rabbit	Abcam ab23892	1:400, o/n 4°C
HA	Mouse	Covance, MMS-101P	1:1000, 1 hr, RT
FLAG	Mouse	Sigma (#F4725)	1:1000, o/n, 4°C
Ubiquitin	Rabbit	#U5379, sigma,	1:1000 o/n, 4°C

Table 9 Secondary antibodies used for western blot.

Secondary Antibody	Catalogue No.	Incubation conditions
Donkey anti-mouse IR Dye 800CW	LI-COR (926-32212)	1:10,000, 1 hr, RT
Donkey anti-mouse IR Dye 680CW	LI-COR (926-32222)	1:10,000, 1 hr, RT
Donkey anti-rabbit IR Dye 800CW	LI-COR (926-32213)	1:10,000, 1 hr, RT
Donkey anti-rabbit IR Dye 680CW	LI-COR (926-32223)	1:10,000, 1 hr, RT
Donkey anti-goat IR Dye 800CW	LI-COR (925-32214)	1:10,000, 1 hr, RT
Donkey anti-sheep IR Dye 680CW	LI-COR (92632224)	1:10,000, 1 hr, RT
Goat anti-rat IR Dye 800CW	LI-COR (926-32219)	1:10,000, 1 hr, RT
IRDye 800CW Streptavidin	LI-COR (C41209-03)	1:10,000 1 hr, RT

2.4.5 Membrane-cytoplasm fractionation

Membrane fractionation was performed to separate membranes from the cytoplasmic sub-cellular compartment. Typically, a single 15 cm^2 confluent dish of cells per condition was used. The cells were scraped in PBS, collected in conical tubes and pelleted at 200 g for 4 minutes in the cold. Pellets were washed in HIM buffer (200 mM Mannitol, 70 mM sucrose, 1 mM EGTA, 10 mM HEPES, pH 7.5) and supplemented with mammalian protease inhibitor cocktail (1:250) and phosphatase inhibitors.

Cells were homogenised by passing through a 23-gauge needle 6-7 times to break the plasma membrane. The homogenate was spun at 500 g for 10 minutes to pellet the nuclear fraction. The nuclei were discarded and excluded from the analysis while the post-nuclear supernatant (PNS) was collected for analysis. A small volume 1/6 of the total PNS was kept for western blotting, while the rest of the PNS

volume was spun at 100, 000g in an ultracentrifuge for 30 minutes. The supernatant (cytoplasmic fraction) was collected for western blotting. The pellets were washed in HIM buffer and then resuspended in 20% of the total homogenization volume in HIM buffer supplemented with MPIs and phosphatase inhibitors.

2.4.6 Exosome enrichment by ultracentrifugation

This protocol is adapted from a previously published paper (Edgar J R, 2016). For exosome enrichment by ultracentrifugation, 1.5 x 10^8 cells were seeded in square 245x245 mm dishes. The cells were treated with 100µM Bafilomycin A1 in media with NEAA but without FBS. After 16 hours, the supernatant media was removed from the plate and spun at 300 g for 10 minutes in the cold. The pellets were discarded, and the supernatant was again spun at 2000 g for 10 minutes in the cold. To remove large vesicles, the supernatant was ultracentrifuged in a 50.2 Ti fixed-angle rotor of a Beckman coulter ultracentrifuge for 30 minutes. The supernatant was removed and ultracentrifuged at 100,000 g for 70 minutes. The membrane pellets were gently washed in PBS and then resuspended in an equal volume of PBS. The resuspended exosome-enriched fractions were diluted in 5x non-reducing sample buffer and heated at 56°C for 5 minutes. The whole volume of each sample was loaded onto 4-12% Nu-PAGE gels for western blotting.

2.4.7 Immunofluorescence

For immunofluorescence, 2x10^5 cells were typically seeded onto 22x22 mm glass coverslips in 9.6 cm^2 wells of a 6-well plates at day 1. Cells were washed in room temperature PBS prior to fixation in 4% paraformaldehyde (PFA) for 15-20 minutes. After a round of 3 PBS washes, fixed cells were quenched with a 50mM NH_4Cl (ammonium chloride) for 10minutes. The cells were permeabilised with 0.2% Triton x-100 for 4 minutes and quenched with 50 mM NH_4Cl for 10 minutes. After additional washes, more often the coverslips were blocked in 10% Goat serum in PBS for 30 minutes, unless otherwise stated. Coverslips were washed and stained with the relevant primary

antibody in 5% goat serum (for conditions see **Table 10**). Then after additional washes, a secondary antibody was incubated onto the coverslips in 5% goat serum (**Table 11**). After further washing in PBS, the coverslips were dipped in millipore H_2O and mounted onto glass slides using Mowiol with 1:5000 DAPI.

Table 10 primary antibodies used for immunofluorescence.

Target	Species	Catalogue No.	Incubation Conditions
AMSH	Rabbit	Home-made, 850-3	PFA, 1:2000, 1h
K63-ubiquitin	Rabbit	Millipore (Sigma), #05-1308	PFA, 1:500, 1h
CD63	Mouse	Novus Biologicals, NBP2-42225SS	PFA, 1:500, 1h
HRS	Rabbit	Home-made 958-3	PFA 1:1000, 1h
HA	Mouse	Covance, MMS-101P	PFA 1:500, 1 hr
FLAG	Mouse	Sigma (#F4725)	PFA 1:250, 1 hr
EEA1	Mouse	Home-made, 243-4	PFA 1:250, 1 hr
LAMP1	Mouse	DSHB Iowa, ID4B	PFA 1:100, 1 hr

Table 11 Secondary antibodies used for immunofluorescence.

Secondary Antibody	Catalogue No.	Incubation
Donkey AF488 anti-mouse	Invitrogen, A21202	1:500
Donkey AF594 anti-mouse	Invitrogen, A21203	1:500
Donkey AF488 anti-rabbit	Invitrogen, A21206	1:500
Donkey AF594 anti-rabbit	Invitrogen, A21207	1:500

Donkey AF594 anti-sheep	Invitrogen, A11016	1:500
Donkey AF647 anti-rat	Invitrogen A21247	1:500

2.4.8 Methods for quantification of fluorescence intensity

The image analysis for immunofluorescence was carried out using Fiji/ImageJ program. Cell outlines were manually traced using the Freehand Selection Tool and quantification of the corrected total cell fluorescence (CTCF) was calculated with the formula CTCF: (IntDen of considered cell - Average of 3 background measurements) X area of considered cell. The single cell measurements were usually plotted as dot plots showing the average and standard deviation (SD).

2.4.9 K63-SUB production and isolation

2.4.10 Biotinylating-competent bacterial system

K63-SUB/K63-Superbinder protein was used in this thesis to enrich mammalian cell lysates for K63Ub, as it is a high-affinity binder of these type of chains. In brief, K63-SUB was produced in the Strain BL21(DE3) that is a chemically competent E. coli B strain, containing an IPTG-inducible BirA expression plasmid and constitutively expressed streptomycin/spectinomycin resistance gene.

Upstream of the UIM, there is a so-called Bioease moiety (AviTag, industrial name) which is readily biotinylated in the BL21 (DE3) bacteria. To isolate the K63-SUB protein, the 6x His moiety at the N-terminus of the protein was used as described below.

2.4.11 K63-Superbinder (K63-SUB) protein production and isolation

The plasmid encoding K63-SUB was provided by the group of Niels Mailand (University of Copenhagen). The pET104Dest (BioEASE-SuperK63-6xHis) plasmid contains the 3X in-tandem repeated UIM domain from the transcription factor protein Rap80. K63-SUB was

reported to bind to K63-linked di-ubiquitin efficiently and specifically (Thorslund et al., 2015a).

Chemically competent BL21 BirA-transformed E. coli cells BL21(DE3) cells were transformed with 50ng of the pET104Dest (BioEASE-SuperK63-6xHis) and the protocol for transformation was followed as described earlier. After starting a 5 ml culture in LB broth supplemented with spectinomycin and ampicillin, the following day the culture was scaled to a 500 ml at a 1:100 dilution. The culture was left to grow in a shaker at 37°C for 2 hours. The optical density (OD) was continuously checked until it reached the OD_{600} value of 0.8. A pre-induction sample was taken at this point. After 1 hour, protein expression was induced by the addition of IPTG (0.5 mM) alongside the addition of Biotin (0.5 mM). Culture was left to cool down at 4°C for 1 hour. After 1 hour, protein expression was induced with IPTG (0.5 mM) and biotin (0.5 mM). Culture was left to shake overnight at 16°C. After 18 hours, samples were pelleted in the Jouan centrifuge at 4 degrees at 4500 rpm for 15 mins.

Supernatant was removed and the pellet washed 1X in ice cold PBS (30ml). Resuspended pellet was transferred into a new tube and spun down as above. Pellets were washed in PBS and transferred to a fresh tube and lysed in 15 ml of lysis buffer (50 mM Na Phosphate pH 7.5 + 150 mM NaCl, 10 mM Imidazole,0.5 mM DTT, 0.5 mg/ml lysozyme, 10 µg/ml DNase and 1:500 bacterial protease inhibitors). Once fully resuspended, the lysate was left on ice for 30 mins, inverting the tube regularly. After 30 mins, the pellet was sonicated 8X 20 seconds at max voltage with 20 seconds rest between bursts.

A sample of the full lysate was taken (100 µl). The lysate was weighed into ultracentrifuge tubes and spun at 100,000 g for 30 mins in an ultracentrifuge using the S80AT3 rotor. After the spin, the supernatant from each tube was collected and combined. A sample of the supernatant was collected (100 µl). The supernatant was filtered through a 0.2 µm button filter before being added to the washed beads.

Ni^{2+} NTA agarose beads 1ml (2 ml of 50% slurry) were washed in 10 volumes of elution buffer, followed by 2 x 10 volumes of binding buffer (50 mM Na Phosphate + 150 mM NaCl, 10 mM Imidazole, 0.5 mM DTT). The beads were then resuspended and then pelleted at 1000 g for 3 mins.

Beads and supernatant were spun together on a wheel in the cold room for 2 hours. After 2 hours, the beads were pelleted at 1000 g for 3 mins. Flow through was collected and a sample taken (100 µl). Beads were washed in 10 volumes of washing buffer (50 mM Na Phosphate, 150 mM NaCl, 30 mM imidazole, 0.5 mM DTT (200 µl 100 mM). A sample of each wash was taken (1 ml). K63-SUB was then eluted in 4 elutions, whereby 1.5 ml of elution buffer was used per elution. Elution buffer was added, and the beads were spun on a wheel at RT for 10 mins. Beads were pelleted, the elution was collected, and a second elution added to spin for 10 mins. This process was repeated 4 times. Once all elutions were collected, a sample of each was taken for a gel (20 µl), then they were pooled together.

2X PD10 columns were equilibrated with exchange buffer (50 mM Na-phosphate pH = 7.5, 150 mM NaCl, 5% glycerol, 0.5 mM DTT). The lid was removed with forceps and the preservative was poured. 4X 5ml of exchange buffer through the column by gravity.

A fifth wash was added and spun through the column at 1000 g for 2 mins. 2.5 ml of sample was applied to each column and spun through as before to remove imidazole and exchange buffers for storage. Exchanges were then pooled and a 660nm assay carried out. After the concentration of the K63-SUB protein was determined, it was aliquoted and frozen in liquid Nitrogen.

For the pre and post induction gel, the pre and post induction samples were spun in a table-top centrifuge at 4500 rpm for 5 mins to pellet bacteria. Supernatant was removed. Pellet was resuspended in 80 µl PBS + 20 µl of 5X sample buffer. Pellets were transferred to threaded vials and boiled at 98°C for 15 mins, vortexing every 3 mins. After 15 mins, samples were spun for 10 mins at full speed in a

tabletop centrifuge. Pre-induction, post-induction, supernatant, flow-through, washes and elutions were loaded onto a 4-12% Nu-PAGE gel was then loaded and run in MES buffer. The gel was stained for 45 minutes in Simply Blue stain before destaining in distilled water and was scanned on the Odyssey the following day.

2.4.12 Test of different bead supports for K63-ubiquitin pull-down on synthetic tetra-ubiquitin chains.

Avidin, Neutravidin and Streptavidin (Thermo-fisher #20219 and #29202; Sigma, #S1638) beads were prepared for pull down overnight. 10 µl of Avidin and Neutravidin beads (20 µl of a 50% slurry) and 20 µl of Streptavidin beads (40 µl of a 50% slurry) were washed 3X in TUBES lysis buffer (100mM Sodium phosphate pH 7.4, 1% NP-40). The beads were resuspended in 250 µl TUBES lysis buffer and conjugated to 5 µg of K63-SUB protein per 10 µl of beads by rotating on a wheel overnight in the cold. Beads were collected and washed 3X in TUBES lysis buffer. 10 µl of nanotag beads (hybrigenics/nanotag technologies, #N1910,) were also washed 3X in TUBES lysis buffer to compare our home-made beads with the commercial alternative.

The beads were tested on a master mix of synthetic tetra-ubiquitin chains K63(4) and K48(4) (Life sensors #SI-6304-0025, SI-4804-0025). The master mix was made up with 250 ng of each chain type per sample. Input was made up of 250 ng of each individual chain type in 10 µl for a single input. The beads were resuspended in 250 µl TUBES lysis buffer and 10 µl of master-mix added to all samples (except mock). Samples spun for 2 hours in the cold room on a wheel. Samples were collected and beads pelleted. After being washed 3X in TUBES lysis buffer, the beads were then dried and diluted in 20 µl of 2X sample buffer. Samples were then boiled at 95°C for 5 mins.

All samples and inputs were loaded onto a 4-12% Nu-PAGE gel in MOPS. The proteins were transferred onto a nitrocellulose membrane that was then boiled for 1h at room temperature. The membrane was

blocked with 0.1% fish-skin gelatin in TBS-T and was first incubated with a total ubiquitin primary antibody (Sigma, #U5379) prior to secondary antibody incubation and scanning on the Odyssey.

2.4.13 Biotin-Streptavidin pull-down for K63-ubiquitin enrichment

For a typical pull-down experiment, HeLa GFP-HRS FlpIN parental, AMSH KO3 and KO4 cells were kept in culture for 48h and lysed in high-stringency RIPA buffer (HS-RIPA) supplemented with 50 mM of CAA, phosphatase inhibitors and mammalian protease inhibitors.

K63-SUB protein (17.6µg) was incubated with 10µl (50% slurry) of Streptavidin agarose beads for 1h on a rotating wheel in the cold. Then the K63-SUB conjugated beads were incubated with the total cell lysate. In all biological repeats a fixed ratio of 125ng of K63-SUB per 125µg of total cell lysates was used per pull-down. For SILAC proteomics experiments, 5mg total lysate of each condition (parental, KO3 and KO4) were pooled to a total 15mg. The mix was incubated with 15µg of K63-SUB and 20µl of streptavidin agarose beads (50% slurry) for 4h on a rotating wheel in the cold. Then the beads were washed with the HS-RIPA lysis buffer devoid of inhibitors, then washed with 10mM Tris-HCl and eluted with a mix of DTT that was freshly added to non-reducing sample buffer on the elutions. The samples were left shaking for 10min at room temperature.

Reduction of the eluate was achieved with 10mM DTT 10min at 70°C. Alkylation was achieved with 55 mM CAA at RT for 1h in the shaker. The sample was then loaded onto a 4-12% Nu-PAGE gel and cut into 12 slices for peptide preparation (as described in the Mass Spectrometry section below).

2.5 Mass Spectrometry

The peptides from the 4 repeats of the K63-ubiquitin related proteome were obtained in Liverpool. Peptides were then sent on dry ice to Leiden University Medical Center (LUMC), Leiden, The Netherlands to Alfred Vertegaal's group where the work in section 2.5.3 and 2.5.4 was carried out thanks to Dr. Fredrick Trulsson.

2.5.1 SILAC Reagents

L-Lys and L-Arg free DMEM (#D633) were purchased from DC biosciences and the FBS (#FB-1001D/500) was from Biosera (France). SILAC labelled media was supplemented with amino acids (Lys, #L8662; Arg, #A-8094; Pro, #P5607; Lys_4, #616192; Arg_6, #643440; Lys_8, #608041; Arg_{10}, #609033) and Iodoacetamide (IAA) (#T-6125) were purchased from Sigma-Aldrich, (Dorset, UK). Dithiothreitol (DTT) (#MB1015) was purchased from Melford biolaboratories (Suffolk, UK). Coomassie stain (#46-5034) was obtained from Invitrogen. LoBind Eppendorf tubes (#022431081) are from Eppendorf (Hamburg, Germany). HPLC grade water (#23595328), HPLC grade formic acid (#20318.297) and HPLC grade acetonitrile (ACN) (#20060320) were all bought from VWR (Leicestershire, UK). Mass spectrometry grade Trypsin Gold (#V5280) was purchased from Promega (WI, USA).

2.5.2 Stable isotope labelling by amino acids in cell culture (SILAC).

SILAC labelling consists of the incorporation of different isotopes of the amino acids Lys, Arg and Pro by cells (Pro-0 is added to prevent conversion of Arg isotopes to Pro). The different amino acids that will be included in the peptides of each cell line represent a distinguishable trace of the cell line that they belong to. HeLa GFP-HRS Flp-IN parental, AMSH KO3 and KO4 cell lines were grown in SILAC DMEM supplemented with 10% dialysed FBS and either “light”, “medium” or “heavy” amino acids for a minimum of 6 passages to incorporate the isotopes in their proteins. The isotope-supplemented media were: ‘Light’ (L-Lys, Lys-0; L-Arg, Arg-0; L-Pro, Pro-0), ‘Medium’ (L-Lys-$^{2}H_4$, Lys-4; L-Arg-$^{13}C_6$, Arg-6; L-Pro, Pro-0) and ‘Heavy’ (L-Lys-$^{2}H_6$-$^{15}N_2$, Lys-8; L-Arg-$^{13}C_6$-$^{15}N_2$, Arg-10; L-Pro, Pro-0). SILAC allows to estimate the exact amount of a specific peptide in different cell lines that are analysed by a Mass Spectrometer at the same time. This method confers the advantage of introducing minimal variability in each experiment and increased reproducibility of the results.

2.5.3 LC-MS (liquid chromatography-mass spectrometry) scan

Fractionated samples were run on an EASY-nLC 1000 system (Proxeon, Odense, Denmark) connected to a Q-Exactive Orbitrap (Thermo-fisher Scientific, Schwerte, Germany) through a nano-electrospray ion source. Peptides were separated in a 15 cm analytical column (MS Wil, Aarle-Rixtel, The Netherlands) with an inner-diameter of 75 µm, in-house packed with 1.8 µm C18 beads (Reprospher-DE, Pur, Dr. Manish, Ammerbuch-Entringen, Germany). The gradient was 90 min from 2% to 95% acetonitrile in 0.1% formic acid at a flow rate of 200 nL/minute. The acquisition mode was set to data-dependent mode. Full-scan MS spectra were acquired at a target value of $3e^6$ and a resolution of 70,000, and the higher-collisional dissociation (HCD) tandem mass spectra (MS/MS) were recorded at a target value of $1e^5$ and with a resolution of 17,500 with a normalized collision energy (NCE) of 25%. The maximum injection times for MS1 and MS2 were 20 ms and 60 ms, respectively. The precursor ion mass of scanned ions was dynamically excluded (DE) from MS/MS analysis for 60 s. Ions with charge 1, or greater than 6 were excluded from triggering MS2 events.

2.5.4 MS data processing and analysis for K63-ubiquitin proteomics

MS data files were analysed using MaxQuant (version 1.6.14) matching to the Uniprot Human Proteome (Reviewed human proteome downloaded from Uniprot on 29th of June 2020) with default settings of FDR and andromeda score filtering, matching to decoy database and common contaminants. Digestion was set to Trypsin digestion allowing maximum 4 missed cleavages. Normalization was done by LFQ (default settings) with matching between runs and matching unidentified features enabled. Cys carbamidomethylation was set as fixed modification and N-terminal acetylation, oxidation of Met and GlyGly modification on Lys (anywhere) were included as variable modifications.

2.6 Biotin-Streptavidin pull-down from Flag-APEX2-AMSH cells

2.6.1 Streptavidin-magnetic beads pull-down

This protocol was adapted from a previous paper by Alice Ting's group. HeLa Flag-APEX2-AMSH were incubated with warm media containing 500 µM biotin-phenol (BP) previously dissolved and warmed up for 5 min in a water bath at 37°C. After incubating the cells with BP for 30 min at 37°C, they were either left untreated or treated with 1 mM hydrogen peroxide (H_2O_2) in PBS for 1 minute at room temperature. The cells were then washed three times in quencher solution (10 mM Sodium azide, 10 mM Sodium ascorbate, 5 mM Trolox) in PBS. The cells were scraped, collected in quencher solution and pelleted by centrifugation at 500 g for 10 min in the cold. After removing the supernatant, the cell pellets were lysed in the eppendrof tube by reuspending them in RIPA lysis buffer supplemented with phosphatase and mammalian protease inhibitors. Debris were pelleted by centrifugation at 14,000 rpm in the cold for 15 min, the lysate concentration was determined by Pierce Assay. For the biotin streptavidin pull-down, Streptavidin magnetic beads (Pierce, #88817) were washed three times in RIPA buffer. After the washes, different amounts of protein lysate were incubated with a fixed volume of beads (15 µl) overnight in the cold on a rotating wheel. The beads were collected and washed twice in RIPA buffer, once in 1M KCl, once with 0.1 M Sodium carbonate (Na_2CO_3), once with 8M UREA in 10 mM Tris-HCl (pH = 8) and twice again with RIPA buffer. The biotinylated proteins were eluted in 3x sample buffer supplemented with 2 mM of free biotin and 20 mM DTT.

2.6.2 Streptavidin-Sepharose beads pull-down

This protocol was adapted from a previous paper by Alice Ting's group and suggestions from Dr. Gunnar Dittmar (Luxembourg Institute of Health).

HeLa Flag-APEX2-AMSH were incubated with warm media containing 500 µM biotin-phenol (BP) previously dissolved and

warmed up for 5 min in a water bath at 37°C. After incubating the cells with BP for 30 min at 37°C, they were washed twice in PBS for 1 min at room temperature. After the washes, the cells were treated with 0.5 mM hydrogen peroxide (H_2O_2) in PBS for 1 minute at room temperature. The cells were then washed three times in quenching solution (10 mM Sodium ascorbate, 10m M Sodium azide, 5 mM Trolox in PBS) for 5min each wash. The cells were then scraped and collected in quenching solution and pelleted for 10min at 3000 g in the cold. The pellets were lysed 0.1% sodium deoxycholate in 50 mM ammonium bicarbonate (AMBIC) buffer supplemented with mammalian protease inhibitors, sonicated 3 times at 5Watts power for 10seconds on ice. The lysates were spun in a Hitachi ultracentrifuge using a S55A-2233 rotor at 100,000g for 30 min in the cold. The cleared supernatant was collected, and the protein concentration was measured with a Pierce Assay. For the pull-down, 5µl of Streptavidin-Sepharose (GE healthcare, #17-5113-01) beads were first washed three times in 40% methanol and twice in the 0.1% sodium deoxycholate in 50 mM AMBIC lysis buffer. The beads were then incubated with different amounts of protein lysate on a rotating wheel at room temperature. After 1 h of incubation, the beads were washed once in 1 M KCl, once in 0.1 M Na_2CO_3, once in 2 M UREA in 50 mM AMBIC (pH = 8), twice in 50 mM AMBIC (pH = 8). The biotinylated proteins eluted with DTT, 2 mM free biotin in 3x sample buffer. The eluate was separated from the beads and the remaining beads were suspended in 10µl of sample buffer to be analysed alongside eluates.

Chapter 3: Generation of HeLa GFP-HRS AMSH KO cells

3.1 Introduction

AMSH is deubiquitylase that is highly specific for K63-linked ubiquitin chains and its depletion affects the downregulation kinetics of the EGFR (McCullough et al., 2004). Loss of AMSH causes a severe neurodevelopmental disorder called MIC-CAP syndrome in which patients show brain atrophy among a complex spectrum of other symptoms(McDonell et al., 2013). In addition, AMSH has been implicated in determining cancer cells invasiveness in the context of melanoma cells (Iwakami et al., 2018). To this day, a definite biological function has not been assigned to AMSH.

The aim of this chapter is to elucidate whether AMSH plays an active role in determining the endo-lysosomal fate of ubiquitylated cargo receptors. The ESCRT-0 components recruit ubiquitylated cargo receptors and reside at the endosomal membrane at AMSH positive microdomains, where STAM recruits AMSH to enhance its catalytic activity. For this reason, it will be important to investigate the link between AMSH loss and the ubiquitin landscape in the cell, to analyse the endosomal morphology and assess the levels of ESCRT-0 components. To this end, I used CRISPR-Cas9 to knock out AMSH in HeLa cells that stably overexpress GFP-HRS (ESCRT-0) to nearly endogenous levels. The advantage of having endosomes which are constitutively labelled with GFP-HRS, is to potentially distinguish them from other organelles by fluorescence microscopy and to adopt GFP-directed immunoprecipitation for their separation, in principle. A potential caveat in this approach is the possibility that the increased levels of HRS in these cell lines are already altering endosomal function. However, these GFP-HRS expressing cells lines, which were established by a former post-Doc Han Liu, express only twice the amount of HRS compared to the

parent HeLa cell line and have been successfully used in a previous study focused on USP8 and EGFR (MacDonald et al., 2018).

In this chapter, I will characterise AMSH knockout cell clones generated from parental HeLa S3 GFP-HRS Flp-In, analyse the K63-ubiquitin landscape and study potential perturbations of the endocytic compartments' structure and functionality.

3.2 AMSH deletion using CRISPR-Cas9

To delete AMSH in HeLa GFP-HRS Flp-In cells (MacDonald et al., 2018) by CRISPR-Cas9 technology, the cells were transfected with the pU6-(BbsI)-CBh-Cas9-T2A-mCherry plasmid containing AMSH-targeting sgRNAs, Cas9 and mCherry that are transcribed into a single mRNA and then cleaved post-translationally into two peptides thanks to self-cleavage of the T2A peptide. The sgRNA1, sgRNA3 and sgRNA4 were introduced into the pU6-(BbsI)-CBh-Cas9-T2A-mCherry plasmid. The sgRNA1, sgRNA3 and sgRNA4 target exons 2, 7 and 8 within the AMSH genomic locus, respectively (**Figure 3.1A**). AMSH protein harbours an N-terminal MIT (microtubule-interacting domain) which mediates its interaction with ESCRT-III proteins, a clathrin interacting region, a STAM binding motif and a C-terminal JAMM catalytic domain, (**Figure 3.1B**) (Dupré et al., 2001; McCullough et al., 2004; McCullough et al., 2006; Nakamura et al., 2006).

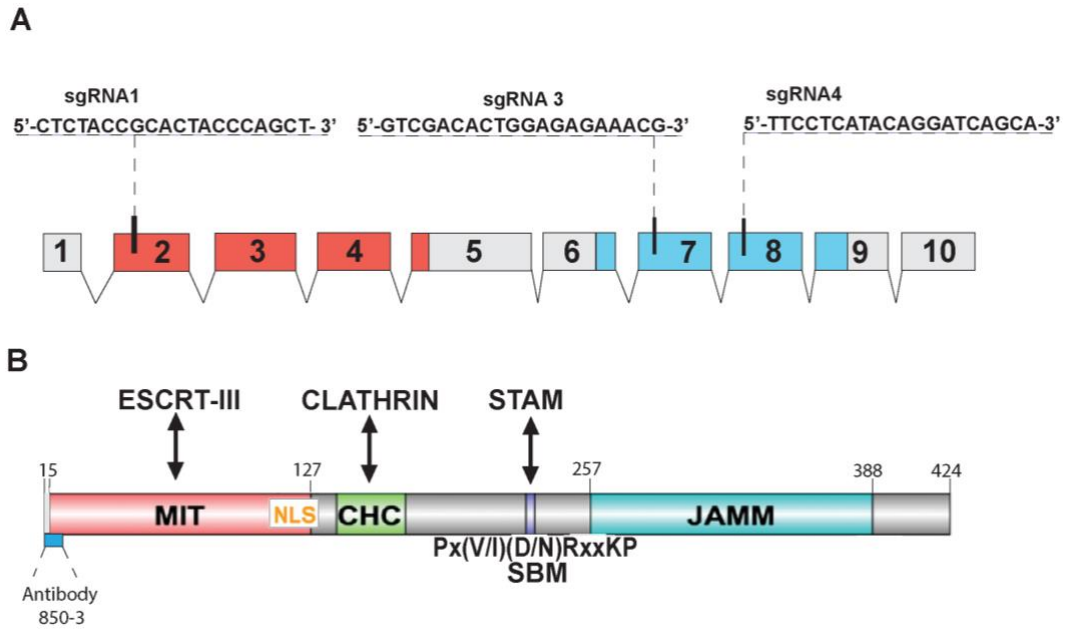

Figure 3.1 sgRNAs targeting AMSH gene and mapping to protein domains.
Exon-intron boundaries of the AMSH gene (gene ID: 10617). The genomic positions targeted by the sgRNAs are indicated A. AMSH protein domain boundaries reflect the annotation in Uniprot. MIT, Microtubule-interacting motif (Uniprot); NLS, nuclear localisation signal; CHC, Clathrin heavy chain interacting motif; SBM, STAM binding motif; JAMM is the JAB1/MPN/MOV34 metalloenzyme domain. The epitope recognised by the polyclonal rabbit antibody (850-3) is also indicated B (McCullough et al., 2004).

At 24 h post-transfection, the cells were sorted by fluorescence-activated cell sorting (FACS) based on dual GFP (HRS) and mCherry (sgRNA) positivity.

Firstly, total cell lysates were produced from the pooled population of sgRNA4-transfected cells. Western Blot analysis showed that AMSH was successfully knocked out and the protein was absent in the cell clone analysed. Furthermore, no compensatory change was observed in the AMSH paralogue AMSH-LP, nor in the other STAM and ESCRT-III interacting endosomal DUB USP8 (**Figure 3.2**).

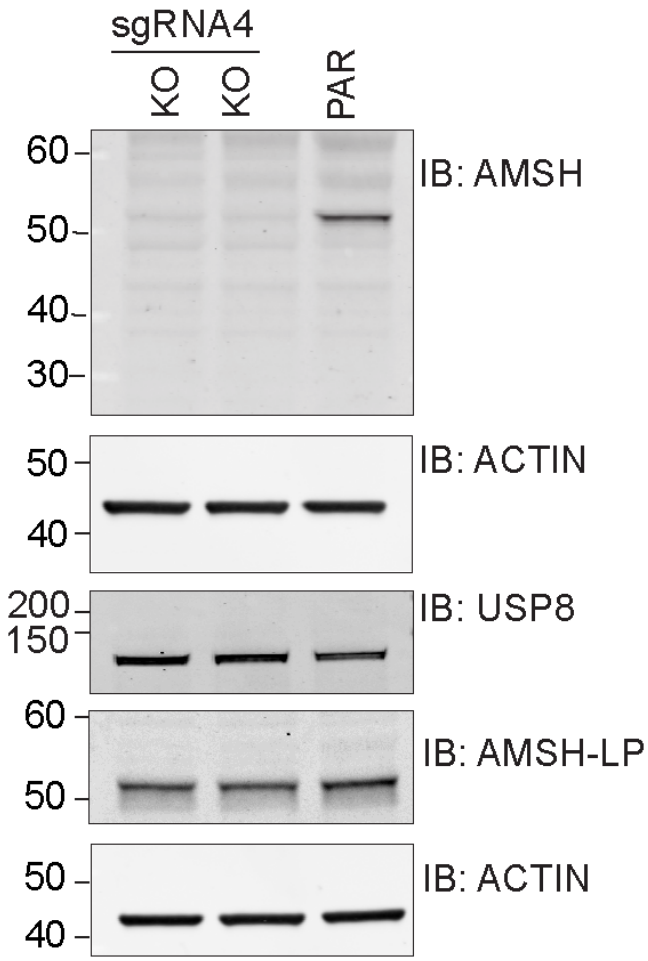

Figure 3.2 CRISPR-Cas9 mediated knockout of AMSH in GFP-HRS cell lines.
A pool of HeLa GFP-HRS FlpIN cells transfected with sgRNA4 were sorted by FACS sorted and lysed in NP-40 lysis buffer along with parentals. The lysates were run on an SDS-PAGE 4-12% gel. The membrane was blotted with AMSH, USP8, AMSH-LP and ACTIN antibodies. PAR: parental cell line (Hela GFP-HRS FlpIN); KO: knockout cells of which two replicate lysates of sgRNA4-transfected cell pools are shown. The membranes were cut and probed with the indicated antibodies. AMSH and AMSH-LP membranes were re-probed for ACTIN.

Then the experiment was repeated with further sgRNA1 and sgRNA3 targeting the exon 2 and exon 7, respectively. The sgRNA-transfected HeLa GFP-HRS cells were sorted as singlets, thus ~30 single AMSH KO clones were kept in culture, lysed, and screened by Western Blot to assess the knockout by blotting for AMSH protein. Out of ~30 clones checked, more than 20 were positive for the knockout (negative for AMSH protein expression) (**Figure 3.3**).

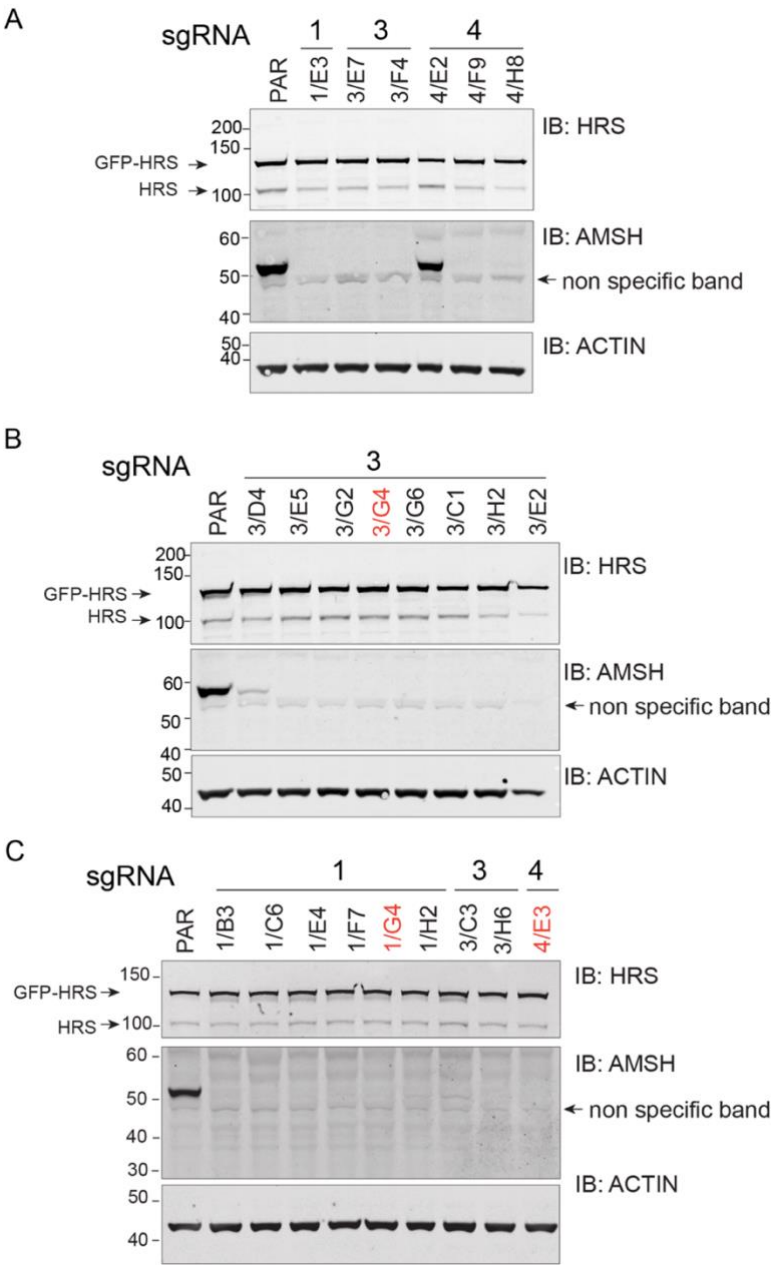

Figure 3.3 Screening of HeLa GFP-HRS Flp-IN AMSH knockout cell clones.

A-C HeLa GFP-HRS Flp-In cells were transfected with the indicated sgRNA, and single cell-derived clones were subsequently screened by Western blot for AMSH and GFP-HRS expression. Clones highlighted in red are positive knockout clones which were selected for further study. These will be subsequently referred to as KO1 (1/G4), KO3 (3/G4) and KO4 (4/E3). The membranes were cut and probed with the indicated antibodies. AMSH membrane was re-probed for ACTIN.

3.3 Characterisation of HeLa GFP-HRS AMSH KO cells

AMSH KO clones 1B3, 1G4 derived from sgRNA1 transfection, sgRNA3 derived clone 3E5, 3G4 (KO3), and sgRNA4 derived clones 4E3 and 4F9

were sequenced across relevant exons. All clones apart from clones 3G4 and 4E3 presented either insertion or deletions in their genomes.

For KO1, sequencing revealed three different mutations, which may correspond to three distinct AMSH alleles, as HeLa cells are known to be polyploid. For AMSH KO3 and KO4 clones, I identified a single mutation which is a single amino acid insertion that in each case results in an early stop codon at L377 and L378 respectively. Both clones have frameshift mutations that result in early stop codons. If translated into protein, would result in a C-terminally truncated protein, and would differ from each other by one amino acid (3.1). If this truncated protein was expressed and stable, I would be able to detect it at 52kDa using our 580-3 antibody which recognises the MSDHGDVSLPPEDRV amino acid sequence at the amino terminal region (AA1 to 15) of AMSH. I could not detect any specific signal for AMSH, suggesting that the protein is rapidly degraded (**Figure 3.3**)

One clone of AMSH KO cells per sgRNA was selected for further analysis. The selected clones were called KO1 (1G4), KO3 (3G4) and KO4 (4E2) as short clone names to readily identify them, as shown in the table below (**Table 12**).

Table 12 Sequencing of KO1, KO3 and KO4 individual clones.
The genomic DNA of AMSH KO1, KO3 and KO4 cell clones was extracted and for every clone a PCR reaction was carried out to amplify the sgRNA targeted regions (exon 2 and exons 7/8, respectively). The PCR products were cloned in the pCR4-TOPO vector and sequenced, and multiple colonies selected for minipreps and sequencing. (Freq.) indicates the number of times a particular mutated allele was detected per minipreps sequenced with the T7 primer provided by the University of Dundee DNA sequencing facility.

Clone name	Short name	Targeted domain	Altered DNA sequence	Altered protein sequence	(Freq)
1B3	none	1 (MIT)	Δ59-71(13nt)	Δ20-33, RR 34-35 match, from 36 frameshift	1/6
1B3	none	1 (MIT)	Δ45-74 (30nt)	Δ16-25	4/6
1B3	none	1 (MIT)	InsT62	Early stop at G22	1/6

1G4	KO1	1 (MIT)	Δ45-66 (22nt)	Early stop at R17	2/4
1G4	KO1	1 (MIT)	Ins (97nt) at G63	Early stop at G46	1/4
1G4	KO1	1 (MIT)	Δ61-79 (19nt)	Early stop at Q20	1/4
3E5	none	3 (JAMM)	Ins A975	Early stop at L377	2/3
3E5	none	3 (JAMM)	Δ975-990 (16nt)	Early stop at R351	1/3
3G4	KO3	3 (JAMM)	Ins A975	Early stop at L377	3/3
4E3	KO4	4 (JAMM)	Ins T1030	Early stop L378	3/3
4F9	none	4 (JAMM)	Δ1027-1042 (16nt)	Early stop R351	1/2
4F9	none	4 (JAMM)	Ins T1030	Early stop L378	1/2

The cells were lysed in NP-40 lysis buffer to characterise them by Western Blotting (**Figure 3.4**). McCullough and colleagues established that AMSH depletion enhances EGF-dependent EGFR downregulation, while another group reported that AMSH localisation to the endosomal membrane via CHMP-III is a requirement for EGFR degradation (Bowers et al., 2006b; McCullough et al., 2004; M. M. Yu et al., 2006). I first checked EGFR steady state levels. EGFR levels were not affected in any of the analysed AMSH KO clones (KO1, KO3 and KO4) (**Figure 3.4**).

McCullough and colleagues had previously shown that a ubiquitylated species of STAM can be stabilised by expression of inactive AMSH (GFP-AMSH D348A)(McCullough et al., 2004) and that the knock down of USP8, another endosomal DUB, affects STAM stability(McCullough et al., 2006; Row et al., 2007). Therefore, I checked STAM2 levels to evaluate any possible effect of AMSH knock out upon STAM stability. The levels of STAM2 were unchanged in the AMSH KO cells lysates.

The levels of the AMSH paralogue AMSH-LP (STAMBPL), GFP-tagged and endogenous HTS were also unchanged in AMSH KO clones (**Figure 3.4**).

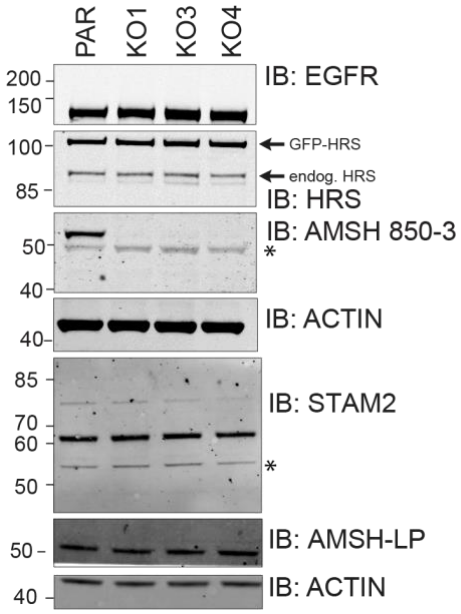

Figure 3.4 AMSH KO clones show no changes in EGFR, HRS, STAM2 and AMSH-LP expression levels.
HeLa GFP-HRS FlpIN Parental (PAR) and AMSH knockout clones generated using sgRNA1 (KO1), sgRNA3 (KO3) and sgRNA4 (KO4) were further analysed by Western blot for EGFR, HRS, AMSH, STAM2 and ACTIN. Cells were lysed in RIPA buffer. * Indicates non-specific band. The membranes were cut and probed with the indicated antibodies. AMSH membrane was re-probed for ACTIN. STAM2 membrane was cut in two pieces, then the upper part probed for AMSH-LP and the lower probed for ACTIN.

I next stained HeLa GFP-HRS Flp-In parental and AMSH clones with antibodies recognising common endosomal markers to check the morphology of these compartments. I noticed that AMSH KO1 cells presented with a rounder and smaller morphology than KO3 and KO4. For this reason, I have mainly focused on and characterised the endosomal morphology of AMSH KO3 and KO4 clones.

The Early endosome antigen 1 (EEA1) is commonly used as an early-endosome marker. The EEA1 signal partially co-localised with GFP-HRS endosomes in AMSH KO cells indicating a normal endosomal morphology similar to the parental cells (**Figure 3.5**).

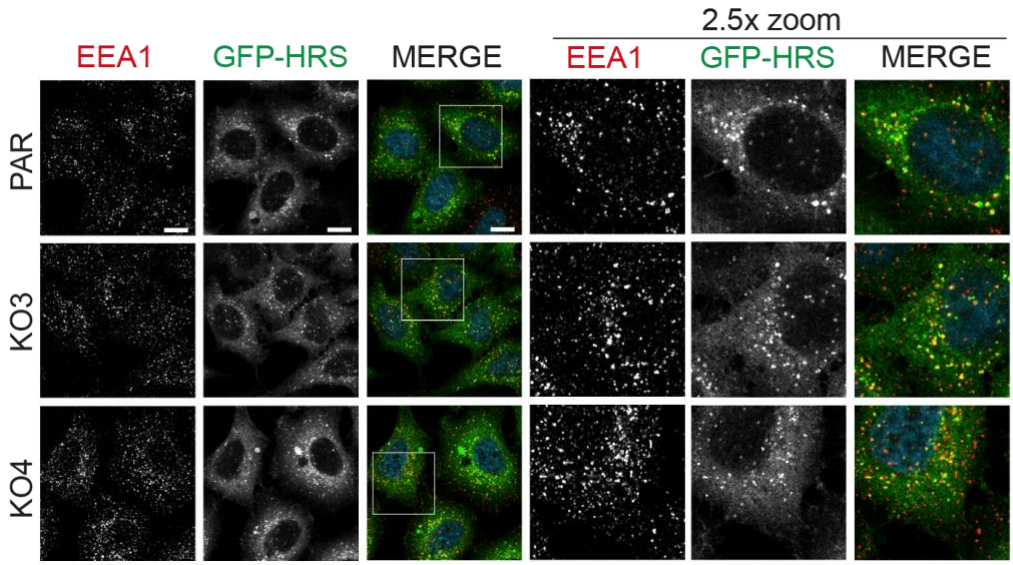

Figure 3.5 Early endosome morphology is unchanged in AMSH KO cells.
HeLa GFP-HRS Flp-In parental, AMSH KO3 and KO4 were fixed in 4% PFA/PBS, permeabilised and stained with the EEA1 antibody. The cells were imaged with an LSM 900 confocal microscope, 63x oil objective. Scalerbar = 10µm. Representative of 3 experiments. Blue = DAPI staining.

HeLa GFP-HRS Flp-In parental and KO cells were also stained for LAMP1 protein is a typical late endosome/lysosomal marker. The total cell fluorescence for LAMP1 was quantified and the intensity of LAMP1 puncta was quantified per cell. LAMP1 is normally expected to segregate from early endosomal markers, which in these cells are marked by the signal of the constitutively expressed GFP-HRS positive puncta. The results show that the GFP-HRS and LAMP1 still segregate in the AMSH KO3 and KO4. The size of the LAMP1 positive structures in the AMSH KOs looks similar to the parentals. (**Figure 3.6A**). A modest increase in the average of LAMP1-positive puncta per cell was apparent in both AMSH KO3 and KO4 compared to the parentals, but not significant, because of the large variability in the number of puncta in both AMSH KO clones.

In order to better appreciate the differences in late endosome abundance in parental and AMSH KO cells, I divided the cells into two categories: those with less than 30 and those with more than 30 LAMP1 puncta. The percentage of cells containing 0-30 and the other 31-80 LAMP1 puncta were divided into two categories. HeLa GFP-HRS parental and both AMSH KO cells have the same % of cells having 0-30 LAMP1 puncta. AMSH KO3 and KO4 contain many more cells having 31-80 LAMP1 puncta. On

average both KO clones have more cells falling in the 31-80 category, but only KO3 has statistically more LAMP1 puncta than the parental cells (**Figure 3.6 B-D**).

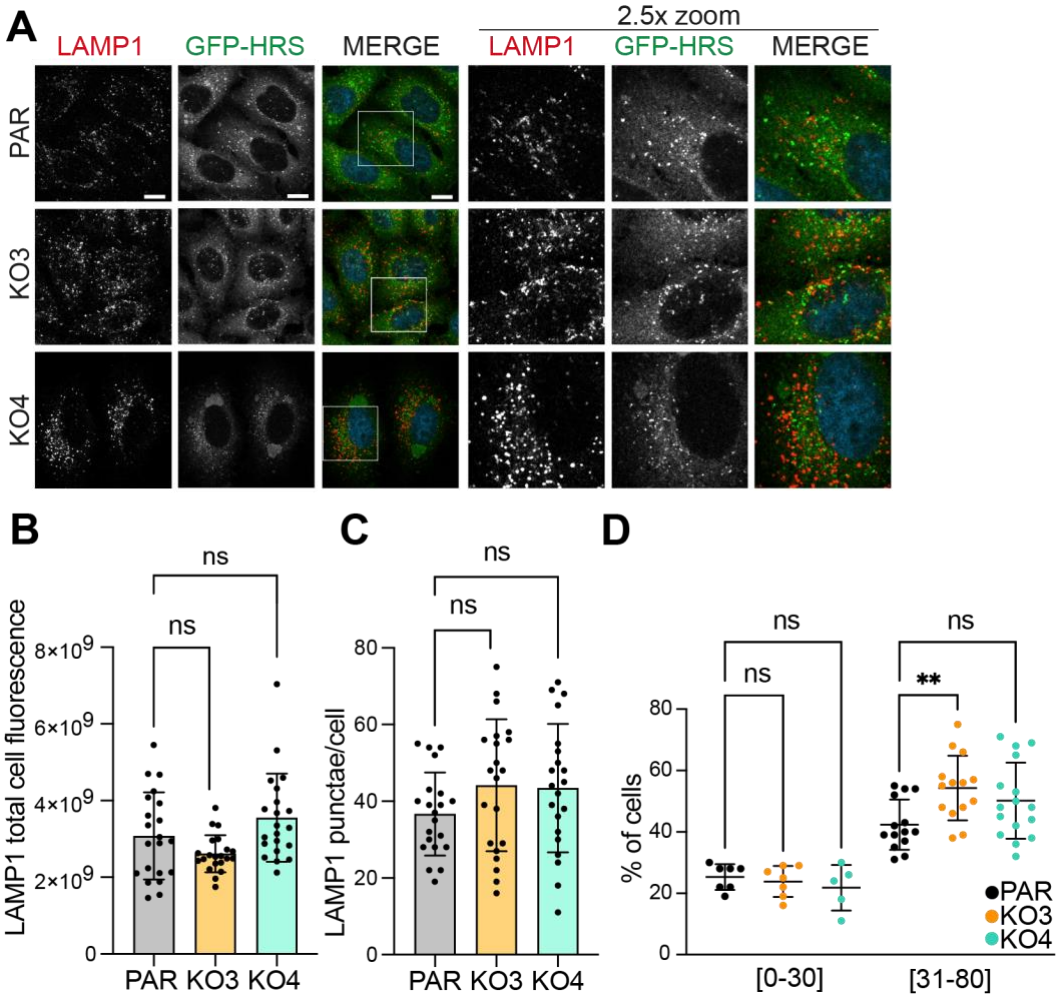

Figure 3.6 Analysis of LAMP1 positive endosomes in AMSH KO cell clones.
A HeLa GFP-HRS Flp-In parental, AMSH KO3 and KO4 were fixed in 4% PFA/PBS, permeabilised and stained with the LAMP1 antibody. The cells were imaged with an LSM 900 confocal microscope, 63x oil objective. Scalebar = 10µm. Blue = DAPI staining. **B-C** Twenty-one cells were analysed to quantify the total cell fluorescence and the number of puncta. D Cells categorised by the number of puncta. One-way Anova (Tukey test) was performed in B and Šidák test in C. In D plotted bars indicate the average and standard deviation n=1.

3.4 Analysis of the ESCRT-0 complex in AMSH KO cells.

Since the western blots incubated with anti-HRS and anti-STAM1/2 showed many background bands, I carried out a knock-down experiment to unequivocally identify the bands specific to HRS and STAM1/2 (**Figure 3.7**).

Bands for STAM1 were identified at ~62 kDa, and those for STAM2 at just below 50kDa, the specific STAM2 bands runs at ~62, ~52 and ~48kDa. I noted that STAM2 knock-down did not affect the levels of STAM1 or HRS, but intriguingly, the knockdown of STAM1 results in a decrease in the levels of endogenous HRS in both Parental and KO4 cells. HRS depletion did not affect the levels of either STAM1, nor STAM2 in AMSH KO4 and parental cells (**Figure 3.7**).

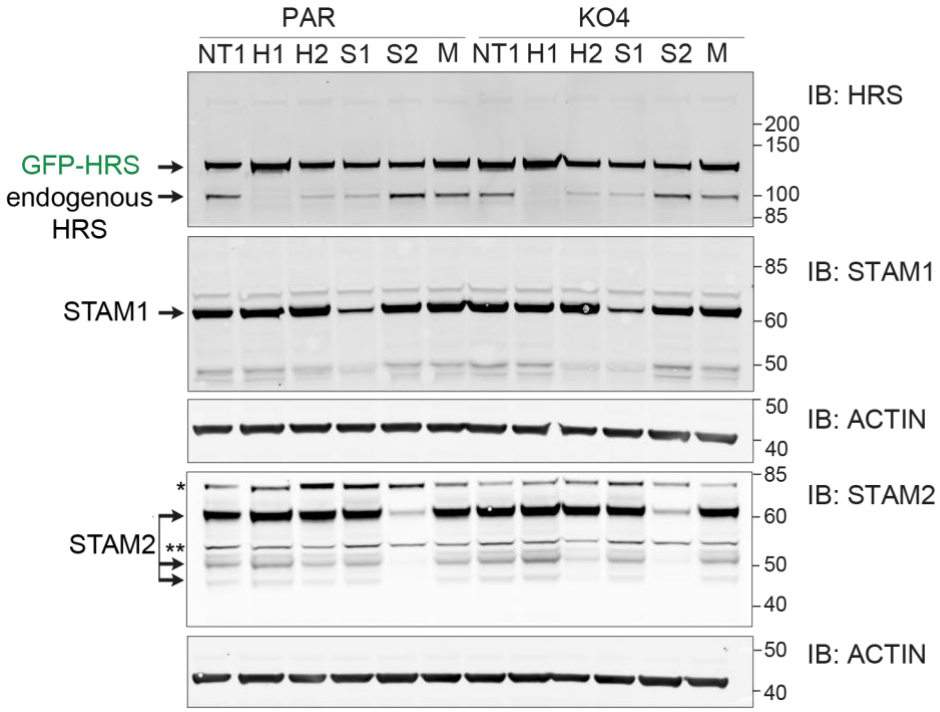

Figure 3.7 Knock-down of ESCRT-0 proteins identifies the specific WB bands for HRS, STAM1/2.
HeLa GPF-HRS Parental and AMSH KO4 were depleted for HRS, STAM1 and STAM2 using NT1 (non-targeting 1), H1 (HRS oligo1), H2 (HRS oligo 2), S1(STAM1) and S2 (STAM2) oligonucleotides, respectively. M (mock transfected). The total lysates were analysed by WB and the membranes were probed with the indicated antibodies. Representative of n=2. *, ** non-specific bands. The membranes were cut and probed with the indicated antibodies. HRS membrane was re-probed for STAM1 and STAM2 blot was re-probed for ACTIN. STAM2 membrane was re-probed for ACTIN.

AMSH uses its STAM-binding motif (SBM) to interact with STAM's SH3 domain at the endosomal membrane. This interaction induces the recruitment of AMSH and stimulates its catalytic activity at the endosomal membrane (McCullough et al., 2006). Conversely, I wanted to assess whether the recruitment of HRS and STAM at the endosome would be

affected by AMSH KO. To this end, I carried out the membrane-cytosol fractionation of HeLa GFP-HRS Parental and three AMSH KO cell clones. The distribution of STAM1 and STAM2 to the membrane fractions was unchanged in all AMSH knockouts. STAM1 and STAM2 are both evenly distributed between cytosol and membranes (**Figure 3.8**).

GFP-HRS is preferentially found in the cytosol, while the endogenous HRS is preferentially associated with the membranes (**Figure 3.8**).

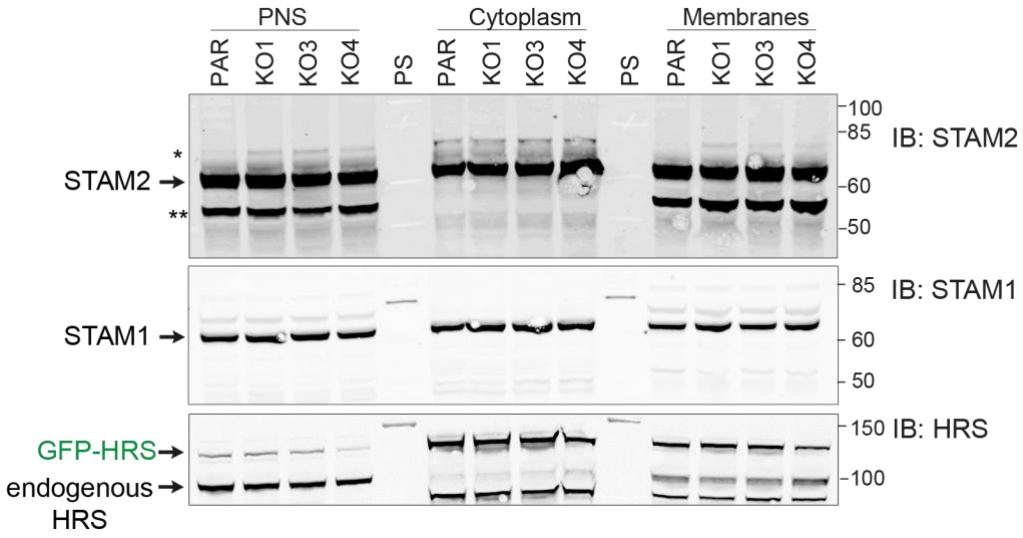

Figure 3.8 The membrane-cytosol distribution of ESCRT-0 proteins is unchanged in AMSH KO cells compared to parentals.
HeLa GFP-HRS Flp-In parental, AMSH KO1/3/4 were homogenised, and the post-nuclear supernatant (PNS) was fractionated to obtain membranes and cytosol. Equal amounts of protein from all fractions were resolved by WB and the membrane was probed with antibodies detecting ESCRT-0 components. * and ** are non-specific bands. PS = protein standard. The membranes were cut and probed with the indicated antibodies. HRS membrane was re-probed for STAM2. A separate membrane was probed for STAM1.

3.5 Ubiquitin chain analysis of AMSH KO cells.

As it was established by McCullough and others, AMSH is uniquely active towards K63-ubiquitin chains. These chains can be found at the endosomal membrane and this type of chains is thought to be the signal responsible for the degradation of the EGFR through the endo-lysosomal pathway (McCullough et al., 2004, 2006,Huang et al., 2013; Lauwers et al., 2009).

Ubiquitin-conjugated proteins have previously been shown to accumulate in MIC-CAP patients derived lymphoblastoid cell lines, AMSH-depleted

neuroblastoma cells as well as in the membrane fraction of AMSH KO mouse model brain cells (Ishii et al., 2001; McDonell et al., 2013). Therefore, I analysed the global abundance of both total ubiquitylated and K63-linked ubiquitylated proteins in cell lysates prepared from HeLa GFP-HRS Flp-In Parental, AMSH KOs (KO1, KO3 and KO4) by western blotting. The lysis buffer was supplemented, alongside protease and phosphatase inhibitors, with N-ethylmaleimide (NEM) to inhibit the DUB activity. For the total conjugated and un-conjugated ubiquitin, I employed the VU-1 antibody, while to detect K63-linked ubiquitin in the total cell lysates, I used the K63-ubiquitin rabbit monoclonal antibody (Millipore, #05-1308). AMSH KO and parental cell lysates displayed the same amount of K63-ubiquitin. Interestingly, in the K63-ubiquitin blot, a 70 kDa band present in both Parental and AMSH KO1 cells disappears in AMSH KO3 and KO4. I observed no obvious difference in total ubiquitin levels. I also noted that the K63-ubiquitin blot displayed several discrete bands from 15 to above 200kDa, while the total ubiquitin blot presented as a smear, except for the region between 15 to 50kDa (**Figure 3.9**).

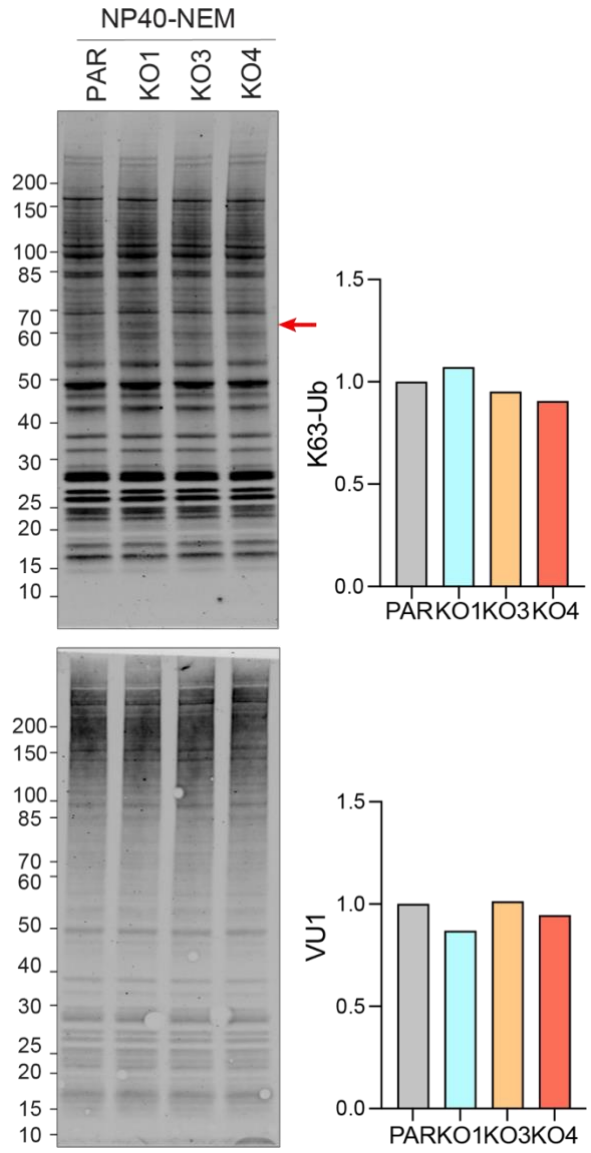

Figure 3.9 The cytosolic ubiquitin levels do not change in AMSH KO cells compared to parentals but a 65 kDa band disappears in KO3 and KO4 cells.
HeLa GFP-HRS Flp-In were lysed in NP-40 + N-ethylmaleimide (NEM) lysis buffer and resolved into a 4-12% nu-page gel. The membrane was incubated with K63-ubiquitin (Millipore, 1:1000) and then with the VU1 antibody. The region from 15 kDa to the top of the membrane was quantified for both blots. Red arrow indicates disappearing band. Two gels were re-run and each membrane probed with the indicated antibody.

I next performed a subcellular fractionation of parental and AMSH KO cells. The cells were homogenised generating a post-nuclear supernatant (PNS) and then total cell membranes were isolated using a 100,000 g centrifugation.

AMSH knockout and parental cell derived fractions were resolved by SDS-PAGE and one set of samples was incubated with the VU1 ubiquitin antibody.

The total ubiquitin in the VU1 blot appeared as smears from ~50kDa to the very top of the membrane reaching 200kDa, and discrete bands below. The lower molecular weight bands below 50kDa did not change in the PNS of AMSH KO3 and KO4, while KO1 PNS showed higher amounts of these proteins than in the parental PNS. The PNS of AMSH KO1, KO3 and KO4 display higher levels of total ubiquitin above 150kDa. Importantly, total ubiquitinated proteins were clearly increased in the membrane fractions of all three AMSH KO cells with the greatest apparent increase above 150kDa.

The cytosolic fraction of all AMSH KO cells showed less total ubiquitin in the region above 150 kDa (**Figure 3.10 A, B**).

The total ubiquitin blot from the subcellular fractionations from 2 biological replicates was quantified and the results plotted. I observed that the total ubiquitin in the MW range above 60kDa in the PNS of KO1 and KO3 consistently increased compared to parentals, while in KO4 this was less clear. Notably, the total ubiquitin in the membrane fractions in the region above 60kDa increased very consistently in all AMSH KO cells compared to parental (**Figure 3.10 C**).

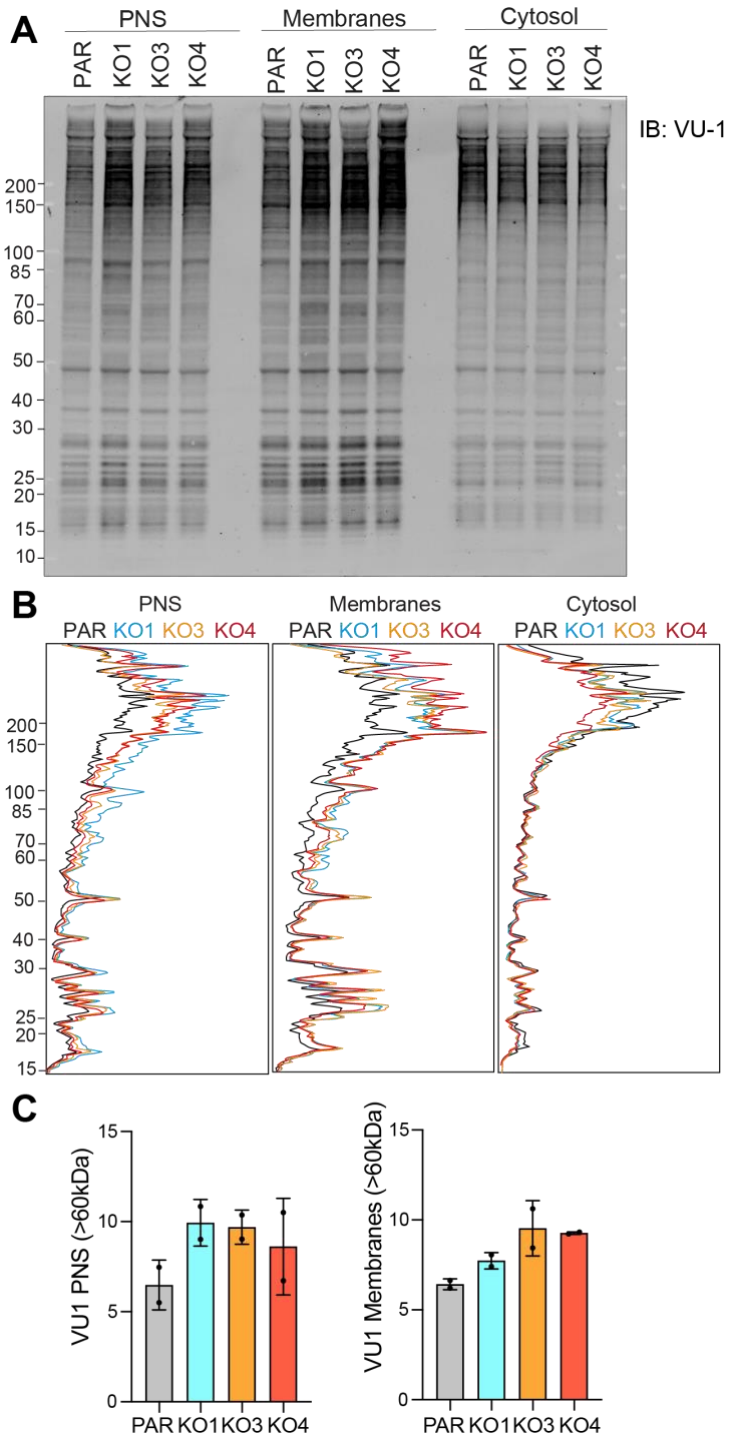

Figure 3.10 Polyubiquitinated proteins increase in the membrane fractions of AMSH KO cells.
A HeLa GHP-HRS Parental and AMSH KO1/3/4 were homogenised and the PNS was fractionated in membrane and cytosol. Equal amounts of protein from all fractions were resolved by WB and the membrane was incubated with the total ubiquitin antibody. Representative of 2 experiments B Line graph corresponding to the signal of the WB bands in A quantified in fiji/ imageJ. C The ubiquitin (VU1) signal in the MW range above 60kDa from the PNS and membranes fractions was quantified. The graph shows the arbitrary units from two independent experiments. Error bars indicate the range.

Another set of samples resolved by WB was incubated with the K63-ubiquitin antibody (Millipore, #05-1308). Overall, there are more K63Ub modified proteins in the membrane fractions than in the cytosol. While a small part of the K63-ubiquitin signal is composed of low molecular weight proteins running at 15-30 kDa, most of the K63-ubiquitin signal presents as a smear between 40 and 200 kDa, both in the PNS and membrane fractions. I observed that this smear was increased in the PNS of KO1 and in the membrane fractions of all three KO cells compared to Parental. The cytosolic fraction of all AMSH KO showed very big variations across multiple experiments. Notably, both in the PNS and membrane fractions of Parental and KO1 cells there was a 60kDa band which disappeared in KO3 and KO4 cells (**Figure 3.11 A**).

The K63-ubiquitin contained in the subcellular fractions from 3 biological replicates was quantified and plotted. The K63-ubiquitin in the whole PNS of all AMSH KOs across 3 biological replicates was variable, only in 2 experiments all AMSH KO cells displayed an increase compared to parentals. On the other hand, the K63-ubiquitin in the whole membranes of all AMSH KO cells was consistently increased compared to parentals (**Figure 3.11 B**).

Similar to the total ubiquitin blots, the differences in the K63-ubiquitin blots are primarily concentrated in the MW range above 60kDa (**Figure 3.11 C**).

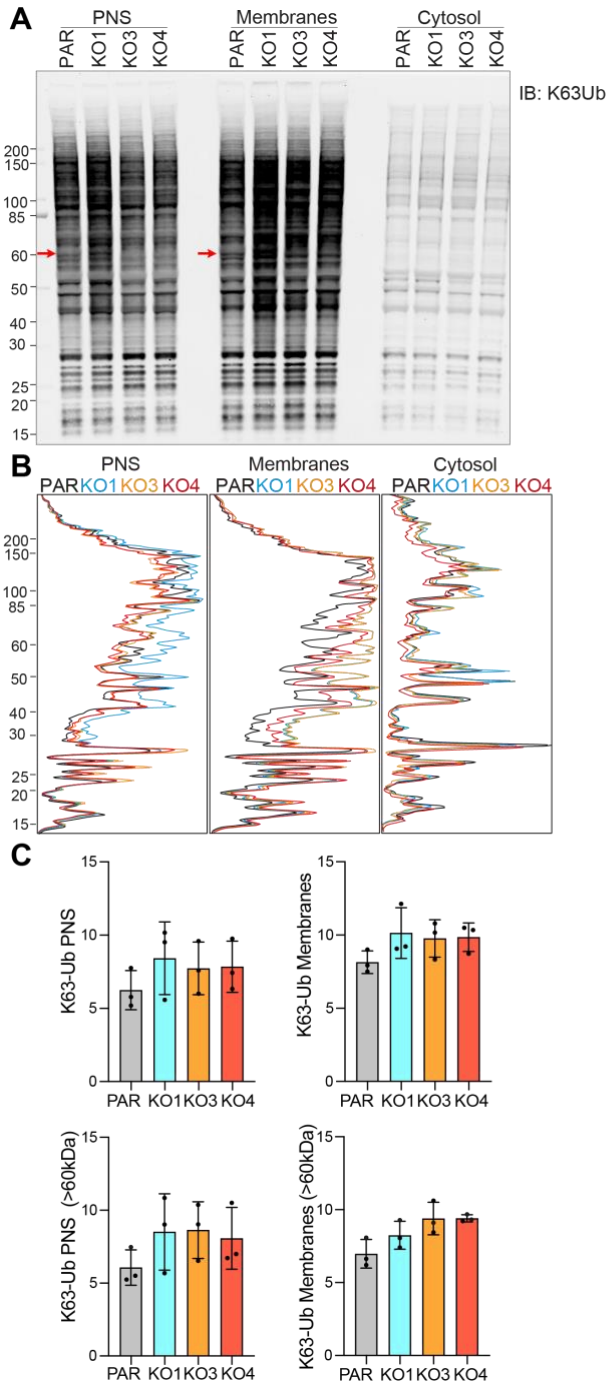

Figure 3.11 K63-linked ubiquitin chain levels are increased in the membrane fractions of AMSH KOs.
A HeLa GHP-HRS Parental and AMSH KO1/3/4 were homogenised and the PNS was fractionated into membrane and cytosol. Equal amounts of protein from all fractions were resolved by WB and the membrane was incubated with the K63Ub antibody (Millipore). The banding pattern is shown as peaks generated in fiji/ imageJ. Representative of three experiments. B Line graph corresponding to the signal of the WB bands in A quantified in fiji/ imageJ. C The K63Ub signal was quantified both across the whole lane (top graphs) and in the MW range above 60kDa (bottom graphs). The non-normalised arbitrary units were plotted and are shown as mean and standard deviation n=3.

I have collaborated with Gunnar Dittmar's lab at LIH in Luxembourg, to evaluate the absolute amounts of each ubiquitin chain linkage type in HeLa GFP-HRS parental, AMSH KO1, KO3 and KO4 by Absolute QUAntification (AQUA). AQUA uses a standard peptide as an internal control to calculate the molar concentration of peptides in a provided sample(Gerber et al., 2003). The relative abundance of K48, K63 and K11 ubiquitin chains was quantified in HeLa GFP-HRS Flp-In parental, AMSH KO1, KO3 and KO4 total cell lysates.

K48-linked ubiquitin chains were the most abundant type of ubiquitin chains in all cells. For K48-linked ubiquitin, two types of ion transition were analysed (2) and (3). In all AMSH KO clones there is a trend towards a higher average content of K48-linked ubiquitin chains for which the differences are however not statistically significant, though.

K63- and K11-linked ubiquitin chains were the second and the third most abundant ubiquitin chain linkages, respectively. Similar to K48-linked chains, for both K63Ub and K11Ub chain linkages, there was an upward trend in AMSH KO1, KO3 and KO4 cells compared to parentals.

Even though the data are not statistically significant due to the big variability between biological replicates, at basal levels all AMSH KO cells displayed a higher average content of K63Ub than parental cells in 3 biological replicates (**Figure 3.12**).

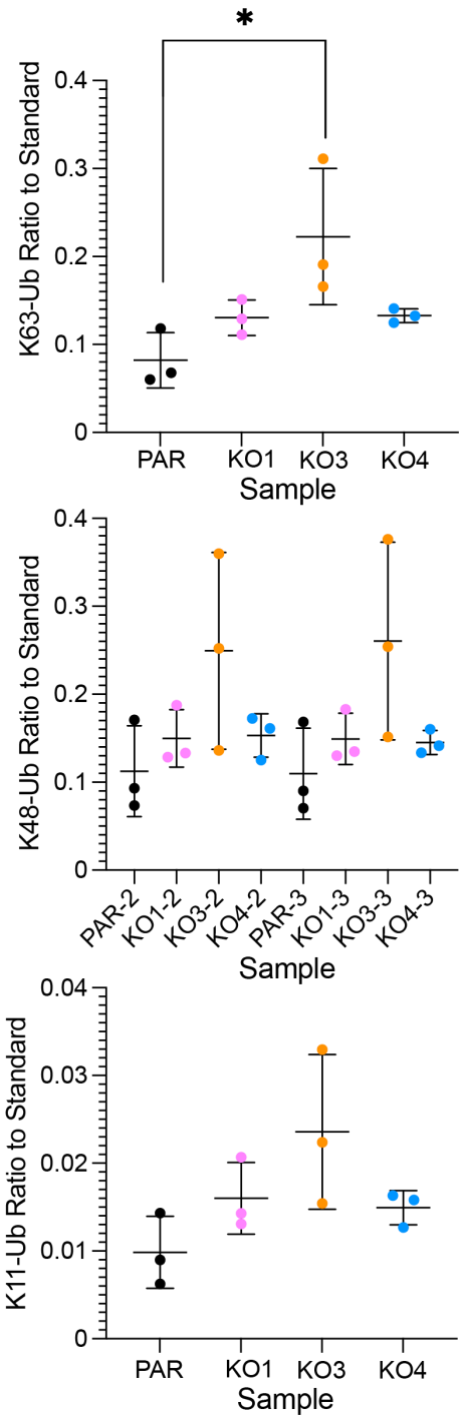

Figure 3.12 The levels of K63-ubiquitin chains follow an upward trend in total lysate of AMSH KO1, KO3 and KO4 cells compared to parentals. The cell pellets from HeLa GFP-HRS parental, AMSH KO1, KO3 and KO4 were resuspended in 8M Urea containing 10mM NEM. Protein concentration was measured using the EXQ Protein Quantitation kit (Thermo-fisher), then 500ng of peptides per sample were run onto QExactive HF coupled to a Ultimate3000 nanoHPLC. The parallel reaction monitoring (PRM) was achieved by analysing every ion transitions simultaneously, the sum of the transition areas for each m/z (mass/charge) were plotted for each condition, n=3.

In **Figure 3.12**, I have shown that higher levels of K63-ubiquitin chains are found in the membranes fraction of AMSH KO cells. I was interested in seeing on where the K63-ubiquitin accumulated in the cell and stained HeLa GFP-HRS parental and the three AMSH KO clones with the K63-ubiquitin antibody. I found much stronger K63-ubiquitin puncta in AMSH KOs, and this phenotype was most obvious in AMSH KO3 and KO4 cells. Interestingly, whilst I observed a clear co-localization between K63-ubiquitin and GFP-HRS in both parental and KO cells, most of the additional K63-ubiquitin signal in AMSH KO3 and KO4 localised on GFP-HRS negative structures (**Figure 3.13**).

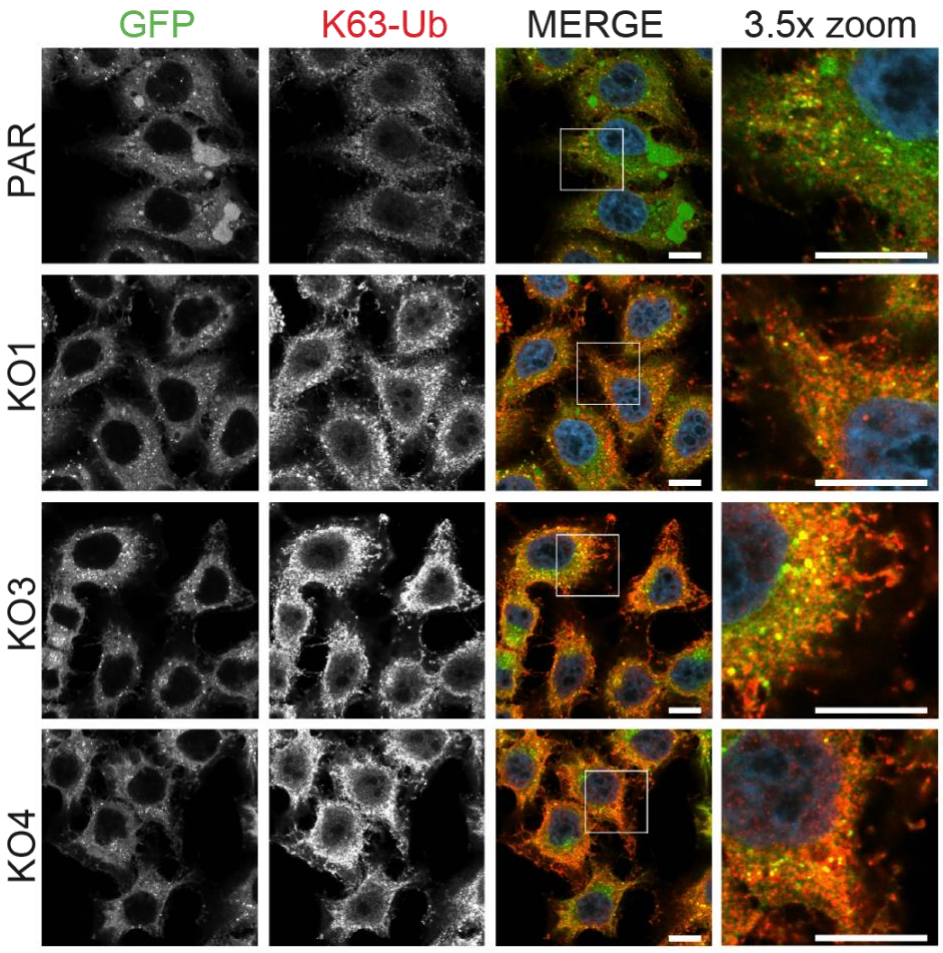

Figure 3.13 Lys63-linked ubiquitin visualisation in AMSH knockout cells.
HeLa GFP-HRS FlpIN (Par), AMSH KO1, KO3 and KO4 cells were fixed in 4% PFA, permeabilised, blocked and stained with a K63-ubiquitin specific antibody (Millipore, #05-1308). The coverslips were imaged with a 63x oil objective at an LSM 900 confocal microscope.
Scale bar = 10µm. Representative of 3 experiments. Blue = DAPI staining.

3.6 Discussion

3.6.1. HeLa AMSH KO clones were produced and JAMM-targeted behaved in a similar fashion.

In this chapter I have generated a series of AMSH knockout cell clones by CRISPR-Cas9 genome editing of HeLa GFP-HRS Flp-In cells. I have characterised the clones and assessed their endo-lysosomal morphology.

I have employed sgRNAs that either targeted the N-terminal MIT domain (sgRNA1) that interacts with the ESCRT-III machinery or target the JAMM catalytic domain (Tsang et al., 2006; Weissenhorn et al., 2011; Kikuchi et al., 2003). If AMSH protein would be transcribed and translated in KO1 cells, this would be an N-terminally truncated version initiated at a downstream codon. On the other hand, if AMSH protein would be produced in AMSH KO3 and KO4 cells, this would lack most of the JAMM catalytic domain (**Figure 3.1**). In fact, the sequencing data suggest that this protein would be truncated in all AMSH KO clones characterised in this chapter (3.1).

I did not see any lower molecular weight bands appearing in the KO cells when probing with the AMSH antibody. However, it should be noted that the antibody recognises the extreme N-terminus of the protein, and thus would not detect N-terminally truncated AMSH deletion mutants.

It is possible that an N-terminally (delta-MIT) mutant of AMSH expressed in KO1 could act in a dominant negative fashion. Indeed, this could underlie the morphological changes I observed in KO1 cells. Alternatively, those features could also be caused by off-target effects of this specific sgRNA. Since both JAMM-targeted AMSH KOs (KO3 and KO4) behave the same gives me confidence that their phenotype does not result from off-target effects. Targeting the C-terminal JAMM domain ensures that there will not be any functional protein produced. For this reason, I mainly focused my attention on AMSH KO3 and KO4 cells. AMSH KO1 cells have not been employed in the following chapters.

I sequenced the genomic AMSH in the KO cells by using primers targeting the region where sgRNAs annealed and detected insertions and deletions.
I could have quantitated the mRNA levels to evaluate gene expression from the putative AMSH KO cells, but this would still not allow me to assess whether the translated protein would be aberrant and possibly unstable.

3.6.2. The ubiquitin landscape appeared changed in all AMSH KO clones and K63-ubiquitin accumulates on their membrane fractions.

A limit to evaluating ubiquitin by Western Blot is that it does not allow for accurate quantitation of different ubiquitin chain types. This prompted me to collaborated with Dittmar's lab to carry out AQUA proteomics. AQUA proteomics suggested that there is a trend for K63-ubiquitin increase in all AMSH KO compared to parentals (**Figure 3.13**). Interestingly, the K63-ubiquitin levels were apparently increased in AMSH KO3 and KO4, and mainly localised to GFP-HRS negative compartments at the cell periphery as observed by confocal microscopy. Moreover, I did not observe an increase in K63-ubiquitin in the nucleus despite the fact that AMSH displays a functional nuclear localisation signal (McCullough et al., 2004) (**Figure 3.14**). Although I could not completely rule out to which compartment does the K63-ubiquitin accumulate at, it cannot be excluded that K63-ubiquitin could accumulate at the endosomal membrane. The NP-40 lysates displayed no change in the levels of total and K63-linked ubiquitin in AMSH KOs (**Figure 3.9**). This result strengthens the idea that the K63-ubiquitin could be increasing on membranes instead of cytosol.
Ishii and colleagues reported that the membrane fractions isolated from AMSH KO mice derived neurons present an elevation of conjugated ubiquitin levels (Ishii et al., 2001; Suzuki et al., 2011). In agreement with these publications, I observed that the levels of both total conjugated ubiquitin and K63-ubiquitin were consistently increased in the membrane fractions of AMSH KO1, KO3 and KO4 compared to parental. The most consistent change observed in the membrane fractions was the increase of K63-ubiquitin in the region above 60kDa. The ubiquitin increase was

concomitant with the disappearance of a 60kDa band in the membranes of AMSH KO3 and KO4 compared to parentals and to AMSH KO1 cells. This suggests that the 60kDa protein present in parentals and AMSH KO1 membranes and disappearing in AMSH KO3 and KO4 is differentially modified with K63-ubiquitin (**Figure 3.11 A-C**).

K63-ubiquitin is the second most abundant ubiquitin modification after K48-ubiquitin (P. Xu et al., 2009). The net shift in the K63-ubiquitin signal in membrane fractions of AMSH KO cells might mean that these cells accumulate K63-ubiquitin chains on a selected group of membrane associated proteins at steady state. Since I observed an increase of K63-ubiquitin chains in the membrane fractions of all 3 AMSH KO clones compared to parental, I hypothesised that there could be a perturbation of the ubiquitin landscape due to AMSH KO.

3.6.3. AMSH KO does not affect the total levels of ECSCRT-0 components.

Maintaining physiological HRS levels is crucial for maintaining endosome physiology, as over-expression of HRS was shown to cluster endosomes that cannot give rise to late endosomes. (Komada & Soriano, 1999; Raiborg et al., 2001; R. L. Williams & Urbé, 2007). That is why I checked the global levels of the two components ESCRT-0 machinery, HRS and STAM. The levels of HRS and STAM2 did not change in AMSH KO which contrasts with the literature reporting that overexpressing the catalytic mutant AMSH results in the stabilisation of a ubiquitylated species of STAM2 (McCullough et al., 2006). EGFR has been shown to be downregulated by AMSH knock-down and that AMSH can cleave K63-ubiquitin chains when it is fused to the EGFR (McCullough et al., 2004; Huang et al., 2013) . In agreement with McCullough et al. 2004, the steady state levels of EGFR were not decreased in all AMSH KO cells indicating that a complete removal of AMSH from HeLa cells does not imbalance the basal turn-over of EGFR likely (**Figure 3.4**).

3.6.4. AMSH and AMSH-LP could not be functionally redundant.

It is a matter of debate whether AMSH and AMSH-LP could have similar roles.

AMSH and AMSH-LP both are K63-ubiquitin specific DUBs and localise to endosomal membranes via their clathrin-binding regions (Kikuchi et al., 2003; Nakamura et al., 2006). AMSH-LP shares 55% of AMSH sequence identity and its 3D structure is preserved, while AMSH-LP lacks a STAM binding motif which is required to interact with the ESCRT-0 (Kikuchi et al., 2003; Clague & Urbé, 2006; Guo et al., 2021).

AMSH protein and mRNA levels were found to be upregulated in a large cohort of NSCLC patients' samples and correlated with an invasive and migratory phenotype (H. Xu et al., 2021).

Some studies point to AMSH-LP as being a valuable target in cancer therapy because its protein levels directly correlate with cancer cell proliferation and invasiveness in gastric cancers (Da-Jun Yu et al., 2019). Similar to AMSH, AMSH-LP is implicated in tumour progression, thus AMSH-LP gene expression directly correlates with the expression of mesenchymal phenotypes in patients' biopsies from lung adenocarcinoma and breast carcinoma (Ambroise et al., 2020).

I checked AMSH-LP levels because this is a paralogue protein to AMSH. It is common that when a paralogue protein is knocked down or knocked out, the other paralogue is upregulated (Thorne et al., 2011). I did not observe paralogue compensation by AMSH-LP; its protein levels were unchanged in AMSH KO1, KO3 and KO4 compared to the parentals. In contrast to what the literature indicates, the observation that AMSH-LP levels are unchanged in all three AMSH KO clones supports the hypothesis of AMSH and AMSH-LP not being functionally redundant (**Figure 3.4**).

Whilst AMSH and AMSH-LP may have similar roles in the context of different signalling pathways, it would be interesting to investigate a possible interplay between these two proteins in the context of protein deubiquitylation at the endosomal membrane.

3.6.5. AMSH is not critical for maintaining early-endosome microdomains segregation but could be involved in determining late-endosome identity.

AMSH is known to localise to the nucleus and to the endosomal membrane via its clathrin binding region(Nakamura et al., 2006). In turn, clathrin is important for HRS to concentrate ubiquitylated membrane proteins at the endosomal membrane and to delineate endosomal microdomains (Clague, 2002; Hicke & Dunn, 2003; Raiborg et al., 2001). The morphology of EEA1 positive endosomes in AMSH KO3 and KO4 appeared normal, as GFP-HRS partially co-localised with EEA1 in all cell types. This indicates that AMSH is not critical to maintain the segregation of EEA1 and HRS microdomains (**Figure 3.5**).

LAMP1 marker segregated from GFP-HRS in AMSH KO3 and KO4 just as in the parental cells indicating that AMSH KO does not alter the morphology of the late endosome compartment (**Figure 3.6 A**). However, I found that there was an apparent increase in the number of LAMP1 puncta in AMSH KO cells. I categorised cells based on the number of particles and showed that AMSH KO3 had significantly more cells that contain between 30 and 80 particles compared to parentals (**Figure 3.6 B-C**). More repeats of that experiment would help to get a definitive picture.

In Chapter 5 I will further explore late endosome physiology in AMSH KO cells.

3.6.6. AMSH could mediate HRS stabilisation via Ub-STAM1

STAM1 and STAM2 share the VHS (Vps/Hrs/STAM) domain, ubiquitin interacting motif (UIM), Src homology domain, and a coiled coil (CC) region. STAM2 has 2 isoforms; STAM2A contains an immune-receptor Tyr-based activation motif (ITAM), similarly to STAM1, whereas STAM2B lacks such motif (Lohi & Lehto, 2001). One functional difference between the STAMs lies in the fact that STAM1A/2B are Tyr-phosphorylated by Jak 1-3 kinases in the ITAM whereas STAM2B is not. HRS depletion has been shown to strongly reduce STAM1/2 levels and to mis localise STAM2 to the cytoplasm (Mizuno, 2004).

In my hands, STAM1 knockdown does not change the levels of endogenous HRS in both Parental and KO4, indicating that AMSH KO there is a normal equilibrium between these two proteins. Then knockdown of either of the STAMs does not influence the other indicating that they may fulfil non-redundant functions in these cells (**Figure 3.7**).

Interestingly, I found that knockdown of STAM1 but not STAM2 destabilised HRS in our AMSH KO4 cells which suggests that AMSH might be involved in stabilising the ESCRT-0 complex via an HRS-independent mechanism. It was shown that a polyubiquitylated STAM1 version is accumulated when overexpressing a catalytically inactive AMSH (D348A) version in HeLa cells (Sierra et al., 2010). One could speculate that HRS stabilisation might be mediated by the AMSH-ubiquitylated-STAM1 interaction.

ESCRT-0 components bear specific ubiquitin binding domains to concentrate plasma membrane protein cargo at the endosomal membrane (Kobayashi et al., 2005; Lohi & Lehto, 2001; Mayers et al., 2011; Ren & Hurley, 2010b; Urbé et al., 2003). The localisation of AMSH to endosomal membranes depends on the STAM UIM domain, and AMSH binding to STAM1 via its STAM binding domain (SBM) (McCullough et al., 2006). For this reason, I checked the sub-cellular distribution of the ESCRT-0 proteins.

The distribution of HRS and STAM in the membrane fractions of AMSH KO cells was unchanged. AMSH is recruited by STAM via its SH3 domain, and this interaction enhances its catalytic activity. Importantly, the catalytically inactive AMSH localises more strongly to endosomes and was seen to stabilise a ubiquitylated form of STAM2 (McCullough et al., 2004).

Whilst overexpressing an inactive enzyme can result in a dominant negative effect by trapping the substrate, in AMSH knockout cells there will be no such trapping thus there will be more cleavage of these substrates by other K63-ubiquitin proteases. I did not observe the stabilisation of any ubiquitylated STAM2 form in AMSH KO cells likely because of more substrates being available for other K63-ubiquitin specific proteases in AMSH KO (**Figure 3.8**).

The AQUA results, together with the membrane fractionations and the K63-ubiquitin immunofluorescence experiments, further strengthen the hypothesis that K63-ubiquitin chains could be either changing their levels in AMSH KO cells or could be changing localisation and be concentrated in compartments that cannot be cleared.

This finding raises the question: what is the identity of the compartments that K63-ubiquitin is accumulating on, and which are the K63 ubiquitylated proteins that are enriched in AMSH KO cells? In the next chapters I will address this question.

Chapter 4: K63-ubiquitin-associated proteome of AMSH KO cells

4.1 Introduction

In the previous chapter I showed that K63-ubiquitin levels were increased in AMSH KO membrane fractions and that by immunofluorescence these chains mostly localise to GFP-HRS negative puncta. In this chapter I build on these findings and try to identify AMSH substrates using Lys63-linked ubiquitin chain specific reagents. By combining this approach with SILAC labelling of isogenic cell pairs, I have sought to gain an unbiased and quantitative insight into AMSH-dependent changes in Lys63 chain modified proteins. By ratioing intensities one can easily filter out background binding to the beads themselves (Trinkle-Mulcahy, 2008).

One commercially available K63-ubiquitin binding tool is a nanobody generated by Hybrigenics/Nanotag which is a single-domain antibody (sdAb) covalently cross-linked to 4% agarose beads (#N1910, NanoTag Biotechnologies). As an alternative, I chose to employ a K63-ubiquitin linkage-specific sensor K63-ubiquitin SUperBinder (K63-SUB). This derives from the 3x UIM of the Rap80 transcription factor and has previously been used by Mailand and colleagues to identify novel substrates of the E3 ligases RNF168 and RNF8 within the DNA double-strand break repair pathway (Thorslund et al., 2015). An advantage of using K63-SUB is that it can be cheaply produced in bulk in our laboratory using bacteria. K63-SUB is appended with an AviTag^{TM} type linear motif of 72 amino acids termed BIOEASE^{TM} which is readily biotinylated in BirA-transformed chemically competent E. coli upon supply of biotin. It also contains a 6x (His) tag that enables its separation from the bacterial protein extracts (Fairhead M. and Howarth M., 2015). I have expressed, purified and benchmarked this reagent. After optimising the protocol, I have used it in mass spectrometry

experiments that have revealed a coherent set of candidate substrate proteins.

4.2 K63-Superbinder (K63-SUB) protein production in E. coli

To produce the K63-SUB fusion protein in bacteria, I used the pET104Dest (BioEASE-SuperK63-6xHis) plasmid that was used by Thorslund and colleagues (Thorslund et al., 2015b) (**Figure 4.1**). The final translated K63-SUB protein contains an N-terminal biotinylated BioEase tag and a C-terminal 6x-His tag (**Table 13**).

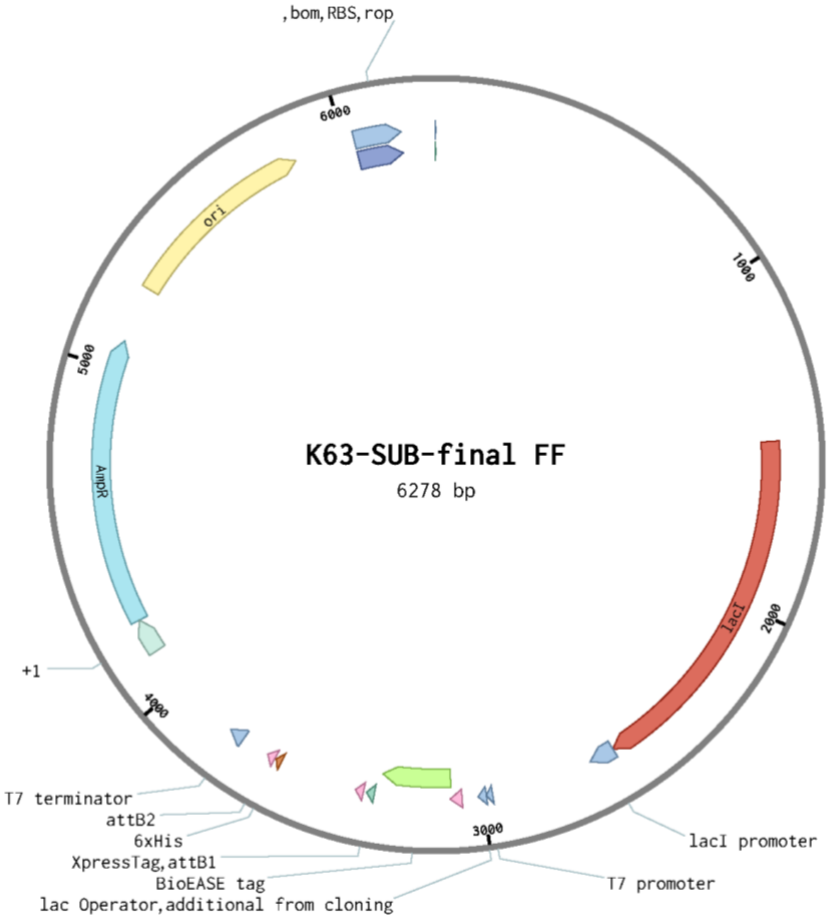

Figure 4.1 Plasmid map of pET104Dest (BioEASE-SuperK63-6xHis). The pET104Dest (BioEASE-SuperK63-6xHis) construct was sequenced using the T7 promoter upstream of the K63-SUB ORF. The plasmid contains the BioEASE tag at the N-terminus, the (2x) UIM1 and UIM2 of the protein Rap80, an Xpress tag and a C-terminal 6x-His tag. The predicted molecular weight of the recombinant protein is 19.8 kDa.

Table 13 Protein sequence annotation of the K63-SUB sensor.
The table shows the amino acid composition of the K63-SUB protein. K63-SUB is made of a BioEASE™ tag which is biotinylated on the Lys 38 (highlighted in red), this is followed by two UIM1 and one UIM2 of the protein Rap80.

K63-SUB domains	Sequence
BioEASE™ (Avi-Tag)	MGAGTPVTAPLAGTIWKVLASEGQTVAAGEVLLIL EAMKMETEIRAAQAGTVRGIAVKAGDAVAVGDTL MTLA
UIM1 (2x)	EEEQFALALKMSEQEA
UIM2 (1x)	EEEELLRKAIAESLNSCRPS
Xpress tag	DLYDDDDK
6x-His Tag	HHHHHH

The pET104Dest (BioEASE-SuperK63-6xHis) plasmid was transfected into chemically competent BL21 BirA-transformed competent E. coli cells (tebu-bio #27462). This E. coli strain contains an IPTG-inducible BirA expression plasmid and constitutively expressed streptomycin/spectinomycin resistance gene (Fairhead M. and Howarth M., 2015). This E. coli strain can simultaneously express and biotinylate recombinant proteins that possess an AviTag™ which in our protein is represented by the BioEASE™ aminoacidic stretch. The BioEASE™ is a biotin-acceptor peptide that is specifically recognised as a substrate and biotinylated by the BirA ligase on the Lys38 residue (Fairhead M. and Howarth M., 2015).
Upon transfection of the BL21 BirA cells with the pET104Dest (BioEASE-SuperK63-6xHis) plasmid, IPTG and biotin are supplied to the media to induce BirA expression that will catalyse the attachment of biotin to the Lys38 within the BioEASE tag (**Figure 4.2**).

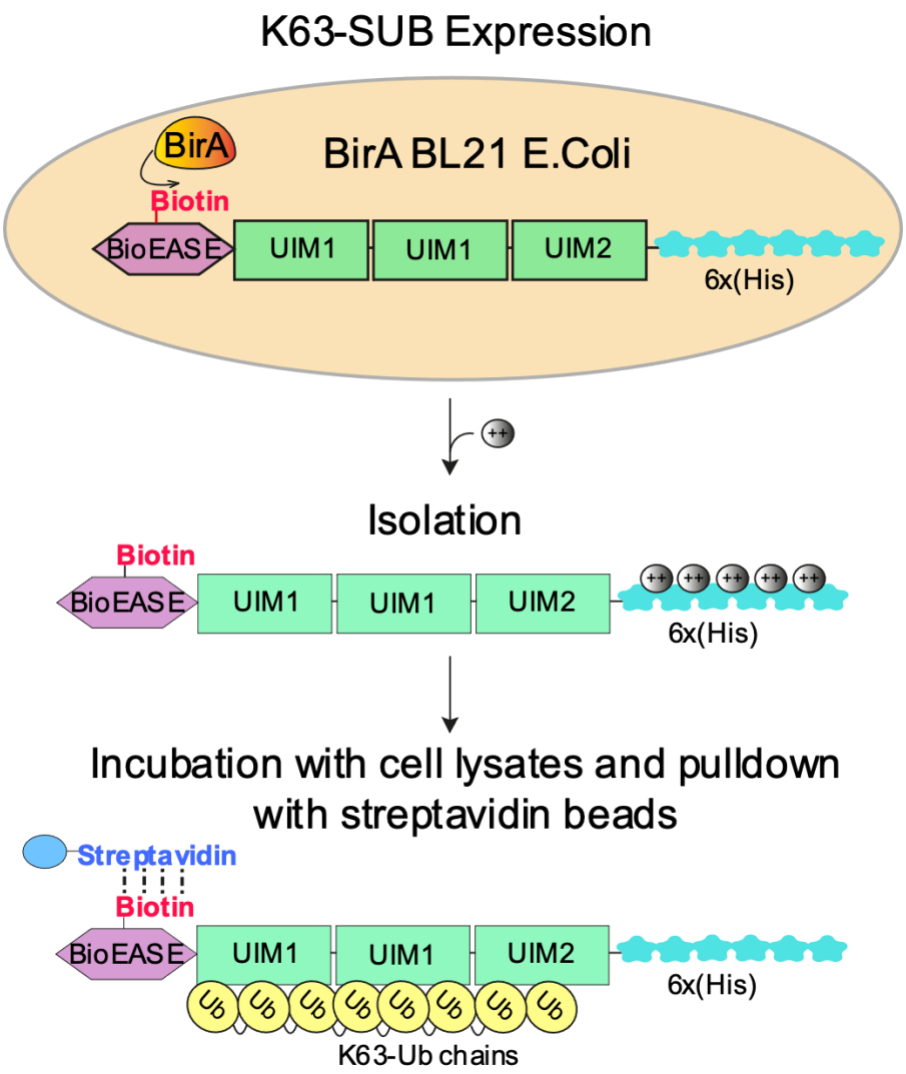

Figure 4.2. Workflow of K63-Superbinder (K63-SUB) production. Diagram showing the workflow for K63-SUB protein production. The K63-SUB (superbinder) is expressed in BL21 competent E. coli and biotinylated by BirA at L BioEASE™ moiety. The bacteria are lysed, and the biotinylated K63-SUB is isolated via its 6x-His tag by Nickel beads and then conjugated to streptavidin agarose beads. The bead-coupled biotinylated K63-SUB can be used to pull-down K63-ubiquitin chains when incubated with cell lysates.

After transformation, the bacteria were spread on Spectinomycin/Ampicillin resistant plates, one colony was picked and cultured the colony in a starter liquid culture in LB broth overnight. The starter culture was diluted 1000 times and after 2 hours the optical density (OD) was measured at 600nm (OD_{600}). At OD_{600}= 0.8, the culture was cooled down to 16°C and a pre-induction sample was taken out. After 1h of cooling, the K63-SUB protein expression was induced by adding 0.5 mM of IPTG along with 0.5 mM of biotin for 20 hours. A post-induction sample was taken and loaded together with the pre-induction sample onto a 4-12% SDS-PAGE gel to resolve the

K63-SUB protein. The gel was incubated with Coomassie blue total protein stain for 30min. Coomassie can be detected in the 700 nm channel of the Licor Odissey CLx^{TM} infrared fluorescence scanner. I identified K63-SUB as 25 kDa band was observed in the post-induction (post-IPTG) sample but not in the pre-induction (pre-IPTG) sample that (expected molecular weight 19.8 kDa). The gel also presented a band at ~35kDa which corresponds to the exact molecular weight of the IPTG-induced BirA ligase (**Figure 4.3**).

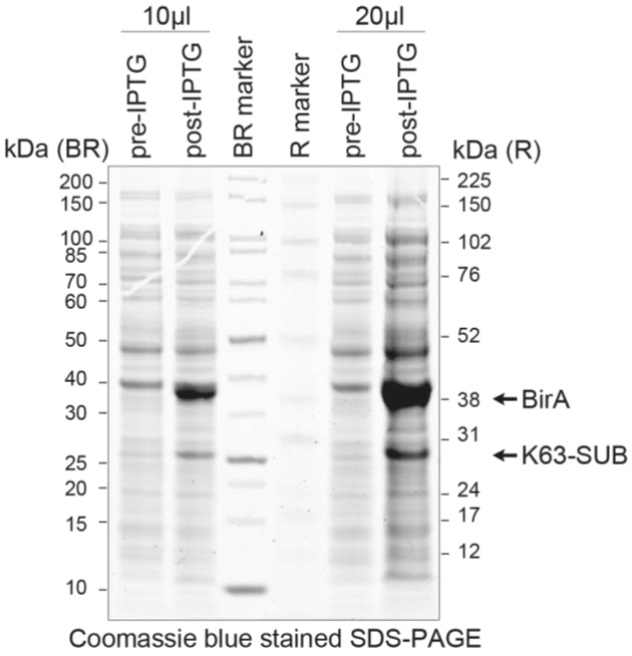

Figure 4.3 BirA protein expression induced by IPTG.
Two different volumes (10µl and 20µl) of pre-IPTG induction and post-induction were loaded onto a 4-12% SDS-PAGE gel and was run in 1x MES buffer. The gel was stained in Coomassie blue stain for 30min and scanned in the 700 nm channel. IPTG (0.5mM) was used to induce the expression of the 25kDa and 35kDa bands which correspond to K63-SUB and BirA proteins, respectively. BR marker =broad range marker. R marker = rainbow marker. Marker scale = broad range.

The bacterial culture was spun down and the resulting pellet was resuspended in the lysis buffer, left on ice for 30min and then sonicated.

I took a small sample of the resuspended pellet and clarified it by spinning at 100,000 g for 30 mins in an ultracentrifuge (Hitachi, S80AT3 fixed angle rotor). After the spin, a small sample of supernatant was taken, and the remaining supernatant was filtered through a 0.2 µm button filter. To separate the K63-SUB from the mixture of the bacterial lysate I took

advantage of Ni^{2+} NTA agarose beads (QIAgen) which can capture K63-SUB by binding to its 6x-His tag.

The Ni^{2+} NTA beads were washed in elution buffer and reconstituted in binding buffer and incubated with the lysate for 2 hours throughout in the cold. After incubation, a sample of the flowthrough was collected. The beads were washed four times, and each wash was saved for analysis on a protein gel later. The bound proteins were eluted from the beads in elution buffer where they while rotating on a wheel for 10min at RT. This step was repeated three times to obtain four eluate samples from which I took a small aliquot to be analysed later. All the small samples collected at each step of the protein production were loaded onto a 4-12% SDS-PAGE gel which was stained with Coomassie blue and scanned in the 700 nm channel (**Figure 4.4**). The biotinylated-K63-SUB protein is expected to run at 20 kDa which is the sum of 19.8 kDa plus the 0.2 kDa of the biotin moiety. Nevertheless, the gel shows that the IPTG-induced eluate sample presents two strong bands at ~25 kDa and 35 kDa which represent the K63-SUB and BirA, respectively. Both are absent in the eluate of the non IPTG-induced sample. In this gel both bands run at an apparently higher mw in the gel because the gel was run for a shorter time than the gel in **Figure 4.3**. The K63-SUB is almost undetectable in the flowthrough sample and is absent in the wash 1 sample (W1). Some background staining observed at the 30-200 kDa range in the W1 and W2 samples was washed away in the samples W3 and W4.

The background present in the wash samples disappeared in the cleared lysate (supernatant) and the flowthrough, the background smear strongly decreases with the washes.

The purity of the K63-SUB protein prep can be appreciated from the elution lanes (E1-E3) where only the K63-SUB band at ~20kDa can be detected. Most of the K63-SUB protein was found in the first and second eluates (single band at ~20kDa). The last elution sample contained no K63-SUB protein indicating that the protein had been efficiently eluted from the Ni^{2+} NTA beads (**Figure 4.4**).

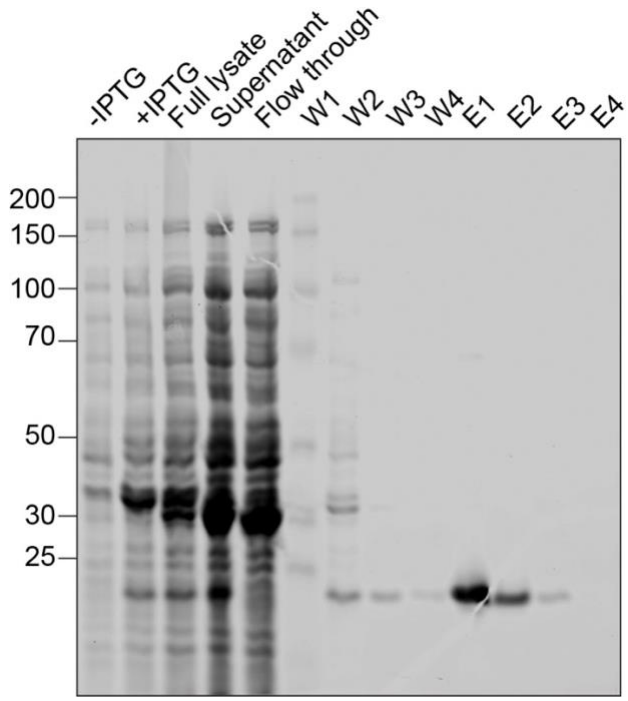

Figure 4.4 K63-SUB protein preparation steps.
The biotinylation competent BL21 E. coli culture transfected with pET104Dest (BioEASE-SuperK63-6xHis) plasmid were induced with 0.5mM IPTG and supplied with 0.5 mM biotin. The lysate was clarified, the supernatant was filtered and incubated with 2ml of Ni^{2+} NTA beads (50% beads slurry). After incubation, the flowthrough and four washes were collected. Elution was achieved in 4 consecutive incubations of the beads with the elution buffer. At all steps, a 20µl aliquot of sample was diluted 5x sample buffer and boiled at 95°C. The protein preparation samples were loaded onto a 4-12% SDS-PAGE gel in 1x MES buffer. The gel was stained for 30min in Coomassie blue stain and scanned in the 700 nm channel.

To dialyse the protein, I followed the protocol established by Mads Gyrd-Hansen group. After, the buffer was exchanged, 0.2 µg of K63-SUB protein preparation both pre-PD10 and post-PD10 buffer exchange were run alongside increasing concentrations of BSA protein standard (0.3, 0.5, 0.8, 1, 2 µg) onto an SDS-PAGE (**Figure 4.5**). I compared the K63-SUB samples with the protein standards, and it was clear that I had over-estimated the amount of K63-SUB protein loaded. The gel shows that the equilibration step left the K63-SUB protein unaffected by the buffer exchange in the PD10 columns.
At this point, the K63-SUB protein can be stored at -80°C indefinitely and defrosted for its use in pull-downs (**Figure 4.5**).

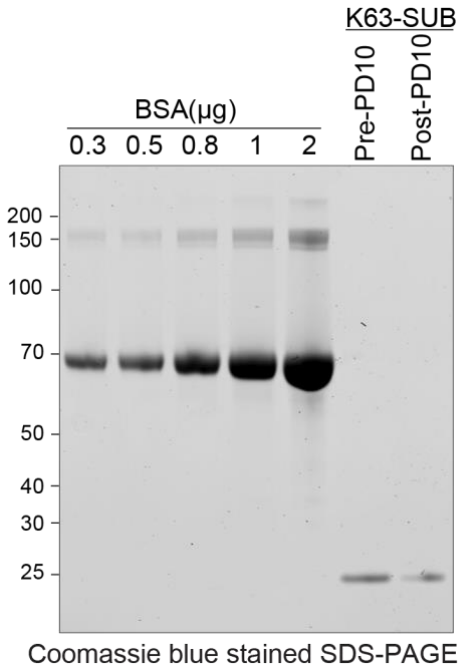

Figure 4.5 K63-SUB protein buffer exchange.
The K63-SUB protein was equilibrated using two PD10 columns in exchange buffer containing 50 mM Na-phosphate (pH7.5), 150 mM NaCl, 5% glycerol, 0.5 mM DTT, in five total equilibration steps. Equal volumes of K63-SUB protein prep sample were applied to each column and spun through. The exchanged K63-SUB samples were pooled, and the protein concentration was determined with Pierce 660nm assay. Conc. = 0.88µg/µl. 20 µl of pre- and post-PD10 samples were loaded onto a 4-12% SDS-PAGE gel in 1x MES buffer. The gel was stained for 30min in Coomassie blue stain and scanned in the 700 nm channel.

4.3 Optimisation of the K63Ub enrichment

As a first step towards assessing the specificity of K63-SUB protein towards K63-linked ubiquitin, I have attempted to pull-down synthetic K48 and K63 tetra-ubiquitin chains. I tested different supports to determine which beads would be the best for use in coupling the biotinylated K63-SUB protein. To this end, K63-SUB was conjugated to Avidin, Neutravidin and Streptavidin beads (10µl of 50% beads slurry) were conjugated to K63-SUB protein (5µg) in TUBES buffer by rotation on a wheel in the cold overnight. Alongside the conjugated beads, I also tested the agarose-beads cross-linked nanotag K63-Selector nanobody (10µl of 50% beads slurry) to compare our K63-SUB protein with a commercial alternative. After conjugation of K63-SUB to the beads, a master mix containing a combination of K48 and K63 tetra-ubiquitin chains was prepared. For each

pull-down, 250ng of each chain type were used. The pull-down was carried out in TUBES buffer for 2 hours in the cold room on a rotating wheel.

As shown in the input lanes of the ubiquitin western blot, we can distinguish the synthetic K48 tetra-ubiquitin that run at ~28kDa, from the K63 tetra-ubiquitin that run at 25kDa (**Figure 4.6**). The K48- linked Ub chains are resolved at a higher MW band compared to the K63-ubiquitin, this could be explained by the fact that they adopt a different topology (Komander & Rape, 2012a). The neutravidin-coupled K63-ubiquitin beads was the support that could best enrich K63-ubiquitin chains over the K48 ones, followed by the streptavidin-coupled beads and the K63-Selector. Nevertheless, the neutravidin beads pull-down was the dirtiest in terms of background. On the other hand, the streptavidin-coupled K63-SUB pull-down was the cleanest. Hence, I decided to continue with the optimisation of the Streptavidin agarose beads- coupled K63-SUB (**Figure 4.6**).

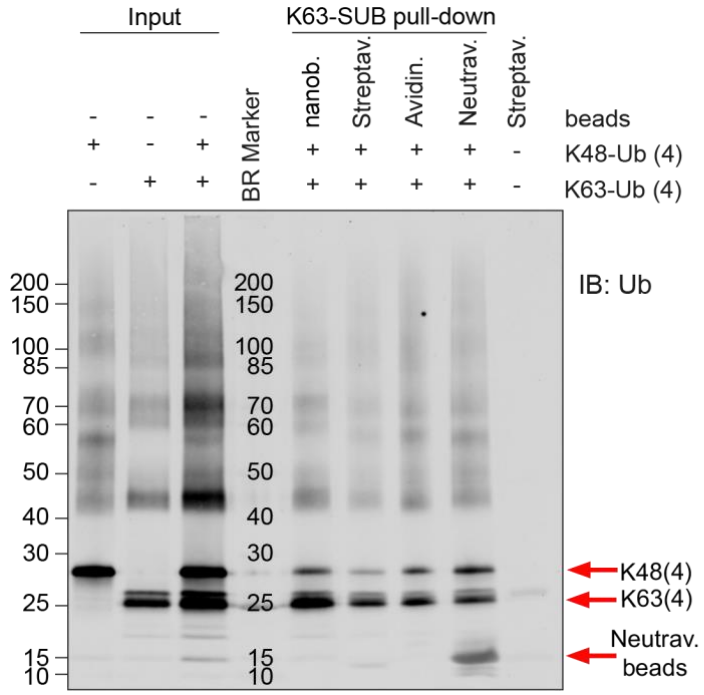

Figure 4.6 Streptavidin-coupled K63-SUB enriches for synthetic tetra-ubiquitin K63-linked versus K48-linked chains.
A combination of 250ng of K63 and K48 synthetic tetra-ubiquitin chains each were incubated with of either avidin, streptavidin, neutravidin agarose beads coupled to 5µg of K63-SUB protein, or with 10µl uncoupled K63-Selector nanobody (10µl of 50% slurry). One streptavidin bead sample was incubated without ubiquitin chains as control. The pull-downs were carried out in TUBES buffer for 2h at 4°C. The beads were pelleted and washed in 3X concentrated TUBES lysis buffer. Elution was achieved with 20 µl of 2X concentrated sample buffer, samples were boiled at 95°C for 5 mins and separated on an SDS-PAGE and transferred onto nitrocellulose. The blot

was incubated with a ubiquitin antibody (Sigma #U5379) overnight in the cold room. The K63/K48 ratios in the pull-down samples were normalised to the K63/K48 ratio in the combined input sample (containing K63 and K48).

In the experiments shown in the **Figure 4.6** I have used the TUBES buffer, a very mild NP-40 based lysis buffer. TUBES buffer allows for detection of weak and transient interactions. I next used a high-stringency RIPA lysis buffer named (HS-RIPA), (Thorslund et al, 2015). The higher salt concentration in HS-RIPA allows to reduce non-specific interactions.

I next carried out a pull-down with K63-SUB coupled to streptavidin agarose from total cell lysates of HeLA GFP-HRS Flp-IN cells. Variable amounts of K63-SUB protein were incubated with a fixed amount of cell lysate prepared using either TUBES or HS-RIPA buffer (**Figure 4.7**). As shown in the K63-ubiquitin Western Blot, the enrichment of K63-ubiquitin chains is directly proportional to the amount of K63-SUB protein employed in the pull-down, both in TUBES and HS-RIPA buffer.

In the TUBES pull-down the K63-ubiquitin signal was detected over a much wider molecular weight range. Contrary to the HS-RIPA pull-down which only shows a higher molecular weight smear, the TUBES pull-down also pulls down low molecular weight proteins. Likely, these reflect proteins with a lower number of ubiquitin moieties or shorter chains attached to them which can be lost by using the HS-RIPA. The K63-SUB contains tandem repeated ubiquitin-binding domains which relies on multivalent interactions; thus K63-SUB is expected to bind to long K63-linked ubiquitin chains much stronger than shorter ones.

Accordingly, using the more stringent HS-RIPA buffer, I preferentially isolated proteins conjugated with K63-ubiquitin in the range of 30-150kDa. The smears identified by K63-ubiquitin pull-down in HS-RIPA are likely long K63-ubiquitin chains.

I noted that the minimum amount of K63-SUB protein to be used to pull-down all K63-ubiquitin from a fixed amount of lysate is higher if using TUBES buffer compared to HS-RIPA. To reach the beads saturation, 500ng of TUBES lysate are required, while 125ng of K63-SUB are sufficient for HS-RIPA lysates. In the TUBES buffer pull-down, the VU1 antibody detected the lower molecular weight ubiquitin chains that

correspond to the bands seen to be enriched in the K63-ubiquitin blot (**Figure 4.7**).

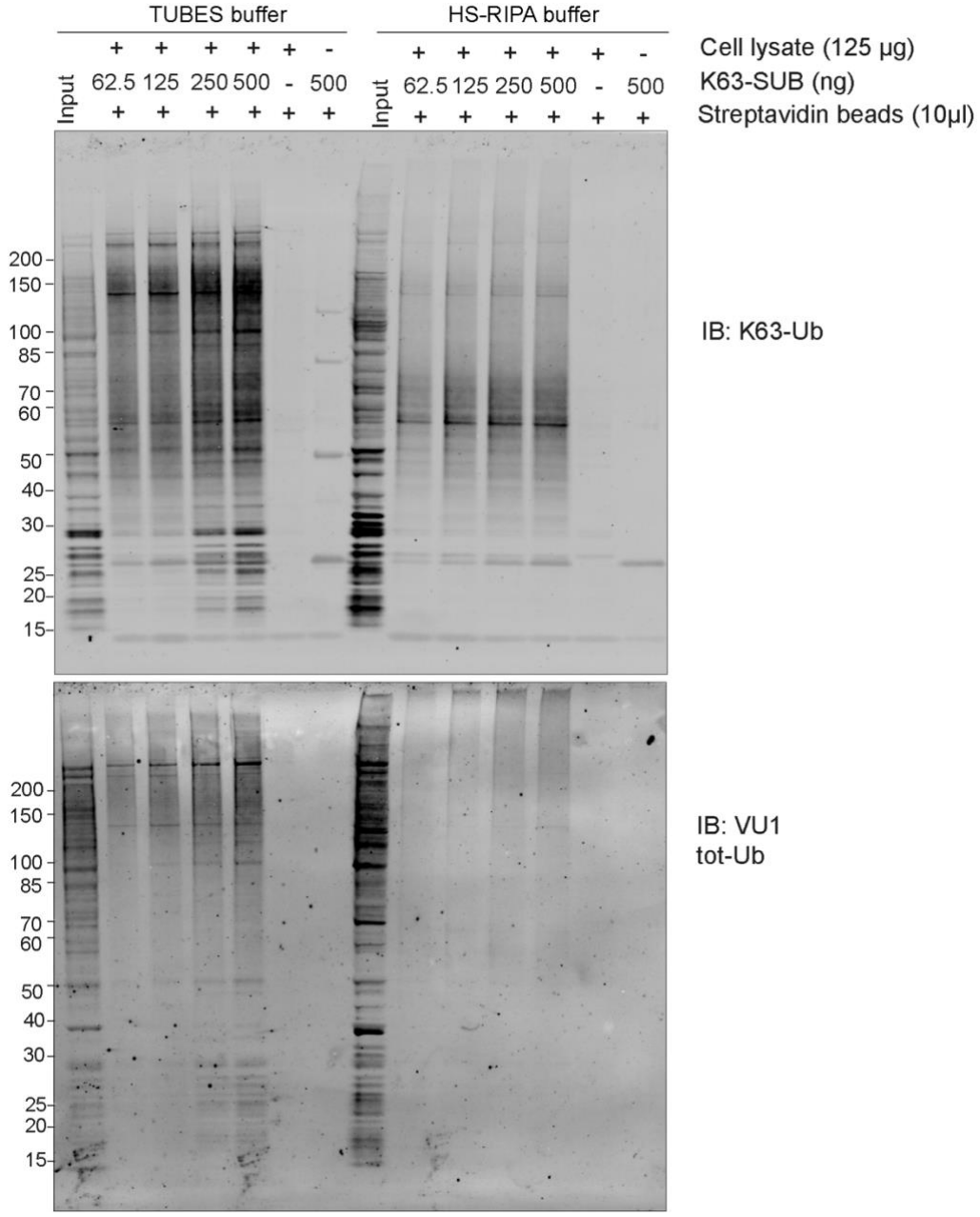

Figure 4.7 HeLa GFP-HRS cells were lysed in either TUBES or HS-RIPA buffer.
A fixed amount of cell lysate (125µg) was incubated with increasing amounts of K63-SUB (62.5, 125, 250, 500 ng) bound to 20µl of Streptavidin-agarose beads (50%slurry). Two control pull-downs were carried out in each buffer, one lacking the K63-SUB in the incubation and a second lacking the lysate. The elutions were loaded onto a 4-12% SDS-PAGE gel and the membrane was probed with the K63-ubiquitin (Millipore, #05-1398) antibody and then re-probed with the VU1 (total ubiquitin) antibody.

4.4 SILAC proteomics of K63-ubiquitin enrichment.

I was interested in identifying proteins that may be differentially modified with K63-ubiquitin in HeLa GFP-HRS AMSH KO compared to parental cells. For this reason, I carried out an unbiased SILAC based proteomic experiment. Parental cells were labelled as “light” (Lys0, Arg0), AMSH KO3 as “medium” (Lys4, Arg6) and KO4 as “heavy” (Lys8, Arg10).
I scaled up the K63-SUB mediated pull-down in HS-RIPA buffer to study the K63-ubiquitin associated proteomes of AMSH KO3 and KO4 by Mass Spectrometry (**Figure 4.8**).

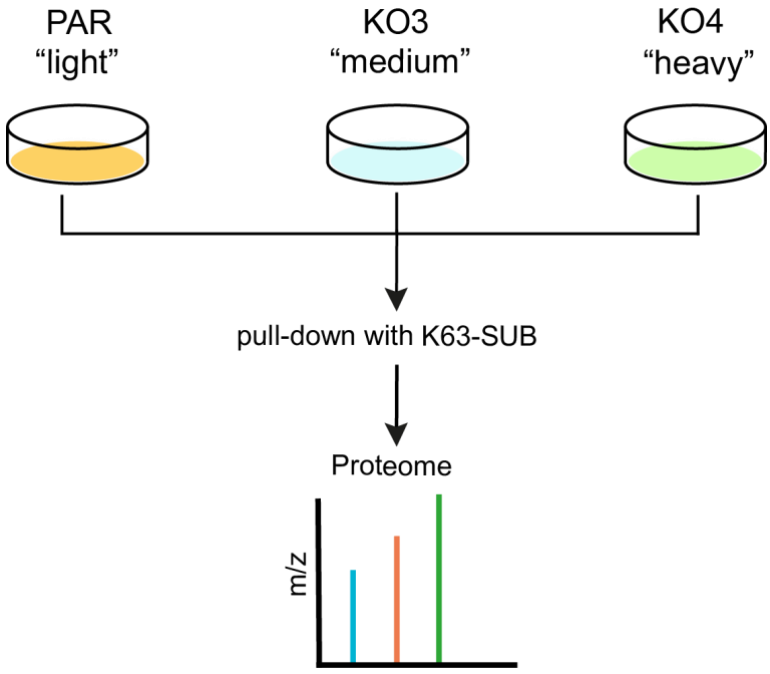

Figure 4.8 Overview of proteomics of K63-ubiquitin pull-down with K63-SUB protein.
HeLa GPF-HRS Parental (PAR), AMSH KO3 and KO4 were labelled each in a different SILAC medium for 8 passages. The cells were lysed in HS-RIPA buffer and 5mg of each condition were pooled together. 15mg cell lysate was incubated with 15µg of streptavidin-coupled K63-SUB protein for 4h in the cold. The eluate of the pull-down was run onto an SDS-PAGE.

Fifteen µg of K63-SUB protein were coupled to streptavidin agarose beads and left to rotate on a wheel for 1h in the cold. Then the three SILAC labelled cell conditions were lysed in HS-RIPA buffer supplemented with 55mM 2-chloroacetamide (CAA) to prevent every DUBs from removing ubiquitin from substrate proteins in these cells. Three mg of each cell

condition were mixed at a 1:1:1 ratio and incubated with the previously coupled streptavidin K63-SUB beads. After 4h of incubation, the beads were washed, and bound proteins were eluted. Each of the eluates of four independent biological replicates were resolved by SDS-PAGE (**Figure 4.9**). The gels were stained with Coomassie blue staining and then 6 equally sized gel slices were cut and subjected to in-gel trypsin digestion in Liverpool.

The LC-MS analysis was run in the lab of Alfred Vertegaal, (Leiden, the Netherlands) by Fredrik Trulsson and the data were inputed in MaxQuant to obtain the ratios of the SILAC label intensity for each protein ID (Cox et al., 2009).

The IDs based on less than 2 peptides were excluded from the analysis. The log_2 of KO3/Parental (Medium/Light) and KO4/Parental (Heavy/Light) were calculated and all protein ID values whose log_2 ratio (FC) KO3/Par and KO4/Par were equal or above 0.7 were taken into consideration as enriched in the K63-ubiquitin proteome of AMSH KO cells.

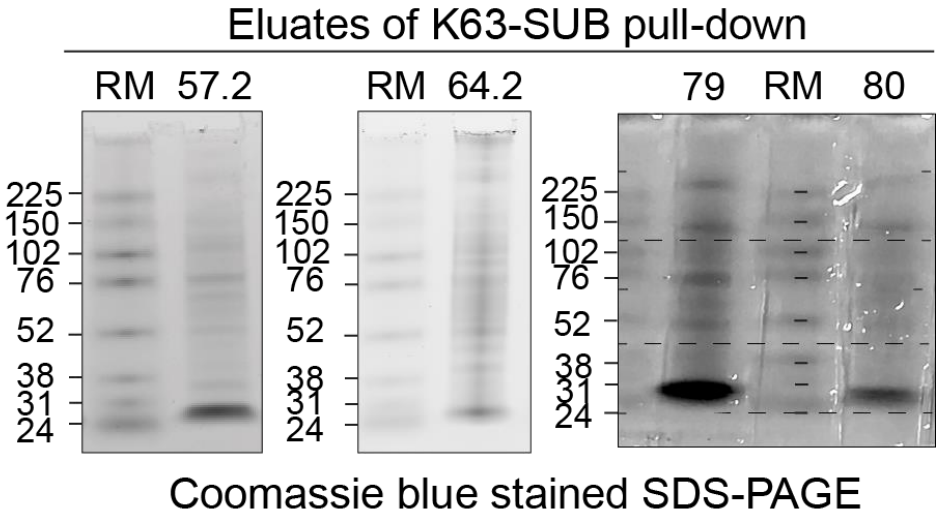

Figure 4.9 Protein gels of the eluates from four K63-SUB pull-downs experiments.
SILAC labelled HeLa GFP-HRS Flp-In parental (Light), AMSH KO3 (Medium) and KO4 (Heavy) were lysed either in TUBES (exp 57.2) or in HS-RIPA lysis buffer (exp 64.2 ,79, and 80). The lysates were pooled in a 1:1:1 ratio and incubated with Streptavidin-agarose beads coupled K63-SUB. The beads were washed, and elution was achieved with 30µl of reducing and alkylating sample buffer. All eluates were run on a 4-12% SDS-PAGE in 1x MOPS buffer. The gel was stained at RT for 1h with Coomassie blue stain and de-stained, thus it was scanned with a Licor Odissey scanner in the 700 nm channel.

The protein IDs of the K63-ubiquitin proteomes from four repeats were plotted in the JMP13 application. Experiment 57-2 displayed the greatest number of proteins upregulated in both AMSH KO clones and the vast majority were enriched more in KO3 than KO4 (**Figure 4.10 A**). In all the other repeats, the protein hits appeared to spread more evenly in the upper-right quadrant of the graph (**Figure 4.10 B**). I observed that in at least two experiments, few protein IDs were enriched in both AMSH KO clones above a fold change $\log_2$ KO/PAR above 0.7: PDCD6IP (ALIX), SDCBP (Syntenin1), ATP6V0D1 and CLCN7 (**Figure 4.10 D**).

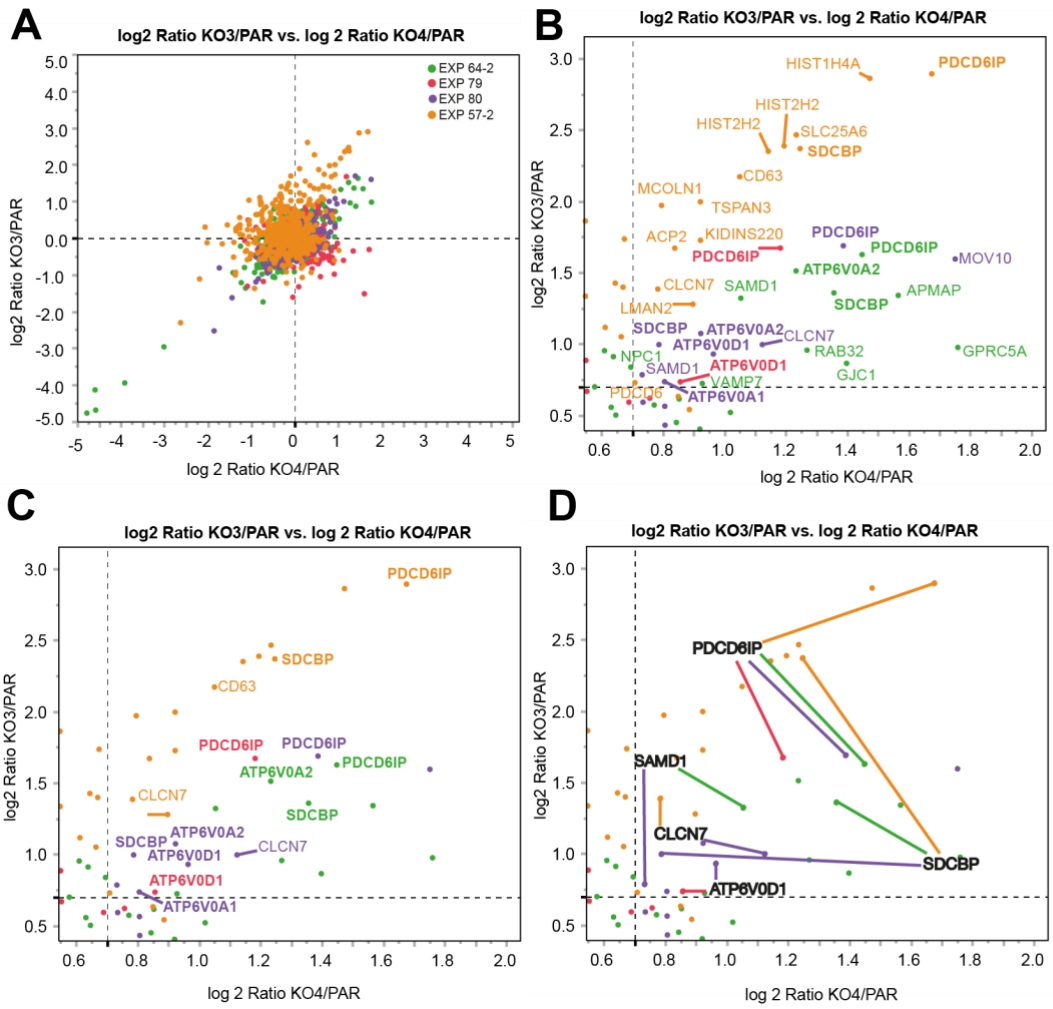

Figure 4.10 Dot plots of K63-ubiquitin enriched proteomes of HeLa AMSH KO3 and KO4 compared to Parentals.
All the protein IDs identified in four independent K63-SUB pull-down experiments were plotted using the JMP13 application. The protein IDs found in all four repeats are shown in A. B shows the protein IDs that are enriched in both AMSH KO clone derived samples. C shows the protein IDs enriched in both KOs compared to parental in at least two experiments,

including proteins that are different subunits of the same protein (ATP6V0A1/2). Lastly, in the panel D, the protein IDs highlighted are those enriched in both KOs compared to parental in at least two experiments, excluding different subunits of the same protein.

Only five K63 SUB interactors were enriched in all 4 experiments in both AMSH KO clones. Interestingly, all but one (SAMD1), have roles in the endo-lysosomal system based on their annotation on Uniprot.

1. PDCD6IP (programmed cell death 6-interacting protein), aka ALIX is involved in endocytosis, multivesicular body biogenesis, membrane repair, cytokinesis, apoptosis and maintenance of tight junction integrity. This protein binds to the phospholipid lysobisphosphatidic acid (LBPA) which is abundant in internal vesicles of MVBs.
2. SDCBP (Syntenin-1) is an adapter protein involved in trafficking of transmembrane proteins, exosome biogenesis and has been implicated in tumorigenesis.
3. ATP6V0A2 is the integral membrane subunit of the V0 complex of vacuolar ATPase.

   ATP6V0A2 can localise both to the plasma membrane and intracellular compartments. The ATP6V0A2 subunit uses ATP to transport protons that acidify intracellular compartments (in particular lysosomes) in eukaryotic cells.
4. ATP6V0D1 is the V-type proton ATPase subunit D1 part of the integral membrane V0 complex of vacuolar ATPase.
5. CLCN7 is a H(+)/Cl(-) exchange transporter 7 that mediates the exchange of chloride ions against protons. This works as an antiporter to increase the acidification of the lysosome lumen.
6. SAMD1 is an unmethylated CpG islands (CGIs)-binding protein that represses transcription by recruiting chromatin modifiers.
7. CD63 is a tetraspanin protein that regulates internalisation of cell surface receptors such as the VEGFR2. CD63 is important in coordinating the signalling mediated by VEGFR and the endothelial cell adhesion. CD63 resides on both the plasma membrane and is enriched at internal vesicles of late endosomes which can be secreted externally as exosomes.
8. NPC1 is a cholesterol transporter from the endosomes to lysosomes. NPC1 mutations have been linked to the Niemann-Pick C1 (NP-C) Disease

which is a genetic lipid storage disorder of low-density lipoprotein (LDL)-derived cholesterol affecting the neuro-visceral system.

Table 14. Proteins enriched in the K63-ubiquitin related proteome of AMSH KO cells in at least two experiments.
The table shows the proteins that are enriched in at least 2 experiments. The protein hits having a value above the 0.7 cut-off are indicated in bold. NaN = not a number. The protein IDs enriched in AMSH KO3 and KO4 over parental cells in at least two biological repeats were entered in the STRING database multiprotein search query. To be able to appreciate both functional and physical interactions, I asked the database to display the protein hits (spheres, nodes) connected by coloured edges with a minimum interaction score of 0.4 which has a medium confidence.

Exp. number	Uniprot number	Gene name	Protein name	FC (log_2) KO3/Par, KO4/Par	Number of peptides
57.2	Q8WUM4	PDCD6IP	ALIX	2.89, 1.67.	17
64.2	Q8WUM4	PDCD6IP	ALIX	1.62, 1.44.	23
79	Q8WUM4	PDCD6IP	ALIX	1.67,1.18.	15
80	Q8WUM4	PDCD6IP	ALIX	1.68, 1.38.	19
57.2	O00560	SDCBP	Syntenin1	2.46, 1.24.	11
64.2	O00560	SDCBP	Syntenin1	1.35, 1,35.	8
79	O00560	SDCBP	Syntenin1	0.88, 0.49.	8
80	O00560	SDCBP	Syntenin1	0.99, 0.78.	7
57.2	Q9Y487	ATP6V0A2	V-type proton ATPase 116 kDa subunit a 2	1.43, 0.34.	8
64.2	Q9Y487	ATP6V0A2	ATPase 116 kDa subunit a 2	1.51,1.23.	8
79	Q9Y487	ATP6V0A2	ATPase 116 kDa subunit a 2	0.93,0.50.	8
80	Q9Y487	ATP6V0A2	ATPase 116 kDa subunit a 2	1.07, 0.92.	7
57.2	P61421	ATP6V0D1	V-type proton	NaN, NaN.	0

			ATPase subunit d 1		
64.2	P61421	ATP6V0D1	V-type proton ATPase subunit d 1	-0.15, 0.06.	3
79	P61421	ATP6V0D1	V-type proton ATPase subunit d 1	0.73,0.85.	3
80	P61421	ATP6V0D1	V-type proton ATPase subunit d 1	0.92, 0.96.	4
57.2	Q93050	ATP6V0A1	V-type proton ATPase 116 kDa subunit a 1	1.05, 0.66.	5
64.2	Q93050	ATP6V0A1	ATPase 116 kDa subunit a 1	-0.33, 0.01.	5
79	Q93050	ATP6V0A1	ATPase 116 kDa subunit a 1	0.59, 0.68.	4
80	Q93050	ATP6V0A1	ATPase 116 kDa subunit a 1	0.73, 0.80.	2
57.2	P51798	CLCN7	H(+)/Cl(-) exchange transporter 7	1.38, 0.78.	7
64.2	P51798	CLCN7	H(+)/Cl(-) exchange transporter 7	0.57,0.77.	3
79	P51798	CLCN7	H(+)/Cl(-) exchange transporter 7	NaN	5
80	P51798	CLCN7	H(+)/Cl(-) exchange transporter	0.99, 1.12.	2

			7		
57.2	Q6SPF0	SAMD1	Sterile alpha motif domain-containing protein 1	NaN, NaN.	0
64.2	Q6SPF0	SAMD1	Sterile alpha motif domain-containing protein 1	1.32, 1.05.	6
79	Q6SPF0	SAMD1	Sterile alpha motif domain-containing protein 1	0.75, 0.25.	5
80	Q6SPF0	SAMD1	Sterile alpha motif domain-containing protein 1	0.78, 0.73	5
57.2	P08962	CD63	CD63 antigen	2.17, 1.05.	2
64.2	P08962	CD63	CD63 antigen	0.50, 0.39.	2
79	P08962	CD63	CD63 antigen	0.68, 0.50.	1
80	P08962	CD63	CD63 antigen	0.69, 0.46.	1
57.2	O15118	NPC1	NPC intracellular cholesterol transporter 1	1.43, 0.03.	3
64.2	O15118	NPC1	NPC intracellular cholesterol transporter 1	0.83, 0.69.	4
79	O15118	NPC1	NPC intracellular cholesterol transporter	0.81, 0.53.	2

			1		
80	O15118	NPC1	NPC intracellular cholesterol transporter 1	0.16, 0.45.	1

The first thing I noted was that there are 2 networks. The first network is composed of (ALIX) and SDCBP (Syntenin1) and CD63 (**Figure 4.11 A**), while a second network is made of the different subunits of the vacuolar ATPase enzyme (v-ATPase) (**Figure 4.11 B**). Lastly, SAMD1 and CLCN7 were not connected neither functionally nor physically with any of the other proteins analysed (**Figure 4.11 C**).

The protein-protein interaction has been experimentally determined for CD63, Syntenin1 and ALIX which typically co-segregate to the same microdomain in late-endosome derived exosomes and interact with each other (Baietti et al., 2012). Although not physically interacting with CD63, NPC1 was reported to be required for the endo-lysosomal recruitment of Rab8 to organelles containing a fluorescently labelled form of cholesterol (Kanerva et al., 2013)

Lastly, the ATP6V0D1, ATP6V0A1 and ATP6V0A2 subunits physically interact since they are different subunits of the same complex (Kissing et al., 2015) (**Figure 4.11 B**).

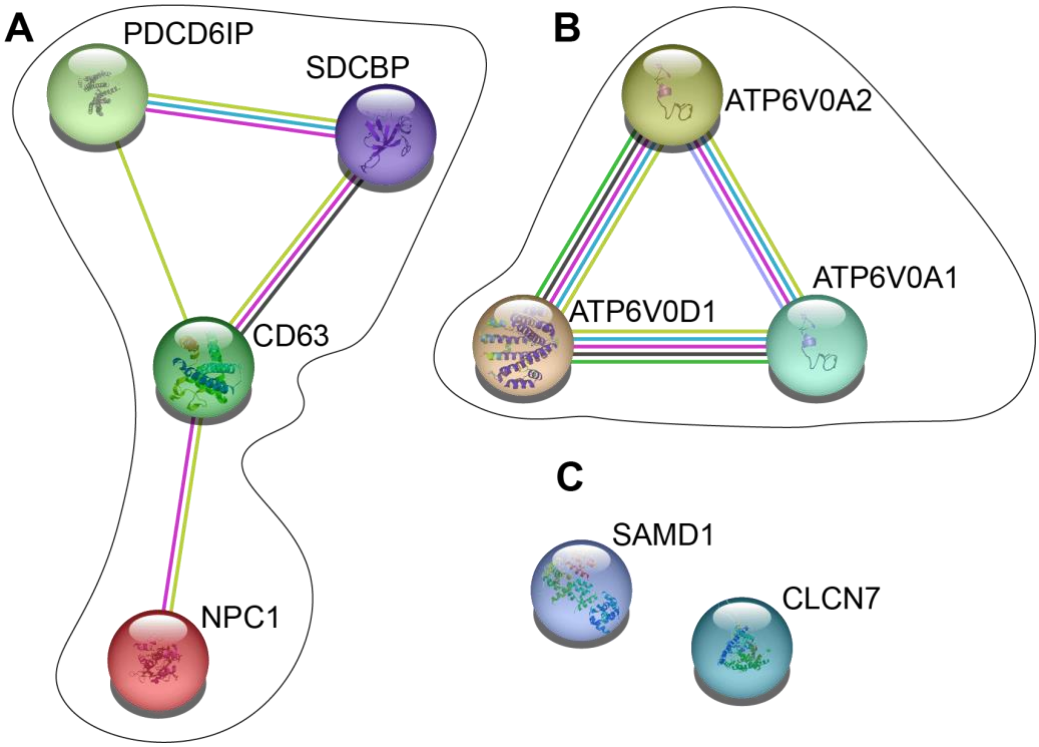

Figure 4.11 Interactions between proteins enriched in the K63-ubiquitin related proteome AMSH KO cells in at least two experiments.

The protein hits enriched in at least two biological repeats of the K63-ubiquitin related proteomes of AMSH KO3 and KO4 over parental were entered in the STRING interaction database. The interactions (both physical and functional) between the proteins (spheres) are showed as coloured lines depending on the type of evidence. Light green= text mining, light blue= from curated databases, dark green= gene neighbourhood, pink= experimentally determined, black= co-expression.

4.5 Discussion

In this chapter, I was able to produce the K63-ubiquitin specific binding domain K63-SUB and use this tool to efficiently enrich K63-ubiquitin linked chains from lysates of SILAC-labelled HeLa GFP-HRS parental, AMSH KO3 and KO4 cells. The proteomes of parental and the two AMSH KO cell lines were analysed by mass-spectrometry and significant differences between both KOs and the parental cells were found. Not all these differences were replicated in 4 independent experiments. I found that a restricted number of proteins are reproducibly enriched in the K63-ubiquitin associated proteomes of AMSH KOs, and most of these have roles in the endo-lysosomal system (**Table 14**).

It should be mentioned that a caveat lies in the fact that I did could not assess the protein levels of these protein hits in our AMSH KO, thus one cannot rule out that they are enriched in the K63-ubiquitin proteome because of an elevation of their total levels.

The attachment of K63-ubiquitin to endosomal cargo proteins is a requirement for their trafficking to MVB in yeast; mutants unable to extend K63-ubiquitin chains have smaller MVBs and fewer ILVs (Erpapazoglou et al., 2012). Endosomal sorting of the EGFR has been shown to be induced by K63-linked ubiquitylation in mammalian cells (F. Huang et al., 2013). It is known that AMSH depletion induces an enhancement of the EGF induced downregulation kinetics (McCullough et al., 2004). This raises questions whether K63-ubiquitin chains that need to be cleaved by AMSH could work as a scaffold for proteins that ensure correct MVB biogenesis. If this is true, then one might expect that AMSH KO would increase sorting of cargoes to other compartments such as lysosomes or MVB-generated exosomes.

The finding that the K63-ubiquitin related proteome of AMSH KO clones had identified proteins that are mostly localised to the endo-lysosomal compartment supports the idea that AMSH could be acting on K63-ubiquitin that impact the biology of endo-lysosomal compartments.

ALIX and Syntenin1 are the main hits, and their strong enrichment in the K63-ubiquitin proteome of AMSH KO clones could be justified by the fact that either of the two is modified with K63-ubiquitin.

Exosomes are organelles arising from the intra-luminal vesicles of multi-vesicular bodies (late-endosomes) that can be released in the extra-cellular environment whose biogenesis depends on recruitment of ALIX and Syntenin1 to MVBs (Baietti et al., 2012).

ALIX and Syntenin1 were identified as strongly enriched in all four biological repeats of the K63-ubiquitin associated proteomes of AMSH KOs. Both ALIX and Syntenin1 have both been shown to co-localise with ubiquitin and interact with K63-ubiquitin which could point to them having a regulatory function upon K63-ubiquitin modified substrates (Dowlatshahi et al., 2012; Rajesh et al., 2011).

ALIX is a Bro1 family protein and is a ubiquitin receptor belonging to the ESCRT complex (Pashkova et al., 2013). ALIX uses its Bro1 domain to bind to ESCRT-III protein Snf/CHMP4, while the central three Pro-rich domains bind TSG-101 (ESCRT-I subunit) (McCullough et al., 2008; Elias et al., 2020). ALIX preferentially binds to K63-linked tetra-ubiquitin chains, via its V domain (Dowlatshahi et al., 2012).

Syntenin1 is a PDZ domain adaptor protein that can interact with a large plethora of membrane proteins like syndecan (Grootjans et al., 1997).

Syntenin1 has been shown to have ubiquitin-binding properties and binds equally well to both K63- and K48-ubiquitin. Syntenin1 dimerisation is critical for its binding to ubiquitin via its $L^{4}YPSL^{8}$ domain (Rajesh et al., 2011).

Syntenin1 interacts with CD63, a tetraspanin protein reported to help cluster plasma membrane proteins in the tetraspanin-enriched microdomains (TERMs). Syntenin1 was reported to be required for the co-precipitation of ubiquitylated proteins from immobilised CD63 fragment, indicating that Syntenin1 uses ubiquitin to interact with CD63 among other transmembrane protein partners (Rajesh et al., 2011).

Importantly, Syntenin1 can be poly-ubiquitylated and in its hyper-ubiquitylated state Syntenin1 binds more tightly to CD63 (Rajesh et al., 2011).

These findings prompt me to speculate that ALIX and/or Syntenin1 could be differentially modified with K63-ubiquitin in AMSH KO cells compared to parentals.

CD63 was enriched only in one of the K63-ubiquitin proteomics repeat but was identified in all four with log2 ratio not too far off the cut-off. This finding points to the possibility that AMSH KO cells could have increased sorting of ubiquitylated proteins that are associated to CD63 TERM microdomains.

The STRING analysis indicated that the strongest functional enrichment in the network analysed in **Figure 4.11** was for biological processes of positive regulation of exosomal secretion and positive regulation of extracellular exosome assembly, GO: 1903543 and GO:1903553, respectively.

In fact, these ALIX and Syntenin1 interact and have been shown to cooperate in exosome biogenesis. Indeed, ALIX and Syntenin1, are adaptor proteins that together with CD63 they regulate exosome biogenesis generating from multi-vesicular bodies and are them-selves sorted in exosomes (Baietti et al., 2012).

Are K63-ubiquitin chains an endosome signalling platform for proteins involved in exosome biogenesis?

In the next chapter, I will undertake further studies to understand the link between K63-ubiquitin, AMSH and exosome biology.

Chapter 5: A role for AMSH in the exosomal pathway.

5.1 Introduction

In the previous chapter I have generated a tool to enrich protein lysates for K63-ubiquitin chains and have unbiasedly analysed the K63-ubiquitin associated proteomes of HeLa GFP-HRS Flp-In Parental and AMSH KO3 and KO4 cells. I have identified a small set of proteins that are coherently enriched in both KOs.

In this chapter, I will report my efforts to validate the protein hits found to be enriched in the K63-ubiquitin proteomics results and determine whether these proteins are differentially expressed or modified with K63-linked ubiquitin chains in AMSH KO cells.

K63-ubiquitin modification is required for cargo receptors to be sequestered at the endosomal membrane and is important to ensure an adequate MVB morphology and size for example in yeast (Erpapazoglou et al., 2012). ALIX and Syntenin1 were the most consistently enriched protein hits in the K63-ubiquitin related proteomes of AMSH KO3 and KO4 cells. Interestingly, ALIX and Syntenin1 together play a pivotal role in the biogenesis of exosomes which are secreted vesicles originating from intra-luminal vesicles of the multi-vesicular bodies/ late endosomes (Baietti et al., 2012).

For this reason, I assessed whether AMSH plays a role in the trafficking of cargo proteins through the exosomal route.

5.2 Validation of results from the K63-ubiquitin associated proteomic dataset.

As the K63-ubiquitin proteomics revealed an enrichment of a small group of proteins in both KO3 and KO4 compared to the parental cells, I sought to validate the mass spectrometry results seen by western blotting.

In principle, proteins may appear enriched in the K63-pull-down in the AMSH KO cells, but in fact just be more highly expressed in the AMSH KO cells rather than being enriched more strongly in the K63-ubiquitin SUB pull-down. These western blots will a) show whether their expression level

is increased or unchanged in the AMSH KO cells, b) show whether the enrichment of these proteins in the K63-SUB pull-down seen in the mass spec is reproducible, and c) potentially reveal higher molecular weight bands as an indication of ubiquitylation.

I started the validation experiments with Alix and Syntenin1, for which antibodies detected multiple bands in western blots. For this reason, I first depleted these proteins using siRNA to help identify the specific bands. I used VPS26A siRNA as a positive control for the knockdown procedure. I also tested an antibody against CD63, a tetraspanin protein that is a major component of exosomes and interacting partner of Syntenin1. CD63 had also been detected as an outlier in the pull-down carried out in TUBES lysis buffer of one K63-ubiquitin-associated proteomic dataset, suggesting its ubiquitylation may be enhanced in AMSH KO cells (**Table 14**).

CD63 is a tetraspanin protein which is heavily glycosylated, and runs as a smear on a WB, ranging from 27-60 kDa (**Figure 5.1).** Two specific ALIX bands were identified: a major one at 110 kDa and a minor one at 85 kDa, compatible with isoforms 1 and 3, while Syntenin1 (predicted MW: 33kDa) is identified as a single ~30 kDa band. Depletion of either ALIX or Syntenin1 does not affect the expression levels of either one nor the expression of CD63 (**Figure 5.1**).

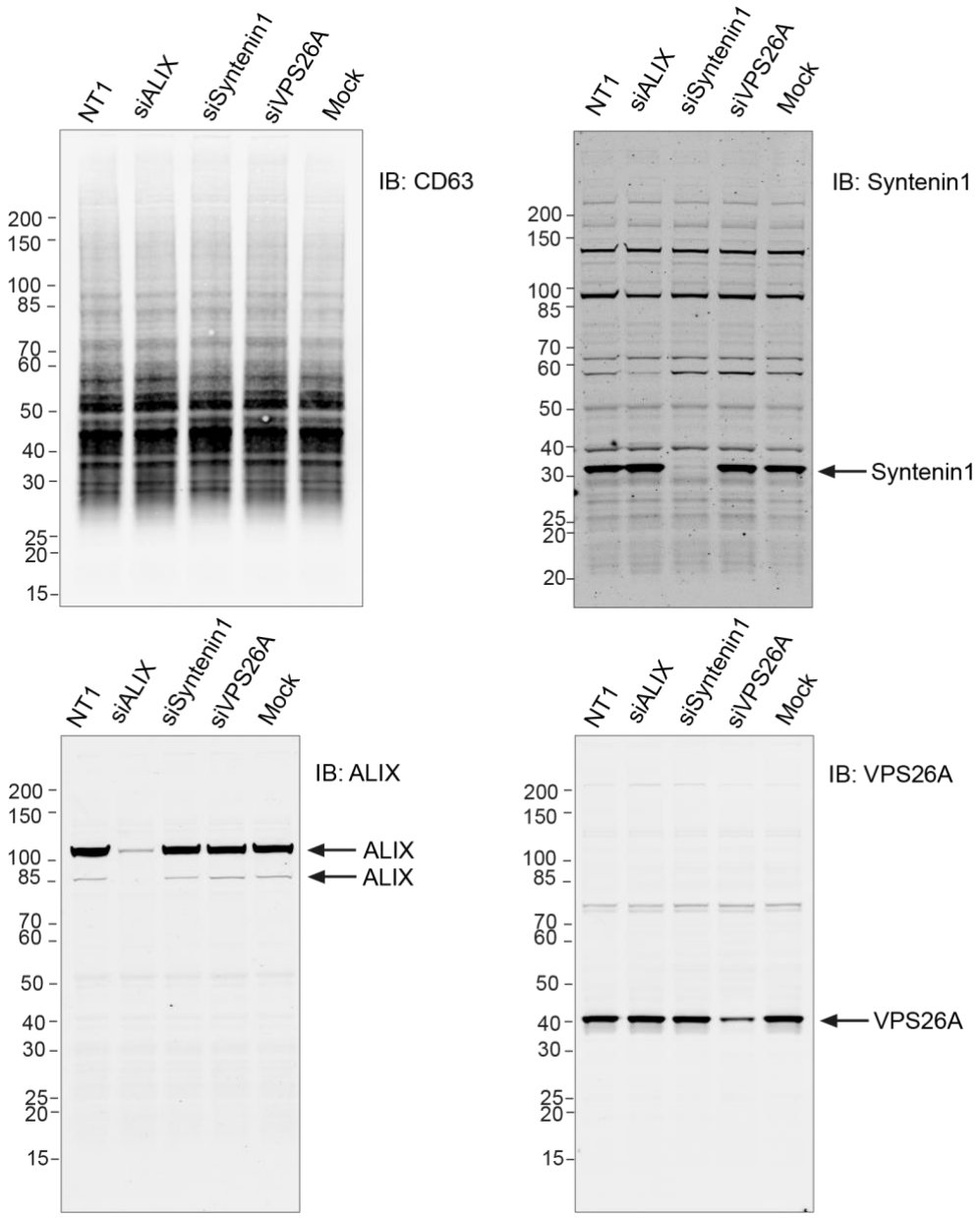

Figure 5.1 Knock down of ALIX and Syntenin1 identifies specific protein bands by Western blot.
HeLa GFP-HRS Flp-In cells were treated with 40 nM of non-targeting siRNA (NT1) or a pool of siRNA oligos targeting ALIX, Syntenin1 or VPS26A (positive control). After 72 h, the cells were lysed in NP-40 lysis buffer. Non reducing sample buffer was added to the sample probed with the CD63 antibody, whereas reducing sample buffer was used for the other samples probed for ALIX, Syntenin1 and Vps26. Arrows indicate specific bands. The ALIX membrane was re-probed for VPS26A.

HeLa GFP-HRS parental, AMSH KO3 and KO4 HeLa cells were lysed in HS-RIPA buffer and subjected to the same K63-ubiquitin pull-down used for

the proteomics experiments. I then eluted the proteins enriched by the K63-SUB coupled streptavidin beads and analysed them by WB.

In samples run in both reducing and non-reducing conditions, the K63-ubiquitin pull-down yields a smear ranging from 30 to 200 kDa (**Figure 5.2 A-C, right hand panels**). The Western Blot quantitation shows that K63-ubiquitin levels in the KO3 eluate are 2 and 2.6-fold, and in KO4 ~1.5 fold more elevated than in the parental cells (**Figure 5.2 A-C, right hand panel and 5.2 D)**. This increase reflects the increase seen in the input samples and for KO3 also in the AQUA experiments (**Figure 3.12)**.

The mass spectrometry data showed that ALIX was enriched in 4 repeats with a Log_2FC between 1.2 and 1.67 and Syntenin1 was enriched in 3 repeats with a Log_2FC between 0.8-1.4 as in the figures and below (**Table 14**).

The western blot of the input samples shows that there are no differences in expression levels between Parental and KO cells for Syntenin1, AMSH or CD63. The ALIX blot shows a discrete band at 100kDa that in the eluates of both KO3 and KO4 was increased more than two-fold compared to parentals and is of the same magnitude as for K63-ubiquitin (**Figure 5.2 A, left hand panel**). In contrast, for Syntenin1, the K63-ubiquitin pull-down yields a band at 30 kDa which is twelve times higher in the KO3 condition and ~4 higher in the KO4 condition compared to parentals. Normalised to K63-ubiquitin, Syntenin1 is enriched 6x in AMSH KO3 and 2x in KO4. compared to parental cells. This is a much higher increase, suggesting that it might be ubiquitylated itself (**Figure 5.2 B, E**). CD63 is likewise enriched over K63-ubiquitin (**Figure 5.2 C, F**).

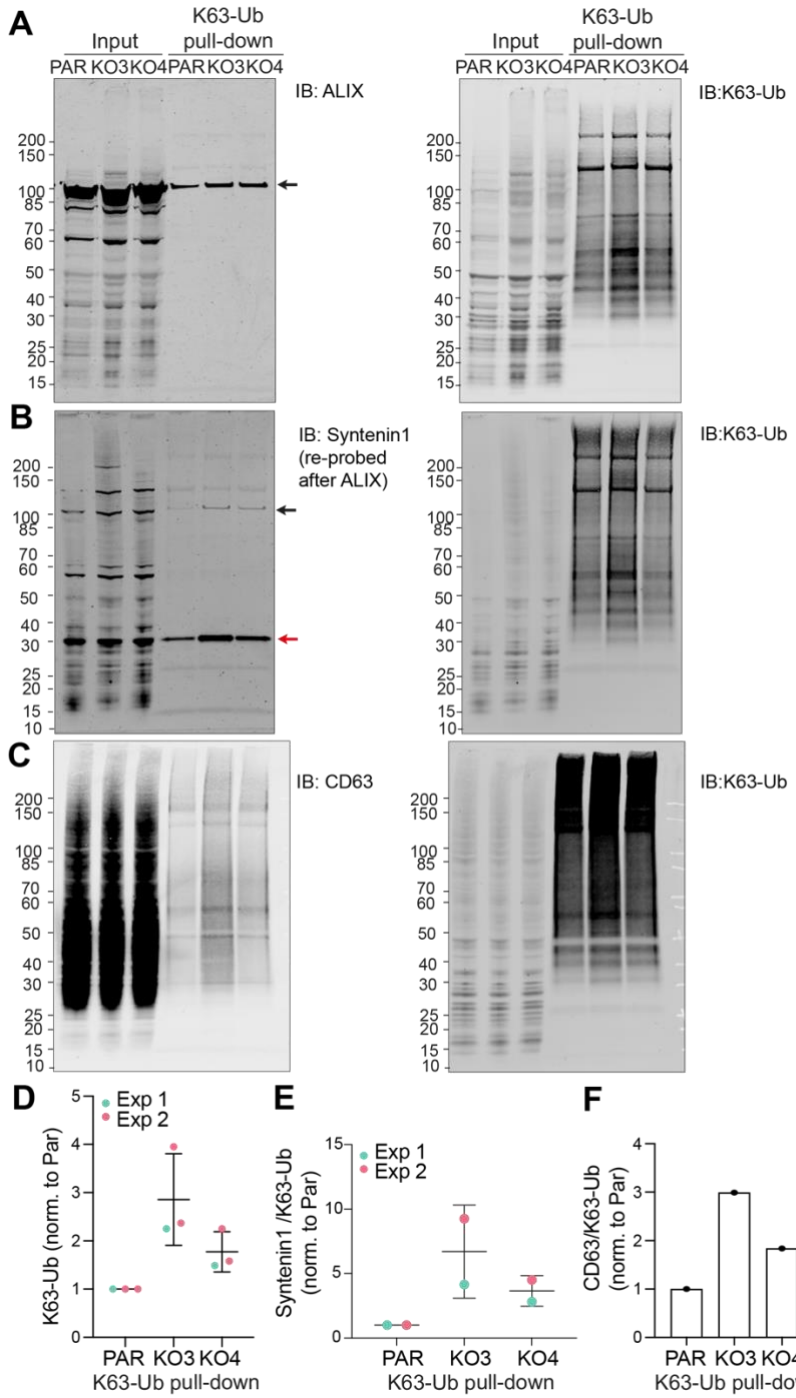

Figure 5.2 Syntenin1 is enriched in K63-ubiquitin pull-downs from AMSH KO cells.

A-C HeLa GFP-HRS Flp-In parental, AMSH KO3 and KO4 were lysed in HS-RIPA buffer. The cell lysates (3 mg) were incubated with 3 µg of K63-SUB for 4 h in the cold. Inputs and eluates were run on 4-12% Nu-PAGE gels and probed with specific antibodies. ALIX, Syntenin1, CD63 membranes were each re-probed for K63-Ub as shown in A, B and C. **D** K63-ubiquitin signal normalised to PAR, 2 biological repeats with 2 technical repeats each. **E** The Syntenin1 signal was normalised to K63-ubiquitin and then parental (PAR) samples. n=2. F CD63 signal was normalised to K63-ubiquitin and to PAR, n=1. A-B black arrow indicates ALIX. **B** red arrow indicates Syntenin1. Error bars indicate range.

The mass spectrometry data showed that the VATP6 V0D1 subunit was only detected in 2 out of 4 repeats and that it was increased each time in both AMSH KOs with a $Log_2FC < 1$ (**Table 14**).

I firstly evaluated the distribution of endogenous VATP6 V0D1 by fixing the cells in 4% PFA (paraformaldehyde) and staining with the subunit specific V0D1 antibody. The immunofluorescence showed a punctate staining pattern for V0D1 that was largely distinct from GFP-HRS and did not differ between parental and AMSH KO cells (**Figure 5.3 A**).

Next, I sought to compare the expression levels of VATP6 V0D1 and potentially ubiquitylated species by lysing the cells in NP-40 lysis buffer supplemented with 20 mM NEM which inhibits ubiquitin E1, E2 and E3 ligases and DUBs that have a catalytic Cys in their active site. Even though AMSH is not a Cys protease, a previous PhD student John McCullough found that AMSH is sensitive to NEM and speculated that this may be due to the presence of a conserved Cys residue at position 353. The Western Blot shows a major VATP6V0D1 band that runs at the expected molecular weight (40 kDa) (**Figure 5.3 B**). This band does not change between parental and AMSH KOs, but interestingly, I observed two bands at 50 and 65 kDa which clearly increase in both the untreated and NEM-treated AMSH KO cells compared to Parentals. Their molecular weight is compatible with a mono and di-ubiquitylated species, respectively (**Figure 5.3 B**).

To check whether V0D1 is indeed differentially modified with K63-ubiquitin in AMSH KO cells, I performed a pull-down with the K63-SUB in Parental and AMSH KO3 and KO4 cells. While in the input lanes the amount of V0D1 is unchanged between parentals and AMSH KO cells, in the K63-ubiquitin pull-down the amount of V0D1 relative to K63-ubiquitin is increased in AMSH KO cells compared to the parental cells. However, I did not detect the high-MW species in the pull-down, despite including another Cys-reactive agent, 2-chloroacetamide (CAA) in the lysis buffer (**Figure 5.3 C, D**).

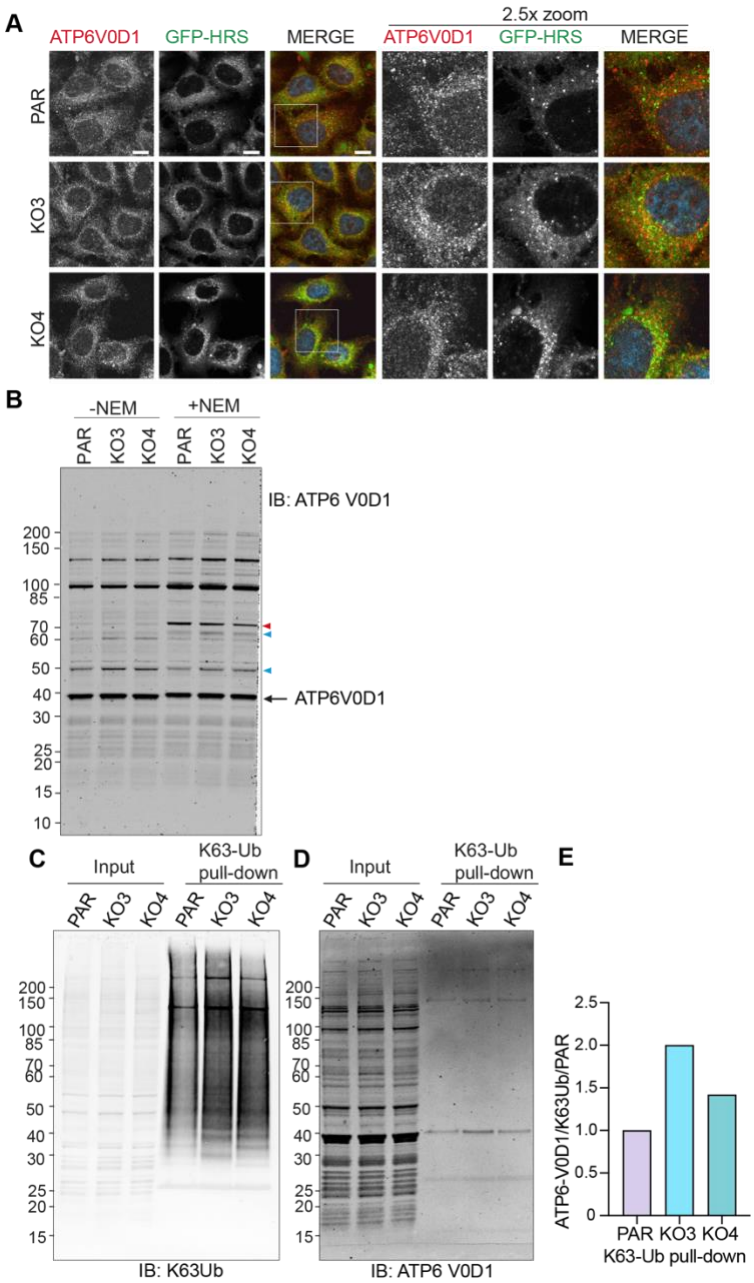

Figure 5.3 The total levels of VATP6 V0D1 subunit do not change in AMSH KOs compared to parental cells.

A HeLa GFP-HRS Flp-In parental, AMSH KO3 and KO4 were fixed in 4% PFA and stained with the ATP6V0D1 antibody. Scale bar = 10 µm, inset shows 2.5x enlarged boxed area. Blue = DAPI staining. **B** The cells were lysed in NP-40 with or without 20 mM NEM. The samples were loaded onto a 4-12% bis-tris gel and the membrane was incubated with ATP6V0D1 antibody. **C-D** The cells were lysed in HS-RIPA buffer with 20 mM CAA. The cell lysates (3 mg) were incubated with 3 µg of K63-SUB for 4 h in the cold. The eluates were loaded onto a 4-12% bis-tris gel and the membrane was incubated with ATP6V0D1 antibody (C), then it was re-probed with K63-ubiquitin (D). Black arrow indicates specific band. Blue arrowheads indicate potential ubiquitylated species. **E** Quantification of data shown in C and D: the VATP6V0D1 signal was normalised to K63-ubiquitin and to parental.

I then sought to find out whether ALIX co-localises with K63-ubiquitin in our cells and whether it is recruited to K63-ubiquitin-positive structures in AMSH KO cells.

Since I was not able to detect the endogenous ALIX by immunofluorescence with the commercial antibody used for WB, I transfected cells with a plasmid expressing Flag tagged full-length ALIX. The cells were then fixed and dually stained with Flag and K63-ubiquitin antibodies to assess co-localisation with K63Ub positive structures (**Figure 5.4)**. The pattern of Flag-ALIX distribution differs between HeLa Parental and both AMSH KO3 and KO4. In parental cells, Flag-ALIX shows a punctate signal and appears to be predominantly localised to the perinuclear area where it partially co-localises with K63-ubiquitin. In AMSH KO clones Flag-ALIX staining shows a diffuse signal but strongly co-localises with K63-ubiquitin and accumulates at cell peripheral structures (**Figure 5.4**). This finding suggests that ALIX might be differentially recruited to peripheral K63-ubiquitin positive structures in AMSH KOs.

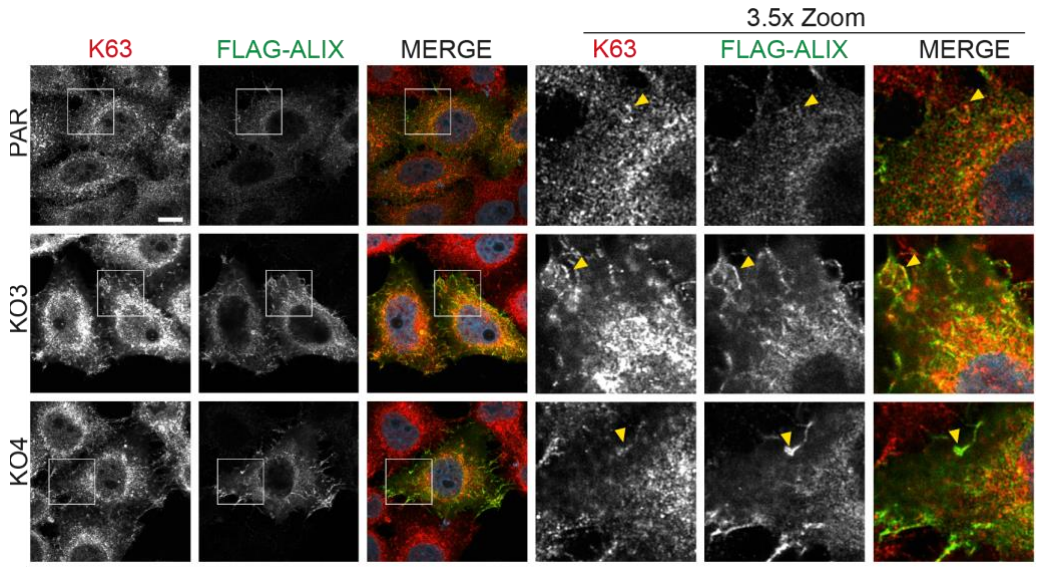

Figure 5.4 Flag-ALIX accumulates at K63-ubiquitin-positive filamentous structures at the cell periphery of AMSH KO cells.
HeLa GFP-HRS FLp-In parental, AMSH KO3 and KO4 were transfected with the Flag-ALIX plasmid. After 24 h, the cells were fixed in 4% PFA and co-stained with the Flag (sigma) and K63-ubiquitin antibodies. Imaging was carried out at the LSM900 with the 63x oil objective. Scale bar= 10 µm, inset shows 3.5x enlarged boxed area. Yellow arrowheads indicate co-localisation.
Blue = DAPI staining.

AMSH cleaves K63-ubiquitin at endosomes and I had previously shown that K63-ubiquitin is accumulating at GFP-HRS negative cellular structures in AMSH KO cells. I wondered whether these structures could be multi-vesicular bodies/late endosomes.

I wondered whether the K63-ubiquitin positive but GFP-HRS negative structures that I had observed in AMSHKO cells in Chapter 3 are in fact CD63-positive MVBs. I co-stained HeLa GFP-HRS parental and AMSH KO clones for K63-ubiquitin and CD63. I did not observe a significant change in the number and distribution of CD63 positive puncta between parentals and AMSH KO cells (**Figure 5.5**).

I found good colocalisation between K63-ubiquitin and CD63 with many K63-ubiquitin positive structures also positive for CD63. However, the K63-ubiquitin increase in the AMSH KO cells was not so apparent in this experiment. This indicates that the AMSH KO cells may have adapted to the K63-ubiquitin accumulation, as these are cells at later passage than the immunofluorescence shown in the previous chapters (**Figure 3.13**).

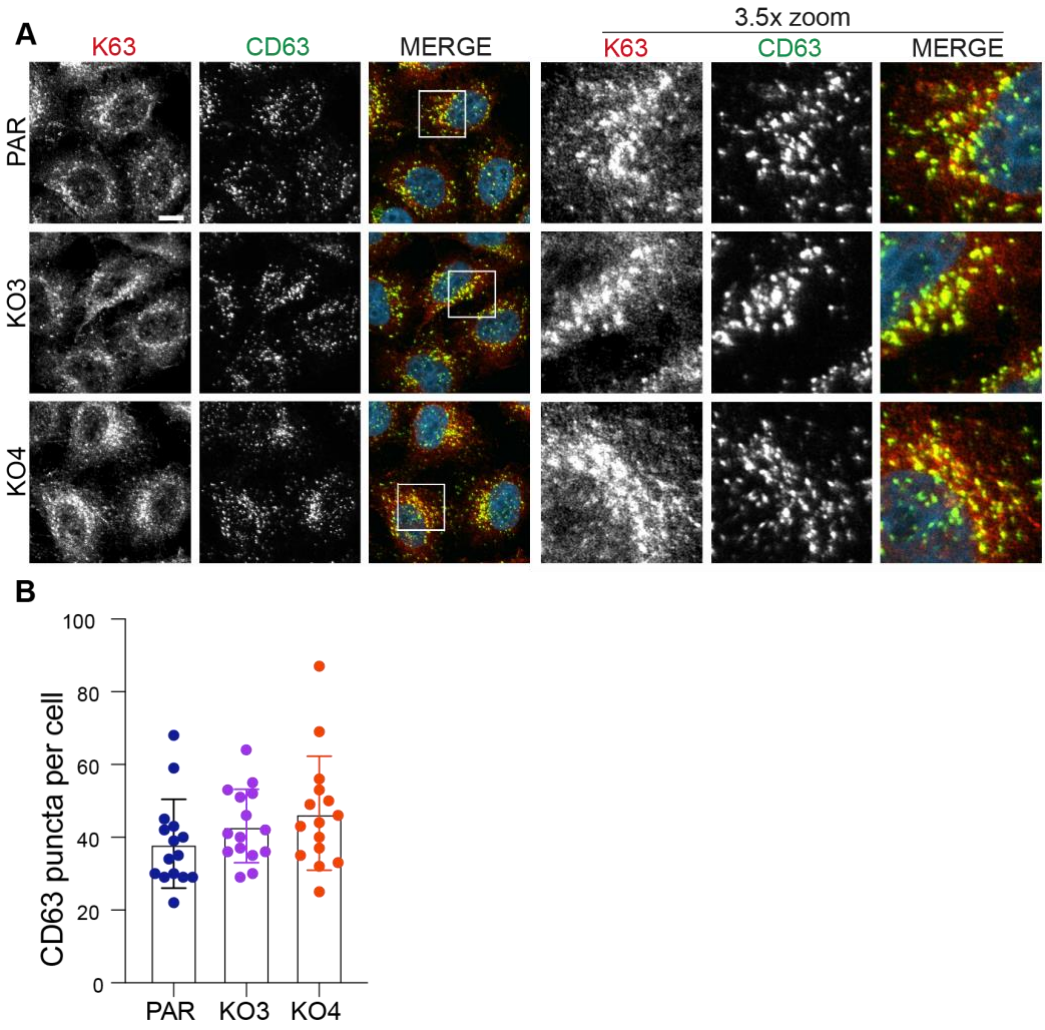

Figure 5.5 K63-ubiquitin strongly co-localises to CD63 positive structures both in Parental and AMSH KO cells.
A HeLa GFP-HRS parental, AMSH KO3 and KO4 were fixed in 4% PFA/PBS and stained with K63-ubiquitin and CD63. The coverslips were imaged at a LSM900 confocal microscope with a 63x oil objective. B Quantification carried out on 9 cells. Error bars indicate range. n=1. Scalebar = 10 µm, inset shows 3.5x enlarged boxed area. Blue = DAPI staining.

To check whether MVB morphology or distribution was affected in AMSH KO cells, I co-stained HeLa GFP-HRS, AMSH KO3 and KO4 with the CD63 antibody and LAMP1 antibody (**Figure 5.6 A**). These two markers are expected to co-localise at the membrane of a subset of MVBs. The average number of LAMP1 positive puncta was not significantly changed in AMSH KO clones compared to parentals cells. Similarly, the number of CD63 positive puncta was again unchanged between parental and AMSH KO cells (**Figure 5.6 A, B**). LAMP1 and CD63 strongly co-localised in both HeLa GFP-HRS Parental cells and AMSH KO cells (**Figure 5.6 A**).

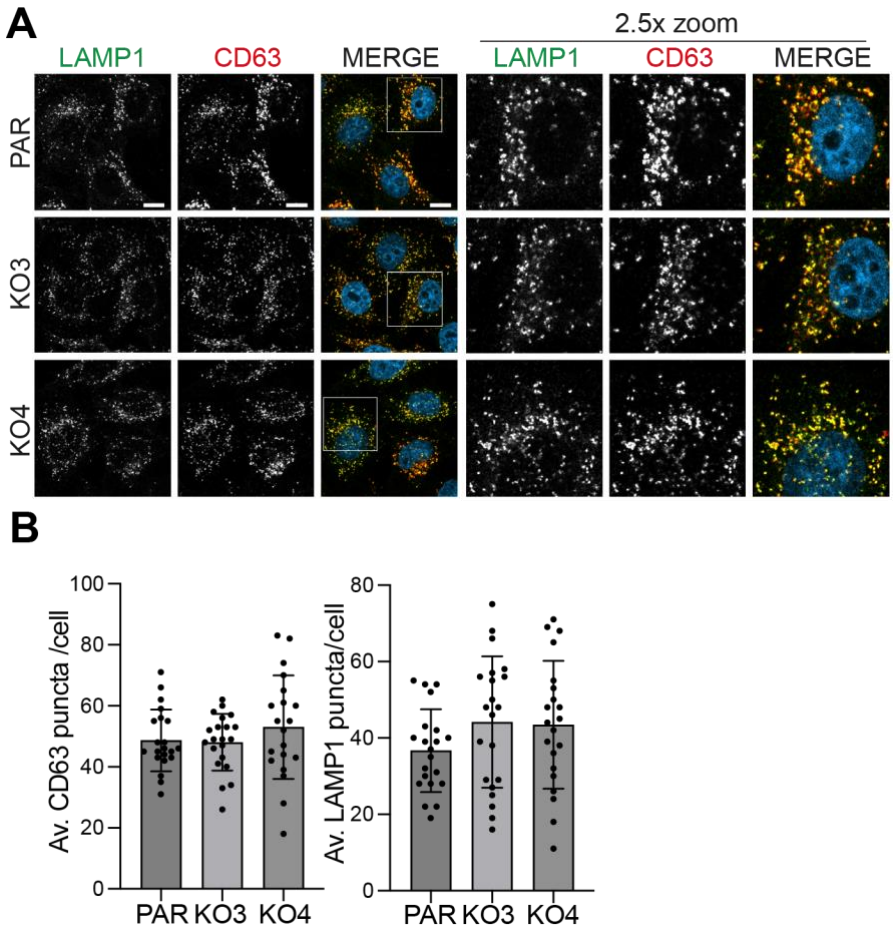

Figure 5.6 AMSH KO does not change the overall abundance of CD63 and LAMP1 positive endolysosomes.
A HeLa GFP-HRS parental, AMSH KO3 and KO4 were fixed in 4% PFA/PBS and stained with CD63 and LAMP1 antibodies. The coverslips were imaged with a 63x oil objective using the LSM900 confocal microscope. Scalebar = 10 µm, inset shows 2.5x enlarged boxed area. Representative of 3 experiments. Blue = DAPI staining. **B** The number of CD63- and LAMP1 positive puncta was quantified for 20 cells, error bars show the range.

I also checked whether overexpression of AMSH affects the morphology or distribution of CD63-positive endosomes/MVBs. HeLa S3 Flp-In cells were transfected with either wild type GFP-AMSH or catalytic mutant GFP-AMSH (D348A) plasmids and were fixed and stained with the CD63 antibody (**Figure 5.7**).

These cells express endogenous AMSH, therefore this experiment was aimed at assessing whether overexpression of wild type or mutant GFP-AMSH had a positive or possibly a dominant negative effect. In order to quantitate the number of CD63-positive MVBs, I took images with a lower magnification objective (40x objective) at the confocal microscope. At this

magnification, individual clustered MVBs are no longer resolved and GFP-AMSH-D385A expressing cells appeared to contain fewer CD63-positive puncta (**Figure 5.7 A, C**).

The cells were also imaged at higher magnification (63x objective). GFP-AMSH (both catalytically inactive and wild type) showed very little co-localisation with CD63-positive MVBs. In the GFP-AMSH D348A mutant transfected cells, CD63-positive puncta appeared larger than those observed in wild type GFP-AMSH transfected cells (**Figure 5.7 B**).

This indicates that despite not strongly colocalising with CD63, catalytically inactive mutant AMSH affects the morphology of CD63-endolysosomes. Indeed, the puncta might appear bigger because of CD63 clustering due to a fission defect.

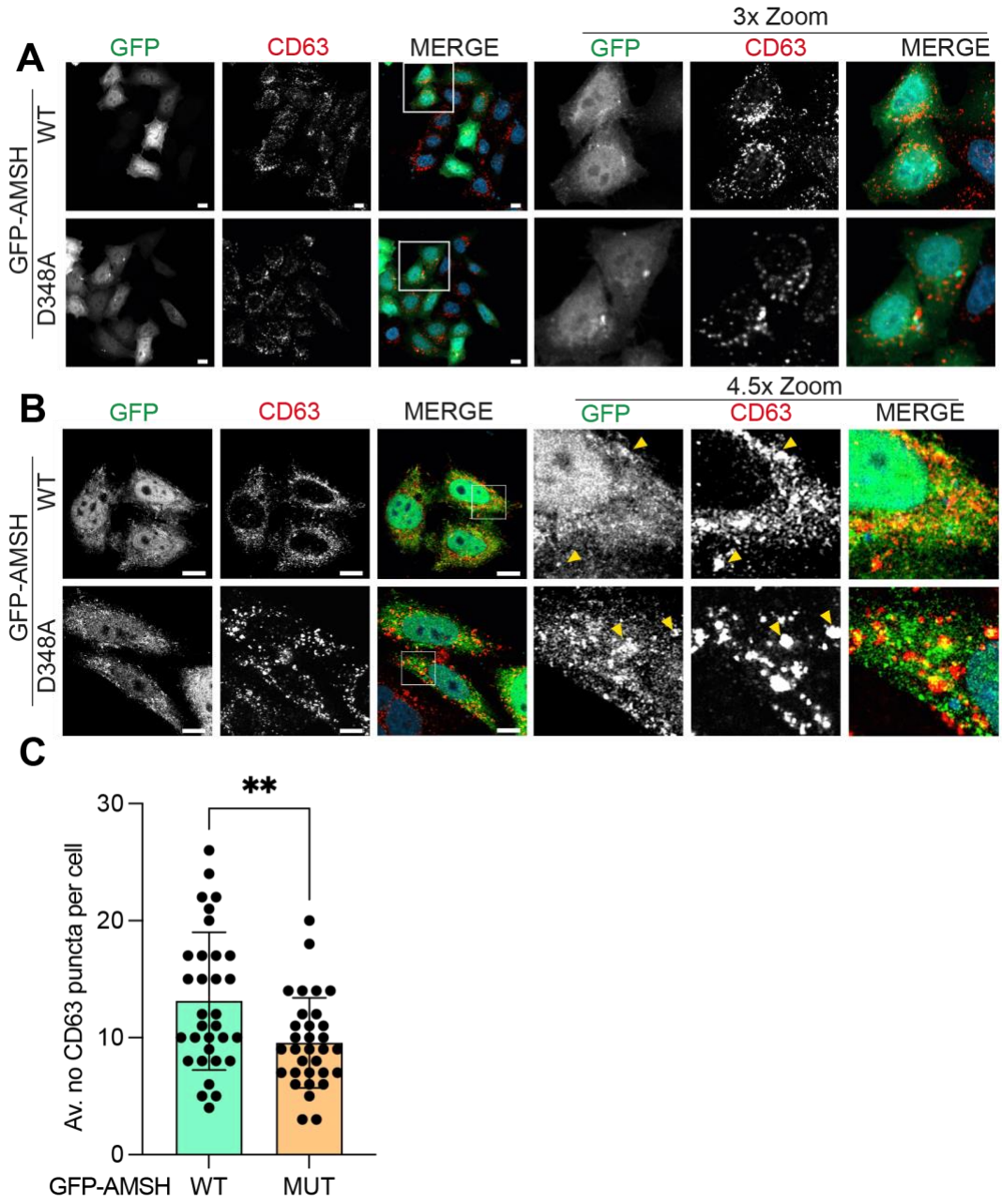

Figure 5.7 Mutant GFP-AMSH (D348A) transfected HeLa cells have fewer and larger CD63-positive MVBs compared to WT GFP-AMSH transfected cells.

A HeLa Flp-In Parental cells were transfected with 1µg of either (WT) GFP-AMSH or GFP-AMSH (D348A) mutant plasmid. After 24 h, the cells were fixed and stained with the CD63 antibody. The coverslips were imaged at the LSM900 confocal microscope with a 40x water objective, scalebar = 10 µm, inset shows 3x enlarged boxed area. **B** The same coverslips were imaged with a 63x oil objective, scale bar = 10 µm, inset shows 4.5x enlarged boxed area. Blue = DAPI staining.**C** The number of CD63-positive puncta was quantified using the "analyse particles" function in FIJI. The graph shows the single measurements, the average, and the standard deviation. Quantification was carried out on 32 cells for each condition. Statistical significance was calculated using an unpaired t-test. P-value <0.01. Error bars show the range.

5.3. Exosome composition and release in AMSH KO cells.

ALIX and Syntenin1 have been reported to be recruited at CD63-positive microdomains of MVBs to ensure correct exosome biogenesis (Baietti et al., 2012).

I sought to assess whether exosomal composition/ biogenesis was affected by AMSH KO. In order to do this, I first applied an exosome enrichment strategy. This approach involves harvesting media from cells grown for 16 hours under serum free conditions. The media were then subjected to an ultracentrifugation step at 100,000g after a first spin at 10,000g. The exosome content can be estimated by probing for the most prominent exosome marker, CD63. In addition, exosome secretion can be enhanced by treatment with Bafilomycin A which inhibits the vacuolar ATP-ase mediating endosomal acidification (Edgar et al., 2016).
The amount of CD63 released via exosomes derived from the media of bafilomycin treated cells was unaffected by AMSH KO. However, the K63-ubiquitin signal associated with the exosomes was clearly increased in the AMSH KO (KO4) cells, and this was most apparent in the MW range above 80 kDa (**Figure 5.8**). This suggests that exosomes released from AMSH KO cells contain increased levels of K63-ubiquitin modified proteins released from AMSH KO4 versus parental cells. A second set of samples was probed for Syntenin1. The expected molecular weight of Syntenin1 is 33 kDa, as shown by the Syntenin1 knock down in **Figure 5.1.** The 33 kDa Syntenin1 band decreases in AMSH KO4 exosomes compared to the parental sample. Interestingly, at the same time, an additional higher molecular weight species of Syntenin1 band was detected at 40 kDa, only in the AMSH KO4 exosome sample. I wondered whether the 40 kDa Syntenin1 band may correspond to a post-translationally modified form of this protein. The fact that the sum of the intensities of the two Syntenin1 bands in the KO4 is equal to the main band in the Parental, could suggest that the 40 kDa band is a dynamic modification affecting a small proportion of the Syntenin1 secreted in exosomes from AMSH KO4 cells (**Figure 5.8**).

On the other hand, the Syntenin1 blot in **Figure 5.1** showed a band at 40 kDa which did not disappear upon Syntenin1 depletion, suggesting this may be a non-specific cross-reactive band (**Figure 5.1**). Since, Syntenin1 can both be ubiquitylated and phosphorylated, further investigation is needed to clarify whether this higher molecular weight Syntenin band is indeed a ubiquitylated species (Rajesh et al., 2011).

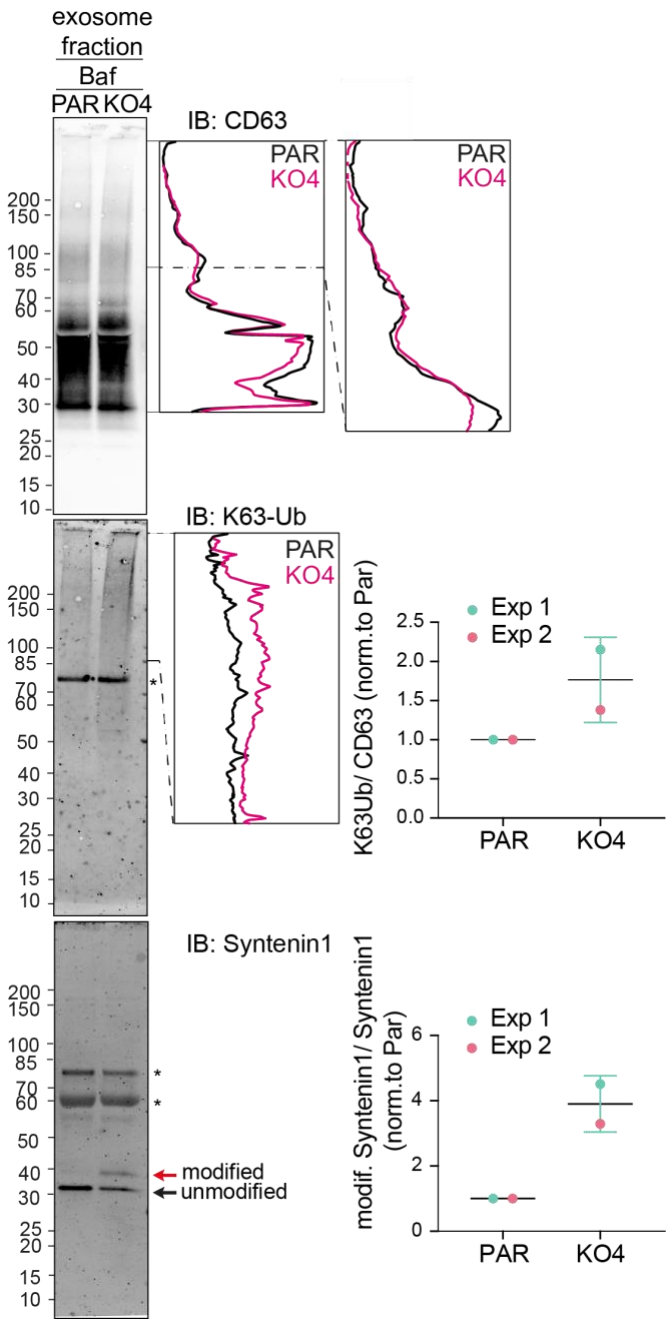

Figure 5.8 Exosome-enriched fractions from AMSH KO4 cells contain more K63-ubiquitin and an additional Syntenin1 band compared to parentals.

HeLa GFP-HRS Flp-In parental and AMSH KO4 cells were treated with 100 nM of bafilomycin A for 16 h. The medium was collected and subjected to a 10,000g and 100,000g spins in a Beckman 50.2Ti rotor. Pellets were resuspended in PBS and boiled with reducing sample buffer (samples probed for Syntenin1) or non-reducing sample buffer (samples probed for CD63 and K63-ubiquitin). The line graphs show the quantification of the whole CD63 smear and of the K63-ubiquitin smear from 80 kDa to the top. The K63-ubiquitin signal was normalised to CD63 and to parental (top plot) and the modified Syntenin1 was normalised to the unmodified, n=2. *non-specific band. Error bars show the range.

Nevertheless, I note that the modified Syntenin1 band found in exosome enrichments has a molecular weight of ~40kDa which is compatible with mono-ubiquitylation (**Figure 5.8**).

The exosome-enriched fractions from HeLa GFP-HRS parental and AMSH KO4 media contain equal levels of CD63, but 1.4-fold higher levels of K63-ubiquitin (**Figure 5.9**). This suggests that the same amount of CD63 is secreted, but it is now more ubiquitylated and this hypothesis remains to be tested (**Figure 5.9).**

I wanted to validate this using an alternative method. I decided to use an HA-tagged Nanoluciferase construct that is fused to CD63 which had previously been used to study exosome secretion from HEK293 cells (Cashikar et al., 2019). The exosome secreted nanoluciferase can then be detected using a highly sensitive luminescent readout.

I also generated a HANL-Syntenin1 construct to look specifically at the Syntenin1 cargo, as I thought this may be ubiquitylated. I wanted to see whether Syntenin1 also co-localised with K63-ubiquitin and assess its potential secretion.

Dr. Phyllis Hanson (University of Michigan) kindly provided us with two dox-inducible expression constructs for HA-NanoLuciferase on its own and fused to CD63 (pcDNA4-TO constructs, referred below as 4TO). I generated two additional constructs that allow for constitutive expression of HANL-Syntenin1 and HANL-CD63 (pEF5 constructs) to check CD63 and Syntenin1 exosomal secretion by luminescence. Both Dox-inducible and constitutive constructs were first tested by western blotting in HEK293 Flp-In TREX and HeLa S3 Flp-In cells (**Figure 5.9**). HeLa S3 cells do not express a tet repressor or activator and thus the transgenes are expected to be expressed in a constitutive manner in both vectors. HEK cells need

the doxycycline treatment for expression from the pCDNA4-TO plasmids, as their gene expression is under an inducible repressor.

As expected, the expression of 4TO-HANL, 4TO-HANL-CD63 and 4TO-HANL-Syntenin1 is constitutive in HeLa S3 cells as is that of the corresponding pEF5 version of the same plasmids. All the doxycycline-inducible plasmids (4TO) show a leaky expression in the untreated HEK cells, while the expression of the pEF5 plasmids looks comparable to the non-induced. The concentration of 0.1 µg/ml of doxycycline is sufficient for maximal expression of the inducible plasmids in HEK cells (**Figure 5.9**).

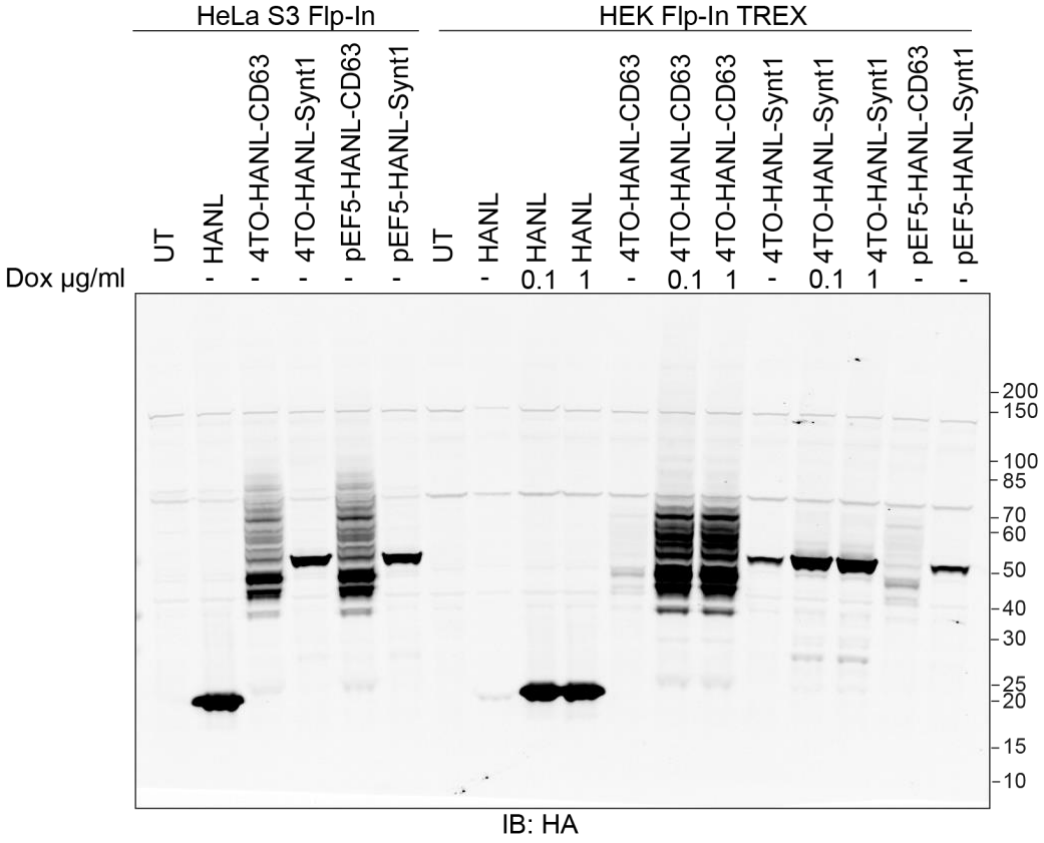

Figure 5.9 HANL-tagged exosome protein test transfection in cells.
HeLa S3 Flp-In cells were either left untransfected (UT) or transfected with 1 µg of pcDNA4-TO-HANL-1-1 (HANL), pcDNA4TO-HANL-CD63 (4TO-HANL-CD63), pcDNA4-TO-HANL-Syntenin1 (4TO-HANL-Synt1), pEF5-HANL-CD63-FRT-D-TOPO (pEF5-HANL-CD63), pEF5-HANL-Syntenin1-FRT-D-TOPO (pEF5-HANL-Synt1) for 18 h. HEK293 Flp-In TREX cells were transfected with the same plasmids as described above but they were either left uninduced, induced with 0.1 µg/ml or with 1 µg/ml of doxycycline after transfection. After 18 h, the cells were lysed in RIPA buffer and samples analysed by 4-12% Nu-PAGE gel and probed with HA antibody.

HeLa GFP-HRS Parental, AMSH KO3 and KO4 were transfected with the constitutively expressed HANL-Syntenin1 plasmid to analyse its

localisation. Syntenin1 has been found to localise to endosomal membranes and the plasma membrane (Fialka et al., 1999; Zimmerman et al., 2005). HANL-Syntenin1 does not co-localise with GFP-HRS positive puncta either in parentals nor in the AMSH KO cells. Instead, HANL-Syntenin1 is detected at both the cell-periphery and at the plasma membrane in parental and AMSH KO (**Figure 5.10**). These findings deviate from the literature showing that FLAG-tagged Syntenin1 has a prevalently punctate staining and localises to STAM1-positive endosomes (Rajesh et al., 2011; Fialka et al., 1999; Zimmerman et al., 2005). I therefore think it is possible that the larger HA-Nanoluciferase tag (180 amino acids) may interfere with the correct localisation of HANL-Syntenin1 (**Figure 5.10**).

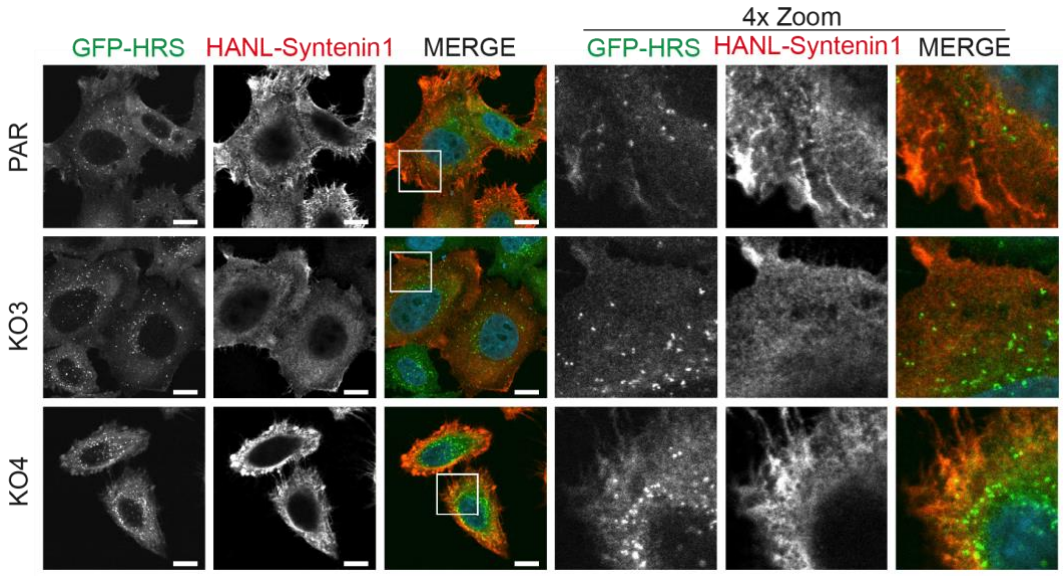

Figure 5.10 HANL-Syntenin1 does not localise to GFP-HRS endosomes but associates preferentially to cell peripheral structures in AMSH KOs versus parental cells.
HeLa GFP-HRS Flp-In parental, AMSH KO3 and KO4 cells were transfected with 1 µg of HANL-Syntenin1 plasmid. After 24 h the cells were fixed in 4% PFA and stained for HA. Scale bar = 10 µm, inset shows a 4x enlarged boxed area. Blue = DAPI staining.

HeLa GFP-HRS Parental, AMSH KO3 and KO4 cells were transfected with either HANL-CD63 or HANL-Syntenin1 plasmids and stained with both anti-HA and anti-LAMP1 to check their distribution respective to the late-endosome marker LAMP1 (**Figure 5.11**).

Under normal conditions, CD63 predominantly localises to the membrane of ILVs and the cell membrane and less strongly to the limiting membrane

of MVBs and to the trans-Golgi network (Pols et al., 2008). In contrast to the mislocalised HANL-Syntenin1, HANL-CD63 staining recapitulates the normal distribution of endogenous CD63 and colocalises extensively with LAMP1 (**Figure 5.11 A, B**).

To assess the exosome secretion in these cells, I determined the fractional release which corresponds to the ratio of luminescence in the media to the luminescence within cells and reflects how many exosomes are secreted (**Figure 5.11 C).** As the HANL-Syntenin fusion protein seemed to be mislocalised, I focused on the CD63-reporter. HeLa GFP-HRS parental, AMSH KO3 and KO4 cells were either left un-transfected or transfected with pEF5-HANL-CD63 plasmid. Twenty-four hours after transfection, the medium was exchanged on all cells either with or without addition of folimycin, which like bafilomycin, inhibits the VATP-ase and induces exosome secretion. After 5h, the media were harvested and the Nanoluciferase luminescence was measured.

For the untreated Parental cells, the secreted HANL-CD63 fraction was higher than that of both AMSH KO clones. However, upon folimycin treatment, both AMSH KO clones, displayed a larger fold increase in the secretion of HANL-CD63 than in the parental cells (**Figure 5.11 C**).

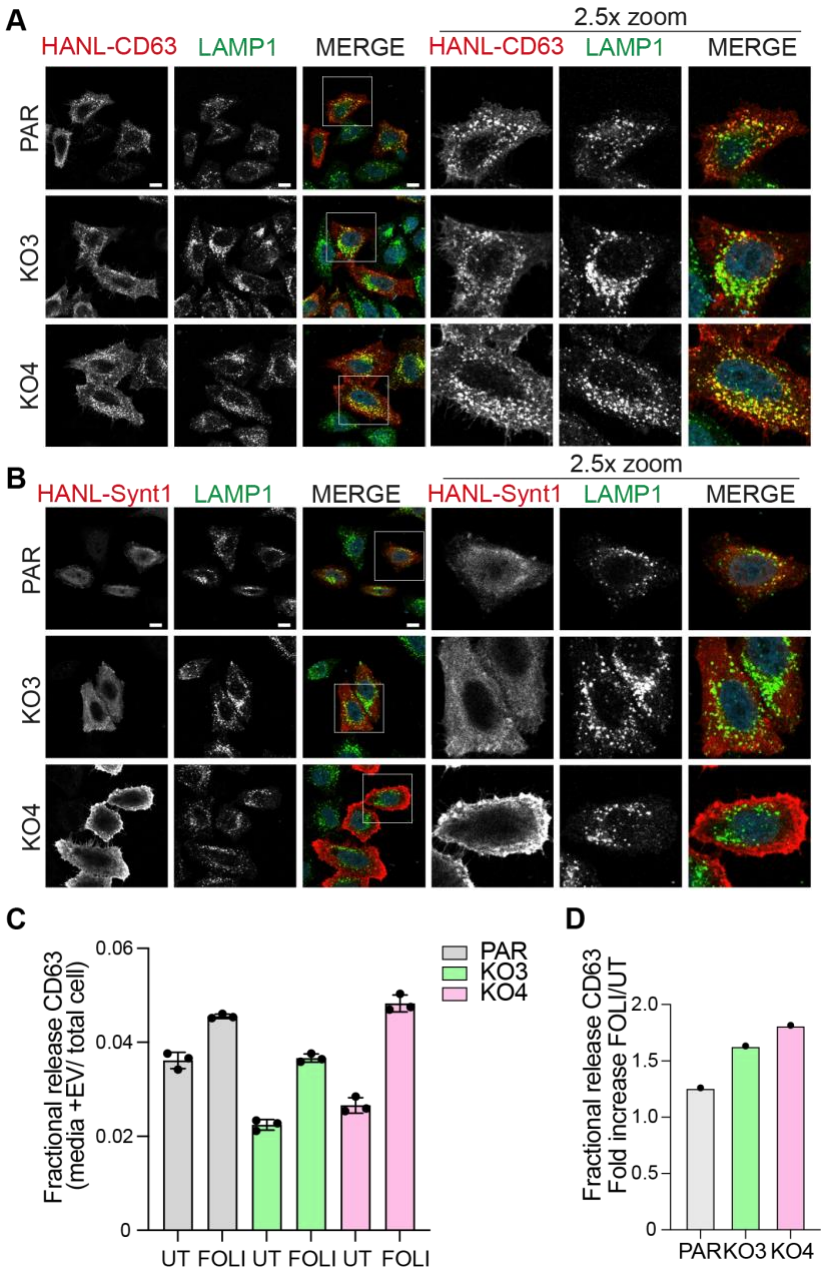

Figure 5.11 The fold increase of folimycin induced secretion of HANL-CD63 is higher in AMSH KO cells compared to parental.

A HeLa GFP-HRS parental, AMSH KO3 and KO4 were transfected with 1 µg of either pEF5-HANL-CD63-FRT-D-TOPO or pEF5-HANL-Syntenin1-FRT-D-TOPO plasmids for 24 h. Scalebar = 10 µm, inset shows a 2.5x enlarged boxed area. **B** The cells were fixed in 4% PFA and were co-stained with HA and LAMP1 antibodies. Imaging was performed at a LSM900 confocal microscope with a 63x oil objective. Scalebar = 10 µm, inset shows a 2.5x enlarged boxed area. Blue = DAPI staining. **C** HeLa GFP-HRS parental, AMSH KO3 and KO4 were transfected with 200 ng of pEF5-HANL-CD63-FRT-D-TOPO plasmid for 24 h. The medium was exchanged onto the cells either without (UT) or with folimycin for 5 h. The fractional release for each condition was plotted as luminescence in “media + EV” fraction /luminescence in “total cell” fraction. Error bars refer to technical replicates. One biological experiment is shown. **D** The fold change of the averages fractional release values normalised to parental for the 3 technical repeats were plotted.

5.4 Discussion

5.4.1 K63-ubiquitin might act as a scaffold to strengthen the interactions in the CD63-Syntenin1-ALIX complex.

In this chapter, I sought to validate the protein hits that were enriched in pull-downs of K63-ubiquitin chains using the K63-SUB domain in AMSH KO clones.

The two most clearly enriched proteins I identified, ALIX and Syntenin1, form a multi-molecular complex with the tetraspanin CD63 to concentrate cargo proteins at the limiting membrane of internal vesicles of MVBs (late endosomes) that are destined to become exosomes (Baietti et al., 2012). Interestingly, CD63 was also enriched in one experimental repeat, the K63-SUB pull-down in TUBES lysis buffer and was enriched ~2-fold in AMSH KO3 and ~1-fold in AMSH KO4 (**Table 14)**. Since the lysates were handled in a low stringency lysis buffer, this might mean that CD63 is co-isolated with ALIX and Syntenin1 in a transiently interacting complex.

Syntenin1 and ALIX were strongly enriched in the K63-ubiquitin pull-down from AMSH KO3 and KO4 clones compared to parentals (**Figure 5.2**). I wondered whether either of these proteins would be differentially ubiquitylated. Syntenin1 has 7 ubiquitylation sites as reported in the PhosphoSitePlus database (Hornbeck et al., 2015a) Two ubiquitylation sites have been identified with high confidence (using proteomics) at K14 and K185 which reside in the first PDZ domain of Syntenin1 (Hornbeck et al., 2015b). No upstream or downstream regulators of Syntenin1 ubiquitylation have yet been identified and the functional impact of this ubiquitylation is unknown. The PDZ domains are involved in binding to CD63, so the ubiquitylation could conceivably interfere with this interaction. ALIX has 32 ubiquitylation sites as reported in the PhosphoSitePlus database (Hornbeck et al., 2015a). Three ubiquitylation sites are reported as high confidence in this database, as they were identified by more than 10 high-throughput studies (K501, K638 and K640). All three ubiquitylation sites reside in the in the V domain of ALIX,

which itself is also known to bind to ubiquitin (Dowlatshahi et al., 2012; Keren-Kaplan et al., 2013) A recent study has shown that NEDD4L and WWP2 can both mono-ubiquitylate ALIX at residues K501 and K510 (Nelson et al., 2023). In addition, NEDD4L and WWP2 can add mono-ubiquitin onto K420 in ALIX (Nelson et al., 2023). Importantly, the mono-ubiquitylated form of ALIX is amorphous meaning less capable of forming fibrils (Nelson et al., 2023). ALIX's ability to form fibrils is important for its scaffolding role in recruiting ESCRT-III proteins (Larios, 2020; Nelson et al., 2023). Indeed, it is possible that the K63-ubiquitin pull-down enriched ALIX monomers rather than fibrils and that these could be modified with mono-ubiquitin rather than long chains. This may explain why I did not see a higher molecular weight ALIX species (**Figure 5.2**).

Another mono-ubiquitylation site was found on ALIX at K638 and this modification is induced by treating cells with vorinostat (suberoylanilide hydroxamic acid), an anticarcinogen which is an inhibitor of the histone deacetylase known to induce cancer cell apoptosis (Wu et al., 2015).

Mono-ubiquitylation of ALIX is proposed to inhibit its dimerization (Nelson et al., 2023).The function of monomeric ALIX is distinct from ALIX dimers, as only monomeric ALIX can sort Syntenin1 to exosomes, while ALIX dimers/multimers are enriched at F-actin polymers to exert a cytoskeleton remodelling function; these dimers are held together by di-sulphide bonds formed within ALIX disordered PRD region (Qiu et al., 2022a).

The K63-ubiquitin pull-down yielded single discrete ALIX and Syntenin1 bands suggesting that neither of the two proteins are differentially modified with K63-ubiquitin (**Figure 5.2**). Studies have shown that Syntenin1 is able to bind K48-linked and K63-linked ubiquitin with the same affinity (Rajesh et al., 2011) whilst ALIX shows a preference for K63-ubiquitin chains (Dowlatshahi et al., 2012). It is possible that I am just not detecting the ubiquitylated species if the epitope that the antibody recognises, is masked. Alternatively, it is conceivable, that ALIX and Syntenin1 are simply isolated together with K63-linked ubiquitin chains through non-covalent interactions. However, there must be a degree of specificity here as the mass spectrometry did not identify other clearly K63-ubiquitin binding proteins as an outlier (i.e. HRS or STAM).

In all 4 technical repeat pull-downs, K63-ubiquitin was enriched in the K63-SUB eluates from AMSH KO3 and KO4 cells compared to parentals. In two biological repeats of these pull-downs, Syntenin1 was the only protein hit that was consistently enriched in both KOs along with K63-ubiquitin (**Figure 5.2**). It is possible that Syntenin1 is enriched because of its tight association with K63-ubiquitin in AMSH KO cells rather than being itself differentially modified with K63-ubiquitin. Nevertheless, in the exosome enrichment of AMSH KO4 I saw an indication that Syntenin1 might be mono-ubiquitylated (**Figure 5.8**).

Differently from all other protein hits, the K63-ubiquitin pull-down showed that CD63 is identified as a higher molecular weight range smear starting at 30 kDa compared to input lanes where the protein runs as a 25-150 kDa smear (**Figure 5.2).** I speculate CD63 could be differentially modified with ubiquitin in AMSH KO cells but to check this one would need to pull-down CD63 and probe for ubiquitin or carry out a UBICREST assay (Hospental et al., 2015). CD63 is reported to be modified with ubiquitin at multiple sites, which all map to the tetraspanin domain (Kim et al., 2011; Wagner et al., 2011), but neither the ubiquitin modifiers involved, nor the functions of this modifications have been described yet. It is possible that in AMSH KO clones the binding of ALIX to both Syntenin1 and CD63 is increased due to ubiquitylation of CD63.

AMSH KO cells secrete less HANL-CD63 exosomes under basal conditions whilst the fold increase of HANL-CD63 exosome release in folimycin treated AMSH KO cells is higher than parentals (**Figure 5.11**). More experiments with the nanoluciferase would be needed to interpret the results, as I found that the parental cells have nearly the same amount release with and without Folimycin, which is at odds with the literature. Indeed, Hanson and colleagues showed that the fold increase of HANL-CD63 secretion upon concanamycin (folimycin) treatment compared to control was much higher than what I observed in my experiment (Cashikar et al., 2019).

In AMSH KO cells, overexpressed Flag-ALIX is localised to both cytoplasm, and peripheral structures, while in parentals it was mostly cytosolic (**Figure 5.4**). The staining pattern in AMSH KO cells resembled

that observed for overexpressed ALIX by others in HEK293 cells and is reminiscent of lamellipodia and filipodia staining (**Figure 5.4**) (Chatellard-Causse et al., 2002). ALIX was shown to localise at filopodium-like projections in muscle cells as it models F-actin cytoskeleton to induce cell protrusions by membrane curvature (Bongiovanni et al., 2012). Interestingly, the authors showed that Ozz E3 ligase can target ALIX and they infer that this ubiquitylation causes a conformational change in ALIX which would expose its V-domain in a so called “open conformation” (Bongiovanni et al., 2012). ALIX is known to bind K63-ubiquitin via its V-domain and this binding is involved in retroviral budding of HIV, for example (D.P. Dowlatshahi, 2012). Retroviral budding from the PM is a topologically equivalent budding reaction to the formation of ILVs and exosomes at MVBs, so I speculate that this binding is also important for exosome formation (Scourfield & Martin-Serrano, 2017). In this scenario, Flag-ALIX may co-localise to K63-ubiquitin puncta in AMSH KO cells to concentrate ubiquitylated cargo that would be sorted to exosomes (**Figure 5.4**). It is possible that ALIX distribution to filopodia is suppressed by AMSH. A link between AMSH and ALIX is also suggested by the corresponding Arabidopsis orthologue. AMSH-3 was shown to recruit the plant homologue of ALIX (Kalinowska et al., 2015). It would have been interesting to co-immunoprecipitate ALIX and AMSH to test whether this interaction is conserved in mammals. The recruitment of mammalian AMSH to endosomes is mediated by the CHMPs (ESCRT-III), STAM and Clathrin and ALIX has not been implicated in this (Agromayor & Martin-Serrano, 2006; McCullough et al., 2006; Nakamura et al., 2006). Interestingly, a paralogue of ALIX, HD-PTP has been shown to recruit USP8 to the ESCRT machinery (Ali et al., 2013).

Since I showed extensive co-localisation of nearly all K63Ub puncta with CD63, and much of the peripheral ALIX structures were also staining positive for K63 Ubiquitin, I speculate that these structures may in fact correspond to immature MVBs that have an exosome fate. In this scenario, AMSH KO may negatively affect assembly of the CD63-ALIX-Syntenin complex at MVBs or at exosomes whose biogenesis is incomplete. Alternatively, they are recruited to exosomes whose

extracellular secretion is hindered because of K63-ubiquitin accumulation (**Figure 5.4 and 5.10**). One way to assess MVB maturation is by either looking at lysobiphosphatidic acid (LBPA) enrichment at the intralumenal vesicles and by visualising the ability of endosomes to form ILVs by electron microscopy (Kobayashi et al., 1998).

In AMSH KO clones neither the number of CD63-positive nor LAMP1-positive puncta is significantly different compared to parentals, although their distribution appeared more clustered in AMSH KO cells (**Figure 5.6**). The CD63 western blot did not show an increase in CD63 protein levels in total lysates of AMSH KO cells (inputs).

However, if CD63 is indeed ubiquitylated in AMSH KO cells, it is conceivable that this could contribute to the clustering of MVBs due to ubiquitin dependent interactions between CD63, ALIX and Syntenin on distinct MVBs. I hypothesise that rather than an increase in the number of MVBs with an exosome fate, it is K63-ubiquitin modification that accumulates at both CD63 positive and negative MVBs in AMSH KO cells (**Figure 5.6**). In fact, the exosome enriched fraction from AMSH KO4 showed that there is more K63-ubiquitin in these fractions (**Figure 5.8**).

5.4.2. Multiple V-ATPase sub-units were co-isolated in the K63-ubiquitin associated proteome and may link AMSH to endosomal acidification and maturation.

The proteomics analysis revealed that the ATP6-V0D1 sub-unit was enriched in 2 biological repeats out of 4 but also that in one of these experiments the V0A1 and V0A2 subunits were also enriched (**Figure 4.10**). The V-ATPase subunit V0D1 is part of the proton pump complex specifically implicated in lysosomal acidification and biogenesis (Yang et al., 2019). The V0A1 and V0A2 subunits exert a structural function as integral membrane domains, the V0D1 couples the proton transport to hydrolysis of ATP (Yang et al., 2019). For the ATP6 V0A1 subunit it was reported that ubiquitylation at K666 can be observed upon proteasome inhibition with MG132 (Wagner et al., 2011). In the ATP6 V0A2 subunit there are two Lys residues, K172 and K374 which are ubiquitylated upon treatment with the vorinostat and MG132 inhibitor, respectively (Wagner et al., 2011; Wu et al., 2015). Similar to the V0A2, the V0D1 subunit, K343

can be ubiquitylated upon vorinostat treatment, indicating they are co-regulated (Wu et al., 2015).

ATP6 V0D1 protein expression levels appeared unchanged in the AMSH KO cells both based on Western Blot and immunofluorescence analysis (**Figure 5.3 A, B**). Interestingly, the K63-ubiquitin pull-down only yielded a single 40 kDa band for V0D1 whose levels were higher in both AMSH KO clones than in parentals. No higher molecular weight species were found to be enriched by K63-ubiquitin pull-down, which would suggest that ATP6-V0D1 was not modified with K63-ubiquitin and that it might be co-isolated with K63-ubiquitin chains (**Figure 5.3 C, D**). Alternatively, ubiquitylation may mask the epitope recognised by the antibody. It would be interesting to investigate whether the V0D1 is differentially ubiquitylated for example by co-expressing a tagged ubiquitin version with and the tagged V0D1 and probing for ubiquitylation.

5.4.3. Overexpression of catalytically inactive GFP-AMSH clusters CD63 positive late endosomes.

I found that overexpression of catalytically inactive GFP-AMSH affected the morphology of CD63-positive MVBs. The results showed that mutant GFP-AMSH transfected HeLa cells contain fewer CD63-positive puncta than WT GFP-AMSH transfected ones (**Figure 5.7**). The apparent decrease in the number and increase in size of CD63 positive endosomes shown in mutant GFP-AMSH transfected cells suggests that they are closely clustered together, and this may be why I cannot discriminate them as individual puncta (**Figure 5.7**). It would be tempting to speculate that AMSH catalytic activity is directly involved in the change in distribution of CD63, but the relative distribution of CD63 and K63-ubiquitin in AMSH KO cells was unchanged (**Figure 5.5**).

Alternatively, one could consider a potential dominant negative role of the mutant AMSH in that it may displace USP8 from their common interactors (STAM, CHMP1A/B, CHMP2A/, CHMP4C, Row et al., 2007; McCullough et al., 2006; Mizuno et al., 2007, Agromayor and Martin-Serrano, 2006; Ridgen et al., 2009; Wenzel et al., 2022). This may then interfere with

deubiquitylation of many endosomal targeted proteins (i.e. EGFR). Indeed, clustered endosomes and lysosomes were observed by immunofluorescence and electron microscopy in USP8-depleted cells (Row et al., 2006).

5.4.4. AMSH KO increases the exosomal sorting of both Syntenin1 and K63-ubiquitin.

Syntenin1 interaction with CD63 is strong and specific to this particular tetraspanin and CD63 trafficking to the ILV is dependent on the Syntenin1 PDZ motif that binds to the C-terminal cytoplasmic tail of CD63 (Latysheva et al., 2006). Syntenin1 uses its PDZ-1 ubiquitin binding motif for recruitment to CD63 positive late endosomes by contacting its C-terminus (Latysheva, 2006; Rajesh et al., 2011). For this reason, I speculate that the high MW Syntenin1 species is enriched in the KO4 exosome fraction by virtue of its enhanced interaction with both the tetraspanin CD63 and long K63-ubiquitin chains (**Figure 5.8**) (Rajesh et al., 2011). The K63-ubiquitin increase in exosome-enriched fractions from AMSH KO4 was accompanied by a decrease of the major Syntenin1 band, while a higher MW Syntenin1 species was present only in AMSH KO4 exosomes but not in parental exosomes (**Figure 5.8**). The total levels of Syntenin1 (sum of modified and un-modified Syntenin1) in AMSH KO4 exosomes equals the levels of the main Syntenin1 band in parentals exosomes. The modified Syntenin1 band is more than two-fold enriched over the main Syntenin1 band in AMSH KO4 exosomes (**Figure 5.8**). This means that modified 40 kDa Syntenin1 band is enriched in exosomes and its molecular weight is compatible with mono-ubiquitylation.

It would have been important to investigate which post-translational modification might be appended onto Syntenin1. I have carried out preliminary experiments to see whether Syntenin1 is differentially ubiquitylated by transiently transfecting Parental, AMSH KO3 and KO4 with HANL-Syntenin1 protein and performing a pull-down by HA-coupled magnetic beads followed by western blotting for ubiquitin. However, the amount of HANL-Syntenin1 expressed and thus precipitated from the lysates was very variable between the different conditions which made it

difficult to appreciate any differential ubiquitylation between Parentals and AMSH KO clones. Ideally these experiments should be carried out using Syntenin1 with a smaller epitope tag or even endogenous Syntenin1.

Collectively, my observations lead me to speculate that K63-ubiquitin at the endosomal membrane plays an important role for the cooperation of the ALIX/Syntenin1/CD63 complex to cooperate to generate exosomes. In conclusion, the results suggest that there may be additional hidden roles to AMSH that still need to be fully explored.

Chapter 6: Generation of HeLa APEX2-AMSH cells

6.1 Introduction

The mechanism of action by which AMSH regulates the turn-over of plasma-membrane proteins through the endo-lysosomal pathway is still elusive.

There are 60 interactors identified with high-throughput unbiased approaches in the Biogrid database. I was interested in expanding this network and to this end, I have generated HeLa Flp-In Flag-APEX2-AMSH cells. These cells can be used for proximity labelling experiments: by fusing the Apex2 peroxidase enzyme to the protein of interest (POI), this enzyme can catalyse a fast biotinylation of the proximal proteins at a distance of less than 20 nm, in the presence of biotin-phenol and hydrogen peroxide (Hung et al., 2016).

The biotinylated proteins are then isolated by biotin-streptavidin affinity capture. This technique allows detection of very transient interactions, i.e. those between an enzyme and its substrate, that would not be detectable using other methods such as immunoprecipitation.

In principle, another use of these cells would be to gain ultrastructural localisation of AMSH, i.e. see which of endosomal domains it is concentrated in. For this purpose, the APEX2 peroxidase can be used to generate osmium tetroxide precipitates after the reaction of DAB tetrahydrochloride mixed with H_2O_2 that allows one to visualise the localisation of the protein of interest as darker stains in a micrograph (Lam et al., 2014; Martell et al., 2012).

In this chapter, I describe the generation, selection and characterisation of HeLa APEX2-AMSH cells and initial experiments demonstrating that these can be used for proximity biotinylation.

6.2 HeLa Flag-APEX2-AMSH FlpIN cell generation and characterisation.

The pEF5-Flag-APEX2-AMSH plasmid was transfected alongside the pOG44 plasmid into HeLa S3 Flp-In which bear a single “FRT” landing

site for recombination of the construct into their genome. To check that the Flag-APEX2-AMSH was expressed constitutively, Parental cells and six APEX2-AMSH transformed clones were lysed and the samples probed for Flag and AMSH (**Figure 6.1**). Importantly, the Flag western blot showed that APEX2-AMSH is identified as a band running under the 85 kDa marker which is present in all Flag-APEX2-AMSH transfected clones but absent in the parental cells' lane. The Flag antibody gave many non-specific bands, including one that runs just under the Flag-APEX2-AMSH (indicated with an asterisk). In order to evaluate the relative expression of Flag-APEX2-AMSH to endogenous, the membrane was re-probed for AMSH (**Figure 6.1**).

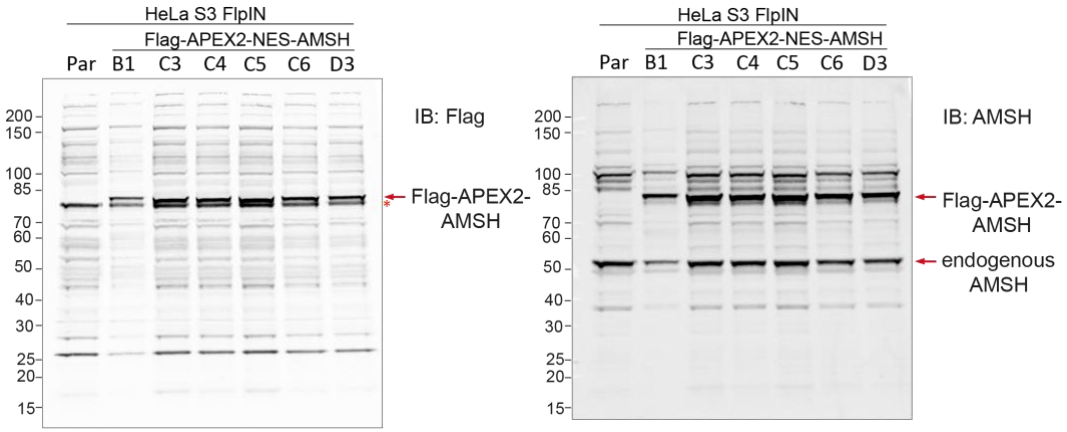

Figure 6.1 Generation of HeLa Flag-APEX2-AMSH clones.
HeLa S3 Flp-In were transfected with the Flag-APEX2-AMSH plasmid. After 4 weeks of growth in selection media supplemented with Hygromycin B, colonies were picked and grown in a well of a 24-well plate. Ten days after picking the clones, they were split both in a 6-well plate for maintenance and in a 24-well plate for screening. The clones were lysed in high-stringency RIPA buffer (HS-RIPA) with phosphatase and protease inhibitors. The concentration of the lysates was very low, and all of the lysate was loaded for each well. The samples were run on a 4-12% SDS-PAGE. The blot was incubated with anti-Flag and re-probed with anti-AMSH antibody. *Indicates non-specific band.

After a first Western blot screen, clone C3 was chosen for further characterisation. An equal amount of cell lysate from parentals and APEX2-AMSH clone C3 were analysed by Western blot. The results showed that the levels of endogenous AMSH are comparable, while the ratio of Flag-APEX2-AMSH: endogenous AMSH was 1:1 (**Figure 6.2**).

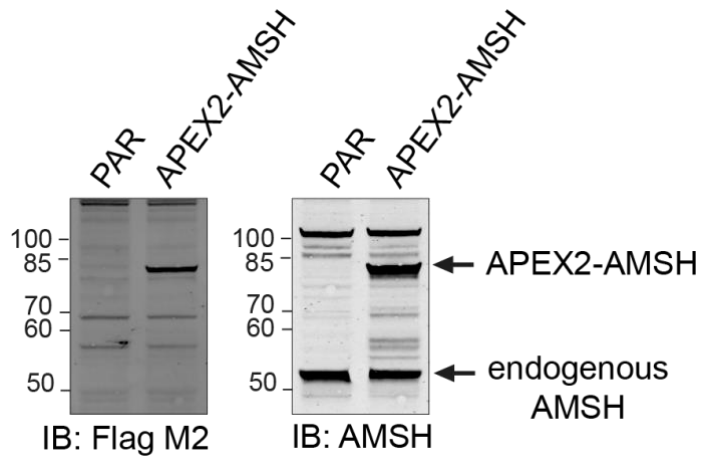

Figure 6.2 HeLa Flag-APEX2-AMSH selected clone C3 stably expresses Flag-Apex2-AMSH at equal levels to endogenous AMSH. HeLa S3 Parental and Flag-APEX2-AMSH Flp-In cells were lysed in RIPA lysis buffer supplemented with protease and phosphatase inhibitors. For every sample, 20 µg were loaded on a 4-12% SDS-PAGE. The blot was incubated with anti-AMSH and re-probed with anti-Flag.

Next, I wanted to check the morphology of early endosomes in two Flag-APEX2-AMSH clones. Parentals, clone C3 and C6 were stained with either anti-HRS or anti-AMSH. The AMSH signal in both clones was comparable and higher than the signal in parentals as expected, the levels of HRS were similar in all the cell lines (**Figure 6.3**).

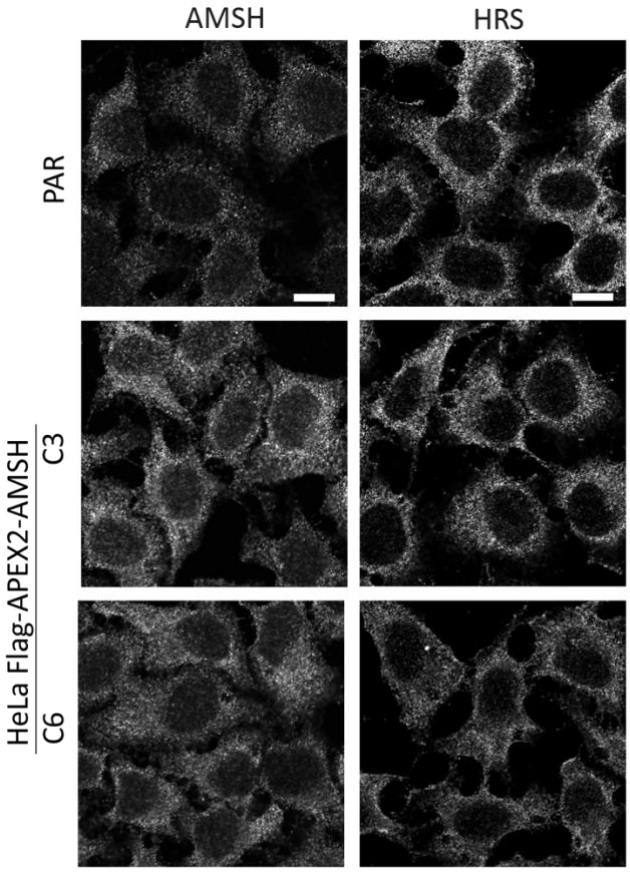

Figure 6.3 HeLa Flag-Apex2-AMSH clone C3 and C6 over-express AMSH compared to the parental cells and have similar levels of total AMSH.
HeLa S3 Parental, Flag-Apex2-AMSH clones C3 and C6 were fixed in 4% PFA, permeabilised, stained with either anti-HRS or anti-AMSH antibodies. The coverslips were imaged at a 63x objective with an LSM900 confocal microscope. Scale bar = 10µm. Representative of two experiments.

Next, I wanted to assess the intracellular distribution of Flag-APEX2-AMSH. HeLa S3 parental, Flag-APEX2-HRS and Flag-APEX2-AMSH cells were stained with anti-Flag. I used Flag-APEX2-HRS HeLa cells generated by a previous PhD student, Doug Grimes, as a positive control. The Flag antibody gave a low amount of non-specific cytosolic and a strong plasma membrane background signal in the parental cells. The Flag signal was clearly increased in the APEX2-HRS and APEX2-AMSH expressing cells, indicating localisation to the cytosol and punctate structures therein. The Flag signal is enhanced in both APEX2-HRS and APEX2-AMSH cell lines, as expected (**Figure 6.4**).

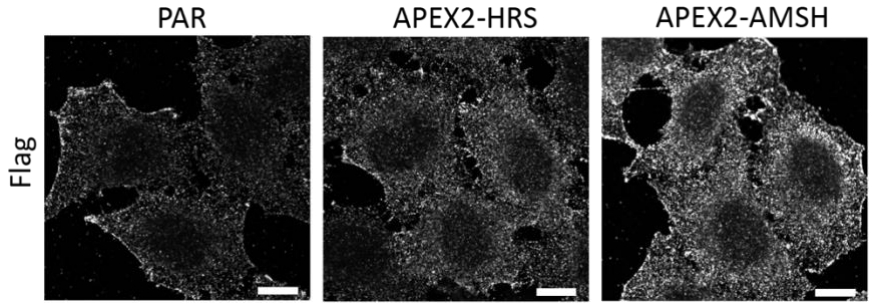

Figure 6.4 Flag-APEX2-AMSH is localised to punctate structures in the cytoplasm.
HeLa S3 parental, Flag-Apex2-HRS and Flag-Apex2-AMSH cells were fixed in 4% PFA, permeabilised, stained with either Flag, EEA1 or LAMP1 antibodies. The coverslips were imaged at a 63x objective with an LSM900 confocal microscope. Scale bar = 10µm. Representative of two experiments.

6.3 HeLa APEX2-AMSH biotinylation mediated proximity labelling.

The HeLa Flag-APEX2-AMSH cells can be used to find new interactors of AMSH. The APEX2 peroxidase catalyses the formation of a covalent adduct between the biotin-phenoxyl and Tyr side chains of proteins found in the proximity of the APEX2-tagged protein, in presence of biotin-phenol (BP) and H_2O_2. The proximity labelling can be appreciated by a Streptavidin Western Blot (Hung et al., 2016).

To check the activity of the APEX2 peroxidase fused to AMSH, I analysed its ability to facilitate labelling with biotin-phenol by western blot. HeLa S3 Flag-APEX2-AMSH Flp-In cells were either left untreated, treated with H_2O_2 only, or pre-incubated with the BP substrate and then treated with H_2O_2. The cells were lysed in two lysis buffers to select for the one that gives the highest levels of biotinylation (**Figure 6.5**). As shown in the Streptavidin blot, in both the untreated lanes of both NP-40 and RIPA lysates, there is a background signal some of which is predicted to derive from proteins in the cell that are prone to hyper-oxidation at their Tyr (likely also tryphtophan, Cys and His rich proteins) (Hung et al., 2016). The strong bands at ~ 80 kDa and ~140 kDa are non-specific, in fact cells treated with H_2O_2 alone, showed the same background as cells that were preincubated with BP. In the cells with double treatment, the overall streptavidin signal increased and I observed the appearance of specific bands at ~25, ~45, ~50 kDa that correspond to true interactors. The most

prominent band at ~50 kDa has a molecular weight that is compatible with the endogenous AMSH biotinylated by the APEX2-AMSH. The intensity of the specific bands was much lower than that of the unspecific ones suggesting that the labelling by the APEX2-AMSH protein was very modest (**Figure 6.5**).

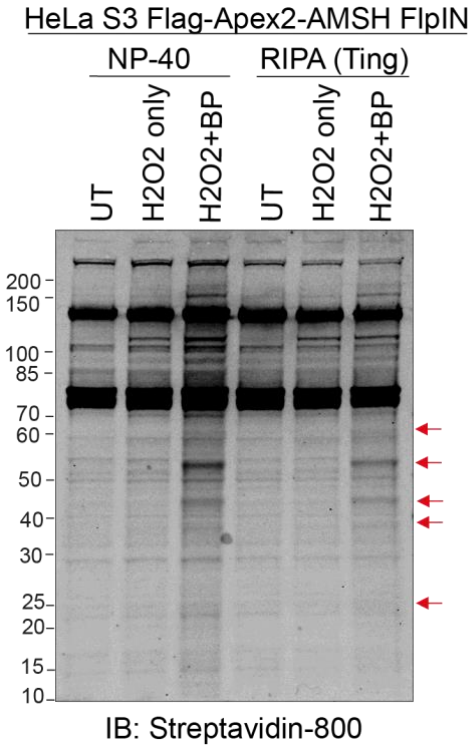

Figure 6.5 APEX2-AMSH biotinylates a subset of proteins in HeLa APEX2-AMSH FlpIN cells.
HeLa S3 Flag-APEX2-AMSH Flp-In cells were seeded in 6 cm dishes. At day 3, the cells were either left untreated (UT), treated with 10 mM hydrogen peroxide only or pre-incubated with 500 µM of bioytin-phenol (BP) and then treated with 10 mM hydrogen peroxide. The cells were washed three times with quenching solution in PBS, then scraped and collected in quenching solution, pelleted, and lysed in either NP-40 or RIPA buffer supplemented with protease and phosphatase inhibitors. For every sample, half the volume of each lysate was loaded on a 4-12% SDS-PAGE. The blot was incubated with the anti-Streptavidin-IR800.

As a first attempt to check that I can enrich for biotinylated substrates in the HeLa APEX2-AMSH Flp-In cells, I performed a streptavidin pull-down. The cells were either left untreated, or pre-incubated with BP and treated with hydrogen peroxide. Then the cells were lysed and increasing amounts of protein lysate were incubated with the streptavidin magnetic beads (**Figure 6.6**). The results showed that the beads are saturated by incubating them with 150 µg of protein lysate. Already in the input lanes

of treated cells, specific bands were found at ~ 50 and ~60 kDa. In the pull-down lanes the more protein input is added, the stronger the streptavidin signal was for specific bands at ~25, ~45, ~50 and ~60 kDa. Nevertheless, much of the signal in the pull-down lanes from the labelled cells was also found in the pull-down lane from the unlabelled cells (**Figure 6.6**).

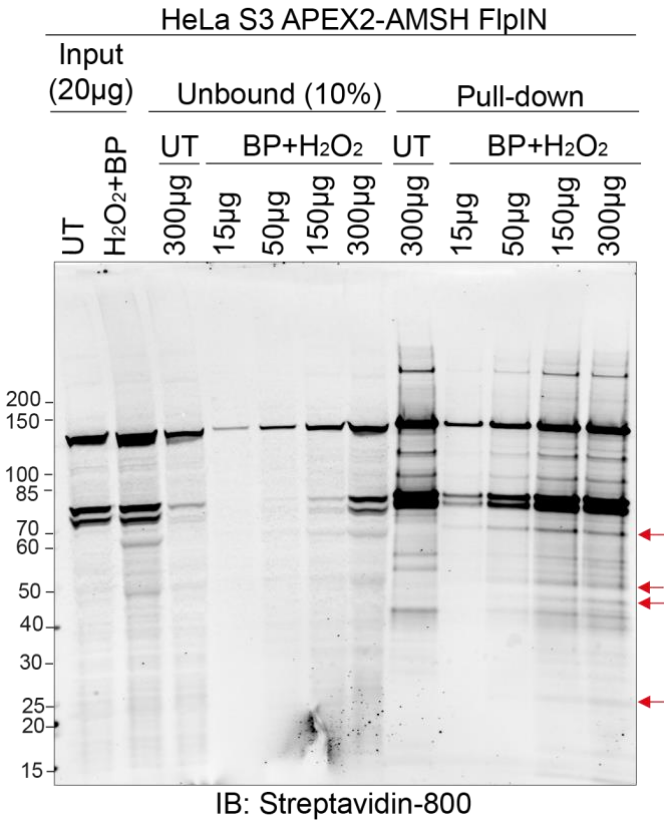

Figure 6.6 Pull-down of APEX2-AMSH biotinylated proteins in HeLa APEX2-AMSH Flp-In cells by streptavidin magnetic beads.
HeLa S3 Flag-APEX2-AMSH Flp-In cells were seeded on 6-well plates. At day 3, the cells were either left untreated (UT), treated with 10 mM hydrogen peroxide only or pre-incubated with 500 µM of biotin-phenol (BP) and then treated with 10 mM hydrogen peroxide. The cells were washed three times with quenching solution in PBS. The cells were scraped and collected in quenching solution, pelleted, and lysed in RIPA buffer supplemented with protease and phosphatase inhibitors. Each sample was incubated with 15 µl of streptavidin magnetic beads (Pierce, #88817) overnight at 4°C on a rotating wheel. The beads were washed twice with RIPA buffer, once with 1M KCl, once with 0.1 M sodium carbonate, once with 8 M UREA and twice with RIPA buffer. The biotinylated proteins were eluted in sample buffer supplemented with 2 mM free biotin and 20 mM DTT. 20 µg of input and unbound fraction and the whole volume of the eluates were loaded on a 4-12% SDS-PAGE. The blot was incubated with the anti-Streptavidin-IR800. This experiment is representative of two biological repeats.

In an attempt to identify more specifically labelled proteins, I adopted a different pull-down approach using Sepharose streptavidin beads instead of the previously tested streptavidin magnetic ones.

For this experiment, I followed the protocol from the collaborator Dr. Gunnar Dittmar (LIH, Luxembourg). After pre-incubation with BP substrate, I treated the cells with a lower concentration of hydrogen peroxide than before, collected all the cells from the plate prior to lysis. The lysates were also subjected to 100,000 g ultracentrifugation to remove insoluble material. Then the lysates were incubated with high-capacity sepharose-streptavidin beads to use these eluates for mass spectrometry.

The eluate samples showed that in both BP-only and BP/ H_2O_2 double treated cells the streptavidin signal increased the more lysate was titrated in, but this increase was much stronger when H_2O_2 was included. However, the pull-down showed a lot of background with BP alone and even in the parental cells which do not express APEX, especially in the region above the 38 kDa marker. The only bands that can be clearly seen are lower MW ones, as there is no background obscuring the signal (**Figure 6.7**).

The streptavidin signal that remains associated with the beads after elution showed the same banding pattern and intensity as the eluate samples. This probably means that the elution step did not work efficiently, ie. not all proteins were eluted (**Figure 6.7**).

The high capacity of these beads is highlighted by the fact that saturation of 5 µl of beads was only reached with 350 ug of lysate whereas three times as many magnetic beads were saturated already with 150 µg of lysate (**Figure 6.6 and 6.7**).

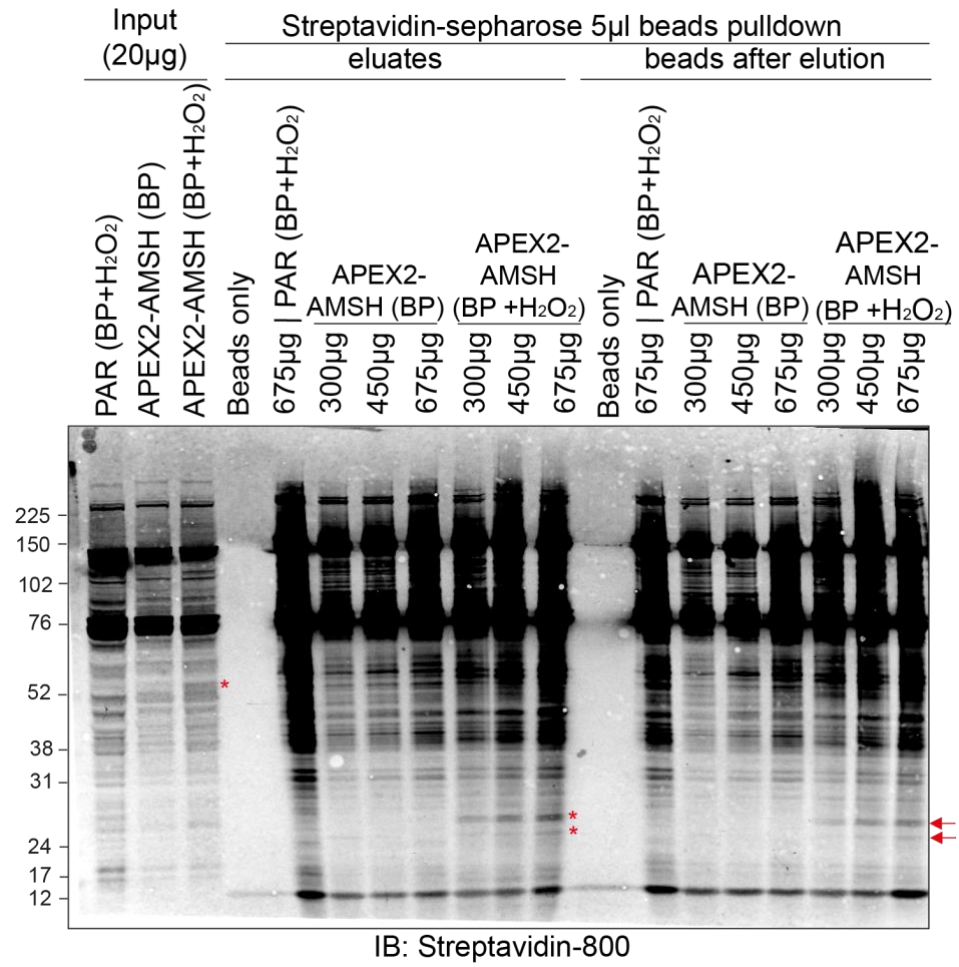

Figure 6.7 Pull-down of APEX2-AMSH biotinylated proteins in HeLa APEX2-AMSH Flp-In cells by streptavidin sepharose beads.
HeLa S3 Flag-APEX2-AMSH Flp-In cells were seeded on 10 cm dishes. At day 3, the cells were pre-incubated with 500 µM BP for 30 min. After washing the cells twice with PBS, one dish of HeLa parental and one of Flag-APEX2-AMSH cells were treated with 0.5 mM hydrogen peroxide/PBS for 1 min at room temperature. Cells in all conditions were washed 3x with quenching solution (10 mM sodium ascorbate, 10 mM sodium azide, 5 mM Trolox in PBS) for 5 min. The cells were scraped and collected in 10 ml of quenching solution, pelleted for 10 min at 3000 g in the cold. The cells were lysed in 0.1% sodium deoxycholate in 50 mM ammonium bicarbonate buffer supplemented with protease inhibitors, sonicated three times on ice. The beads (5 µl) were incubated with 300, 450, or 675 µg of protein lysate on a rotating wheel for 1 h at room temperature. The beads were washed and eluted with DTT, free biotin and reducing sample buffer. The eluate was separated from the beads and the remaining beads were suspended in sample buffer. The whole volume of each eluate and remaining beads was loaded on a 4-12% SDS-PAGE. Proteins were transferred onto a nitrocellulose membrane and was blocked in 5% BSA/TBST o/n 4°C and then incubated for 1 h at room temperature with the anti-Streptavidin-IR800.

6.4 Conclusions

There are ~31 entries for known interactors of AMSH in the Bioplex database (CHMP1A, CHMP2a and CHMP2b (Huttlin et al., 2021; Schweppe et al., 2018) and ~60 interactors for AMSH in the Biogrid database, but only few of these interactors have been extensively characterised (i.e. STAM, CHC, and CHMPs, especially CHMP3 (Agromayor and Martin-Serrano, 2006; McCullough et al., 2006).

In this chapter I have generated HeLa S3 Flag-APEX2-AMSH as a valuable new tool to expand the knowledge of the biological role of AMSH. These cells express Flag-APEX2-AMSH at near physiological levels at a 1:1 ratio to those of endogenous AMSH (**Figure 6.1,6.2 and 6.3**).

Flag-APEX2-AMSH shows a largely cytosolic localisation with a few punctate structures which agrees well with what has been shown before using transient overexpression of GFP-AMSH or Myc-AMSH (McCullough et al., 2004, 2006; Sierra et al., 2010b). I have not carried out a colocalization experiment, as the punctate staining seen was very weak and the Flag antibody gave a lot of background.

It should be highlighted that Flag-APEX2-AMSH contains a nuclear export signal (NES) which will localise it to the cytoplasm, thus detection of nuclear interactors may not be optimal.

John McCullough, a former student had shown that when AMSH is overexpressed at high levels, it can re-distribute STAM to different subdomains (McCullough et al. 2006). This is likely not the case in HeLa APEX2-AMSH cells, because the protein is expressed at endogenous levels (**Figure 6.2**).

I tested the biotinylation capability of APEX2-AMSH and showed that it can catalyse an appreciable level of biotinylation in the presence of biotin-phenol and hydrogen peroxide together. Some specific bands can be identified directly in the lysates like the 50 kDa band seen in the input of APEX2-AMSH cells treated with BP and hydrogen peroxide.

I showed that specific bands running at ~25, ~45, ~50 and ~60 kDa corresponding to biotinylated proteins could be enriched using magnetic streptavidin beads (**Figure 6.6**). However, to aim for a proteomic survey

of the biotinylated proteome in these cells, I employed sepharose streptavidin beads.

Even though the beads have high capacity, the streptavidin signal in eluates from cells incubated with BP and hydrogen peroxide was too much dominated by non-specific bands. Only 2 specific bands at low molecular weight could be seen, contrary to the pull-down with the magnetic beads which yielded many more specific bands (**Figure 6.6 and 6.7**). This protocol will require further optimisation, for example to improve the currently inefficient elution step. Another possibility would be to extend the time of hydrogen peroxide treatment in the attempt of increasing the signal/noise ratio of labelling with the APEX2-AMSH protein.

I am confident that in the future the APEX2-AMSH cells can be used to unveil new interactors. In fact, two different pull-down supports and protocols, each identified a band running between the 24-31 kDa marker (**Figure 6.6 and 6.7**). I speculate that this protein could correspond to one of the CHMPs which are oligomerising components of the ESCRT-III complex and are known to interact with AMSH (Agromayor & Martin-Serrano, 2006). They have a molecular weight ranging from 25-30 kDa and specific antibodies could be used to probe these streptavidin pull-downs to test this hypothesis.

I tried to use SILAC supplemented media to label these cells, but they were dying when cultured in the FBS-dialysed media. For this reason, after I performed the pull-down with the Sepharose-streptavidin beads, the peptides were sent for a label-free proteomics survey to our collaborators Marta Mendes and Gunnar Dittmar at Luxembourg Institute of Health, Luxembourg. Unfortunately, the MS analysis did not return sufficient specific IDs to warrant reporting here, but these cells could now potentially be used to identify novel interactors of AMSH. APEX-mediated labelling could not be used to identify AMSH interactors and possible substrates as the APEX2-AMSH cells were dying in SILAC media. Other approaches could have been used to evaluate AMSH

substrates such as precipitation of substrates by antibodies specific for the diGly remnant that identifies ubiquitylated lysines in tryptic peptides of previously ubiquitylated proteins (Kim et al., 2011).

I tried to visualise the APEX-AMSH localisation using the DAB staining approach discussed above but failed to detect a specific signal. Since my positive control sample APEX2-HRS expressing cells also likewise did not show a specific signal on endosomes, I concluded that the methodology requires further optimising.

Overall, I provide the first example of HeLa APEX2-AMSH stably expressing cells. This methodology allows detection of interactors in the radius of 20 nm distance from the protein of interest, and it is more accurate in detecting very transient interactions due to the short labelling time that is required compared to the BirA biotinylation enzyme (Mehta & Trinkle-Mulcahy, 2016). It is also faster than the Turbo-ID method which consists of fusing a hyperactive version of the BirA biotinylase to the POI but can only detect proteins in a 10 nm radius and has a longer biotinylation time (10 minutes) compared to APEX2 (Branon et al., 2018).

Importantly, these cells will be ideal to study dynamic interactions of AMSH for example in response to growth factor stimulation. I conclusion, these cells will provide an important resource for future studies exploring new roles of AMSH.

Chapter 7: Conclusions

7.1 K63-ubiquitin accumulates in AMSH KO cells.

At the beginning of my PhD, some key points were known about AMSH that came from previous work of Dr. John McCullough:

Firstly, AMSH preferentially cleaves K63-ubiquitin chains *in vitro* (McCullough et al. 2004). Secondly, AMSH can localise to both the nucleus and endosomal membranes where it interacts with ESCRT-0 (STAM), ESCRT-III and clathrin (Agromayor & Martin-Serrano, 2006; McCullough et al., 2004, 2006; Nakamura et al., 2006; Row et al., 2007). Thirdly, AMSH depletion enhances the downregulation of EGFR and other receptors suggesting that it opposes K63-ubiquitin mediated sorting into MVBs and promotes their recycling (McCullough et al., 2004; Sierra et al., 2010b).

In this thesis I have generated and characterised HeLa AMSH KO cells and found that:

1. AMSH KO cells display higher levels of K63-ubiquitin on membrane fractions. This increase was not necessarily expected, as AMSH is not the only K63-ubiquitin competent DUB, as its paralogue AMSH-LP has the same selectivity as AMSH. In addition, there are other endosomal DUBs that share ESCRT binding partners with AMSH, such as USP8 that does not discriminate between K48- and K63-linked polyubiquitin (Row et al., 2006; Sato et al., 2008). Interestingly, some other K63-ubiquitin specific DUBs have been implicated in endocytosis, such as BRCC36, a catalytic sub-unit associated with the cytoplasmic BRISC-SHMT complex which deubiquitylates and regulates the turn-over of the type-1 interferon (IFN) receptor chain 1 (IFNAR1) (H. Zheng et al., 2013b).
2. AMSH KO cells showed accumulation of K63-ubiquitin by immunostaining, prevalently at GFP-HRS negative structures indicating that early endosomes are not the main compartment affected by this increase.

7.2 AMSH is involved in exosome biogenesis.

I undertook an unbiased approach to analyse changes in the K63-ubiquitin associated proteome of AMSH KO cells using a K63-selective ubiquitin binding domain as an enrichment strategy. The proteomics identified a specific set of proteins involved in exosome biogenesis. I then sought to validate the enrichment of ALIX, Syntenin1, CD63 and K63-ubiquitin by western blotting, but I was unable to demonstrate that these proteins are directly modified with K63-ubiquitin chains. Further experiments will be needed to assess whether any of these proteins are differentially modified with ubiquitin. Interestingly, in the eluates from K63-ubiquitin pull-down experiments, discrete bands of ALIX and Syntenin1 were increased in cell lysates from AMSH KO cells suggesting that a CD63, ALIX and Syntenin1 complex is enriched by virtue of non-covalent interactions of either of these proteins with the K63-ubiquitin modification.

It is known that Syntenin1 forms a multi-molecular complex with the tetraspanin CD63 to concentrate cargo proteins at the limiting membrane of internal vesicles of MVBs (late endosomes) that are destined to become exosomes. Syntenin controls the number of CD63 positive exosomes relased (Baietti et al., 2012).

This finding prompted me to look at whether exosome formation is impaired in AMSH KO cells. Exosomes released from AMSH KO cells contained the same amount of CD63 but higher levels of K63-ubiquitin, alongside with an increase of a higher molecular weight Syntenin1 form. It is not known whether a modified version of Syntenin1 is sorted to exosomes and what this might mean, but I speculate that this is a result of a failed chain editing event at the MVB prior to its sorting to exosomes. This finding suggests that AMSH may cleave K63-ubiquitin from exosome cargos.

Studies have shown that Syntenin1 is able to bind K48-linked and K63-linked ubiquitin with the same affinity (Rajesh et al., 2011) whilst ALIX shows a preference for K63-ubiquitin chains (Dowlatshahi et al., 2012). It is possible that the Syntenin1 and ALIX bind tightly to the K63-ubiquitin

chains in AMSH KO cells and are recruited along with other ubiquitin modifying enzymes (i.e. E3 ligases) which generate the high molecular weight Syntenin1 species.

CD63 is normally sorted to late endosome domains defined by the LAMP1 marker and it is not known whether it is ubiquitylated with K63-ubiquitin chains. I did not observe a change in CD63 levels in AMSH KO cells, but I suggest that it may be differentially modified in AMSH KO cells, as in the eluates from the K63-ubiquitin pull-down it runs as at a higher molecular weight species. For this reason, I speculate that AMSH may be involved in the recruitment of the exosomal proteins ALIX and Syntenin via K63-ubiquitin likely appended onto CD63. Further studies are required to test this hypothesis.

K63-ubiquitin extensively co-localised with CD63, while Flag-ALIX is partially colocalised with K63-ubiquitin at cell peripheral structures in AMSH KO cells. In this context it is interesting to note that K63-ubiquitin binding to the ALIX V-domain is critical for retroviral budding of HIV (D.P. Dowlatshahi, 2012). Retroviral budding from the PM is a topologically equivalent budding reaction to the formation of ILVs and exosomes at MVBs (Scourfield & Martin-Serrano, 2017). This led me to hypothesise that these structures may be immature MVBs that have an exosome fate. In this scenario, AMSH KO may negatively affect assembly of the CD63-ALIX-Syntenin complex at MVBs or leading to the generation of exosomes. Alternatively, they are recruited to exosomes whose extracellular secretion is hindered because of K63-ubiquitin accumulation.

Upon overexpressing catalytically inactive AMSH, I have observed an accumulation of the CD63 positive structures which strengthened the idea that MVB maturation is hindered in AMSH KO cells.

Together my findings suggest that AMSH acts as a modulator of MVB maturation or exosome biogenesis by affecting the recruitment of the Syntenin/ALIX/CD63 complex at K63-ubiquitin.

7.3 Future outlook

Exosomes are cargo loaded organelles which are secreted to remove metabolites, DNA, RNA, lipids and protein material from the cell and can target distant cell to change their phenotype. miRNA-containing exosomes can carry information from the secreting cell and modulate the gene expression of the target cells, for example (Kalluri & LeBleu, 2020) Cancer cell derived exosomes can be secreted from different body organs and contain cancer biomarkers (Melo et al., 2015). Importantly, in the context of tumour microenvironment regulation, exosomes are involved in promoting tumour angiogenesis which facilitates tumour dissemination, and they can induce the expression of invasive morphological changes such as the formation of invadopodia (Hoshino et al., 2013; Le et al., 2014; Ribeiro et al., 2013).

AMSH deletion was implicated in accumulation of ubiquitylated protein species both in mice brains and in lymphocytes from neuro-developmentally compromised patient's cells affected by the MIC-CAP syndrome (Ishii et al., 2001; Suzuki et al., 2011; McDonell et al., 2013). In addition to these findings, AMSH is known to oppose the downregulation of receptors implicated in cancer growth (McCullough et al., 2004; Sierra et al., 2010).

Syntenin1 is a scaffold protein that interacts with multiple proteins involved in many different pathways such as cell motility, tumour metastasis and exosome biogenesis, to cite a few (Lee et al., 2023) Interestingly, Syntenin1 interacts with both protein partners and miRNAs. Firstly, Syntenin1 interacts with Merlin to promote filopodia extension leading to cell motility and tumour metastasis. Secondly, Syntenin1 phosphorylation by the oncogenic c-Src kinase promotes its binding to ALIX and induces exosome release. Lastly, Syntenin1 has been proposed to transport miRNAs into exosomes suggesting it may modulate gene expression of target cells (Hikita et al., 2019; Jannatipour et al., 2001; Zhang et al., 2015).

The finding that Syntenin1 is potentially differentially modified in AMSH KO cells is important because Syntenin1 upregulation is known to correlate with tumour progression and is proposed to be sorted to exosomes as a way to reduce its intracellular protein levels (Qiu et al., 2022). It has never been assessed whether Syntenin1 or CD63 can be modified with K63-ubiquitin or whether either of them can bind to K63-ubiquitin in exosomes. Further studies are needed to determine whether either or both proteins are indeed differentially modified with K63-ubiquitin and check whether this changes tumour cell invasiveness and/or morphology in target cells.

The catalytic activity of AMSH towards K63-ubiquitin on receptors was proposed to be required for their sorting into ILVs, but AMSH has never been linked to the sorting of ubiquitylated cargo to exosomes. Therefore, my thesis adds novel information on the role of K63-ubiquitin chains in intracellular trafficking. Further studies are required to investigate whether there are additional proteins other than Syntenin that are either differentially modified or sorted in exosomes upon AMSH deletion.

Interestingly, exosomes contain poly-ubiquitylated proteins, and a proteomics study conducted on specific ubiquitin chain linkages determined that K63-linked ubiquitin is the main chain type contained in exosomes (Buschow et al., 2005; Huebner A.R. et al., 2016). The intracellular increase in K63-ubiquitin levels in AMSH KO cells was reflected in an increase in the exosome-enriched fraction from KO4 which led me to propose that K63-ubiquitin chains must normally be cleaved before the MVBs fuse with the plasma membrane to secrete their ILVs as exosomes in the media (extracellular environment). Therefore, I propose that AMSH protein carries out an editing function that is dependent on concomitant recruitment of K63-ubiquitin specific ubiquitin binding proteins to assist the exosome sorting of ubiquitylated cargo receptors (**Figure 1.11**).

The findings in this thesis might be helpful first for a better comprehension of AMSH biological role in intracellular trafficking. The finding that K63-ubiquitin homeostasis is compromised in AMSH deleted cells and that may be involved in opposing exosome biogenesis could open a new area

of investigation for DUBs in regulating the extracellular tumour micro-environment.

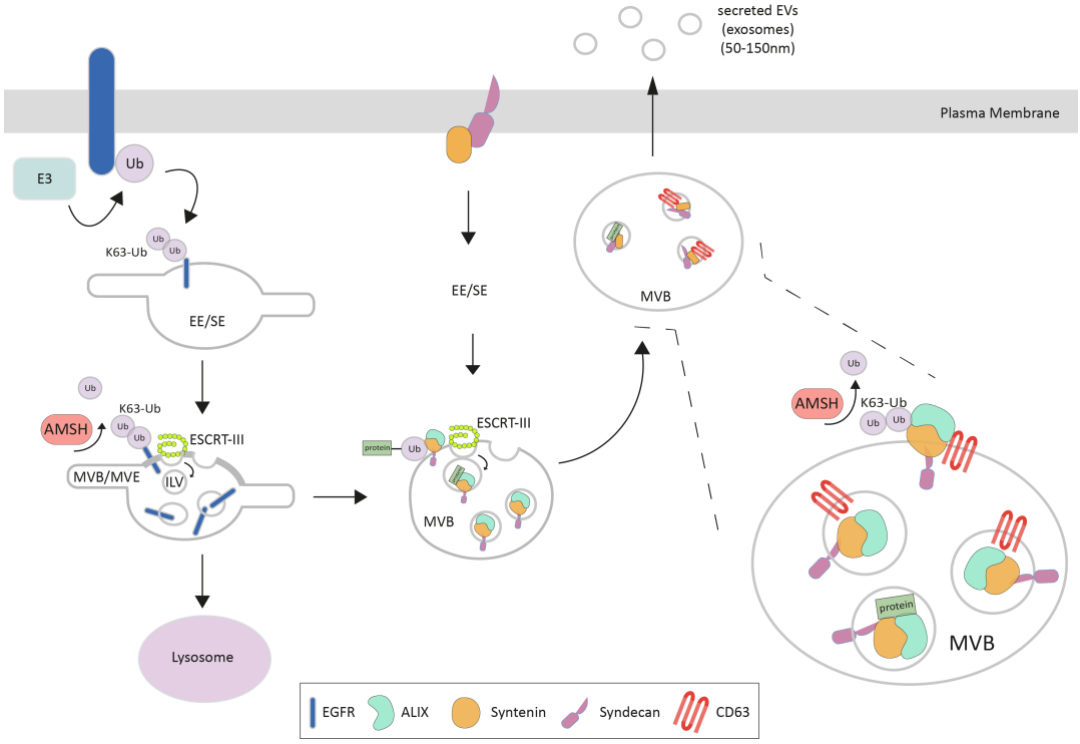

Figure 7.1 Proposed model of AMSH role in intracellular trafficking. The diagram shows a proposed model for AMSH in intracellular trafficking. K63-ubiquitin chains must normally be cleaved before the MVBs fuse with the plasma membrane to secrete their ILVs as exosomes in the media (extracellular environment).

Bibliography

Abdul Rehman, S. A., Kristariyanto, Y. A., Choi, S. Y., Nkosi, P. J., Weidlich, S., Labib, K., Hofmann, K., & Kulathu, Y. (2016). MINDY-1 Is a Member of an Evolutionarily Conserved and Structurally Distinct New Family of Deubiquitinating Enzymes. *Molecular Cell*. https://doi.org/10.1016/j.molcel.2016.05.009

Agromayor, M., & Martin-Serrano, J. (2006). Interaction of AMSH with ESCRT-III and deubiquitination of endosomal cargo. *Journal of Biological Chemistry*, *281*(32), 23083–23091. https://doi.org/10.1074/jbc.M513803200

Akutsu, M., Dikic, I., & Bremm, A. (2016). Ubiquitin chain diversity at a glance. *Journal of Cell Science*. https://doi.org/10.1242/jcs.183954

Ali, N., Zhang, L., Taylor, S., Mironov, A., Urbé, S., & Woodman, P. (2013a). Recruitment of UBPY and ESCRT exchange drive hd-ptp-dependent sorting of egfr to the mvb. *Current Biology*. https://doi.org/10.1016/j.cub.2013.02.033

Ali, N., Zhang, L., Taylor, S., Mironov, A., Urbé, S., & Woodman, P. (2013b). Recruitment of UBPY and ESCRT exchange drive hd-ptp-dependent sorting of egfr to the mvb. *Current Biology*, *23*(6), 453–461. https://doi.org/10.1016/j.cub.2013.02.033

Ambroise, G., Yu, T. ting, Zhang, B., Kacal, M., Hao, Y., Queiroz, A. L., Ouchida, A. T., Lindskog, C., Norberg, E., & Vakifahmetoglu-Norberg, H. (2020). Systematic analysis reveals a functional role for STAMBPL1 in the epithelial–mesenchymal transition process across multiple carcinomas. *British Journal of Cancer*, *123*(7), 1164. https://doi.org/10.1038/S41416-020-0972-X

Amerik, A., Sindhi, N., & Hochstrasser, M. (2006). A conserved late endosome-targeting signal required for Doa4 deubiquitylating enzyme function. *Journal of Cell Biology*, *175*(5), 825–835. https://doi.org/10.1083/jcb.200605134

Andersen, P. L., Zhou, H., Pastushok, L., Moraes, T., McKenna, S., Ziola, B., Ellison, M. J., Dixit, V. M., & Xiao, W. (2005). Distinct regulation of Ubc13 functions by the two ubiquitin-conjugating enzyme variants Mms2 and Uev1A. *The Journal of Cell Biology*, *170*(5), 745. https://doi.org/10.1083/JCB.200502113

Antonescu, C. N., McGraw, T. E., & Klip, A. (2014). Reciprocal Regulation of Endocytosis and Metabolism. *Cold Spring Harbor Perspectives in Biology*, *6*(7). https://doi.org/10.1101/CSHPERSPECT.A016964

Asao, H., Sasaki, Y., Arita, T., Tanaka, N., Endo, K., Kasai, H., Takeshita, T., Endo, Y., Fujita, T., & Sugamura, K. (1997). Hrs is associated with STAM, a signal-transducing adaptor molecule. It's suppressive effect on cytokine-induced cell growth. *Journal of Biological Chemistry*. https://doi.org/10.1074/jbc.272.52.32785

Babst, M., Katzmann, D. J., Estepa-Sabal, E. J., Meerloo, T., & Emr, S. D. (2002). ESCRT-III: An endosome-associated heterooligomeric protein complex required for MVB sorting. *Developmental Cell*. https://doi.org/10.1016/S1534-5807(02)00220-4

Babst, M., Katzmann, D. J., Snyder, W. B., Wendland, B., & Emr, S. D. (2002). Endosome-associated complex, ESCRT-II, recruits transport machinery for protein sorting at the multivesicular body. *Developmental Cell*, *3*(2), 283–289. https://doi.org/10.1016/S1534-5807(02)00219-8

Babst, M., Sato, T. K., Banta, L. M., & Emr, S. D. (1997). Endosomal transport function in yeast requires a novel AAA-type ATPase, Vps4p. *The EMBO Journal*, *16*(8), 1820–1831. https://doi.org/10.1093/EMBOJ/16.8.1820

Babst, M., Wendland, B., Estepa, E. J., & Emr, S. D. (1998). The Vps4p AAA ATPase regulates membrane association of a Vps protein complex required for normal endosome function. *The EMBO Journal*, *17*(11), 2982–2993. https://doi.org/10.1093/EMBOJ/17.11.2982

Bache, K. G., Brech, A., Mehlum, A., & Stenmark, H. (2003). Hrs regulates multivesicular body formation via ESCRT recruitment to endosomes. *The Journal of Cell Biology*, *162*(3), 435. https://doi.org/10.1083/JCB.200302131

Baer, R., & Ludwig, T. (2002). The BRCA1/BARD1 heterodimer, a tumor suppressor complex with ubiquitin E3 ligase activity. In *Current Opinion in Genetics and Development*. https://doi.org/10.1016/S0959-437X(01)00269-6

Baietti, M. F. et al. (2012). Syndecan syntenin ALIX regulates the biogenesis of exosomes. *Nature Cell Biology*. https://doi.org/DOI: 10.1038/ncb2502

Baietti, M. F., Zhang, Z., Mortier, E., Melchior, A., Degeest, G., Geeraerts, A., Ivarsson, Y., Depoortere, F., Coomans, C., Vermeiren, E., Zimmermann, P., & David, G. (2012). Syndecan–syntenin–ALIX regulates the biogenesis of exosomes. *Nature Cell Biology 2012 14:7*, *14*(7), 677–685. https://doi.org/10.1038/ncb2502

Baker, R. T., & Board, P. G. (1991). The human ubiquitin-52 amino acid fusion protein gene shares several structural features with mammalian ribosomal protein genes. *Nucleic Acids Research*, *19*(5), 1035. https://doi.org/10.1093/NAR/19.5.1035

Ballabio, A., & Bonifacino, J. S. (2019). Lysosomes as dynamic regulators of cell and organismal homeostasis. *Nature Reviews Molecular Cell Biology 2019 21:2*, *21*(2), 101–118. https://doi.org/10.1038/s41580-019-0185-4

Bankaitis, V. A., Johnson, L. M., & Emr, S. D. (1986). Isolation of yeast mutants defective in protein targeting to the vacuole. *Proceedings of the National Academy of Sciences*, *83*(23), 9075–9079. https://doi.org/10.1073/PNAS.83.23.9075

Basters, A., Geurink, P. P., Röcker, A., Witting, K. F., Tadayon, R., Hess, S., Semrau, M. S., Storici, P., Ovaa, H., Knobeloch, K. P., & Fritz, G. (2017). Structural basis of the specificity of USP18 toward ISG15. *Nature Structural and Molecular Biology*. https://doi.org/10.1038/nsmb.3371

Beck, F., Unverdorben, P., Bohn, S., Schweitzer, A., Pfeifer, G., Sakata, E., Nickell, S., Plitzko, J. M., Villa, E., Baumeister, W., & Förster, F. (2012). Near-atomic resolution structural model of the yeast 26S proteasome. *Proceedings of the National Academy of Sciences of the United States of America*. https://doi.org/10.1073/pnas.1213333109

Bednash, J. S., & Mallampalli, R. K. (2016). Regulation of inflammasomes by ubiquitination. In *Cellular and Molecular Immunology*. https://doi.org/10.1038/cmi.2016.15

Bednash, J. S., Weathington, N., Londino, J., Rojas, M., Gulick, D. L., Fort, R., Han, S. H., McKelvey, A. C., Chen, B. B., & Mallampalli, R. K. (2017a). Targeting the deubiquitinase STAMBP inhibits NALP7 inflammasome activity. *Nature Communications 2017 8:1*, *8*(1), 1–13. https://doi.org/10.1038/ncomms15203

Bednash, J. S., Weathington, N., Londino, J., Rojas, M., Gulick, D. L., Fort, R., Han, S. H., McKelvey, A. C., Chen, B. B., & Mallampalli, R. K. (2017b).

Targeting the deubiquitinase STAMBP inhibits NALP7 inflammasome activity. *Nature Communications*. https://doi.org/10.1038/ncomms15203
Bhogaraju, S., Kalayil, S., Liu, Y., Bonn, F., Colby, T., Matic, I., & Dikic, I. (2016). Phosphoribosylation of Ubiquitin Promotes Serine Ubiquitination and Impairs Conventional Ubiquitination. *Cell*. https://doi.org/10.1016/j.cell.2016.11.019
Bilodeau, P. S., Urbanowski, J. L., Winistorfer, S. C., & Piper, R. C. (2002). The Vps27p-Hse1p complex binds ubiquitin and mediates endosomal protein sorting. *Nature Cell Biology*. https://doi.org/10.1038/ncb815
Bongiovanni, A., Romancino, D. P., Campos, Y., Paterniti, G., Qiu, X., Moshiach, S., Di Felice, V., Vergani, N., Ustek, D., & D'Azzo, A. (2012). Alix protein is substrate of Ozz-E3 ligase and modulates actin remodeling in skeletal muscle. *Journal of Biological Chemistry*, *287*(15), 12159–12171. https://doi.org/10.1074/jbc.M111.297036
Booth, A. M., Fang, Y., Fallon, J. K., Yang, J. M., Hildreth, J. E. K., Gould, S. J., Sandefur, S., & Varthakavi, V. (2006). Exosomes and HIV Gag bud from endosome-like domains of the T cell plasma membrane. *Journal of Cell Biology*, *172*(6), 923–935. https://doi.org/10.1083/JCB.200508014
Bowers, K., Lottridge, J., Helliwell, S. B., Goldthwaite, L. M., Luzio, J. P., & Stevens, T. H. (2004). Protein–Protein Interactions of ESCRT Complexes in the Yeast Saccharomyces cerevisiae. *Traffic*, *5*(3), 194–210. https://doi.org/10.1111/J.1600-0854.2004.00169.X
Bowers, K., Piper, S. C., Edeling, M. A., Gray, S. R., Owen, D. J., Lehner, P. J., & Luzio, J. P. (2006a). Degradation of endocytosed epidermal growth factor and virally ubiquitinated major histocompatibility complex class I is independent of mammalian ESCRTII. *The Journal of Biological Chemistry*, *281*(8), 5094–5105. https://doi.org/10.1074/JBC.M508632200
Bowers, K., Piper, S. C., Edeling, M. A., Gray, S. R., Owen, D. J., Lehner, P. J., & Luzio, J. P. (2006b). Degradation of endocytosed epidermal growth factor and virally ubiquitinated major histocompatibility complex class I is independent of mammalian ESCRTII. *Journal of Biological Chemistry*, *281*(8), 5094–5105. https://doi.org/10.1074/jbc.M508632200
Branon, T. C., Bosch, J. A., Sanchez, A. D., Udeshi, N. D., Svinkina, T., Carr, S. A., Feldman, J. L., Perrimon, N., & Ting, A. Y. (2018). Efficient proximity labeling in living cells and organisms with TurboID. *Nature Biotechnology*, *36*(9), 880. https://doi.org/10.1038/NBT.4201
Bremm, A., Freund, S. M. V., & Komander, D. (2010). Lys11-linked ubiquitin chains adopt compact conformations and are preferentially hydrolyzed by the deubiquitinase Cezanne. *Nature Structural and Molecular Biology*. https://doi.org/10.1038/nsmb.1873
Brzovic, P. S., Keeffe, J. R., Nishikawa, H., Miyamoto, K., Fox, D., Fukuda, M., Ohta, T., & Klevit, R. (2003). Binding and recognition in the assembly of an active BRCA1/BARD1 ubiquitin-ligase complex. *Proceedings of the National Academy of Sciences of the United States of America*. https://doi.org/10.1073/pnas.0836054100
Buetow, L., & Huang, D. T. (2016). Structural insights into the catalysis and regulation of E3 ubiquitin ligases. *Nature Reviews. Molecular Cell Biology*, *17*(10), 626. https://doi.org/10.1038/NRM.2016.91
Buschow, S. I., Liefhebber, J. M. P., Wubbolts, R., & Stoorvogel, W. (2005). Exosomes contain ubiquitinated proteins. *Blood Cells, Molecules, and Diseases*, *35*(3), 398–403. https://doi.org/10.1016/J.BCMD.2005.08.005

Cavadini, S., Fischer, E. S., Bunker, R. D., Potenza, A., Lingaraju, G. M., Goldie, K. N., Mohamed, W. I., Faty, M., Petzold, G., Beckwith, R. E. J., Tichkule, R. B., Hassiepen, U., Abdulrahman, W., Pantelic, R. S., Matsumoto, S., Sugasawa, K., Stahlberg, H., & Thomä, N. H. (2016). Cullin–RING ubiquitin E3 ligase regulation by the COP9 signalosome. *Nature 2016 531:7596*, *531*(7596), 598–603. https://doi.org/10.1038/nature17416

Chang, L., & Barford, D. (2014). Insights into the anaphase-promoting complex: A molecular machine that regulates mitosis. In *Current Opinion in Structural Biology*. https://doi.org/10.1016/j.sbi.2014.08.003

Chatellard-Causse, C., Blot, B., Cristina, N., Torch, S., Missotten, M., & Sadoul, R. (2002). Alix (ALG-2-interacting protein X), a protein involved in apoptosis, binds to endophilins and induces cytoplasmic vacuolization. *The Journal of Biological Chemistry*, *277*(32), 29108–29115. https://doi.org/10.1074/jbc.M204019200

Choi, Y. S., Bollinger, S. A., Prada, L. F., Scavone, F., Yao, T., & Cohen, R. E. (2019). High-affinity free ubiquitin sensors for quantifying ubiquitin homeostasis and deubiquitination. *Nature Methods 2019 16:8*, *16*(8), 771–777. https://doi.org/10.1038/s41592-019-0469-9

Ciechanover, A., & Ben-Saadon, R. (2004). N-terminal ubiquitination: more protein substrates join in. *Trends in Cell Biology*, *14*(3), 103–106. https://doi.org/10.1016/J.TCB.2004.01.004

Clague, M. J. (2002). Membrane transport: A coat for ubiquitin. In *Current Biology*. https://doi.org/10.1016/S0960-9822(02)01030-8

Clague, M. J., Barsukov, I., Coulson, J. M., Liu, H., Rigden, D. J., & Urbé, S. (2013). Deubiquitylases from genes to organism. *Physiological Reviews*. https://doi.org/10.1152/physrev.00002.2013

Clague, M. J., Heride, C., & Urbé, S. (2015). The demographics of the ubiquitin system. In *Trends in Cell Biology*. https://doi.org/10.1016/j.tcb.2015.03.002

Clague, M. J., Liu, H., & Urbé, S. (2012). Governance of endocytic trafficking and signaling by reversible ubiquitylation. *Developmental Cell*, *23*(3), 457–467. https://doi.org/10.1016/J.DEVCEL.2012.08.011

Clague, M. J., & Urbé, S. (2006a). Endocytosis: the DUB version. *Trends in Cell Biology*, *16*(11), 551–559. https://doi.org/10.1016/j.tcb.2006.09.002

Clague, M. J., & Urbé, S. (2006b). Endocytosis: the DUB version. In *Trends in Cell Biology*. https://doi.org/10.1016/j.tcb.2006.09.002

Clague, M. J., & Urbé, S. (2010). Ubiquitin: Same molecule, different degradation pathways. In *Cell*. https://doi.org/10.1016/j.cell.2010.11.012

Clague, M. J., Urbé, S., & Komander, D. (2019). Breaking the chains: deubiquitylating enzyme specificity begets function. In *Nature Reviews Molecular Cell Biology*. https://doi.org/10.1038/s41580-019-0099-1

Colombo, M., Moita, C., Van Niel, G., Kowal, J., Vigneron, J., Benaroch, P., Manel, N., Moita, L. F., Théry, C., & Raposo, G. (2013). Analysis of ESCRT functions in exosome biogenesis, composition and secretion highlights the heterogeneity of extracellular vesicles. *Journal of Cell Science*, *126*(24), 5553–5565. https://doi.org/10.1242/JCS.128868/263554/AM/ANALYSIS-OF-ESCRT-FUNCTIONS-IN-EXOSOME-BIOGENESIS

Conigliaro, A., Costa, V., Lo Dico, A., Saieva, L., Buccheri, S., Dieli, F., Manno, M., Raccosta, S., Mancone, C., Tripodi, M., De Leo, G., & Alessandro, R. (2015). CD90+ liver cancer cells modulate endothelial cell phenotype through the release of exosomes containing H19 lncRNA. *Molecular Cancer*, *14*(1), 1–11. https://doi.org/10.1186/S12943-015-0426-X/FIGURES/5

Cook, W. J., Jeffrey, L. C., Carson, M., Chen, Z., & Pickart, C. M. (1992). Structure of a diubiquitin conjugate and a model for interaction with ubiquitin conjugating enzyme (E2). *Journal of Biological Chemistry*. https://doi.org/10.2210/pdb1aar/pdb

Cooper, E. M., Boeke, J. D., & Cohen, R. E. (2010). Specificity of the BRISC deubiquitinating enzyme is not due to selective binding to Lys63-linked polyubiquitin. *The Journal of Biological Chemistry*, *285*(14), 10344–10352. https://doi.org/10.1074/JBC.M109.059667

Cooper, E. M., Cutcliffe, C., Kristiansen, T. Z., Pandey, A., Pickart, C. M., & Cohen, R. E. (2009). K63-specific deubiquitination by two JAMM/MPN+ complexes: BRISC-associated Brcc36 and proteasomal Poh1. *EMBO Journal*. https://doi.org/10.1038/emboj.2009.27

Cope, G. A., & Deshaies, R. J. (2003). COP9 signalosome: A multifunctional regulator of SCF and other cullin-based ubiquitin ligases. In *Cell*. https://doi.org/10.1016/S0092-8674(03)00722-0

Cope, G. A., Suh, G. S. B., Aravind, L., Schwarz, S. E., Zipursky, S. L., Koonin, E. V., & Deshaies, R. J. (2002). Role of predicted metalloprotease motif of Jab1/Csn5 in cleavage of Nedd8 from Cul1. *Science*. https://doi.org/10.1126/science.1075901

Couchman, J. R. (2003). Syndecans: proteoglycan regulators of cell-surface microdomains? *Nature Reviews Molecular Cell Biology 2003 4:12*, *4*(12), 926–938. https://doi.org/10.1038/nrm1257

Cox, J. et al. (2009). A practical guide to the MaxQuant computationalplatform for SILAC-based quantitative proteomics. *Nature Protocols*, *4*(5), 698–705.

Cstorer, A., & Ménard, R. (1994). Catalytic mechanism in papain family of cysteine peptidases. *Methods in Enzymology*. https://doi.org/10.1016/0076-6879(94)44035-2

Cullen, P. J., & Steinberg, F. (2018). To degrade or not to degrade: mechanisms and significance of endocytic recycling. *Nature Reviews Molecular Cell Biology 2018 19:11*, *19*(11), 679–696. https://doi.org/10.1038/s41580-018-0053-7

Cunningham, C. N., Baughman, J. M., Phu, L., Tea, J. S., Yu, C., Coons, M., Kirkpatrick, D. S., Bingol, B., & Corn, J. E. (2015). USP30 and parkin homeostatically regulate atypical ubiquitin chains on mitochondria. *Nature Cell Biology*, *17*(2), 160–169. https://doi.org/10.1038/NCB3097

Da-Jun Yu et al. (2019). STAMBPL knockdown has antitumour effects on gastric cancer biological activities. *Oncology Letters*, *18*(5), 4421–4428.

Datta, A. B., Hura, G. L., & Wolberger, C. (2009). The Structure and Conformation of Lys63-Linked Tetraubiquitin. *Journal of Molecular Biology*. https://doi.org/10.1016/j.jmb.2009.07.090

Dautry Varsat, A., Ciechanover, A., & Lodish, H. F. (1983). pH and the recycling of transferrin during receptor-mediated endocytosis. *Proceedings of the National Academy of Sciences of the United States of America*, *80*(8), 2258–2262. https://doi.org/10.1073/PNAS.80.8.2258

Davies, C. W., Paul, L. N., & Das, C. (2013). Mechanism of recruitment and activation of the endosome-associated deubiquitinase AMSH. *Biochemistry*, *52*(44), 7818–7829. https://doi.org/10.1021/BI401106B/SUPPL_FILE/BI401106B_SI_001.PDF

de Duve, C., & Wattiaux, R. (1966). Functions of Lysosomes. *Annual Review of Physiology*. https://doi.org/10.1146/annurev.ph.28.030166.002251

Deshaies, R. J. (1999). SCF and Cullin/RING H2-Based Ubiquitin Ligases. *Annual Review of Cell and Developmental Biology*. https://doi.org/10.1146/annurev.cellbio.15.1.435

Dikic, I., & Schulman, B. A. (2022). An expanded lexicon for the ubiquitin code. *Nature Reviews Molecular Cell Biology 2022 24:4*, *24*(4), 273–287. https://doi.org/10.1038/s41580-022-00543-1

Dikic, I., Wakatsuki, S., & Walters, K. J. (2009). Ubiquitin-binding domains from structures to functions. In *Nature Reviews Molecular Cell Biology*. https://doi.org/10.1038/nrm2767

Doherty, G. J., & McMahon, H. T. (2009). Mechanisms of Endocytosis. *Https://Doi.Org/10.1146/Annurev.Biochem.78.081307.110540*, *78*, 857–902. https://doi.org/10.1146/ANNUREV.BIOCHEM.78.081307.110540

Dou, H., Buetow, L., Sibbet, G. J., Cameron, K., & Huang, D. T. (2012). BIRC7-E2 ubiquitin conjugate structure reveals the mechanism of ubiquitin transfer by a RING dimer. *Nature Structural and Molecular Biology*. https://doi.org/10.1038/nsmb.2379

Dowlatshahi, D. P., Sandrin, V., Vivona, S., Shaler, T. A., Kaiser, S. E., Melandri, F., Sundquist, W. I., & Kopito, R. R. (2012). ALIX is a Lys63-specific polyubiquitin binding protein that functions in retrovirus budding. *Developmental Cell*, *23*(6), 1247–1254. https://doi.org/10.1016/J.DEVCEL.2012.10.023

Doyotte, A., Mironov, A., McKenzie, E., & Woodman, P. (2008). The Bro1-related protein HD-PTP/PTPN23 is required for endosomal cargo sorting and multivesicular body morphogenesis. *Proceedings of the National Academy of Sciences of the United States of America*. https://doi.org/10.1073/pnas.0707601105

D.P. Dowlatshahi. (2012). ALIX Is a Lys63-Specific Polyubiquitin Binding Protein that Functions in Retrovirus Budding. *Developmental Cell*.

Dupré, S., Volland, C., & Haguenauer-Tsapis, R. (2001). Membrane transport: Ubiquitylation in endosomal sorting. In *Current Biology*. https://doi.org/10.1016/S0960-9822(01)00558-9

Eddins, M. J., Carlile, C. M., Gomez, K. M., Pickart, C. M., & Wolberger, C. (2006). Mms2–Ubc13 covalently bound to ubiquitin reveals the structural basis of linkage-specific polyubiquitin chain formation. *Nature Structural & Molecular Biology 2006 13:10*, *13*(10), 915–920. https://doi.org/10.1038/nsmb1148

Eddins, M. J., Varadan, R., Fushman, D., Pickart, C. M., & Wolberger, C. (2007). Crystal Structure and Solution NMR Studies of Lys48-linked Tetraubiquitin at Neutral pH. *Journal of Molecular Biology*. https://doi.org/10.1016/j.jmb.2006.12.065

Edgar J R. (2016). Tetherin is an exosomal tether. *ELife*.

Elias, R. D., Ma, W., Ghirlando, R., Schwieters, C. D., Reddy, V. S., & Deshmukh, L. (2020). Proline-rich domain of human ALIX contains multiple TSG101-UEV interaction sites and forms phosphorylation-mediated reversible amyloids. *Proceedings of the National Academy of Sciences of the United States of America*, *117*(39), 24274–24284. https://doi.org/10.1073/PNAS.2010635117/SUPPL_FILE/PNAS.2010635117.SAPP.PDF

El-Sayed, A., & Harashima, H. (2013). Endocytosis of gene delivery vectors: from clathrin-dependent to lipid raft-mediated endocytosis. *Molecular Therapy : The Journal of the American Society of Gene Therapy*, *21*(6), 1118–1130. https://doi.org/10.1038/MT.2013.54

Erpapazoglou, Z. (2012). A dual role for K63-linked ubiquitin chains in multivesicular body biogenesis and cargo sorting. *Molecular Biology of the Cell*.

Etlinger, J. D., & Goldberg, A. L. (1977). A soluble ATP dependent proteolytic system responsible for the degradation of abnormal proteins in reticulocytes. *Proceedings of the National Academy of Sciences of the United States of America*. https://doi.org/10.1073/pnas.74.1.54

Fader, C. M., Sánchez, D. G., Mestre, M. B., & Colombo, M. I. (2009). TI-VAMP/VAMP7 and VAMP3/cellubrevin: two v-SNARE proteins involved in specific steps of the autophagy/multivesicular body pathways. *Biochimica et Biophysica Acta (BBA) - Molecular Cell Research*, *1793*(12), 1901–1916. https://doi.org/10.1016/J.BBAMCR.2009.09.011

Faesen, A. C., Luna-Vargas, M. P. A., Geurink, P. P., Clerici, M., Merkx, R., Van Dijk, W. J., Hameed, D. S., El Oualid, F., Ovaa, H., & Sixma, T. K. (2011). The Differential Modulation of USP Activity by Internal Regulatory Domains, Interactors and Eight Ubiquitin Chain Types. *Chemistry & Biology*, *18*(12), 1550–1561. https://doi.org/10.1016/J.CHEMBIOL.2011.10.017

Fairhead M. and Howarth M. (2015). Site-specific biotinylation of purified proteins using BirA. *Methods in Molecular Biology*, *1266*, 171–184.

Feng, L., Wang, J., & Chen, J. (2010). The Lys63-specific deubiquitinating enzyme BRCC36 is regulated by two scaffold proteins localizing in different subcellular compartments. *Journal of Biological Chemistry*. https://doi.org/10.1074/jbc.M110.135392

Fialka. (1999). Identification of Syntenin as a Protein of the Apical Early Endocytic Compartment in Madin-Darby Canine Kidney Cells. *J Biol Chem*, *274*(37).

Finley, D. (2009). Recognition and processing of ubiquitin-protein conjugates by the proteasome. *Annual Review of Biochemistry*, *78*, 477–513. https://doi.org/10.1146/ANNUREV.BIOCHEM.78.081507.101607

Freemont, P. S. (2000). Ubiquitination: RING for destruction? *Current Biology*, *10*(2), R84–R87. https://doi.org/10.1016/S0960-9822(00)00287-6

Futter, C. E., Pearse, A., Hewlett, L. J., & Hopkins, C. R. (1996). Multivesicular endosomes containing internalized EGF-EGF receptor complexes mature and then fuse directly with lysosomes. *The Journal of Cell Biology*, *132*(6), 1011–1023. https://doi.org/10.1083/JCB.132.6.1011

Gerber, S. A., Rush, J., Stemman, O., Kirschner, M. W., & Gygi, S. P. (2003). Absolute quantification of proteins and phosphoproteins from cell lysates by tandem MS. *Proceedings of the National Academy of Sciences of the United States of America*. https://doi.org/10.1073/pnas.0832254100

Gersch, M., Gladkova, C., Schubert, A. F., Michel, M. A., Maslen, S., & Komander, D. (2017). Mechanism and regulation of the Lys6-selective deubiquitinase USP30. *Nature Structural & Molecular Biology*, *24*(11), 920–930. https://doi.org/10.1038/NSMB.3475

Goldknopf, I. L., & Busch, H. (1977). Isopeptide linkage between nonhistone and histone 2A polypeptides of chromosomal conjugate protein A24. *Proceedings of the National Academy of Sciences of the United States of America*. https://doi.org/10.1073/pnas.74.3.864

Goldstein, G., Scheid, M., Hammerling, U., Schlesinger, D. H., Niall, H. D., & Boyse, E. A. (1975). Isolation of a polypeptide that has lymphocyte differentiating properties and is probably represented universally in living cells. *Proceedings of the National Academy of Sciences of the United States of America*. https://doi.org/10.1073/pnas.72.1.11

Grootjans, J. J., Zimmermann, P., Reekmans, G., Smets, A., Degeest, G., Dürr, J., & David, G. (1997). Syntenin, a PDZ protein that binds syndecan cytoplasmic domains. *Proceedings of the National Academy of Sciences of the United States of America*, *94*(25), 13683–13688. https://doi.org/10.1073/PNAS.94.25.13683

Gruenberg, J., & Maxfield, F. R. (1995). Membrane transport in the endocytic pathway. *Current Opinion in Cell Biology*. https://doi.org/10.1016/0955-0674(95)80013-1

Guo, Y., Liu, Q., Mallette, E., Caba, C., Hou, F., Fux, J., LaPlante, G., Dong, A., Zhang, Q., Zheng, H., Tong, Y., & Zhang, W. (2021). Structural and functional characterization of ubiquitin variant inhibitors for the JAMM-family deubiquitinases STAMBP and STAMBPL1. *Journal of Biological Chemistry*, *297*(4), 101107. https://doi.org/10.1016/J.JBC.2021.101107

Gurung, S., Perocheau, D., Touramanidou, L., & Baruteau, J. (2021). The exosome journey: from biogenesis to uptake and intracellular signalling. *Cell Communication and Signaling 2021 19:1*, *19*(1), 1–19. https://doi.org/10.1186/S12964-021-00730-1

Haahr, P., Borgermann, N., Guo, X., Typas, D., Achuthankutty, D., Hoffmann, S., Shearer, R., Sixma, T. K., & Mailand, N. (2018). ZUFSP Deubiquitylates K63-Linked Polyubiquitin Chains to Promote Genome Stability. *Molecular Cell*, *70*(1), 165-174.e6. https://doi.org/10.1016/J.MOLCEL.2018.02.024

Haas et al. (1982). Ubiquitin-activating enzyme. Mechanism and role in protein-ubiquitin conjugation. *JBC*, *257*(5), 2543–2548.

Haguenauer-Tsapis, R., & André, B. (2004). *Membrane trafficking of yeast transporters: mechanisms and physiological control of downregulation*. 273–323. https://doi.org/10.1007/B97215

Han, S. H., Lear, T. B., Jerome, J. A., Rajbhandari, S., Snavely, C. A., Gulick, D. L., Gibson, K. F., Zou, C., Chen, B. B., & Mallampalli, R. K. (2015). Lipopolysaccharide primes the NALP3 inflammasome by inhibiting its ubiquitination and degradation mediated by the SCFFBXL2 E3 ligase. *Journal of Biological Chemistry*. https://doi.org/10.1074/jbc.M115.645549

Harbour, M. E., Breusegem, S. Y., & Seaman, M. N. J. (2012). Recruitment of the endosomal WASH complex is mediated by the extended “tail” of Fam21 binding to the retromer protein Vps35. *The Biochemical Journal*, *442*(1), 209–220. https://doi.org/10.1042/BJ20111761

Heride, C., Urbé, S., & Clague, M. J. (2014). Ubiquitin code assembly and disassembly. *Current Biology*, *24*(6), R215–R220. https://doi.org/10.1016/j.cub.2014.02.002

Hermanns, T., Pichlo, C., Woiwode, I., Klopffleisch, K., Witting, K. F., Ovaa, H., Baumann, U., & Hofmann, K. (2018). A family of unconventional deubiquitinases with modular chain specificity determinants. *Nature Communications 2018 9:1*, *9*(1), 1–13. https://doi.org/10.1038/s41467-018-03148-5

Hershko, A., & Ciechanover, A. (1998). THE UBIQUITIN SYSTEM. *Annual Review of Biochemistry*. https://doi.org/10.1146/annurev.biochem.67.1.425

Hershko, A., Ciechanover, A., & Rose, I. A. (1979). Resolution of the ATP dependent proteolytic system from reticulocytes: A component that interacts with ATP. *Proceedings of the National Academy of Sciences of the United States of America*. https://doi.org/10.1073/pnas.76.7.3107

Heusermann, W., Hean, J., Trojer, D., Steib, E., von Bueren, S., Graff-Meyer, A., Genoud, C., Martin, K., Pizzato, N., Voshol, J., Morrissey, D. V., Andaloussi,

S. E. L., Wood, M. J., & Meisner-Kober, N. C. (2016). Exosomes surf on filopodia to enter cells at endocytic hot spots, traffic within endosomes, and are targeted to the ER. *Journal of Cell Biology*, *213*(2), 173–184. https://doi.org/10.1083/JCB.201506084/VIDEO-9

Hewings, D. S., Heideker, J., Ma, T. P., Ahyoung, A. P., El Oualid, F., Amore, A., Costakes, G. T., Kirchhofer, D., Brasher, B., Pillow, T., Popovych, N., Maurer, T., Schwerdtfeger, C., Forrest, W. F., Yu, K., Flygare, J., Bogyo, M., & Wertz, I. E. (2018). Reactive-site-centric chemoproteomics identifies a distinct class of deubiquitinase enzymes. *Nature Communications 2018 9:1*, *9*(1), 1–17. https://doi.org/10.1038/s41467-018-03511-6

Hicke, L., & Dunn, R. (2003). Regulation of Membrane Protein Transport by Ubiquitin and Ubiquitin-Binding Proteins. *Annual Review of Cell and Developmental Biology*. https://doi.org/10.1146/annurev.cellbio.19.110701.154617

Hicke, L., & Riezman, H. (1996). Ubiquitination of a yeast plasma membrane receptor signals its ligand-stimulated endocytosis. *Cell*, *84*(2), 277–287. https://doi.org/10.1016/S0092-8674(00)80982-4

Hikita, T., Kuwahara, A., Watanabe, R., Miyata, M., & Oneyama, C. (2019). Src in endosomal membranes promotes exosome secretion and tumor progression. *Scientific Reports 2019 9:1*, *9*(1), 1–14. https://doi.org/10.1038/s41598-019-39882-z

Hjerpe, R., Aillet, F., Lopitz-Otsoa, F., Lang, V., England, P., & Rodriguez, M. S. (2009). Efficient protection and isolation of ubiquitylated proteins using tandem ubiquitin-binding entities. *EMBO Reports*, *10*(11), 1250. https://doi.org/10.1038/EMBOR.2009.192

Hoeller, D., Crosetto, N., Blagoev, B., Raiborg, C., Tikkanen, R., Wagner, S., Kowanetz, K., Breitling, R., Mann, M., Stenmark, H., & Dikic, I. (2006). Regulation of ubiquitin-binding proteins by monoubiquitination. *Nature Cell Biology*. https://doi.org/10.1038/ncb1354

Hofmann, K., & Falquet, L. (2001). A ubiquitin-interacting motif conserved in components of the proteasomal and lysosomal protein degradation systems. In *Trends in Biochemical Sciences*. https://doi.org/10.1016/S0968-0004(01)01835-7

Hofmann, R. M., & Pickart, C. M. (1999). Noncanonical MMS2-encoded ubiquitin-conjugating enzyme functions in assembly of novel polyubiquitin chains for DNA repair. *Cell*, *96*(5), 645–653. https://doi.org/10.1016/S0092-8674(00)80575-9

Horazdovsky, B. F., Davies, B. A., Seaman, M. N. J., McLaughlin, S. A., Yoon, S. H., & Emr, S. D. (1997). A sorting nexin-1 homologue, Vps5p, forms a complex with Vps17p and is required for recycling the vacuolar protein-sorting receptor. *Molecular Biology of the Cell*, *8*(8), 1529–1541. https://doi.org/10.1091/MBC.8.8.1529

Hornbeck, P. V., Zhang, B., Murray, B., Kornhauser, J. M., Latham, V., & Skrzypek, E. (2015a). PhosphoSitePlus, 2014: Mutations, PTMs and recalibrations. *Nucleic Acids Research*. https://doi.org/10.1093/nar/gku1267

Hornbeck, P. V., Zhang, B., Murray, B., Kornhauser, J. M., Latham, V., & Skrzypek, E. (2015b). PhosphoSitePlus, 2014: mutations, PTMs and recalibrations. *Nucleic Acids Research*, *43*(D1), D512–D520. https://doi.org/10.1093/NAR/GKU1267

Hoshino, D., Kirkbride, K. C., Costello, K., Clark, E. S., Sinha, S., Grega-Larson, N., Tyska, M. J., & Weaver, A. M. (2013). Exosome secretion is enhanced by

invadopodia and drives invasive behavior. *Cell Reports*, *5*(5), 1159–1168. https://doi.org/10.1016/j.celrep.2013.10.050
Hospenthal, M. K., Mevissen, T. E. T., & Komander, D. (2015). Deubiquitinase-based analysis of ubiquitin chain architecture using Ubiquitin Chain Restriction (UbiCRest). *Nature Protocols*, *10*(2), 349–361. https://doi.org/10.1038/NPROT.2015.018
Huang, A., de Jong, R. N., Wienk, H., Winkler, G. S., Timmers, H. T. M., & Boelens, R. (2009). E2-c-Cbl Recognition Is Necessary but not Sufficient for Ubiquitination Activity. *Journal of Molecular Biology*. https://doi.org/10.1016/j.jmb.2008.10.044
Huang, F., Zeng, X., Kim, W., Balasubramani, M., Fortian, A., Gygi, S. P., Yates, N. A., & Sorkin, A. (2013). Lysine 63-linked polyubiquitination is required for EGF receptor degradation. *Proceedings of the National Academy of Sciences of the United States of America*. https://doi.org/10.1073/pnas.1308014110
Huang, L., Kinnucan, E., Wang, G., Beaudenon, S., Howley, P. M., Huibregtse, J. M., & Pavletich, N. P. (1999). Structure of an E6AP-UbcH7 complex: Insights into ubiquitination by the E2-E3 enzyme cascade. *Science*. https://doi.org/10.1126/science.286.5443.1321
Huebner A.R. et al. (2016). Deubiquitylation of Protein Cargo Is Not an Essential Step in Exosome Formation. *Molecular and Cellular Proteomics*.
Hung, V., Udeshi, N. D., Lam, S. S., Loh, K. H., Cox, K. J., Pedram, K., Carr, S. A., & Ting, A. Y. (2016). Spatially resolved proteomic mapping in living cells with the engineered peroxidase APEX2. *Nature Protocols 2016 11:3*, *11*(3), 456–475. https://doi.org/10.1038/nprot.2016.018
Huotari, J., & Helenius, A. (2011). Endosome maturation. In *EMBO Journal*. https://doi.org/10.1038/emboj.2011.286
Hurley, J. H. (2015). ESCRT s are everywhere . *The EMBO Journal*. https://doi.org/10.15252/embj.201592484
Husnjak, K., & Dikic, I. (2012). Ubiquitin-Binding Proteins: Decoders of Ubiquitin-Mediated Cellular Functions. *Annual Review of Biochemistry*. https://doi.org/10.1146/annurev-biochem-051810-094654
Huttlin, E. L., Bruckner, R. J., Navarrete-Perea, J., Cannon, J. R., Baltier, K., Gebreab, F., Gygi, M. P., Thornock, A., Zarraga, G., Tam, S., Szpyt, J., Gassaway, B. M., Panov, A., Parzen, H., Fu, S., Golbazi, A., Maenpaa, E., Stricker, K., Guha Thakurta, S., … Gygi, S. P. (2021). Dual proteome-scale networks reveal cell-specific remodeling of the human interactome. *Cell*, *184*(11), 3022-3040.e28. https://doi.org/10.1016/J.CELL.2021.04.011/ATTACHMENT/9D45895F-3A8F-4F89-9279-12FF7DCE96A4/MMC7.ZIP
Ishii, N., Owada, Y., Yamada, M., Miura, S., Murata, K., Asao, H., Kondo, H., & Sugamura, K. (2001). Loss of Neurons in the Hippocampus and Cerebral Cortex of AMSH-Deficient Mice. *Molecular and Cellular Biology*. https://doi.org/10.1128/mcb.21.24.8626-8637.2001
Iwakami, Y., Yokoyama, S., Watanabe, K., & Hayakawa, Y. (2018). STAM-binding protein regulates melanoma metastasis through SLUG stabilization. *Biochemical and Biophysical Research Communications*. https://doi.org/10.1016/j.bbrc.2018.11.068
Jannatipour, M., Dion, P., Khan, S., Jindal, H., Fan, X., Laganière, J., Chishti, A. H., & Rouleau, G. A. (2001). Schwannomin Isoform-1 Interacts with Syntenin via PDZ Domains. *Journal of Biological Chemistry*, *276*(35), 33093–33100. https://doi.org/10.1074/jbc.M105792200

Johnson, S. A., Pleiman, C. M., Pao, L., Schneringer, J., Hippen, K., & Cambier, J. C. (1995). Phosphorylated immunoreceptor signaling motifs (ITAMs) exhibit unique abilities to bind and activate Lyn and Syk tyrosine kinases. *Journal of Immunology (Baltimore, Md. : 1950)*.

Kalinowska, K., Nagel, M. K., Goodman, K., Cuyas, L., Anzenberger, F., Alkofer, A., Paz-Ares, J., Braun, P., Rubio, V., Otegui, M. S., Isono, E., & Raikhel, N. V. (2015). Arabidopsis ALIX is required for the endosomal localization of the deubiquitinating enzyme AMSH3. *Proceedings of the National Academy of Sciences of the United States of America*, *112*(40), E5543–E5551. https://doi.org/10.1073/PNAS.1510516112/-/DCSUPPLEMENTAL

Kalluri, R., & LeBleu, V. S. (2020). The biology, function, and biomedical applications of exosomes. *Science*, *367*(6478). https://doi.org/10.1126/SCIENCE.AAU6977

Kanaseki, T., & Kadota, K. (1969). The “vesicle in a basket”. A morphological study of the coated vesicle isolated from the nerve endings of the guinea pig brain, with special reference to the mechanism of membrane movements. *The Journal of Cell Biology*, *42*(1), 202–220. https://doi.org/10.1083/JCB.42.1.202

Kanelis, V., Rotin, D., & Forman-Kay, J. D. (2001). Solution structure of a Nedd4 WW domain-ENaC peptide complex. *Nature Structural Biology*. https://doi.org/10.1038/87562

Kanerva, K., Uronen, R. L., Blom, T., Li, S., Bittman, R., Lappalainen, P., Peränen, J., Raposo, G., & Ikonen, E. (2013). LDL Cholesterol Recycles to the Plasma Membrane via a Rab8a-Myosin5b-Actin-Dependent Membrane Transport Route. *Developmental Cell*, *27*(3), 249–262. https://doi.org/10.1016/J.DEVCEL.2013.09.016

Katzmann, D. J., Babst, M., & Emr, S. D. (2001). Ubiquitin-dependent sorting into the multivesicular body pathway requires the function of a conserved endosomal protein sorting complex, ESCRT-I. *Cell*. https://doi.org/10.1016/S0092-8674(01)00434-2

Katzmann, D. J., Stefan, C. J., Babst, M., & Emr, S. D. (2003). Vps27 recruits ESCRT machinery to endosomes during MVB sorting. *Journal of Cell Biology*, *162*(3), 413–423. https://doi.org/10.1083/JCB.200302136

Keith D. Wilkinson, M. K. U. and A. L. H. (1980). Ubiquitin Is the ATP-dependent Proteolysis Factor I of Rabbit Reticulocytes. *The Journal of Biological Chemistry*, *255*(16), 7529–7532.

Keren-Kaplan, T., Attali, I., Estrin, M., Kuo, L. S., Farkash, E., Jerabek-Willemsen, M., Blutraich, N., Artzi, S., Peri, A., Freed, E. O., Wolfson, H. J., & Prag, G. (2013). Structure-based in silico identification of ubiquitin-binding domains provides insights into the ALIX-V:ubiquitin complex and retrovirus budding. *The EMBO Journal*, *32*(4), 538. https://doi.org/10.1038/EMBOJ.2013.4

Keusekotten, K., Elliott, P. R., Glockner, L., Fiil, B. K., Damgaard, R. B., Kulathu, Y., Wauer, T., Hospenthal, M. K., Gyrd-Hansen, M., Krappmann, D., Hofmann, K., & Komander, D. (2013). OTULIN antagonizes LUBAC signaling by specifically hydrolyzing Met1-linked polyubiquitin. *Cell*, *153*(6), 1312. https://doi.org/10.1016/J.CELL.2013.05.014

Kikuchi, K., Ishii, N., Asao, H., & Sugamura, K. (2003). Identification of AMSH-LP containing a Jab1/MPN domain metalloenzyme motif. *Biochemical and Biophysical Research Communications*. https://doi.org/10.1016/S0006-291X(03)01009-X

Kim, W., Bennett, E. J., Huttlin, E. L., Guo, A., Li, J., Possemato, A., Sowa, M. E., Rad, R., Rush, J., Comb, M. J., Harper, J. W., & Gygi, S. P. (2011).

Systematic and quantitative assessment of the ubiquitin-modified proteome. *Molecular Cell*, *44*(2), 325–340. https://doi.org/10.1016/J.MOLCEL.2011.08.025

Kissing, S., Hermsen, C., Repnik, U., Nesset, C. K., Von Bargen, K., Griffiths, G., Ichihara, A., Lee, B. S., Schwake, M., De Brabander, J., Haas, A., & Saftig, P. (2015). Vacuolar ATPase in Phagosome-Lysosome Fusion. *The Journal of Biological Chemistry*, *290*(22), 14166. https://doi.org/10.1074/JBC.M114.628891

Klumperman, J., & Raposo, G. (2014). The complex ultrastructure of the endolysosomal system. *Cold Spring Harbor Perspectives in Biology*, *6*(10). https://doi.org/10.1101/CSHPERSPECT.A016857

Kobayashi, H., Tanaka, N., Asao, H., Miura, S., Kyuuma, M., Semura, K., Ishii, N., & Sugamura, K. (2005). Hrs, a mammalian master molecule in vesicular transport and protein sorting, suppresses the degradation of ESCRT proteins signal transducing adaptor molecule 1 and 2. *Journal of Biological Chemistry*. https://doi.org/10.1074/jbc.M409969200

Komada, M., & Kitamura, N. (1995). Growth factor-induced tyrosine phosphorylation of Hrs, a novel 115-kilodalton protein with a structurally conserved putative zinc finger domain. *Molecular and Cellular Biology*. https://doi.org/10.1128/mcb.15.11.6213

Komada, M., Masaki, R., Yamamoto, A., & Kitamura, N. (1997). Hrs, a tyrosine kinase substrate with a conserved double zinc finger domain, is localized to the cytoplasmic surface of early endosomes. *Journal of Biological Chemistry*. https://doi.org/10.1074/jbc.272.33.20538

Komada, M., & Soriano, P. (1999). Hrs, a FYVE finger protein localized to early endosomes, is implicated in vesicular traffic and required for ventral folding morphogenesis. *Genes and Development*. https://doi.org/10.1101/gad.13.11.1475

Komander, D., Clague, M. J., & Urbé, S. (2009). Breaking the chains: Structure and function of the deubiquitinases. In *Nature Reviews Molecular Cell Biology*. https://doi.org/10.1038/nrm2731

Komander, D., & Rape, M. (2012a). The Ubiquitin Code. *Annual Review of Biochemistry*. https://doi.org/10.1146/annurev-biochem-060310-170328

Komander, D., & Rape, M. (2012b). The Ubiquitin Code. *Https://Doi.Org/10.1146/Annurev-Biochem-060310-170328*, *81*, 203–229. https://doi.org/10.1146/ANNUREV-BIOCHEM-060310-170328

Komander, D., Reyes-Turcu, F., Licchesi, J. D. F., Odenwaelder, P., Wilkinson, K. D., & Barford, D. (2009). Molecular discrimination of structurally equivalent Lys 63-linked and linear polyubiquitin chains. *EMBO Reports*. https://doi.org/10.1038/embor.2009.55

Kulak, N. A., Pichler, G., Paron, I., Nagaraj, N., & Mann, M. (2014). Minimal, encapsulated proteomic-sample processing applied to copy-number estimation in eukaryotic cells. *Nature Methods 2014 11:3*, *11*(3), 319–324. https://doi.org/10.1038/nmeth.2834

Kumar, R., Tang, Q., Müller, S. A., Gao, P., Mahlstedt, D., Zampagni, S., Tan, Y., Klingl, A., Bötzel, K., Lichtenthaler, S. F., Höglinger, G. U., & Koeglsperger, T. (2020). Fibroblast growth factor 2-mediated regulation of neuronal exosome release depends on VAMP3/cellubrevin in hippocampal neurons. *Wiley Online LibraryR Kumar, Q Tang, SA Müller, P Gao, D Mahlstedt, S Zampagni, Y Tan, A Klingl, K BötzelAdvanced Science, 2020•Wiley Online Library*, *7*(6). https://doi.org/10.1002/advs.201902372

Kumari, S., Mg, S., & Mayor, S. (2010). Endocytosis unplugged: multiple ways to enter the cell. *Cell Research 2010 20:3*, *20*(3), 256–275. https://doi.org/10.1038/cr.2010.19

Kwasna, D., Abdul Rehman, S. A., Natarajan, J., Matthews, S., Madden, R., De Cesare, V., Weidlich, S., Virdee, S., Ahel, I., Gibbs-Seymour, I., & Kulathu, Y. (2018). Discovery and Characterization of ZUFSP/ZUP1, a Distinct Deubiquitinase Class Important for Genome Stability. *Molecular Cell*, *70*(1), 150-164.e6. https://doi.org/10.1016/j.molcel.2018.02.023

Kyuuma, M., Kikuchi, K., Kojima, K., Sugawara, Y., Sato, M., Mano, N., Goto, J., Takeshita, T., Yamamoto, A., Sugamura, K., & Tanaka, N. (2006). AMSH, an ESCRT-III associated enzyme, deubiquitinates cargo on MVB/late endosomes. *Cell Structure and Function*. https://doi.org/10.1247/csf.06023

Lam, S. S., Martell, J. D., Kamer, K. J., Deerinck, T. J., Ellisman, M. H., Mootha, V. K., & Ting, A. Y. (2014). Directed evolution of APEX2 for electron microscopy and proximity labeling. *Nature Methods 2014 12:1*, *12*(1), 51–54. https://doi.org/10.1038/nmeth.3179

Larios, J. (2020). ALIX- and ESCRT-III–dependent sorting of tetraspanins to exosomes. *Journal of Cell Biology*, *219*(3).

Lata, S., Roessle, M., Solomons, J., Jamin, M., Gottlinger, H. G., Svergun, D. I., & Weissenhorn, W. (2008). Structural Basis for Autoinhibition of ESCRT-III CHMP3. *Journal of Molecular Biology*. https://doi.org/10.1016/j.jmb.2008.03.030

Latysheva. (2006). Syntenin-1 Is a New Component of Tetraspanin-Enriched Microdomains: Mechanisms and Consequences of the Interaction of Syntenin-1 with CD63. *Molecular and Cellular Biology*, *26*(20).

Lauwers, E., Jacob, C., & Andre, B. (2009). K63-linked ubiquitin chains as a specific signal for protein sorting into the multivesicular body pathway. *Journal of Cell Biology*. https://doi.org/10.1083/jcb.200810114

Le, M. T. N., Hamar, P., Guo, C., Basar, E., Perdigão-Henriques, R., Balaj, L., & Lieberman, J. (2014). miR-200-containing extracellular vesicles promote breast cancer cell metastasis. *The Journal of Clinical Investigation*, *124*(12), 5109–5128. https://doi.org/10.1172/JCI75695

Lee, K. M., Seo, E. C., Lee, J. H., Kim, H. J., & Hwangbo, C. (2023). The Multifunctional Protein Syntenin-1: Regulator of Exosome Biogenesis, Cellular Function, and Tumor Progression. *International Journal of Molecular Sciences 2023, Vol. 24, Page 9418*, *24*(11), 9418. https://doi.org/10.3390/IJMS24119418

Li, P., Blademosi, A. T., Luo, J., & Meunier, F. A. (2018). Actin Remodeling in Regulated Exocytosis: Toward a Mesoscopic View. *Trends in Cell Biology*, *28*(9), 685–697. https://doi.org/10.1016/J.TCB.2018.04.004

Lohi, O., & Lehto, V. P. (2001). STAM/EAST/Hbp adapter proteins - Integrators of signalling pathways. In *FEBS Letters*. https://doi.org/10.1016/S0014-5793(01)03079-4

Maaike S. Pols, J. K. (2008). Trafficking and function of the tetraspanin CD6. *Experimental Cell Research*.

MacDonald, E., Brown, L., Selvais, A., Liu, H., Waring, T., Newman, D., Bithell, J., Grimes, D., Urbé, S., Clague, M. J., & Zech, T. (2018). HRS-WASH axis governs actin-mediated endosomal recycling and cell invasion. *Journal of Cell Biology*, *217*(7), 2549–2564. https://doi.org/10.1083/JCB.201710051/VIDEO-5

Malakhov, M. P., Malakhova, O. A., Il Kim, K., Ritchie, K. J., & Zhang, D. E. (2002). UBP43 (USP18) specifically removes ISG15 from conjugated

proteins. *Journal of Biological Chemistry*. https://doi.org/10.1074/jbc.M109078200

Martell, J. D., Deerinck, T. J., Sancak, Y., Poulos, T. L., Mootha, V. K., Sosinsky, G. E., Ellisman, M. H., & Ting, A. Y. (2012). Engineered ascorbate peroxidase as a genetically encoded reporter for electron microscopy. *Nature Biotechnology 2012 30:11*, *30*(11), 1143–1148. https://doi.org/10.1038/nbt.2375

Mastoridis, S., Bertolino, G. M., Whitehouse, G., Dazzi, F., Sanchez-Fueyo, A., & Martinez-Llordella, M. (2018). Multiparametric Analysis of Circulating Exosomes and Other Small Extracellular Vesicles by Advanced Imaging Flow Cytometry. *Frontiers in Immunology*, *9*(JUL). https://doi.org/10.3389/FIMMU.2018.01583

Mattila, P. K., & Lappalainen, P. (2008). Filopodia: molecular architecture and cellular functions. *Nature Reviews Molecular Cell Biology 2008 9:6*, *9*(6), 446–454. https://doi.org/10.1038/nrm2406

Maxfield, F. R., & McGraw, T. E. (2004). Endocytic recycling. *Nature Reviews. Molecular Cell Biology*, *5*(2), 121–132. https://doi.org/10.1038/NRM1315

Mayers, J. R., Fyfe, I., Schuh, A. L., Chapman, E. R., Edwardson, J. M., & Audhya, A. (2011). ESCRT-0 assembles as a heterotetrameric complex on membranes and binds multiple ubiquitinylated cargoes simultaneously. *Journal of Biological Chemistry*. https://doi.org/10.1074/jbc.M110.185363

Maytal-Kivity, V., Reis, N., Hofmann, K., & Glickman, M. H. (2002). MPN+, a putative catalytic motif found in a subset of MPN domain proteinsfrom eukaryotes and prokaryotes, is critical for Rpn11 function. *BMC Biochemistry*. https://doi.org/10.1186/1471-2091-3-28

McCullough, J., Clague, M. J., & Urbé, S. (2004). AMSH is an endosome-associated ubiquitin isopeptidase. *Journal of Cell Biology*, *166*(4), 487–492. https://doi.org/10.1083/jcb.200401141

McCullough, J., Fisher, R. D., Whitby, F. G., Sundquist, W. I., & Hill, C. P. (2008). ALIX-CHMP4 interactions in the human ESCRT pathway. *Proceedings of the National Academy of Sciences of the United States of America*. https://doi.org/10.1073/pnas.0801567105

McCullough, J., Row, P. E., Lorenzo, Ó., Doherty, M., Beynon, R., Clague, M. J., & Urbé, S. (2006). Activation of the endosome-associated ubiquitin isopeptidase AMSH by STAM, a component of the multivesicular body-sorting machinery. *Current Biology*. https://doi.org/10.1016/j.cub.2005.11.073

McDonell, L. M., Mirzaa, G. M., Alcantara, D., Schwartzentruber, J., Carter, M. T., Lee, L. J., Clericuzio, C. L., Graham, J. M., Morris-Rosendahl, D. J., Polster, T., Acsadi, G., Townshend, S., Williams, S., Halbert, A., Isidor, B., David, A., Smyser, C. D., Paciorkowski, A. R., Willing, M., … Boycott, K. M. (2013). Mutations in STAMBP, encoding a deubiquitinating enzyme, cause microcephaly-capillary malformation syndrome. *Nature Genetics*. https://doi.org/10.1038/ng.2602

McKenna, S., Spyracopoulos, L., Moraes, T., Pastushok, L., Ptak, C., Xiao, W., & Ellison, M. J. (2001). Noncovalent Interaction between Ubiquitin and the Human DNA Repair Protein Mms2 Is Required for Ubc13-mediated Polyubiquitination. *Journal of Biological Chemistry*, *276*(43), 40120–40126. https://doi.org/10.1074/jbc.M102858200

McNally, K. E., & Cullen, P. J. (2018). Endosomal Retrieval of Cargo: Retromer Is Not Alone. *Trends in Cell Biology*, *28*(10), 807–822. https://doi.org/10.1016/J.TCB.2018.06.005

Mehta, V., & Trinkle-Mulcahy, L. (2016). Recent advances in large-scale protein interactome mapping. *F1000Research*, *5*. https://doi.org/10.12688/F1000RESEARCH.7629.1

Melo, S. A., Luecke, L. B., Kahlert, C., Fernandez, A. F., Gammon, S. T., Kaye, J., LeBleu, V. S., Mittendorf, E. A., Weitz, J., Rahbari, N., Reissfelder, C., Pilarsky, C., Fraga, M. F., Piwnica-Worms, D., & Kalluri, R. (2015). Glypican-1 identifies cancer exosomes and detects early pancreatic cancer. *Nature 2015 523:7559*, *523*(7559), 177–182. https://doi.org/10.1038/nature14581

Mercker, M., & Marciniak-Czochra, A. (2015). Bud-Neck Scaffolding as a Possible Driving Force in ESCRT-Induced Membrane Budding. *Biophysical Journal*. https://doi.org/10.1016/j.bpj.2014.12.040

Metzger, M. B., Pruneda, J. N., Klevit, R. E., & Weissman, A. M. (2014). RING-type E3 ligases: Master manipulators of E2 ubiquitin-conjugating enzymes and ubiquitination. *Biochimica et Biophysica Acta*, *1843*(1), 47. https://doi.org/10.1016/J.BBAMCR.2013.05.026

Mevissen, T. E. T., Hospenthal, M. K., Geurink, P. P., Elliott, P. R., Akutsu, M., Arnaudo, N., Ekkebus, R., Kulathu, Y., Wauer, T., El Oualid, F., Freund, S. M. V., Ovaa, H., & Komander, D. (2013). OTU deubiquitinases reveal mechanisms of linkage specificity and enable ubiquitin chain restriction analysis. *Cell*, *154*(1), 169. https://doi.org/10.1016/J.CELL.2013.05.046

Mevissen, T. E. T., & Komander, D. (2017). Mechanisms of Deubiquitinase Specificity and Regulation. *Annual Review of Biochemistry*. https://doi.org/10.1146/annurev-biochem-061516-044916

Mevissen, T. E. T., Kulathu, Y., Mulder, M. P. C., Geurink, P. P., Maslen, S. L., Gersch, M., Elliott, P. R., Burke, J. E., Van Tol, B. D. M., Akutsu, M., El Oualid, F., Kawasaki, M., Freund, S. M. V., Ovaa, H., & Komander, D. (2016). Molecular basis of Lys11-polyubiquitin specificity in the deubiquitinase Cezanne. *Nature*, *538*(7625), 402–405. https://doi.org/10.1038/NATURE19836

Mizuno, E. (2004). Association with Hrs is required for the early endosomal localization, stability, and function of STAM. *J Bioch*.

Mizuno, E., Kawahata, K., Kato, M., Kitamura, N., & Komada, M. (2003). STAM proteins bind ubiquitinated proteins on the early endosome via the VHS domain and ubiquitin-interacting motif. *Molecular Biology of the Cell*. https://doi.org/10.1091/mbc.E02-12-0823

Morton, C. J., & Campbell, I. D. (1994). SH3 Domains: Molecular 'Velcro'1. *Current Biology*. https://doi.org/10.1016/S0960-9822(00)00134-2

Murphy, D. A., & Courtneidge, S. A. (2011). The "ins" and "outs" of podosomes and invadopodia: characteristics, formation and function. *Nature Reviews. Molecular Cell Biology*, *12*(7), 413. https://doi.org/10.1038/NRM3141

Nakamura, M., Tanaka, N., Kitamura, N., & Komada, M. (2006). Clathrin anchors deubiquitinating enzymes, AMSH and AMSH-like protein, on early endosomes. *Genes to Cells*. https://doi.org/10.1111/j.1365-2443.2006.00963.x

Nelson, S. L., Li, Y., Chen, Y., & Deshmukh, L. (2023). Avidity-Based Method for the Efficient Generation of Monoubiquitinated Recombinant Proteins. *Journal of the American Chemical Society*, *145*(14), 7748–7752. https://doi.org/10.1021/JACS.3C01943/SUPPL_FILE/JA3C01943_SI_002.AVI

Norris, A., & Grant, B. D. (2020). Endosomal microdomains: Formation and function. *Current Opinion in Cell Biology*. https://doi.org/10.1016/j.ceb.2020.02.018

Nothwehr, S. F., & Hindes, A. E. (1997). The yeast VPS5/GRD2 gene encodes a sorting nexin-1-like protein required for localizing membrane proteins to the late Golgi. *Journal of Cell Science*, *110 (Pt 9)*(9), 1063–1072. https://doi.org/10.1242/JCS.110.9.1063

Ogunjimi, A. A., Briant, D. J., Pece-Barbara, N., Le Roy, C., Di Guglielmo, G. M., Kavsak, P., Rasmussen, R. K., Seet, B. T., Sicheri, F., & Wrana, J. L. (2005). Regulation of Smurf2 ubiquitin ligase activity by anchoring the E2 to the HECT domain. *Molecular Cell*. https://doi.org/10.1016/j.molcel.2005.06.028

Ohtake, F., Saeki, Y., Sakamoto, K., Ohtake, K., Nishikawa, H., Tsuchiya, H., Ohta, T., Tanaka, K., & Kanno, J. (2015). Ubiquitin acetylation inhibits polyubiquitin chain elongation. *EMBO Reports*. https://doi.org/10.15252/embr.201439152

Omerovic, J., Hammond, D. E., Prior, I. A., & Clague, M. J. (2012). Global snapshot of the influence of endocytosis upon EGF receptor signaling output. *Journal of Proteome Research*, *11*(11), 5157–5166. https://doi.org/10.1021/PR3007304/SUPPL_FILE/PR3007304_SI_008.PDF

Özkaynak, E., Finley, D., & Varshavsky, A. (1984). The yeast ubiquitin gene: head-to-tail repeats encoding a polyubiquitin precursor protein. *Nature 1984 312:5995*, *312*(5995), 663–666. https://doi.org/10.1038/312663a0

Pandey, A., Fernandez, M. M., Steen, H., Blagoev, B., Nielsen, M. M., Roche, S., Mann, M., & Lodish, H. F. (2000). Identification of a novel immunoreceptor tyrosine-based activation motif-containing molecule, STAM2, by mass spectrometry and its involvement in growth factor and cytokine receptor signaling pathways. *Journal of Biological Chemistry*. https://doi.org/10.1074/jbc.M007849200

Pareja, F., Ferraro, D. A., Rubin, C., Cohen-Dvashi, H., Zhang, F., Aulmann, S., Ben-Chetrit, N., Pines, G., Navon, R., Crosetto, N., Köstler, W., Carvalho, S., Lavi, S., Schmitt, F., Dikic, I., Yakhini, Z., Sinn, P., Mills, G. B., & Yarden, Y. (2012). Deubiquitination of EGFR by Cezanne-1 contributes to cancer progression. *Oncogene*, *31*(43), 4599. https://doi.org/10.1038/ONC.2011.587

Parkinson, M. D. J., Piper, S. C., Bright, N. A., Evans, J. L., Boname, J. M., Bowers, K., Lehner, P. J., & Luzio, J. P. (2015). A non-canonical ESCRT pathway, including histidine domain phosphotyrosine phosphatase (HD-PTP), is used for down-regulation of virally ubiquitinated MHC class I. *Biochemical Journal*. https://doi.org/10.1042/BJ20150336

Pashkova, N., Gakhar, L., Winistorfer, S. C., Sunshine, A. B., Rich, M., Dunham, M. J., Yu, L., & Piper, R. C. (2013). The yeast alix homolog bro1 functions as a ubiquitin receptor for protein sorting into multivesicular endosomes. *Developmental Cell*. https://doi.org/10.1016/j.devcel.2013.04.007

Patki, V., Virbasius, J., Lane, W. S., Toh, B. H., Shpetner, H. S., & Corvera, S. (1997). Identification of an early endosomal protein regulated by phosphatidylinositol 3-kinase. *Proceedings of the National Academy of Sciences of the United States of America*, *94*(14), 7326. https://doi.org/10.1073/PNAS.94.14.7326

Pearse, B. M. F. (1975). Coated vesicles from pig brain: purification and biochemical characterization. *Journal of Molecular Biology*, *97*(1). https://doi.org/10.1016/S0022-2836(75)80024-6

Pickart, C. M. (2001). Mechanisms Underlying Ubiquitination. *Annual Review of Biochemistry*. https://doi.org/10.1146/annurev.biochem.70.1.503

Piper, R. C., Cooper, A. A., Yang, H., & Stevens, T. H. (1995). VPS27 controls vacuolar and endocytic traffic through a prevacuolar compartment in

Saccharomyces cerevisiae. *Journal of Cell Biology*. https://doi.org/10.1083/jcb.131.3.603

Pires, R., Hartlieb, B., Signor, L., Schoehn, G., Lata, S., Roessle, M., Moriscot, C., Popov, S., Hinz, A., Jamin, M., Boyer, V., Sadoul, R., Forest, E., Svergun, D. I., Göttlinger, H. G., & Weissenhorn, W. (2009). A Crescent-Shaped ALIX Dimer Targets ESCRT-III CHMP4 Filaments. *Structure*. https://doi.org/10.1016/j.str.2009.04.007

Plechanovov, A., Jaffray, E. G., Tatham, M. H., Naismith, J. H., & Hay, R. T. (2012). Structure of a RING E3 ligase and ubiquitin-loaded E2 primed for catalysis. *Nature*. https://doi.org/10.1038/nature11376

Poteryaev, D., Datta, S., Ackema, K., Zerial, M., & Spang, A. (2010). Identification of the switch in early-to-late endosome transition. *Cell*. https://doi.org/10.1016/j.cell.2010.03.011

Pruneda, J. N., Littlefield, P. J., Soss, S. E., Nordquist, K. A., Chazin, W. J., Brzovic, P. S., & Klevit, R. E. (2012). Structure of an E3:E2~Ub Complex Reveals an Allosteric Mechanism Shared among RING/U-box Ligases. *Molecular Cell*. https://doi.org/10.1016/j.molcel.2012.07.001

Py, B. F., Kim, M. S., Vakifahmetoglu-Norberg, H., & Yuan, J. (2013). Deubiquitination of NLRP3 by BRCC3 Critically Regulates Inflammasome Activity. *Molecular Cell*. https://doi.org/10.1016/j.molcel.2012.11.009

Qiu, X., Campos, Y., van de Vlekkert, D., Gomero, E., Tanwar, A. C., Kalathur, R., Weesner, J. A., Bongiovanni, A., Demmers, J., & d'Azzo, A. (2022). Distinct functions of dimeric and monomeric scaffold protein Alix in regulating F-actin assembly and loading of exosomal cargo. *Journal of Biological Chemistry*, *298*(10), 102425. https://doi.org/10.1016/J.JBC.2022.102425

Rabl, J., Bunker, R. D., Schenk, A. D., Cavadini, S., Gill, M. E., Abdulrahman, W., Andrés-Pons, A., Luijsterburg, M. S., Ibrahim, A. F. M., Branigan, E., Aguirre, J. D., Marceau, A. H., Guérillon, C., Bouwmeester, T., Hassiepen, U., Peters, A. H. F. M., Renatus, M., Gelman, L., Rubin, S. M., … Thomä, N. H. (2019). Structural Basis of BRCC36 Function in DNA Repair and Immune Regulation. *Molecular Cell*, *75*(3), 483. https://doi.org/10.1016/J.MOLCEL.2019.06.002

Raiborg, C., Bache, K. G., Gillooly, D. J., Madshus, I. H., Stang, E., & Stenmark, H. (2002). Hrs sorts ubiquitinated proteins into clathrin-coated microdomains of early endosomes. *Nature Cell Biology*, *4*(5), 394–398. https://doi.org/10.1038/NCB791

Raiborg, C., Grønvold Bache, K., Mehlum, A., Stang, E., & Stenmark, H. (2001). Hrs recruits clathrin to early endosomes. *EMBO Journal*. https://doi.org/10.1093/emboj/20.17.5008

Raiborg, C., Wesche, J., Malerød, L., & Stenmark, H. (2006). Flat clathrin coats on endosomes mediate degradative protein sorting by scaffolding Hrs in dynamic microdomains. *Journal of Cell Science*, *119*(Pt 12), 2414–2424. https://doi.org/10.1242/JCS.02978

Rajesh et al. (2011). Binding to Syntenin-1 Protein Defines a New Mode of Ubiquitin-based Interactions Regulated by Phosphorylation. *Journal of Biological ChemistryBC*.

Raymond, C. K., Howald-Stevenson, I., Vater, C. A., & Stevens, T. H. (1992). Morphological classification of the yeast vacuolar protein sorting mutants: Evidence for a prevacuolar compartment in class E vps mutants. *Molecular Biology of the Cell*. https://doi.org/10.1091/mbc.3.12.1389

Ren, X., & Hurley, J. H. (2010a). VHS domains of ESCRT-0 cooperate in high-avidity binding to polyubiquitinated cargo. *The EMBO Journal*, *29*(6), 1045–1054. https://doi.org/10.1038/EMBOJ.2010.6

Ren, X., & Hurley, J. H. (2010b). VHS domains of ESCRT-0 cooperate in high-avidity binding to polyubiquitinated cargo. *EMBO Journal*. https://doi.org/10.1038/emboj.2010.6

Renault, L., Kuhlmann, J., Henkel, A., & Wittinghofer, A. (2001). Structural basis for guanine nucleotide exchange on Ran by the regulator of chromosome condensation (RCC1). *Cell*. https://doi.org/10.1016/S0092-8674(01)00315-4

Ribeiro, M. F., Zhu, H., Millard, R. W., & Fan, G. C. (2013). Exosomes Function in Pro- and Anti-Angiogenesis. *Current Angiogenesis*, *2*(1), 54–59. https://doi.org/10.2174/22115528113020020001

Richter, C., West, M., & Odorizzi, G. (2007). Dual mechanisms specify Doa4-mediated deubiquitination at multivesicular bodies. *The EMBO Journal*, *26*(10), 2454. https://doi.org/10.1038/SJ.EMBOJ.7601692

Rink, J., Ghigo, E., Kalaidzidis, Y., & Zerial, M. (2005). Rab conversion as a mechanism of progression from early to late endosomes. *Cell*. https://doi.org/10.1016/j.cell.2005.06.043

Rivkin, E., Almeida, S. M., Ceccarelli, D. F., Juang, Y. C., MacLean, T. A., Srikumar, T., Huang, H., Dunham, W. H., Fukumura, R., Xie, G., Gondo, Y., Raught, B., Gingras, A. C., Sicheri, F., & Cordes, S. P. (2013). The linear ubiquitin-specific deubiquitinase gumby regulates angiogenesis. *Nature 2013 498:7454*, *498*(7454), 318–324. https://doi.org/10.1038/nature12296

Rotin, D., & Kumar, S. (2009). Physiological functions of the HECT family of ubiquitin ligases. In *Nature Reviews Molecular Cell Biology*. https://doi.org/10.1038/nrm2690

Roucourt, B., Meeussen, S., Bao, J., Zimmermann, P., & David, G. (2015). Heparanase activates the syndecan-syntenin-ALIX exosome pathway. *Cell Research*, *25*(4), 412–428. https://doi.org/10.1038/CR.2015.29

Row, P. E., Liu, H., Hayes, S., Welchman, R., Charalabous, P., Hofmann, K., Clague, M. J., Sanderson, C. M., & Urbé, S. (2007). The MIT Domain of UBPY Constitutes a CHMP Binding and Endosomal Localization Signal Required for Efficient Epidermal Growth Factor Receptor Degradation. *Journal of Biological Chemistry*, *282*(42), 30929–30937. https://doi.org/10.1074/JBC.M704009200

Row, P. E., Prior, I. A., McCullough, J., Clague, M. J., & Urbé, S. (2006). The ubiquitin isopeptidase UBPY regulates endosomal ubiquitin dynamics and is essential for receptor down-regulation. *The Journal of Biological Chemistry*, *281*(18), 12618–12624. https://doi.org/10.1074/JBC.M512615200

Sachse, M., Urbé, S., Oorschot, V., Strous, G. J., & Klumperman, J. (2002). Bilayered clathrin coats on endosomal vacuoles are involved in protein sorting toward lysosomes. *Molecular Biology of the Cell*. https://doi.org/10.1091/mbc.01-10-0525

Saksena, S., Wahlman, J., Teis, D., Johnson, A. E., & Emr, S. D. (2009). Functional Reconstitution of ESCRT-III Assembly and Disassembly. *Cell*. https://doi.org/10.1016/j.cell.2008.11.013

Sato, Y., Goto, E., Shibata, Y., Kubota, Y., Yamagata, A., Goto-Ito, S., Kubota, K., Inoue, J. I., Takekawa, M., Tokunaga, F., & Fukai, S. (2015). Structures of CYLD USP with Met1- or Lys63-linked diubiquitin reveal mechanisms for dual specificity. *Nature Structural & Molecular Biology 2015 22:3*, *22*(3), 222–229. https://doi.org/10.1038/nsmb.2970

Sato, Y., Okatsu, K., Saeki, Y., Yamano, K., Matsuda, N., Kaiho, A., Yamagata, A., Goto-Ito, S., Ishikawa, M., Hashimoto, Y., Tanaka, K., & Fukai, S. (2017). Structural basis for specific cleavage of Lys6-linked polyubiquitin chains by USP30. *Nature Structural & Molecular Biology 2017 24:11*, *24*(11), 911–919. https://doi.org/10.1038/nsmb.3469

Sato, Y., Yoshikawa, A., Yamagata, A., Mimura, H., Yamashita, M., Ookata, K., Nureki, O., Iwai, K., Komada, M., & Fukai, S. (2008). Structural basis for specific cleavage of Lys 63-linked polyubiquitin chains. *Nature*. https://doi.org/10.1038/nature07254

Scheffner, M., Nuber, U., & Huibregtse, J. M. (1995). Protein ubiquitination involving an E1–E2–E3 enzyme ubiquitin thioester cascade. *Nature 1995 373:6509*, *373*(6509), 81–83. https://doi.org/10.1038/373081a0

Schlesinger, D. H., & Goldstein, G. (1975). Molecular conservation of 74 amino acid sequence of ubiquitin between cattle and man. *Nature*. https://doi.org/10.1038/255423a0

Schmid, E. M., & McMahon, H. T. (2007). Integrating molecular and network biology to decode endocytosis. *Nature*, *448*(7156), 883–888. https://doi.org/10.1038/NATURE06031

Schmid, S. L., Fuchs, R., Male, P., & Mellman, I. (1988). Two distinct subpopulations of endosomes involved in membrane recycling and transport to lysosomes. *Cell*. https://doi.org/10.1016/0092-8674(88)90532-6

Schöneberg, J., Lee, I. H., Iwasa, J. H., & Hurley, J. H. (2016). Reverse-topology membrane scission by the ESCRT proteins. In *Nature Reviews Molecular Cell Biology*. https://doi.org/10.1038/nrm.2016.121

Schroder, K., & Tschopp, J. (2010). The Inflammsomes. *Cell*.

Schulz, S., Chachami, G., Kozaczkiewicz, L., Winter, U., Stankovic-Valentin, N., Haas, P., Hofmann, K., Urlaub, H., Ovaa, H., Wittbrodt, J., Meulmeester, E., & Melchior, F. (2012). Ubiquitin-specific protease-like 1 (USPL1) is a SUMO isopeptidase with essential, non-catalytic functions. *EMBO Reports*, *13*(10), 930–938. https://doi.org/10.1038/EMBOR.2012.125

Schweppe, D. K., Huttlin, E. L., Harper, J. W., & Gygi, S. P. (2018). BioPlex Display: An Interactive Suite for Large-Scale AP-MS Protein-Protein Interaction Data. *Journal of Proteome Research*, *17*(1), 722–726. https://doi.org/10.1021/ACS.JPROTEOME.7B00572/SUPPL_FILE/PR7B00572_SI_001.PDF

Scourfield, E. J., & Martin-Serrano, J. (2017). Growing functions of the ESCRT machinery in cell biology and viral replication. *Biochemical Society Transactions*, *45*(3), 613–634. https://doi.org/10.1042/BST20160479

Seaman, M. N. J., McCaffery, J. M., & Emr, S. D. (1998). A membrane coat complex essential for endosome-to-Golgi retrograde transport in yeast. *Journal of Cell Biology*. https://doi.org/10.1083/jcb.142.3.665

Seidah, N. G., Poirier, S., Denis, M., Parker, R., Miao, B., Mapelli, C., Prat, A., Wassef, H., Davignon, J., Hajjar, K. A., & Mayer, G. (2012). Annexin A2 is a natural extrahepatic inhibitor of the PCSK9-induced LDL receptor degradation. *PloS One*, *7*(7). https://doi.org/10.1371/JOURNAL.PONE.0041865

Shao, G., Lilli, D. R., Patterson-Fortin, J., Coleman, K. A., Morrissey, D. E., & Greenberg, R. A. (2009). The Rap80-BRCC36 de-ubiquitinating enzyme complex antagonizes RNF8-Ubc13-dependent ubiquitination events at DNA double strand breaks. *Proceedings of the National Academy of Sciences of the United States of America*. https://doi.org/10.1073/pnas.0807485106

Shields, S. B., & Piper, R. C. (2011). How ubiquitin functions with ESCRTs. In *Traffic*. https://doi.org/10.1111/j.1600-0854.2011.01242.x

Shim, S., Kimpler, L. A., & Hanson, P. I. (2007). Structure/function analysis of four core ESCRT-III proteins reveals common regulatory role for extreme C-terminal domain. *Traffic*. https://doi.org/10.1111/j.1600-0854.2007.00584.x

Shrestha, R. K., Ronau, J. A., Davies, C. W., Guenette, R. G., Strieter, E. R., Paul, L. N., & Das, C. (2014). Insights into the mechanism of deubiquitination by jamm deubiquitinases from cocrystal structures of the enzyme with the substrate and product. *Biochemistry*, *53*(19), 3199–3217. https://doi.org/10.1021/BI5003162/SUPPL_FILE/BI5003162_SI_001.PDF

Sierra, M. I., Wright, M. H., & Nash, P. D. (2010a). AMSH interacts with ESCRT-0 to regulate the stability and trafficking of CXCR4. *Journal of Biological Chemistry*. https://doi.org/10.1074/jbc.M109.061309

Sierra, M. I., Wright, M. H., & Nash, P. D. (2010b). AMSH Interacts with ESCRT-0 to Regulate the Stability and Trafficking of CXCR4. *Journal of Biological Chemistry*, *285*(18), 13990–14004. https://doi.org/10.1074/JBC.M109.061309

Sönnichsen, B., De Renzis, S., Nielsen, E., Rietdorf, J., & Zerial, M. (2000). Distinct membrane domains on endosomes in the recycling pathway visualized by multicolor imaging of Rab4, Rab5, and Rab11. *Journal of Cell Biology*. https://doi.org/10.1083/jcb.149.4.901

Spratt, D. E., Walden, H., & Shaw, G. S. (2014). RBR E3 ubiquitin ligases: New structures, new insights, new questions. In *Biochemical Journal*. https://doi.org/10.1042/BJ20140006

Staub, O., Dho, S., Henry, P., Correa, J., Ishikawa, T., McGlade, J., & Rotin, D. (1996). WW domains of Nedd4 bind to the proline-rich PY motifs in the epithelial Na+ channel deleted in Liddle's syndrome. *The EMBO Journal*. https://doi.org/10.1002/j.1460-2075.1996.tb00593.x

Stewart et al. (2016). E2 enzymes: more than just middle men. *Cell Reasearch*, *26*, 423–440.

Suzuki, S., Tamai, K., Watanabe, M., Kyuuma, M., Ono, M., Sugamura, K., & Tanaka, N. (2011). AMSH is required to degrade ubiquitinated proteins in the central nervous system. *Biochemical and Biophysical Research Communications*. https://doi.org/10.1016/j.bbrc.2011.04.065

Swaney, D. L., Beltrao, P., Starita, L., Guo, A., Rush, J., Fields, S., Krogan, N. J., & Villén, J. (2013). Global analysis of phosphorylation and ubiquitylation cross-talk in protein degradation. *Nature Methods*. https://doi.org/10.1038/nmeth.2519

Takata, H., Kato, M., Denda, K., & Kitamura, N. (2000). A Hrs binding protein having a Src homology 3 domain is involved in intracellular degradation of growth factors and their receptors. *Genes to Cells*. https://doi.org/10.1046/j.1365-2443.2000.00303.x

Takeshita, T., Arita, T., Asao, H., Tanaka, N., Higuchi, M., Kuroda, H., Kaneko, K., Munakata, H., Endo, Y., Fujita, T., & Sugamura, K. (1996). Cloning of a novel signal-transducing adaptor molecule containing an SH3 domain and ITAM. *Biochemical and Biophysical Research Communications*. https://doi.org/10.1006/bbrc.1996.1290

Takeshita, T., Arita, T., Higuchi, M., Asao, H., Endo, K., Kuroda, H., Tanaka, N., Murata, K., Ishii, N., & Sugamura, K. (1997). STAM, signal transducing adaptor molecule, is associated with janus kinases and involved in signaling for cell growth and c-myc induction. *Immunity*. https://doi.org/10.1016/S1074-7613(00)80288-5

Tanaka, N., Kaneko, K., Asao, H., Kasai, H., Endo, Y., Fujita, T., Takeshita, T., & Sugamura, K. (1999). Possible involvement of a novel STAM-associated molecule “AMSH” in intracellular signal transduction mediated by cytokines. *Journal of Biological Chemistry*. https://doi.org/10.1074/jbc.274.27.19129

Teis, D., Saksena, S., & Emr, S. D. (2008). Ordered Assembly of the ESCRT-III Complex on Endosomes Is Required to Sequester Cargo during MVB Formation. *Developmental Cell*. https://doi.org/10.1016/j.devcel.2008.08.013

Tenno, T., Fujiwara, K., Tochio, H., Iwai, K., Morita, E. H., Hayashi, H., Murata, S., Hiroaki, H., Sato, M., Tanaka, K., & Shirakawa, M. (2004). Structural basis for distinct roles of Lys63- and Lys48-linked polyubiquitin chains. *Genes to Cells*. https://doi.org/10.1111/j.1365-2443.2004.00780.x

Thorne, C., Eccles, R. L., Coulson, J. M., Urbé, S., & Clague, M. J. (2011). Isoform-Specific Localization of the Deubiquitinase USP33 to the Golgi Apparatus. *Traffic*, *12*(11), 1563–1574. https://doi.org/10.1111/J.1600-0854.2011.01261.X

Thorslund, T., Ripplinger, A., Hoffmann, S., Wild, T., Uckelmann, M., Villumsen, B., Narita, T., Sixma, T. K., Choudhary, C., Bekker-Jensen, S., & Mailand, N. (2015a). Histone H1 couples initiation and amplification of ubiquitin signalling after DNA damage. *Nature 2015 527:7578*, *527*(7578), 389–393. https://doi.org/10.1038/nature15401

Thorslund, T., Ripplinger, A., Hoffmann, S., Wild, T., Uckelmann, M., Villumsen, B., Narita, T., Sixma, T. K., Choudhary, C., Bekker-Jensen, S., & Mailand, N. (2015b). Histone H1 couples initiation and amplification of ubiquitin signalling after DNA damage. *Nature*. https://doi.org/10.1038/nature15401

Trinkle-Mulcahy, L. (2008). Identifying specific protein interaction partners using quantitative mass spectrometry and bead proteomes. *Journal of Cell Biology*, *183*(2), 223–239.

Tsang, H. T. H., Connell, J. W., Brown, S. E., Thompson, A., Reid, E., & Sanderson, C. M. (2006). A systematic analysis of human CHMP protein interactions: Additional MIT domain-containing proteins bind to multiple components of the human ESCRT III complex. *Genomics*, *88*(3), 333–346. https://doi.org/10.1016/J.YGENO.2006.04.003

Tupone, M. G., D’Aguanno, S., Di Martile, M., Valentini, E., Desideri, M., Trisciuoglio, D., Donzelli, S., Sacconi, A., Buglioni, S., Ercolani, C., Biagioni, A., Fibbi, G., Fattore, L., Mancini, R., Ciliberto, G., Blandino, G., & Del Bufalo, D. (2020). microRNA-378a-5p iS a novel positive regulator of melanoma progression. *Oncogenesis*. https://doi.org/10.1038/s41389-020-0203-6

Urbe, S., Mills, I. G., Stenmark, H., Kitamura, N., & Clague, M. J. (2000). Endosomal Localization and Receptor Dynamics Determine Tyrosine Phosphorylation of Hepatocyte Growth Factor-Regulated Tyrosine Kinase Substrate. *Molecular and Cellular Biology*. https://doi.org/10.1128/mcb.20.20.7685-7692.2000

Urbé, S., Sachse, M., Row, P. E., Preisinger, C., Barr, F. A., Strous, G., Klumperman, J., & Clague, M. (2003). The UIM domain of Hrs couples receptor sorting to vesicle formation. *Journal of Cell Science*. https://doi.org/10.1242/jcs.00723

Van Der Sluijs, P., Hull, M., Zahraoui, A., Tavitian, A., Goud, B., & Mellman, I. (1991). The small GTP-binding protein rab4 is associated with early endosomes. *Proceedings of the National Academy of Sciences of the United States of America*, *88*(14), 6313–6317. https://doi.org/10.1073/PNAS.88.14.6313

Varadan, R., Assfalg, M., Haririnia, A., Raasi, S., Pickart, C., & Fushman, D. (2004). Solution Conformation of Lys63-linked Di-ubiquitin Chain Provides Clues to Functional Diversity of Polyubiquitin Signaling. *Journal of Biological Chemistry*. https://doi.org/10.1074/jbc.M309184200

Varadan, R., Walker, O., Pickart, C., & Fushman, D. (2002). Structural properties of polyubiquitin chains in solution. *Journal of Molecular Biology*. https://doi.org/10.1016/S0022-2836(02)01198-1

Verdecia, M. A., Joazeiro, C. A. P., Wells, N. J., Ferrer, J. L., Bowman, M. E., Hunter, T., & Noel, J. P. (2003). Conformational flexibility underlies ubiquitin ligation mediated by the WWP1 HECT domain E3 ligase. *Molecular Cell*. https://doi.org/10.1016/S1097-2765(02)00774-8

Verma, R., Aravind, L., Oania, R., McDonald, W. H., Yates, J. R., Koonin, E. V., & Deshaies, R. J. (2002). Role of Rpn11 metalloprotease in deubiquitination and degradation by the 26S proteasome. *Science*. https://doi.org/10.1126/science.1075898

Vietri, M., Radulovic, M., & Stenmark, H. (2020). The many functions of ESCRTs. In *Nature Reviews Molecular Cell Biology*. https://doi.org/10.1038/s41580-019-0177-4

Virdee, S., Ye, Y., Nguyen, D. P., Komander, D., & Chin, J. W. (2010). Engineered diubiquitin synthesis reveals Lys29-isopeptide specificity of an OTU deubiquitinase. *Nature Chemical Biology*, *6*(10), 750–757. https://doi.org/10.1038/NCHEMBIO.426

Wagner, S. A., Beli, P., Weinert, B. T., Nielsen, M. L., Cox, J., Mann, M., & Choudhary, C. (2011). A proteome-wide, quantitative survey of in vivo ubiquitylation sites reveals widespread regulatory roles. *Molecular & Cellular Proteomics : MCP*, *10*(10), M111.013284. https://doi.org/10.1074/MCP.M111.013284

Walden, M., Masandi, S. K., Pawłowski, K., & Zeqiraj, E. (2018). Pseudo-DUBs as allosteric activators and molecular scaffolds of protein complexes. In *Biochemical Society Transactions*. https://doi.org/10.1042/BST20160268

Wang, D., Xu, C., Yang, W., Chen, J., Ou, Y., Guan, Y., Guan, J., & Liu, Y. (2022). E3 ligase RNF167 and deubiquitinase STAMBPL1 modulate mTOR and cancer progression. *Molecular Cell*, *82*(4), 770-784.e9. https://doi.org/10.1016/j.molcel.2022.01.002

Weeks, S. D., Grasty, K. C., Hernandez-Cuebas, L., & Loll, P. J. (2009). Crystal structures of Lys-63-linked tri- and di-ubiquitin reveal a highly extended chain architecture. *Proteins: Structure, Function and Bioinformatics*. https://doi.org/10.1002/prot.22568

Weissenhorn, W., Solomons, J., Sabin, C., Poudevigne, E., Usami, Y., Hulsik, D. L., Macheboeuf, P., Hartlieb, B., & Gottlinger, H. (2011). Structural Basis for ESCRT-III CHMP3 Recruitment of AMSH. *Structure*.

Wenzel, D. M., Lissounov, A., Brzovic, P. S., & Klevit, R. E. (2011). UBCH7 reactivity profile reveals parkin and HHARI to be RING/HECT hybrids. *Nature*. https://doi.org/10.1038/nature09966

Wiborg, O., Pedersen, M. S., Wind, A., Berglund, L. E., Marcker, K. A., & Vuust, J. (1985). The human ubiquitin multigene family: some genes contain multiple directly repeated ubiquitin coding sequences. *The EMBO Journal*, *4*(3), 755. https://doi.org/10.1002/J.1460-2075.1985.TB03693.X

Williams, J. K., Ngo, J. M., Lehman, I. M., & Schekman, R. (2023). Annexin A6 mediates calcium-dependent exosome secretion during plasma membrane repair. *ELife*, *12*. https://doi.org/10.7554/ELIFE.86556

Williams, R. L., & Urbé, S. (2007). The emerging shape of the ESCRT machinery. *Nature Reviews Molecular Cell Biology 2007 8:5*, *8*(5), 355–368. https://doi.org/10.1038/nrm2162

Wolf, P. (1967). The Nature and Significance of Platelet Products in Human Plasma. *British Journal of Haematology*, *13*(3), 269–288. https://doi.org/10.1111/J.1365-2141.1967.TB08741.X

Worden, E. J., Padovani, C., & Martin, A. (2014). Structure of the Rpn11-Rpn8 dimer reveals mechanisms of substrate deubiquitination during proteasomal degradation. *Nature Structural and Molecular Biology*. https://doi.org/10.1038/nsmb.2771

Wu, Q., Cheng, Z., Zhu, J., Xu, W., Peng, X., Chen, C., Li, W., Wang, F., Cao, L., Yi, X., Wu, Z., Li, J., & Fan, P. (2015). Suberoylanilide Hydroxamic Acid Treatment Reveals Crosstalks among Proteome, Ubiquitylome and Acetylome in Non-Small Cell Lung Cancer A549 Cell Line. *Scientific Reports 2015 5:1*, *5*(1), 1–11. https://doi.org/10.1038/srep09520

Xia, Z. P., Sun, L., Chen, X., Pineda, G., Jiang, X., Adhikari, A., Zeng, W., & Chen, Z. J. (2009). Direct activation of protein kinases by unanchored polyubiquitin chains. *Nature*. https://doi.org/10.1038/nature08247

Xu, H., Yang, X., Xuan, X., Wu, D., Zhang, J., Xu, X., Zhao, Y., Ma, C., & Li, D. (2021). STAMBP promotes lung adenocarcinoma metastasis by regulating the EGFR/MAPK signaling pathway. *Neoplasia (New York, N.Y.)*, *23*(6), 607. https://doi.org/10.1016/J.NEO.2021.05.011

Xu, P., Duong, D. M., Seyfried, N. T., Cheng, D., Xie, Y., Robert, J., Rush, J., Hochstrasser, M., Finley, D., & Peng, J. (2009). Quantitative Proteomics Reveals the Function of Unconventional Ubiquitin Chains in Proteasomal Degradation. *Cell*, *137*(1), 133. https://doi.org/10.1016/J.CELL.2009.01.041

Yan, J., & Jetten, A. M. (2008). RAP80 and RNF8, key players in the recruitment of repair proteins to DNA damage sites. *Cancer Letters*, *271*(2), 179. https://doi.org/10.1016/J.CANLET.2008.04.046

Yan, Y., Jiang, W., Liu, L., Wang, X., Ding, C., Tian, Z., & Zhou, R. (2015). Dopamine controls systemic inflammation through inhibition of NLRP3 inflammasome. *Cell*. https://doi.org/10.1016/j.cell.2014.11.047

Yáñez-Mó, M., Siljander, P. R. M., Andreu, Z., Zavec, A. B., Borràs, F. E., Buzas, E. I., Buzas, K., Casal, E., Cappello, F., Carvalho, J., Colás, E., Cordeiro-Da Silva, A., Fais, S., Falcon-Perez, J. M., Ghobrial, I. M., Giebel, B., Gimona, M., Graner, M., Gursel, I., … De Wever, O. (2015). Biological properties of extracellular vesicles and their physiological functions. *Journal of Extracellular Vesicles*, *4*(2015), 1–60. https://doi.org/10.3402/JEV.V4.27066

Yang, X.-P. (2019). The macrophage-specific V-ATPase subunit ATP6V0D2 restricts inflammasome activation and bacterial infection by facilitating autophagosome-lysosome fusion. *Autophagy*, *15*(6).

Yao, T., & Cohen, R. E. (2002). A cryptic protease couples deubiquitination and degradation by the proteasome. *Nature*. https://doi.org/10.1038/nature01071

Yu, H., Chen, J. K., Feng, S., Dalgarno, D. C., Brauer, A. W., & Schrelber, S. L. (1994). Structural basis for the binding of proline-rich peptides to SH3 domains. *Cell*. https://doi.org/10.1016/0092-8674(94)90367-0

Yu, M. M., Boucrot, E., Villén, J., Affar, E. B., Gygi, S. P., Göttlinger, H. G., & Kirchhausen, T. (2006). Targeting of AMSH to endosomes is required for epidermal growth factor receptor degradation. *Journal of Biological Chemistry*, *282*(13), 9805–9812. https://doi.org/10.1074/jbc.M611635200

Yu, Z., Shi, M., Stewart, T., Fernagut, P. O., Huang, Y., Tian, C., Dehay, B., Atik, A., Yang, D., de Giorgi, F., Ichas, F., Canron, M. H., Ceravolo, R., Frosini, D., Kim, H. J., Feng, T., Meissner, W. G., & Zhang, J. (2020). Reduced oligodendrocyte exosome secretion in multiple system atrophy involves SNARE dysfunction. *Brain*, *143*(6), 1780–1797. https://doi.org/10.1093/BRAIN/AWAA110

Zamborlini, A., Usami, Y., Radoshitzky, S. R., Popova, E., Palu, G., & Göttlinger, H. (2006). Release of autoinhibition converts ESCRT-III components into potent inhibitors of HIV-1 budding. *Proceedings of the National Academy of Sciences of the United States of America*. https://doi.org/10.1073/pnas.0603788103

Zeng, W., Sun, L., Jiang, X., Chen, X., Hou, F., Adhikari, A., Xu, M., & Chen, Z. J. (2010). Reconstitution of the RIG-I pathway reveals a signaling role of unanchored polyubiquitin chains in innate immunity. *Cell*. https://doi.org/10.1016/j.cell.2010.03.029

Zhai, Q., Landesman, M. B., Chung, H.-Y., Dierkers, A., Jeffries, C. M., Trewhella, J., Hill, C. P., & Sundquist, W. I. (2011). Activation of the Retroviral Budding Factor ALIX. *Journal of Virology*. https://doi.org/10.1128/jvi.02653-10

Zhang, J., Li, S., Li, L., Li, M., Guo, C., Yao, J., & Mi, S. (2015). Exosome and Exosomal MicroRNA: Trafficking, Sorting, and Function. *Genomics, Proteomics & Bioinformatics*, *13*(1), 17–24. https://doi.org/10.1016/J.GPB.2015.02.001

Zhao, Y., Mudge, M. C., Soll, J. M., Rodrigues, R. B., Byrum, A. K., Schwarzkopf, E. A., Bradstreet, T. R., Gygi, S. P., Edelson, B. T., & Mosammaparast, N. (2018). OTUD4 Is a Phospho-Activated K63 Deubiquitinase that Regulates MyD88-Dependent Signaling. *Molecular Cell*, *69*(3), 505-516.e5. https://doi.org/10.1016/J.MOLCEL.2018.01.009

Zheng, H., Gupta, V., Patterson-Fortin, J., Bhattacharya, S., Katlinski, K., Wu, J., Varghese, B., Carbone, C. J., Aressy, B., Fuchs, S. Y., & Greenberg, R. A. (2013a). A BRISC-SHMT Complex Deubiquitinates IFNAR1 and Regulates Interferon Responses. *Cell Reports*. https://doi.org/10.1016/j.celrep.2013.08.025

Zheng, H., Gupta, V., Patterson-Fortin, J., Bhattacharya, S., Katlinski, K., Wu, J., Varghese, B., Carbone, C. J., Aressy, B., Fuchs, S. Y., & Greenberg, R. A. (2013b). A BRISC-SHMT Complex Deubiquitinates IFNAR1 and Regulates Interferon Responses. *Cell Reports*, *5*(1), 180–193. https://doi.org/10.1016/j.celrep.2013.08.025

Zheng, N., & Shabek, N. (2017). Ubiquitin Ligases: Structure, Function, and Regulation. *Annual Review of Biochemistry*. https://doi.org/10.1146/annurev-biochem-060815-014922

Zhu, P., Zhou, W., Wang, J., Puc, J., Ohgi, K. A., Erdjument-Bromage, H., Tempst, P., Glass, C. K., & Rosenfeld, M. G. (2007). A Histone H2A Deubiquitinase Complex Coordinating Histone Acetylation and H1 Dissociation in Transcriptional Regulation. *Molecular Cell*. https://doi.org/10.1016/j.molcel.2007.07.024

Zimmerman. (2005). Syndecan recycling [corrected] is controlled by syntenin-PIP2 interaction and Arf6. *Developmental Cell*, *9*(3).

Zimmerman, E. S., Schulman, B. A., & Zheng, N. (2010). Structural assembly of cullin-RING ubiquitin ligase complexes. In *Current Opinion in Structural Biology*. https://doi.org/10.1016/j.sbi.2010.08.010